Haptic Teleoperation for Robotic-Assisted Surgery

Abdulrahman Albakri

THÈSE

Pour obtenir le grade de

Docteur

Délivré par l'**Université de Montpellier**

Préparée au sein de l'école doctorale **Information, Structures, Systèmes (I2S)**

Et de l'unité de recherche **Laboratoire d'Informatique, de Robotique et de Microélectronique de Montpellier (LIRMM)**

Spécialité: **System Automatique et Microélectronique (SyAM)**

Présentée par **Abdulrahman ALBAKRI**

Haptic Teleoperation for Robotic-Assisted Surgery

Soutenue le 16 Decembre 2015 devant le jury composé de

M. Tanneguy Redarce	Professeur	INSA de Lyon	Rapporteur
M. Gérard Poisson	Professeur	Univ. d'Orleans	Rapporteur
Mme. Marilena Vendittelli	Ass. Professor	Univ. de Rome	Examinateur
M. Nabil Zemiti	Maître de Conférence	Univ. Montpellier	Examinateur
M. Philippe Poignet	Professeur	Univ. Montpellier	Directeur de thèse
M. Chao Liu	Chargé de Recherche	LIRMM-CNRS	Co-Encadrant

The work of this dissertation was supported by Syrian Ministry of Higher Education (University of Aleppo) Grant.

.

To my family ...

Contents

Contents v

List of Figures ix

List of Tables xiii

Nomenclature 1

1 Introduction 3
- 1.1 Statement of Purposes . . . 3
- 1.2 Contributions . . . 4
- 1.3 Summary of remaining chapters . . . 5

2 Telerobotics for Surgery: Telesurgery 7
- 2.1 Terminology . . . 7
- 2.2 Conception and Foundation . . . 9
- 2.3 Historic Overview and Applications . . . 11
  - 2.3.1 Teleoperation for Medical care . . . 13
  - 2.3.2 Robotics for Surgical assistance . . . 13
- 2.4 Research Thematics . . . 14
  - 2.4.1 Human-Master interconnection . . . 15
  - 2.4.2 Master System design . . . 21
  - 2.4.3 Communication layer design . . . 25
  - 2.4.4 Slave System . . . 28
  - 2.4.5 Environment and interaction modelling . . . 32

2.4.6 Teleoperation design and assessment . . . 35
2.5 Conclusion . . . 38

3 Teleoperation Design and Evaluation 39
3.1 Modelling . . . 39
3.1.1 Basic Notions . . . 40
3.1.2 Human and Environment modelling . . . 43
3.1.3 Teleoperator's model . . . 44
3.2 Design . . . 49
3.3 Evaluation . . . 52
3.4 Conclusion . . . 54

4 On the Selection of Teleoperation Control Architecture 55
4.1 Introduction . . . 56
4.2 Contributions . . . 60
4.3 Stability and Performance Analysis of 3-Channel Architectures . . . 62
4.3.1 Position-Position Force Control Architecture ($P-PF$, $Fig.4.2.a$) . . . 62
4.3.2 Force-Position Force Control Architecture ($F-PF$, $Fig.4.2.b$) . . . 67
4.3.3 Position Force-Position Control Architecture ($PF-P$, $Fig.4.2.c$) . . . 71
4.3.4 Position Force-Force Control Architecture ($PF-F$, $Fig.4.2.d$) . . . 74
4.4 Teleoperation control architecture for medical application . . . 76
4.5 Conclusions . . . 79

5 Environment Modeling with Physiological Motion Disturbance for Surgical Teleoperation 81
5.1 Introduction . . . 81
5.2 Teleoperation Scheme Reformulation . . . 83
5.2.1 Heart electromechanical properties . . . 84
5.2.2 Problem reformulation . . . 85
5.2.3 Environment Impedance . . . 88
5.3 Interaction Impedance with a Moving Environment . . . 88
5.3.1 Soft Tissue Modeling $Z_e(s)$ . . . 89
5.3.2 Motion Modelling . . . 89
5.3.3 Interaction modeling . . . 92
5.4 Case Study . . . 94
5.4.1 Beating heart motion modeling . . . 94
5.4.2 Slave Robot Motion Modelling . . . 95
5.4.3 Interaction Impedance . . . 96
5.5 Conclusion . . . 98

6 Slave-Environment Interaction Control Based Haptic Teleoperation 99

6.1 Introduction . . . 100
6.2 Chapter Contributions and Organisation: . . . 102
6.3 Teleoperation Structure . . . 102
6.3.1 Modelling . . . 103
6.3.2 Stability . . . 104
6.3.3 Transparency . . . 105
6.3.4 The role of G_v transfer function (a discussion) . . . 107
6.4 An Enhanced Interaction Controller . . . 110
6.4.1 Tissue interaction model . . . 111
6.4.2 Model based interaction controller . . . 113
6.5 Experimental validation: . . . 120
6.5.1 Experiments set-up . . . 120
6.5.2 Haptic data measurements . . . 124
6.5.3 Experiments results . . . 125
6.6 Conclusion . . . 127

7 Conclusions and Discussion **129**
7.1 Conclusions . . . 129
7.2 Future Directions . . . 131

A Appendix A: Model based interaction control, a comparative study **133**
A.1 Model Identification . . . 133
A.1.1 Experiment Setup . . . 133
A.1.2 Parameter Estimation . . . 135
A.1.3 Reconstructed Force Analysis . . . 135
A.2 Comparative Studies . . . 136
A.2.1 Numerical Studies . . . 136
A.2.2 Experimental Studies . . . 137
A.2.3 Discussion . . . 139
A.3 Conclusion . . . 139

B Appendix B: Prove of Equation 3.7 **141**

C Publications **143**

Bibliography **145**

List of Figures

2.1 Multimodal Teleoperation Concept 10
2.2 Unilateral and Bilateral teleoperation 10
2.3 Milestones in teleoperation idea start-up: (left) General Electric Master-Slave Manipulator, John Payne 1948 [Pathe, 1948]. (middle) Electro-Mechanical Manipulator, Ray Goertz 1954 [Goertz, 1953]. (right) Garco, Harvey Chapman, 1953 [Chapman, 1958]. 11
2.4 Milestones in tele-operation idea start-up: Telemedicine (teledactyl) (left) & tele-doctor (the doctor of the future) (right) as imagined in 1925[Novak]. 12
2.5 teleoperation main topic: 1. Human-Master Interaction, 2. Master (haptic) device design, 3. Communication Layer design (Time delay effect), 4. Slave robot design (task oriented), 5. Environment (Interaction) modelling and 6. Teleoperation design. 15
2.6 Touch exploration examples [Lederman and Klatzky, 1997] [Lederman and Klatzky, 1987] 17
2.7 Haptic perception system [Chu and Myer, 2013] 17
2.8 Human asymmetric input/output capabilities [Brooks, 1990] 18
2.9 Forces applied to various sutures during a knot tie by an attending surgeon. Instrument tie force levels and standard deviations of the hand tie and instrument tie are similar, while those of the robot tie are different. [Okamura et al., 2011b] 20
2.10 Human-Machine interaction modelling [Srinivasan and Basdogan, 1997] 21
2.11 Commercialized Haptic interfaces Classification [euroVR] 24
2.12 Human-Master interaction (red region) in a.) teleoperation and b.) virtual reality context 25
2.13 Operating room set-up [Higuchi and Gettman, 2011] 30

2.14 a. Remote centre of motion (RCM) constraints and surgeon workspace, b. spherical and c. the parallelogram mechanisms to satisfy RCM constraints [Rosen et al., 2011] . . . 31
2.15 Bilateral Teleoperation Modelling . . . 36

3.1 Teleoperation Modelling . . . 40
3.2 Teleoperation Modelling . . . 42
3.3 Human and environment dynamics modelling . . . 43
3.4 Bilateral Teleoperation Modelling . . . 44
3.5 Extended Lawrence 4-Channel Teleoperation Control Architecture . . . 48
3.6 One and two-port networks as a basic components in teleoperation system . . . 50

4.1 Bilateral Control Architectures, M: master, S: slave, P, Pc position signal and position based control, F and F_c force and force based control. . . . 58
4.2 Three-Channel teleoperation control architectures . . . 61
4.3 Stability condition $\eta \geq 1$ . . . 65
4.4 Transparency: $Z_{to} \equiv Z_e$ . . . 65
4.5 $|Z_{tomin}| < |Z_e|$ . . . 66
4.6 Transparency: $|Z_{towidth}| > |Z_e|$ . . . 66
4.7 Stability condition $\eta \geq 1$ . . . 69
4.8 Transparency: $Z_{to} \equiv Z_e$ . . . 69
4.9 $|Z_{tomin}| < |Z_e|$ . . . 70
4.10 Transparency: $|Z_{tomax}| > |Z_e|$ . . . 70
4.11 Stability condition $\eta \geq 1$ . . . 72
4.12 Transparency: $Z_{to} \equiv Z_e$ . . . 72
4.13 $|Z_{tomin}| < |Z_e|$ . . . 73
4.14 Transparency: $|Z_{tomax}| > |Z_e|$ . . . 73
4.15 Stability condition $\eta \geq 1$ . . . 75
4.16 Transparency: $Z_{to} \equiv Z_e$ . . . 75
4.17 $|Z_{tomin}| < |Z_e|$ . . . 76
4.18 Transparency: $|Z_{towidth}| > |Z_e|$ . . . 76
4.19 1^{st} Example: Absolute stability parameter (upper), Performance parameters $|Z_{tomin}|$ (middle) and $|Z_{towidth}|$ (lower). . . . 77
4.20 2^{st} Example: Absolute stability parameter (upper), Performance parameters $|Z_{tomin}|$ (middle) and $|Z_{towidth}|$ (lower). . . . 77

5.1 Teleoperation Modelling . . . 82
5.2 Conventional teleoperation modelling . . . 84
5.3 Heart conducting system [Guyton and Hall, 2010] . . . 84
5.4 The cardiac cycle for left ventricular function [Guyton and Hall, 2010] . . . 84
5.5 Section in a blood vessel . . . 85

5.6 Muscle fibre general model . . . 85
5.7 Myocardium model (reconstructed [Marieb and Hoehn, 2007]) . . . 86
5.8 Tool-tissue interaction . . . 86
5.9 Teleoperation scheme reformulation . . . 87
5.10 Heart motion data . . . 95
5.11 The real part of the interaction impedance . . . 97

6.1 Interaction control based haptic teleoperation as proposed in [Park and Khatib, 2006] . 101
6.2 Bilateral teloperation scheme . . . 103
6.3 Teleoperation scheme reformulation . . . 106
6.4 Hunt-Crossly model linearisation around an equilibrium configuration . . . 112
6.5 Linearised decoupled model of a robot control in Cartesian space . . . 115
6.6 Observer based slave controller . . . 115
6.7 Master Sigma 7 robot . . . 121
6.8 . . . 122
6.9 Raven II robot slave site . . . 123
6.10 Relaxation test and model reconstruction behaviour . . . 124
6.11 Relaxation test and model reconstruction behaviour . . . 125
6.12 Interaction force measurement facility: a.) ATI/FT force sensing system b.) force sensor transducer attached to slave end-effector c.) force sensor attached to sigma-7. . . . 126
6.13 Force, Position and Velocity tracking measures on $Z_{direction}$; m: master and s: slave . . . 127
6.14 Impedance matching . . . 128

A.1 Relaxation test using Raven II robot . . . 134
A.2 Reconstructed forces for the Trial 3: (a) ramp deformation and force measurement, (b) reconstructed forces, (c) zoomed in reconstructed transient responses, (d) reconstructed hysteresis behaviors . . . 134
A.3 System performances for different pole p assignments with $p = -2rad/s$ (left), $p = -5rad/s$ (middle) and $p = -8rad/s$ (right) . . . 137
A.4 Experiment results with pole at $p = -2\ rad/s$ . . . 138
A.5 Experiment results with pole at $p = -5\ rad/s$ . . . 138
A.6 Experiment results with pole at $p = -8\ rad/s$ . . . 138

List of Tables

2.1 Task requirements of abdomen surgery in terms of workspace and interaction wrench [Rosen et al., 2011] . . . 30

3.1 Signals analogy of mechanical-electrical systems . . . 41
3.2 Components analogy of mechanical-electrical systems . . . 41

4.1 Teleoperator Parameters . . . 59

5.1 Interpolation using DFT . . . 95

6.1 Candidate models . . . 111
6.2 Robot-Environment system plant . . . 116
6.3 Experimental Parameters . . . 125

A.1 Values of the estimated parameters . . . 135
A.2 Average values of MFE [N] and STD [N] for the four relaxation tests . . . 136
A.3 Transient responses of the three control force . . . 137
A.4 Experimental results . . . 139

Nomenclature

Acronyms

AOB	Active OBserver
A-V node	AtrioVentricular node
CA	Control Architecture
CAs	Control Architectures
DoF(s)	Degree(s) of Freedom
DFT	Direct Fourier Transform
ELA	Extended Lawrence Architecture
HC	Hunt-Crossley
HMI	Human-Machine Interface
JND	Just Noticeable Difference
KB	Kelvin-Boltzmann
KV	Kelvin-Voigt
LTI	Linear Time Invariant
LHP	Left Half Plane
MSD	Mass Spring Damper
MIS	Minimally Invasive surgery
MIRS	Minimally Invasive Robotic Surgery
MIBHS	Minimally Invasive Beating Heart Surgery
MICS	Minimally Invasive Cardiac Surgery
MSN	Master Slave Network
MFE	Mean Force Error
OR	Operating Room
POI	Point Of Interest
PBC	Passivity-Based Control
RHP	Right Half Plane
S-A node	SinoAtrial node
STD	STandard Deviation
TF	Transfer Function

General notations

a	scalar
$\mathbf{a}$	vector
$\mathbf{A}$	matrix

Mathematical Symboles

$\overline{a}$	complex conjugate of a
$\|\|a\|\|$	Euclidean norm ($\sqrt{\overline{a}a}$)
$\mathbf{a}^T$, $\mathbf{A}^T$	vector and matrix transpose
$\mathbf{A}^{-1}$	matrix inverse
$\Re\{a\}$	real part of a
$\Im\{a\}$	imaginary part of a
$\mathbf{e}$	effort
$\mathbf{f}$	flow
E	energy
P	power
p	pressure
$\mathbf{I}$	identity matrix
b, $\mathbf{B}$	viscous damping coefficient
k, $\mathbf{K}$	stiffness
m, $\mathbf{M}$	mass
s	Laplace variable ($\sigma + j\omega$)
t	time
ω	frequency
v, $\mathbf{v}$	velocity
$\mathbf{x}$, $\mathbf{y}$, $\mathbf{z}$	position information
F	force vector $\in \mathbb{R}^n, \quad n \leq 6$
Z	impedance transfer function
$\mathbb{H}$	hybrid matrix model of a 2-port network
$\mathbb{G}$	inverse hybrid matrix model of a 2-port network
$\mathbb{Z}$	impedance matrix model of a 2-port network
$\mathbb{Y}$	admittance matrix model of a 2-port network
$\mathbb{P}$	immittance matrix model of a 2-port network

CHAPTER

1 Introduction

1.1 Statement of Purposes

Medicine performed wide steps during the last century. One of the landmarks was the integration of surgical robot in the operating room(OR) to assist surgeons and enable more complex and sometimes unachievable therapeutic techniques. There are still many details to improve, one of them is represented by integrating haptic feedback in the telesurgical platform. The main objective of haptic augmentation in telesurgery is to minimize the exceed in forces exerted by the surgeon to execute his/her task on the operated tissue and to provide at the same time the surgeon with an adequate sensation of the manipulated tissue mechanical properties.

Nevertheless haptic feedback is complementary in teleoperation context where the task can be successfully accomplished under vision feedback, haptic augmentation represents a remarkable added value in medical robotic because:

i Sensing tissue impedance helps the surgeon to inject the required amount of forces to execute the task. Consequently, the exceed in exerted forces on the operated tissue will vanish or will be simplified which reduces proportionally the potential of damage.

ii It reduces stress load endured by surgeon due to his/her increased confidence of how much forces he/she applied on the operated tissues.

iii It is an essential part of minimally invasive surgery (MIS) perfection which improves the surgical intervention outcome by reducing patient after-operation stay.

iv Providing a transparent teleoperation system would cope with the some short-handed medical specialities in the rural countryside regions and/or disasters' areas where palpation is a frequent elementary test in medical examination.

This thesis aims to improve telesurgical systems' transparency for challenging applications where number of uncertainties are present (such as physiological motion disturbances and tissue modelling uncertainties). It is possible to summarise this thesis objectives in the following two main goals:

* **First goal:** Defining the major elements that affect a teleoperation transparency.
* **Second:** Analysing the role of these factors in providing a transparent teleoperation.

To realize these objectives, a wide state of art survey is carried out to identify the effects of each component of a teleoperation system on its transparency. Consequently, some but not limited to the major effective factors on a system transparency are identified as follows:

- Master design: defines action generation and haptic sense stimulation methods.
- Slave design: defines haptic variables acquisition accuracy of a required interaction.
- The implemented control architecture to achieve master-slave bilateral coupling.
- Action-perception latency (Time delay).
- Disturbance and uncertainties presence in the operated environment.
- Tissue model accuracy affects the force control based haptic teleoperation.

For a given teleoperation system, the connected master slave network is already imposed on the designer, we reduced therefore our focus of interest on the last four elements.

1.2 Contributions

The contributions in the context of this thesis can be summarised in the following folds:

* **First**: a new proposition and classification to explore haptic teleoperation literature. Haptic teleoperation encompasses a wide variety of applications and developments. To obtain a simple indication to the challenging exploration of haptic teleoperation literature, it is sufficient to search for its main keywords (combined or separately) on the most famous scientific research engines like IEEE Xplore, ScienceDirect, google scholar, CiteSeer and/or PubMed. The concerned person will find thousands of publications ($\gg 500$ for "haptic teleoperation", $\gg 1500$ for "teleoperation" and $\gg 3000$ for "haptics") which is worth to be noticed before dealing with a teleoperation haptic transparency. To the best of the author's knowledge, the available surveys to explore haptic teleoperation literature like [Sheridan, 1992] [Hokayem and Spong, 2006] [Passenberg et al., 2010] [Hirche and Buss, 2012] have focussed on partial issues in teleoperation. In the first chapter we propose a new point of view to handle the wide varieties of developments that can be classified under haptic teleoperation context by referring to its contribution on teleoperation generalised well known scheme.
* **The second contribution** treats the role of the implemented bilateral control architecture (CA) in achieving a required level of transparency. This contribution provides a comparative analytical study on the performance of 3-Channel control architectures group. An illustrative case study is presented to clarify the usability of the proposed guideline to select a suitable CA that meets a set of requirements.

* **The third contribution** studies the role of physiological disturbance presence in the operated tissue on achieved transparency. This contribution extends environment model to encompass physiological disturbances presence. A recursive method to calculate this model is proposed to enable its integration in the design of interaction control based haptic teleoperation which is the subject of the following contribution.
* **The last contribution** proposes a new transparent teleoperation CA that involves interaction based control of the surgical robot because this feature is desired in operating room. The performance of the interaction based controller (known also as AOB) is enhanced by integrating Hunt-Crossly model to represent the viscoelastic properties of the operated soft tissues. The proposed teleoperation CA is designed and is examined experimentally on Raven II-Sigma 7 telesurgery test-bed.

1.3 Summary of remaining chapters

The contributions of this thesis are organised in six chapters. Each chapter analyses one factor of the aforementioned factors that affect a system transparency as follows:

Chapter 2 and 3 introduce the state of the art on haptic teleoperation research topic. In the second chapter, a new point of view is proposed to organize and survey the diverse and rich literature of haptic teleoperation. This literature is organised based on its focus of interest inside teleoperation standard scheme (i.e. human-master-communication-slave-environment). This proposition enabled the identification of the major factors that affect a system transparency by analysing the role of each component in whole system transparency. On the other hand, the third chapter introduces the haptic teleoperation study from technical point of view. The necessary tools to design and to assess a haptic teleoperation are surveyed and supported with a numerical example.

Chapter 4 analyses the role of applied control architecture in achieving a desirable performance and a controllable level of transparency. First of all, all the possible control architectures that can be used to realise a bilateral teleoperation are surveyed and the so called haptic and non-haptic control architectures are identified. Haptic architecture is the control architecture that is capable of achieving a reliable kinaesthetic coupling between human operator and the remote task. The lack of 3-channel control architecture analysis is fulfilled by showing through numerical studies the role of each robot controller in achieving the desired level of transparency.

Chapter 5 focuses on the effect of the possible presence of motion disturbance in the operated soft tissue. Human has a limited capacity of compensating manually any motion disturbance. In the context of MIRS it is possible to compensate automatically, by assistance of a robotic system, the presence of motion disturbance in some vital organs during many frequent interventions. Unfortunately, robot-moving tissue interaction problem is not well understood yet and therefore in this chapter we propose an adequate analysis of this interaction and the effect of disturbance presence on the system transparency.

Chapter 6 introduces e new haptic CA that adopts (**Position-Force**) teleoperation CA form and involves model based interaction control of slave robot as a desired feature in OR. First, the proposed CA is designed and assessed using teleoperation literature standard tools. Second, the performance of the model based interaction controller is enhanced by using Hunt-Crossly model to represent robot-tissue interaction. Hunt-Crossly model and showed a preferred performance in model based interaction control in comparison with state of art known linear models. The proposed teleoperation CA is examined experimentally by its realisation on Raven II-Sigma 7 teleoperation test-bed that exists in LIRMM and the obtained results is discussed on commented.

The thesis is closed by a general conclusion to readdress the thesis main results and its general short-term and long-term perspectives

CHAPTER

2 Telerobotics for Surgery: Telesurgery

Preamble

This chapter is an essay to provide a resumed overview of the state of the art on the key words included in haptic teleoperation for **M***inimally* **I***nvasive* **B***eating* **H***eart* **S***urgery* **(MIBHS)** *research field.*

Teleoperation is the adopted concept to extend human presence through action. Introducing teleoperation to operating room maximized the outcome of surgery for patients and therapists. Haptic augmentation is proved to further improve the surgery benefits but unfortunately non of the available commercialised surgical robots afford the surgeon with an adequate haptic sense of the treated tissues. In this chapter, we explore the performed research work on the keywords treated by a research subject that aims to improve the transparency of haptic teleoperation system for minimally invassive cardiac surgery.

2.1 Terminology

Tele- means *to, at* or *over a (long) distance,* a prefix that is thought to be derived from Greek (*tēle-* "far off") to refer to the distant presence or action referred by the connected word [Longman Dictionary] [Oxford Dictionary]. For example, **tele-robotics** and **tele-operation** address the distance in robotics and operation. These aptronyms are coined to point out the extension of human sense and dexterity and therefore imply the presence of human (operator) in control or human-in-the-loop [Sheridan, 1992]. In fact, these neologisms are used to refer to the overcoming of barriers between the user and the targeted environment by remote controlling a robot who's replacing the human in action to directly

carry out the required task(s) [Basañez and Suárez, 2009]. The barriers can be that the environment locates in inaccessible place (deep oceans, space ... etc.), the hazardous nature of the performed task(s) or the environment scale is beyond the human scale capacity. The commune property of all barriers is that the aimed environment is not physically reachable/accessible for the user [Niemeyer et al., 2008]. The medium between the human operator and the remote environment is called **Master Slave Network (MSN)** and its ultimate objective is to provide a **telepresence** for the human operator [Hannaford, 1989a].

Telepresence implies not only the extension of user's capabilities of manipulation but also his/her skills to perceive the remote environment. In other words, an ideal *MSN* extends the five external senses of human nature (sense of touch, sense of vision (sight), sense of hearing, smelling and tasting) [Ferre et al., 2007]. Although visual feedback is crucial for *teleoperation* success, the later area of research focuses mostly on the sense of touch because it is created through the robotic hardware and its control system(s). *Teleoperator* that provides a sufficient level of *telepresence* is said to be **transparent**. Ideally, a *MSN* is *transparent* when human operator and remote environment interact with each other while they are fooled into forgetting the medium itself [Niemeyer et al., 2008].

The sense of *touch* is perceived through **tactile** and **proprioceptive** (also referred as **haptic**) modules. **Tactile** (from Latin *tactilis* and means "to touch") is the sensation arising from stimulus to the skin such as heat, pressure, vibration, slip, pain ..., and is generally used in *teleoperation* literature to address the perception of surfaces nature and features. On the other hand, **haptic** (from Greek *haptikos* which conveys the "ability to touch or grasp") is related to the **kinaesthetic** perception of the manipulated environment. **Kinaesthesia**, by definition, is the precise awareness of muscles and joints internal forces and positions [Hannaford and Okamura, 2008] [MacLean, 2008]. This thesis is a contribution to **haptic teleoperation in thoracic surgery**. This thesis focuses on the *kinaesthetic* force feedback in **telesurgery** as an essential skill required by surgeon(s) (physician) to assess the quality of his/her surgical (therapeutic) examination and intervention. The *tactile* sense does not locate in the scope of concern of this thesis. Nevertheless haptic perception is essential for the successful completion of numerous daily tasks, it may become decisive in many of **tele-examination** and **telesurgical** applications.

Integrating *MSN(s)* in therapy and healthcare area gives rise to several new coined terminologies that can be listed for example but not limited to as: **teletherapy**, **tele-examination**, **tele-rehabilitation**, **telesurgery** etc. Each of the aforementioned terms refer to the same concept, that is: using MSN and robotic technology to serve healthcare, but they differ in their emphasize and area of implication. For example, *tele-examination* highlights the physician-patient interaction through MSN to remotely determine the reason(s) of client complaint, while *telesurgery* emphasizes the remote level of robot assisted surgery, and this applies to all the previously mentioned idioms.

2.2 Conception and Foundation

Extending human presence implies the existence of an intermediate between the two remote sites, i.e. operator site and the performed task site, which locates in an inaccessible environment. This notion of *telepresence* is interpreted conceptually, using available robotic technology, by connected **M**aster **S**lave **N**etwork (**MSN**). Considering human operator point of view, in the local site, he/she interacts with a robotic device (the master robot) while in the remote site, a robot (the slave) embodies human gestures to perform the required task(s) in a remote inaccessible environment. The necessary perception information to perform a successful useful task(s) is acquired and fed back to the operator through adequate facilities. The Fig. 2.1 presents the concept of multi-modal teleoperation which ultimate objective is to provide a complete telepresence of human operator by extending all of his/her sense of nature. As already stated, the main scope of focus of this thesis is the telepresence provided though the robotic devices. This level of teleoperaion is closely related to the indirect force-position kinaesthetic (haptic) interaction between human and environment through **MSN** and is briefly referred as **Haptic Teleoperation**.

Haptic teleoperation is realised when a slave robot is controlled to imitate master motion and simultaneously the master is controlled to convey slave experienced interaction forces to human operator. Hence, it also referred as **bilateral teleoperation** because master and slave are controlled bilaterally to provide a complete kinaesthetic coupling between human and remote performed task. In an ideally transparent *haptic teleoperation*, the human feels through the MSN as if he/she touches directly the remote environment. By observing Fig. 2.1, it can be noticed that the chain connecting the operator to the task can be seen as a serial connection of two port networks that transmit energy between the source (operator) and the client (task) and vice versa. In other words, master robot transmits human injected energy to the communication facility(ies), communication devices deliver the received energy from master to slave and slave conveys this energy to the environment to perform the task and to reflect back through the same logic the reaction energy to human operator. This energetic interpretation of *haptic teleoperation* is subsequently used to design and evaluate haptic (force reflecting) MSNs (Section 2.4.6). On the other hand, at the very beginning of teleoperation field, and still used for many applications for its simplicity and lower cost, teleoperation is performed **unilaterally**, i.e. only the slave is controlled to perform human action on the remote environment without feeding back any type of haptic perception to the operator. This type of teleoperation is addressed in literature as **unilateral teleoperation** [Sheridan, 1992] [Niemeyer et al., 2008].

Although the first successful teleoperator appeared in mid 40s, teleoperation has had to wait till end of 90s to find its way to **O**perating **R**ooms (**OR**). Nowadays, MSNs are common in therapy centres through the world. It is worth noting that all commercialized MSNs in present adopt only a unilateral control protocol while the necessary haptic sense augmentation is still limited to laboratories developments. A graphical comparison between unilateral and bilateral teleoperation is presented in Fig. 2.2. The physical regions represented

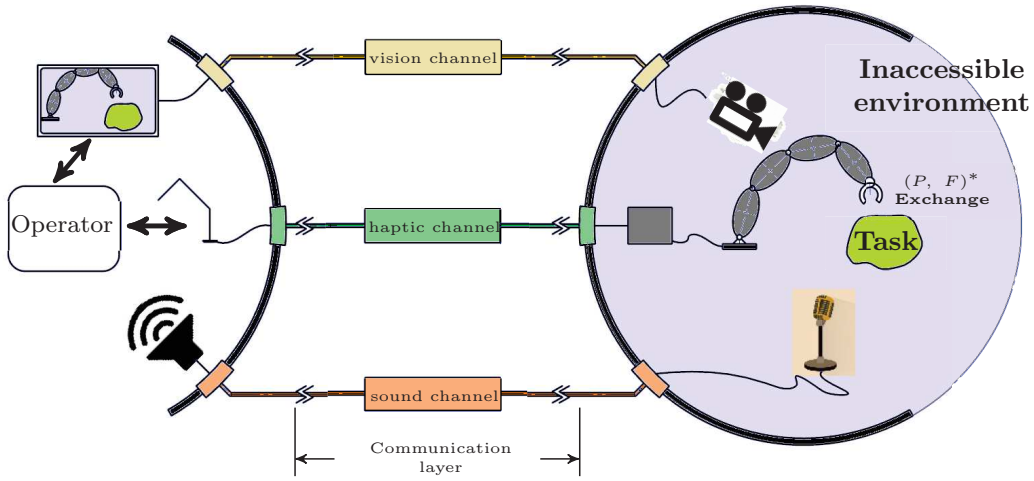

Figure 2.1: Multimodal Teleoperation Concept

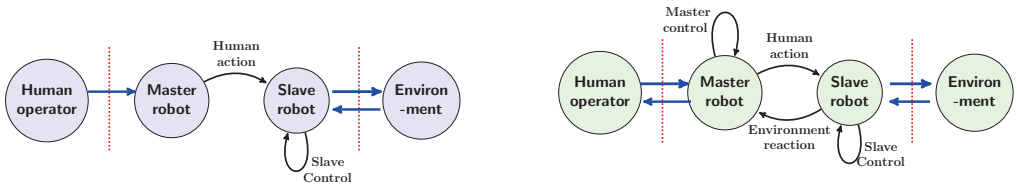

Figure 2.2: Unilateral and Bilateral teleoperation

by red lines in (Figs. 2.2.a and 2.2.b) are the regions of interaction between Human-Master and Environment-Slave and their characteristics will be presented afterwards in Section 3.1.1.

Before detailing the use of haptic teleoperation in surgical therapy, a general overview of teleoperation development will be provided. Teleoperation has been an active field of research since mid 50s with wide range variety of developments and applications. Hence, to provide a satisfactory overview of teleoperation evolution over the past six decades, it is introduced through two folds, the first is the history of teleoperation through applications and milestone (commercialised) products Section 2.3. The second fold addresses this history through the research topics covered in teleoperation literature Section 2.4. This redundancy of presentation is intentional, in the aim of well identifying the factors that play a decisive role in improving a MSN transparency.

2.3 Historic Overview and Applications

Teleoperation represents one of the earliest applications of robotic technology where its history can be traced down till the beginning of the second half of 20th century. Since then, teleoperation has been an extensive field of inspiration and foundation. Nevertheless, the first remote manipulator is patented early 50s, the teleoperation and telepresence idea is reported quite earlier in science fiction literature by *Hugo Gernsback*, notably the notion of telemedicine (referred at that time as **teledactyl** (Fig. 2.4)) [Novak]. Master-Slave telerobotic systems are thought to be essentially motivated by the issue of human safety in hazardous environment (eg. nuclear or chemical plants). Three major milestone patents reported,closely in time, (in the same decade) to declare the renaissance of teleoperation era [Payne, 1949] [Pathe, 1948] [Goertz, 1953] [Chapman, 1958] [Goertz] [Vertut and Coiffet, 1985] (Figs. 2.3 and 2.4). A codified presentation of early developments can be traced in [Niemeyer et al., 2008] [Sheridan, 1992] [Garcia et al., 2007]. It is worth to note that force feedback importance in teleoperation is recognised very early [Goertz, 1952], haptic (force-reflecting) teleoperation enjoys therefore a rich literature with wide range of applications.

Remarkably affected by networking technology, the use of digital computer in robotics and computer vision, teleoperation spread to encompass countless applications of engineering. Teleoperation has been useful in underwater exploration, space navigation [Fong et al., 2013], medical care and rehabilitation applications, agriculture, mining, industrial, construction and yet in service and elderly assistance applications. Following the evolution time-line of teleoperation analysis reveals the following conclusion, even-though the early reported analysis started to appear in the 60s [Sheridan and Ferrell, 1963] , the rigorous analysis of haptic MSNs is delayed around four decades (till mid 80s) to start to reap-

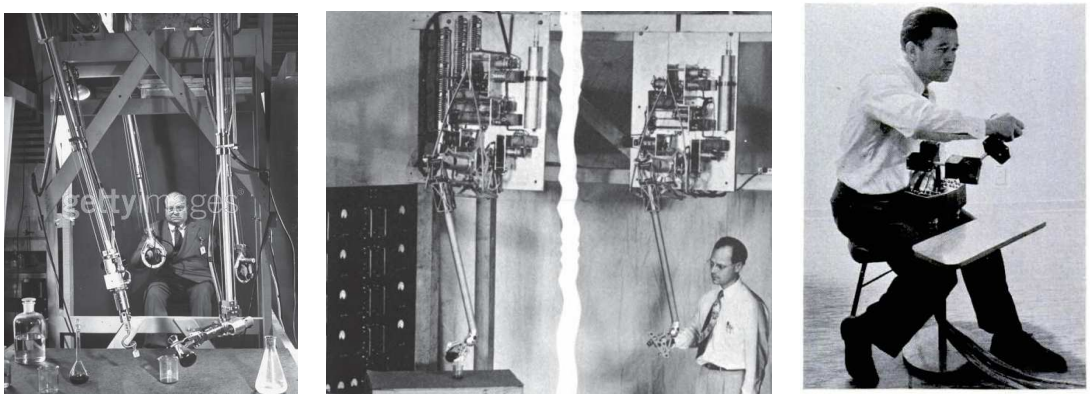

Figure 2.3: Milestones in teleoperation idea start-up: (left) General Electric Master-Slave Manipulator, John Payne 1948 [Pathe, 1948]. (middle) Electro-Mechanical Manipulator, Ray Goertz 1954 [Goertz, 1953]. (right) Garco, Harvey Chapman, 1953 [Chapman, 1958].

pear in literature [Sheridan, 1989], between this two remarkable milestones, the reported documentation is quite limited [McCloy and Harris, 1986]. In fact, it has had to wait the robotic and networking literature to be sophisticated. Since then, several methods has been adopted to classify teleoperation developments. One of the earliest approaches organised teleoperation literature by considering human role in the control closed loop into three main categories [Sheridan, 1992]:

* **Direct control**: Slave motion is directly controlled by operator hand motion and the MSN controller does not employ any type of autonomy or intelligence. This group encompasses unilateral and bilateral control of MSN(s).
* **Shared control**: the MSN controller assists task execution with the human operator, i.e. the task is distributed between human operator and MSN. For example: In Beating heart surgery, the surgical robot compensates automatically heart beats while the surgeon carries out his intervention as on a static environment.
* **Supervisory control**: the operator gives a high-level command to be refined and executed by the MSN. For example, the user selects the task and the sub-tasks based on a set of keywords and the MSN assumes the task accomplishment.

The following attempts to survey bilateral teleoperation adopted the aforementioned approach[Hokayem and Spong, 2006] i.e. it is always organised based on the role of applied control [Passenberg et al., 2010] or the benefits brought to its user [Hirche and Buss, 2012].

Before bringing surgical MSNs to the spotlight, it is important to note for teleoperation readers that even though the core logic of the design guidelines used to develop MSNs adopt always the same basic engineering rules and conceptions, but these design guidelines are considerably affected by the application nature and design specifications. This point will be better addressed in research thematic section (Section. 2.4).

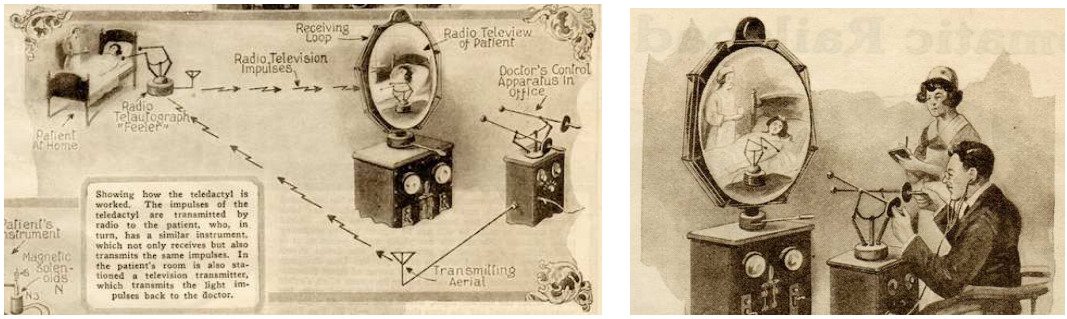

Figure 2.4: Milestones in tele-operation idea start-up: Telemedicine (teledactyl) (left) & tele-doctor (the doctor of the future) (right) as imagined in 1925[Novak].

2.3.1 Teleoperation for Medical care

Medical telecare, more concisely telemedicine, started not only as an imaginative idea in science fiction literature but also with some early pioneer experiments as in **t**elecardiogram with *Willem Einthoven*. Since then medical service represents one of the essential motives of technological developments by contributing to and benefiting from its quick wide steps happened during the 20th century [Bashshur and Shannon, 2009]. This thesis scope of telepresence is restricted to this achieved through robotic technology and devices. Therefore medical care, in its two main branches *diagnosis* and *therapy*, attained but not through robotic telepresence is excluded.

This thesis contributes to medical robotic community where robotic telepresence can bring a meaningful assessment to medical service like: expanding the reachability and enhancing the delivery time of medical services, improving diagnosis and intervention quality, compensating/completing human limitation of fatigue, observation, dexterity and precision etc. For example, it is possible to compensate the lack of some resident specialities and deliver a quick efficient health service and/or specialised consultation for isolated communities and rural countrysides. Nowadays, a serious research work is oriented to provide a remote complete medical care through multi-modal teleoperation systems and physician-patient haptic interaction locates in the core of such services because palpation and tapping are frequent procedures to perform a successful diagnosis. Moreover, with the wide spread of human exploration, this may be a considerable added value in space exploration and tourism, exploration expeditions (to the outlying territories ex. Antarctica) or even urgent medical support in disaster/warfare regions.

In the recent decade, robotic assistance has already performed wide steps in its integration inside **OR** for medical intervention therapy. For example, **Da Vinci** (Intuitive Surgical, Inc., Sunnyvale, CA, USA) robot performs nowadays a wide variety of surgical interventions around the world. **Da Vinci** represents an exemplary successful commercialized surgical robotic MSN. Before evaluating its contribution to the therapeutic community, a brief introduction of the surgical robotics is performed. Because surgical MSNs are used mainly to overcome the limits and drawbacks of minimally invasive surgery, this surgical procedure is introduced and evaluated through benefits and drawbacks. Finally the interventional MSN system is presented through well known approved products.

2.3.2 Robotics for Surgical assistance

In the light of the Robot Institute of America (**RIA**) definition of a robot [1], a very wide variety of robotic tools has been useful for medical care assessment. The main success of telerobotics has been achieved in surgical robotic assessment. Therefore, this section

1. In 1979, **RIA** defined the **robot** as *"a reprogrammable, multifunctional manipulator designed to move materials, parts, tools, or other specialized devices through various programmed motions for the performance of a variety of tasks."*

will focus on the surgical robotics. But it is useful to note that nevertheless its faltering commercial footsteps, telerehabilitation represents also a promising field of contribution for haptic teleoperation community.

The first explicit advent of robotic technology in medical service was in stereotactic brain surgery to perform CT-guided brain tumor biopsies [Kwoh et al., 1988]. Since then, robotic technology infiltrated all medical care aspects most notably in surgical and residual care[Dario et al., 1996]. The main idea is that robot is not meant to replace surgeon, but to provide a useful tool to overcome human capabilities limitation or enabling better advantageous surgical intervention as minimally invasive surgery (MIS) to be performed where it is not possible to be performed manually. To have better overview of the surgical robotics technical advances, the reader can refer to [Hill and Jensen, 1998] [Taylor et al., 2008] [Beasley, 2012] [Badaan and Stoianovici, 2011] [Gomes, 2011] [Moustris et al., 2011] [Najarian et al., 2011] [Park and Lee, 2011] [Singh, 2011] [Stüer et al., 2011] [Okamura et al., 2010] [sssr13, 2013] [NASSSR14 presentations, 2014] [NASSSR14 videos, 2014] for a sophisticated state of the art surveys.

2.4 Research Thematics

Teleoperator is defined as an intermediate master slave network between human operator and manipulated environment. While teleoperation is the performed task under human control on the remote inaccessible environment. The optimal objective of any teleoperated task is to be safe (i.e. stable) while giving the human operator the feeling of telepresence (i.e. transparency). Teleoperation is a multidisciplinary field of research and has been the active area of contribution for wide variety of scientific communities with wide variety of thematics and applications. Therefore, to ease the introduction of the contributed effort in the context of teleoperation field, research in teleoperation community has been divided in sub-thematics, then the objective of each sub-field is introduced and some key works and applications are cited. Good comprehension of each sub-field's role and objective will affect positively on improving the MSN transparency.

Teleoperation can be seen, as presented in (Fig 2.2.b), as a cascade of interconnecting dynamic systems that exchange energy. Briefly, the operator injects energy in the MSN as a position input, the MSN conveys this energy to the remote environment by performing a required task, the environment reaction is reflected back to the human operator through the same MSN as a reaction force. Based on this understanding, teleoperation can be divided into the following main field of research. The area of implication of each sub-field is represented by a region in (Fig 2.5) and then its main aspects and objectives are introduced in brief details in the referred subsection:

1. **Human-Master interconnection:** (Fig. 2.5-region 1), presented in (section2.4.1) .
2. **Master System design:** presented in (section 2.4.2) (Fig 2.5-region 2).

3. **Communication layer design:** presented in (section 2.4.3) (Fig 2.5-region 3).
4. **Slave System design:** presented in (section 2.4.4) (Fig 2.5-region 4).
5. **Slave-Environment interaction:** presented in (section 2.4.5) (Fig 2.5-region 5).
6. **Teleoperation and MSN design and assessment:** presented in (section 2.4.6) (Fig 2.5-region 6).

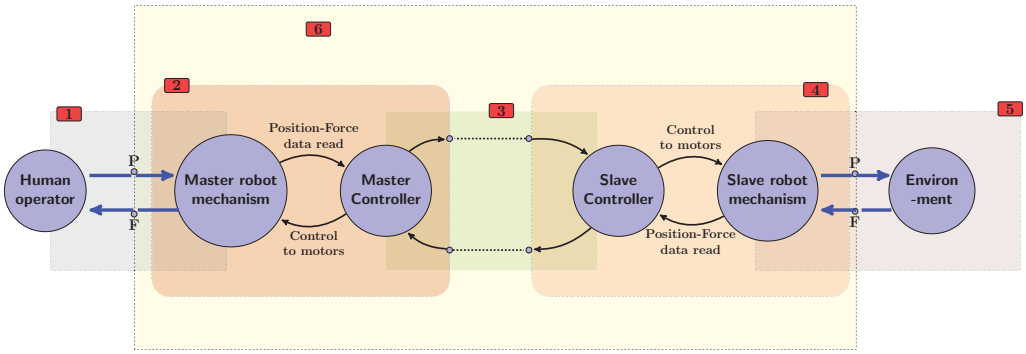

Figure 2.5: teleoperation main topic: 1. Human-Master Interaction, 2. Master (haptic) device design, 3. Communication Layer design (Time delay effect), 4. Slave robot design (task oriented), 5. Environment (Interaction) modelling and 6. Teleoperation design.

Back to teleoperation history, the first two main issues that have been remarked for the researchers were time-delay effect and multi-modality influence on the user up to mid 60s because the two main targeted applications at the epoch were space and ocean exploration. One more additional important issues is the force feedback reflection, what is later called the haptic feedback [Sheridan, 1989]. After the beginning of the last decade of the 20th century and for as much as the robotic and communication fields has got matured, teleoperation has infiltrated many technological aspects to provide useful service in numerous applications. This fact can justify the difficulty of drawing a complete image of teleoperation field in terms of analysis and application. This survey can be seen as a step in the consequence series of surveys appeared in teleopration field [Sheridan, 1992], [Hokayem and Spong, 2006], [Niemeyer et al., 2008], [MacLean, 2008], [Basañez and Suárez, 2009], [Passenberg et al., 2010], [Hirche and Buss, 2012] with an attempt to identify the main factors that affect teleoperation transparency.

2.4.1 Human-Master interconnection

This area of analysis and investigation brings the human, as a subject, to the centre of interest. The main objective, from teleoperation point of view, is to provide the best design of a MSN through the analysis and knowledge of human needs, capabilities and

performances during a designed teleoperated task. To the author best of knowledge, the performed effort of research in this area, in the light of teleoperation perspectives, can be organized in the following main topics:

1. Human system's philosophy of touch perception:

Human system conception has been a tremendous source of inspiration for researchers. Understanding the human sense of touch system helps researchers to design meaningful devices that can convey correctly and efficiently the targeted user with an engineered sense of touch through the knowledge of human system philosophy of acquisition and psychophysics. Generally, ***the objective*** of these studies is to understand the quantitative laws governing the relationship between mental sensation and body stimuli through the following landmarks:(1) defining the receptors locations and types, (2) knowing the stimulation method(s) and threshold(s), (3) specifying the sensitivity toward stimulation so called also Just Noticeable Difference (JND) [Allin et al., 2002], (4) defining the required time for successful stimulation, (5) examining and assessing the quality of the artificially stimulated sense, etc. Sophisticated answers for these problematics, from neuroscience perspectives, can be found in [Kandel et al., 2012].

The sought answers of the aforementioned listed questions can be achieved either through psychophysical, perceptual and/or performance experiments. Psychophysical experiments define the fundamental relations of dependency between body and mind. On the other hand perceptual experiments are performed through objective questions about the perception. Finally, performance experiments concentrate on the human subject performance during a designed task with and without the sense of touch. This set of tests will be the subject of the following teleoperation task assessment section.

To summarize the research results in this field from ***haptic teleoperation*** standpoint, the sense of touch is divided into two main categories tactile and haptic. **Tactile** sense arises from skin's stimuli while **haptic** sense is closely related to force-position kinaesthetic sensation. The main focus of these thesis is the second category, therefore we reduce our discussion to haptic sense. A sophisticated reading about tactile receptors and physiology can be sought in [Gescheider et al., 2010] [Goldstein, 2013] and from engineering point of view [Dahiya et al., 2013] [Lederman and Jones, 2011] [Lederman and Klatzky, 2009].

Haptics is the human perceived sense of mechanical properties of the in-touch surrounding environment, this properties include shape, stiffness, inertia, etc. Physics quantifies this mechanical values through relationships between force and motion information and therefore haptics is defined as the sense of touch that is closely related to force-position kinaesthesia. A set of haptic exploration examples is introduced in (Fig. 2.6) including pressure palpation, weight perception, shape and stiffness definition through manipulation ..., haptic perception is performed through proprioceptive receptors, also known as muscle mechanoreceptors. These receptors are embedded in human muscle fibres and joints. Therefore, haptic sense works closely with the motor control system to coordinate our daily activities with the considerable dynamic constraints surrounding us.

The force sensors (Golgi tendon organs)are located serially between muscles and ten-

dons and measures the local tension inside the muscle fibre. On the other hand, position and motion sensors are muscle spindles. Muscle spindles are excited by changes in muscle length (e.g., active and passive stretching) where they are located in parallel among muscle fibres (Fig. 2.7). Each of these sensor types plays a special role in motor control. A clear idea about the type of psychophysical and perceptual experiments, that can be carried out on the proprioceptive receptors, can be found in [Mai et al., 1985] [Louw et al., 2000] [Lederman and Klatzky, 2004] [Kuschel et al., 2008] [Goldstein, 2013] [Klatzky and Wu, 2014].

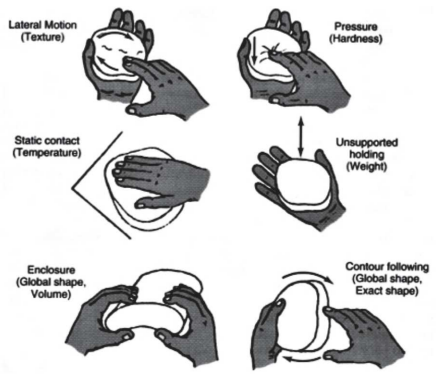

Figure 2.6: Touch exploration examples [Lederman and Klatzky, 1997] [Lederman and Klatzky, 1987]

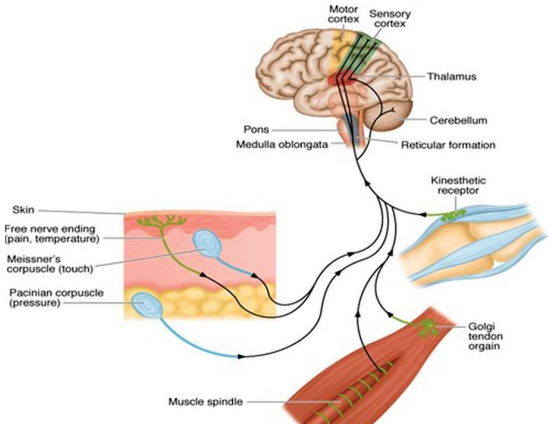

Figure 2.7: Haptic perception system [Chu and Myer, 2013]

As a conclusion of the psychophysical experiments on human position-force acquisition capabilities, the following point may represent a source of interest for haptic technology designers and developers [Tan et al., 1994] [MacLean, 2008]: (1) Humans are reported to track small forces quite accurately (with errors range 2% – 3% for gripping [Mai et al., 1985] to 15% when pushing against a normal surface [Srinivasan and Chen, 1993]), the maximum forces' rage, that can be applied by human user on haptic interface, varies from 5 to hundreds of newtons. (2) Human performance, during manipulation task, degrades without visual feedback or access to texture [Lederman and Klatzky, 2004]. (3) A JND of n percent implies an exponential resolution curve. At low torque levels,we can sense values relatively close together, but as the absolute torque or force level increases, absolute sensory resolution decreases accordingly. (4) For dexterous manipulation, what counts is the relationship between force and position rather than either one individually [Wu et al., 1999] and the actual sensation probably depends on the work performed in during the manipulation task. (5) Human motor control bandwidth, which represents how fast we can move our own limbs or digits, has to be lower than the rate of motion we can perceive. Indeed, proprioceptive sensing occurs around 20-30 Hz, compared with 10-10,000 Hz for tactile sensing. Control, however, saturates around 5-10 Hz, a sophisticated details can be

sought in [Brooks, 1990] [Shimoga, 1992] (Fig. 2.8). Finally, it should be stated that during manipulation task, the human system employs simultaneously three distinct systems. The **sensory system** by detecting cutaneous and kinaesthetic sensations. The **motor system**, to perform the required task, and the **cognitive system**, to provide a successful perception-action coordination. The complicated simultaneous effective performance of these three physiological system during a manipulation task will result in haptic sense in an unconscious form.

Understanding human system philosophy of perception helps not only to design meaningful tools that meet his/her requirements but also can be useful to conceive relevant experiments to assess his/her needs of haptic feedback in a predefined context as in MIRS for example. This set of performance experiments is the subject of the following section.

2. Haptic Feedback Contribution Assessment (Importance):

Haptic feedback is always emerging and contributing in multi-modal context. During any manipulation task, human sees (vision), feels the manipulated object's surface texture nature and heat (tactile), its shape [van der Horst and Kappers, 2008] [Vogels et al., 1999] and mechanical impedance characteristics (haptics) [Riley et al., 2002]. Researchers and designers in haptics and teleoperation field of research need to be aware of the contribution of each sense in the targeted set of tasks of the designed MSN (haptic technology)

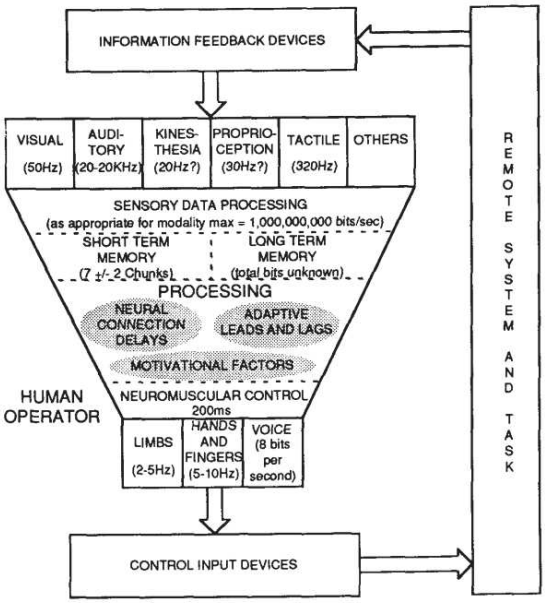

Figure 2.8: Human asymmetric input/output capabilities [Brooks, 1990]

because it has a remarkable influence on the design requirements, simplicity trade-off and hence product efficiency and cost.

A spontaneous intuition would tell that although to feel the touch feedback (tactile and haptic) of a manipulated object would improve remarkably the human performance, this task would be extremely difficult to be achievable in case of vision sense absence. This intuitive judgement of vision sense dominance when it comes to conflict with touch sense has been subject to an early revision [Power, 1980] to show that sense dominance is found to be task-dependent and is integrated, by human neural system, in a statistical optimal fashion with a predictable model [Ernst and Banks, 2002]. Indeed, the haptic sense could be dominant in some circumstances like concentrating on mechanical impedance changes discrimination [Tholey et al., 2005] [Kaim and Drewing, 2011]. This adaptive behaviour makes it difficult to derive a generic conclusion about the contribution of each sense, the inter-sensory interactions, and how the conflicting information are resolved. In fact, haptic feedback importance assessment in improving operator performance is a task dependent evaluation, i.e *the task matters* as [MacLean, 2008] concludes. Although the focus scope of this thesis implies to limit the evaluation of haptic feedback benefit on operator performance to MIRS context, a further insight can be found elsewhere as for the assessment experiments of other application [Wildenbeest et al., 2013].

Assessing the haptic feedback influence is carried out through performance experiments by measuring the impact of haptic sense absence/presence on human performance during the medical diagnosis/therapy. Haptic feedback is essential in medical diagnosis and intervention. The diagnostic procedure requires frequently touch interaction between physician and patient. Moreover, touch interaction is key during any therapeutic intervention. For example, when an anaesthetist inserts his/her epidural needle, he/she judges the depth of insertion by his/her haptic sense, when a surgeon makes an incision, a dental surgeon drills into a carious lesion etc., the therapist relies always on his/her sense of touch [Okamura et al., 2011a]. Simultaneously to the integration of surgical MSN in the Operating Room (OR), the importance of evaluating surgeon performance in closed-loop during the teleoperated surgical intervention is arisen and started to be reported in the literature, always with a special attention to the importance of providing a faithful kinaesthetic coupling between the surgeon ad the teleoperated site [Ben-Porat et al., 2000] [Kazi, 2001].

In conclusion, haptic feedback could bring better enhancement to surgeon performance than only vision feedback while providing both feedbacks simultaneously would be optimal, especially when task requires a mechanical impedance changes discrimination [Tholey et al., 2005]. Providing the surgeon with faithful force-position kinaesthetic feedback of the manipulated tissue improves the task performance through reducing the task completion time, reducing the exerted force on the manipulated tissues and reducing the consumed energy and the committed errors and the users cognitive workload during the required task performance [Wagner et al., 2007] [Hannaford et al., 1991] [Massimino and Sheridan, 1989] [Vitense et al., 2003] [Bethea et al., 2004] [Talasaz et al., 2012] (Fig. 2.9).

Hence, adding the sense of touch to the existing sense of vision into robotic assisted

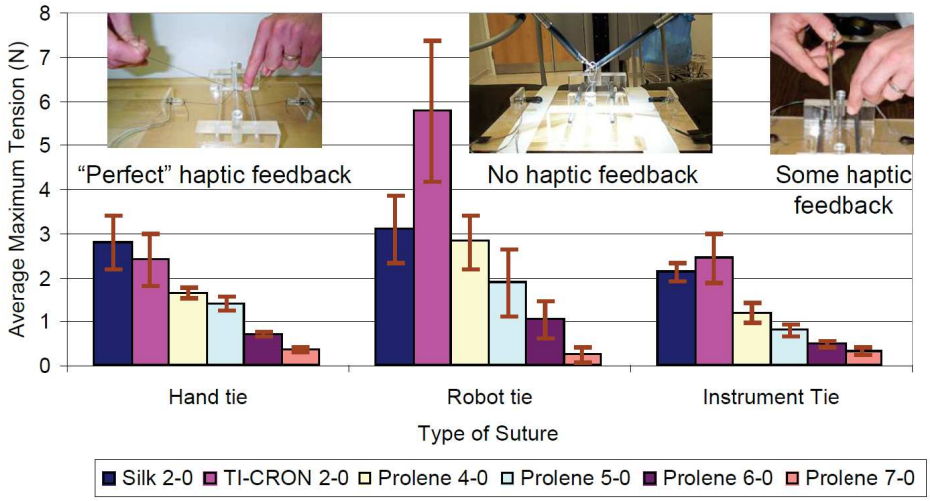

Figure 2.9: Forces applied to various sutures during a knot tie by an attending surgeon. Instrument tie force levels and standard deviations of the hand tie and instrument tie are similar, while those of the robot tie are different. [Okamura et al., 2011b]

surgery platform will improve the telesurgery outcome by reducing the undesired "side-effect" possible damage to the treated tissue and reducing the surgeon cognitive workload. Furthermore, understanding the aforementioned psychophysical test results output would help researcher in interactive-robotics field to develop a useful models of human in-loop to be used in design and evaluation process of haptic devices as in the following point of this research thematic or in teleoperation as in the 6^{th} research thematic.

3. Man-Machine interaction modelling:

The objective of this research area is to understand Human-Machine haptic Interaction in the coupled situation. In other words, Is it possible to provide a meaningful model of human in-loop performance when he is performing his tele-task through manipulating the master device? This question was motivated by simultaneously developing several robotic technology aspects, the desire of designing a dexterously interactive robots, understanding the human in-loop role in teleoperative context and developing interfaces for haptic interaction with computer integrated virtual environments (input-output devices).

The required dexterous interactive robotics motivated the research on force control and then so called interaction control [Villani and De Schutter, 2008] [Hogan, 1985a] [Colgate and Hogan, 1988]. Considering the output of the aforementioned psychophysical and biomedical (human-performance focussed) experiments [Cannon and Zahalak, 1982], Hogan ([Hogan, 1989]) proposed to model the human limb as a passive impedance linked in serial with a neural active source. This model is proved experimentally and reformu-

lated in teleloperative and for virtual environment interaction context [Kazerooni et al., 1990] [Kazerooni and Her, 1994] [Srinivasan and Basdogan, 1997].

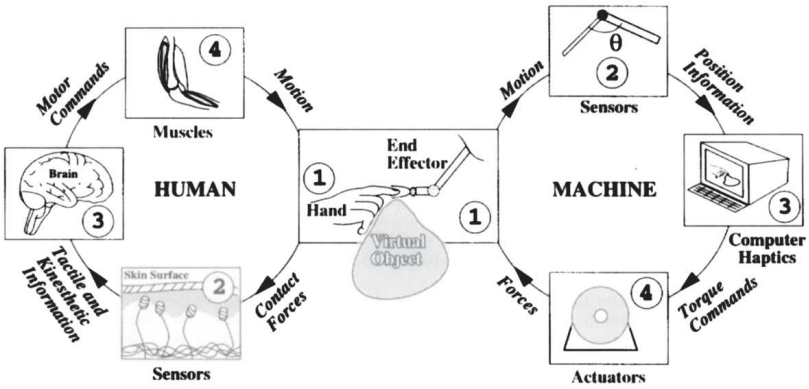

Figure 2.10: Human-Machine interaction modelling [Srinivasan and Basdogan, 1997]

Simultaneously, research effort focussed on human limbs' impedance model identification [Tsuji et al., 1995] [De Vlugt et al., 2002] [Van der Helm et al., 2002] [De Vlugt et al., 2006] [Hajian and Howe, 1997] [Hasser and Cutkosky, 2002] [Hogan, 1985b] [Mussa-Ivaldi et al., 1985] and human arm motion "in coupled situation" modelling [Flash and Hogan, 1985]. Later and by introducing robots to operating rooms, this models has been improved to suit the surgical robotics applications [Ahmidi et al., 2012] [Ahmidi et al., 2013] [Osa et al., 2014].

As a conclusion to this research topic, the objective of investigating human-machine interaction is first to understand human needs and requirements second to provide a useful models that can be used an inputs to the haptic interfaces and MSNs design process. To this limit, the first thematic of research in teleoperation context is closed and the next thematic will address the haptic devices technology.

2.4.2 Master System design

Providing telepresence through touch implies the need to design devices that can convey the required sense of touch or ***to engineer the sense of touch*** as *Alison Okamura* introduces it. In other words, to design devices that respond to human action in a way that mimic the remote environment reaction to generate in human mind a sense of telepresence through touch. At the same time developing computer graphics arose the need of input-output devices that can meet human haptic requirements for a specific set of applications and enable computers to communicate with users through touch channel. This necessity gave birth to a new technology branch called haptics [Hayward et al., 2004]

[Otaduy and Lin, 2005]. Subsequently, hapic interfaces design and technology is classified as Human-Computer Interaction (HCI) technology. Therefore, haptic teleoperation for surgical robotic systems locates in the dynamic area of intersection between three major research fields, teleoperation, HCI through haptics and medical robotics.

This section tries to investigates the role of master system design in achieving a transparent teleoperation. Haptic interfaces comprise hardware and software components aiming at providing computer-controlled, programmable sensations of mechanical nature. Many methods have been adopted to provide artificial haptic sensations , four techniques are dominating and can be used separately or together in a single master system. They include vibrotactile devices, distributed tactile displays, surface displays and force-feedback systems [Hayward and MacLean, 2007]. Because master system design defines through interaction with human the action generation and reaction (haptic sense) stimulation methodology, its effects on teleoperation transparency investigated through the following principal folds [Zadeh, 2010]: Human-machine interaction from technical view point, The adopted electro-mechanical structures to realise master the device. and haptic feedback techniques. A brief conclusion pursues to summarize the main factors affecting teleoperation transparency.

1. Human-Master interaction:

In coupled state, human and machine exchange energy. This energy is quantified by knowing force and velocity values at the interaction region(s) (known as ***interaction port(s)***) [Raju et al., 1989]. The objective here is to define the design measures that have to be considered in haptic interfaces by Knowing the human ergonomics and needs of haptic display [Tan et al., 1994]. These measures are very useful in assessing the telepresence.

To achieve the aforementioned objective, the phenomena arisen from human-machine physical interaction is firstly subjected to deep analysis [Kazerooni and Tsay, 1988] [Colgate and Hogan, 1988] [Lawrence and Chapel, 1994] [Lawrence et al., 2000], not only for teleoperation perspectives but also for other applications that make use of human-robot interaction phenomena (ex. neural rehabilitation) [Hogan, 1989] [Igo Krebs et al., 1998] [Holden, 2005]. To arrive finally to define a set of requirements that should be fulfilled by a haptic device [Colgate and Brown, 1994] [Rosenberg, 1995] [Hayward and Astley, 1996] [Ellis et al., 1996] [Moreyra and Hannaford, 1998] [Cavusoglu et al., 2001]. This requirements can be organised into two main groups: first, design requirements (ex. defining the body part of interaction, the range of motion of the haptic interface and the range of forces that can be conveyed through this interface). Second, assessment requirements, the most important to bilateral MSNs designer is three measures: low impedance(inertia) device (negligible will be ideal), a capacity of reflecting a wide range of impedances [2] and a sensitive

2. In physical systems: The **Impedance** is defined as mapping ratio between the flow as an input and effort as an output while **Admittance** takes effort values as input and gives flow as output.

device with capacity of impedance discrimination higher than humans. This requirements will be addressed analytically in the following chapter.

2. Master electro-mechanical design

Haptics as stand alone field of research encompasses a wide variety of technical approaches to convey a user with the sense of touch. Although this thesis focus is on teleoperation and hence the robotic haptic devices, a comprehensive introduction to this and other techniques of haptic feedback can be found in [Hayward et al., 2004] [Hayward and MacLean, 2007] [MacLean and Hayward, 2008] [MacLean, 2008] and [Hannaford and Okamura, 2008]. The objective of this section is to provide a brief overview of the haptic interface design and hardware with a further reading resources.

Telepresence objectives can be resumed, using teleoperation terms of description, in ***transparency***. As it will be further explained in the 6^{th} research thematic in this chapter and the following chapters, transparency is remarkably affected by the physical characteristic (mass, damping, etc.) of master-slave network, and especially these of the master because it is in direct contact with the operator. Therefore, the haptic device has to satisfy several contrasting, not only in terms of human ergonomics and suitable effective (singularity-free) workspace but also in terms of low inertia, low friction, zero or near-zero backlash, high stiffness, stability, etc. For an example of step by step robotic haptic interface design see [Hayward, 1995] [Stocco et al., 2001] [Çavuşoğlu et al., 2002b] [Uchiyama et al., 2007]. Moreover, for an overview of the used kinematic structures to realise haptic interfaces [Kim, 2010], for actuation side [Conti and Khatib, 2009], preferred sampling techniques [Shahabi et al., 2001] and for gravity compensation [Checcacci et al., 2002].

Generally, several comprehensive classification methods had been adopted to organise the developed sets of haptic technology [Hayward and Astley, 1996]. For example, haptic devices can be classified, regarding the Human-device interaction method, into ***grounded devices*** (with one locus interaction) which encompasses all devices that are manipulated through an affordable end-effector and ***non-grounded devices*** (attached to a part of human body(limbs)) with its two main categories hand and arm exoskeletons. Moreover, haptic interfaces can be classified based on the provided DoFs into low, high and very high DoFs devices or even can be classified based on position workspace-force feedback capabilities as in (Fig 2.11) for commercialized devices, more on laboratories interfaces and classifications can be found in [euroVR]. Finally, based on physical causality, force-feedback devices can be either impedance or admittance like devices. Although the wide majority of haptic interfaces lay under the impedance like category, an increasing focus on admittance like haptic interfaces is taking place [Peer and Buss, 2008] [Peer, 2008].

The following research issue addresses the stability of haptic interfaces and haptic feedback. Further selective reading, on haptic interface designing issue, can be found in [Brooks et al., 1990] [Iwata, 1990] [Millman and Colgate, 1991] [Adelstein and Rosen, 1992] [Buttolo and Hannaford, 1995] [Yoon and Ryu, 2001] [Melchiorri and Vassura, 2001] [Ven-

ema and Hannaford, 2001] [Birglen et al., 2002] [Grant, 2004] [Murayama et al., 2004] [Campion et al., 2005] [Lawrence et al., 2004] [Massie and Salisbury, 1994] [Frisoli and Bergamasco, 2003] [Conti and Khatib, 2005] [Janot et al., 2007] [Tobergte et al., 2011].

3. Haptic interface controller and force (haptic) feedback

Haptic interfaces are computer controlled devices that combines discrete and continuous phenomenons. While the human-device interaction happens in the continuous reality, the force feedback happens in the discrete virtual space. The rendered forces can be derived from real (as in teleoperation) or virtual interaction (as in virtual reality simulation). Regardless the nature of the original rendered interaction, the control and stability issues in force feedback stay always the same.

For the most known devices that adopt impedance like physical systems, the motor driving current is proportional to the force feedback [Hayward and MacLean, 2007]. It is generally sufficient to feedback the force by applying open-loop force control [Hannaford and Okamura, 2008]. Actuation and Transmission system selection should be carefully treated in design step to provide a low friction, backlash-free, well compensated gravity effect master console, because the rendered forces quality is highly affected by these issues.

An abstraction of human-master interaction is addressed in (Fig. 2.12) for teleoperation and virtual reality interaction context [Handlykken and Turner, 1980]. The main dif-

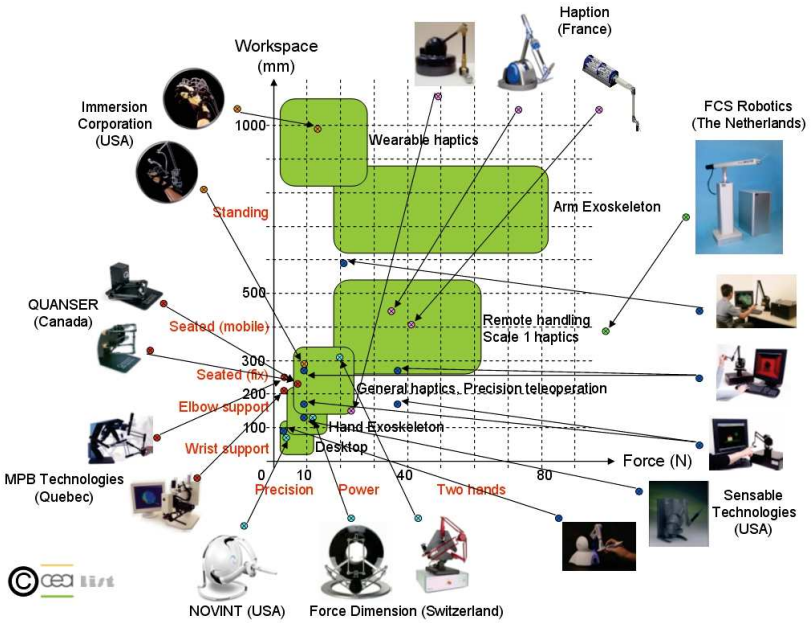

Figure 2.11: Commercialized Haptic interfaces Classification [euroVR]

ference in two cases is the nature of the rendered force origin. In teleoperation context, the force feedback is the slave-environment (scaled) interaction forces which is acquired through a proper sensing modality and reflected back to feedback on the master device. On the other hand, in virtual context, the force feedback is artificially generated based on the modelled virtual object physical properties (surface or impedance). In both cases the stability of rendered system should be insured [Weir and Colgate, 2008] [Minsky et al., 1990]. Further selective reading on haptic rending and stability issue can be traced in [Gillespie and Cutkosky, 1996] [Ellis et al., 1997] [Colgate and Schenkel, 1997] [Sirouspour et al., 2000] [Adams and Hannaford, 2002] [Hannaford and Ryu, 2002] [Gil et al., 2004] [Miller et al., 2004] [Abbott and Okamura, 2005] [Diolaiti et al., 2006] [An and Kwon, 2006] [Basdogan and Srinivasan, 2002] [Robles-De-La-Torre, 2008] [Gil et al., 2009].

In conclusion, Master system influences teleoperation transparency through the adopted human-interface interaction geometry (i.e. haptic sense stimulation method) and the accuracy of force feedback technique. Furthermore, the required criteria to assess the haptic feedback are also discussed. The next research topic investigates the influence of communication layer on teleoperation transparency.

2.4.3 Communication layer design

Master-Slave Network (MSN) is designed to overcome the barrier that exists between operator and targeted task. To overcome this barrier, a proper communication method has to be established between master and slave controllers (as illustrated in Fig. 2.5) in order to exchange the necessary data to provide a proper kinaesthetic coupling between human and environment through MSN. Starting with electromechanical transmission to provide the kinaesthetic coupling [Goertz, 1954], teleoperation has benefited from the wide technological advances in telecommunication [Haykin, 1970]. A survey on data transmission techniques that can be used in bilateral teleoperation can be found in [Kokkonis et al., 2012] [Sankaranarayanan et al., 2007] [Mitsuishi et al., 2003] [Harnett et al., 2008].

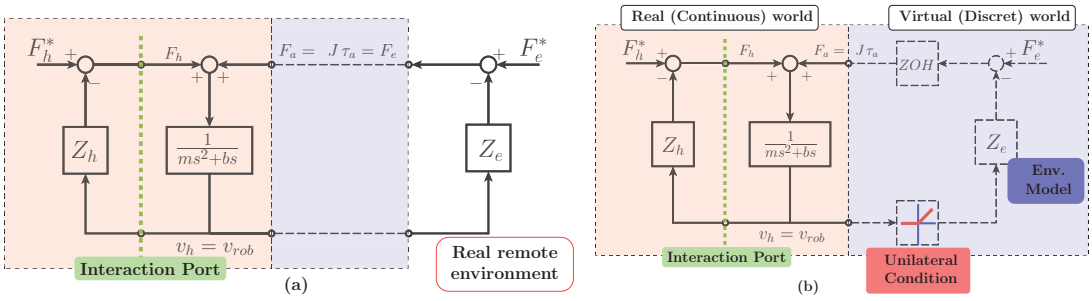

Figure 2.12: Human-Master interaction (red region) in a.) teleoperation and b.) virtual reality context

Bilateral (haptic) teleoperation aims to control the relationship between the interaction values (motion and forces) at master-human and Environment-Slave interaction ports. Hence, the two remote sites have to exchange position P_i and force F_i values also called haptic data , where ($i = m,\ s$) stand for master and slave interaction ports. If the size of transmitted data packets is greater than the network bandwidth, the transmitted information has to subject to a parametric reduction before being sent through the network to the other side which replicates the received data [Hinterseer et al., 2008] [Kuschel et al., 2009] [Steinbach et al., 2011]. The combination of these three steps (reduction, transmission and replication) is known idiomatically as ***communication layer*** in teleoperation literature.

The communication layer is always characterised by the time delay imposed on the transmitted data. Time latency between human actions and his/her perception of environment reactions represents one of the major issues that affect teleoperation transparency. Considering the adopted technique to stabilise a time delayed MSN, this section presents the communication layer analysis in the literature through two main folds: the Non-passivity based and the passivity-based approaches [3] [Hokayem and Spong, 2006].

a. Non-passivity based approaches

In the dawn of telerobotic era, researchers noticed the influence of time delay on human performance then these effects have been analysed on the performance and stability of the system itself. The strategies adopted in this category can be summarised in the following main points:

1. **Move and wait strategy:** *Sheridan and Ferrell* noticed during their early experiments that human adapts his performance in teleoperation to adopt *move-and-wait* strategy. Where the human operator performs his action and waits till seeing the effects of this action before launching the next step [Ferrell, 1965].
2. **Supervisory and /or shared control:** Operator sets occasionally sequences of subgoals for the slave robot to be executed automatically and then compensate for its limited decision-making capability [Ferell and Sheridan, 1967] [Whitney, 1969]. With the progress of computing technology, the supervisory control has been refined by introducing a proper language and by adopting modular techniques in software and hardware level [Sheridan, 1992] [Kim et al., 1992] [Hokayem and Spong, 2006].
3. **Augmented reality to beat time delay effects:** With the advances of haptic technology, researchers proposed to encounter the remote environment delayed reaction through providing the operator with adaptive virtual model to interact with without latency and using the time delayed signals coming from the remote site to update this virtual model [Mitra and Niemeyer, 2008] [Huijun and Aiguo, 2007].

3. A system is said to be **passive** if this system is dissipative and does not produce any sort of energy. Considering a period of interest $T = [t_{start}, t_{end}]$, a system is dissipative if its stored energy is positive i.e. $S(T) = E(t_{end}) - E(t_{start}) \geq 0$. Based on this notion, passivity theorem is used to examine the stability of interconnecting systems based on their input-output relationship [Khalil, 2002] [Colgate and Hogan, 1988]

4. **Stability using classical non-linear systems design tools:** This group makes use of the classical nonlinear tools to design a stable bilateral time-delayed MSN with other types of uncertainties through implying H_∞, μ-synthesis [Leung et al., 1995], optimization [Yan and Salcudean, 1996] or even through frequency domain damping design [Suzuki and Ohnishi, 2013].

b. Passivity based approaches

At the end of 80s, the immense progress in network theory [Haykin, 1970] started to be integrated in teleoperation literature. Based on network theory inspired bilateral teleoperation modelling [Raju et al., 1989], the communication layer can be seen as a two-port delayed transmission network with know inputs and outputs. Consequently, the time-delay problem is reduced to become how to design a passive 2-port delayed network. Employing passivity theorem [Khalil, 2002], several techniques are adopted to derive suitable solutions to resolve time-delay stability issue because time-delayed member is unstable. This techniques can be summarised into the following main points:

1. **Passivity-based intermediate transformation:** Before transmitting the required signals through the communication lines, the input signals are submitted to a special transformation technique (coding) to produce a new input sent through the communication line. The received transformed signals are subject to a new transformation inverse of the first one (decoding) to extract the required outputs. This coding/decoding steps are designed in a form that changes the time-delay into a passive member as in the scattering transformation [Anderson and Spong, 1992] or as in the wave variable transformation [Niemeyer and Slotine, 1991] [Niemeyer, 2004]. In fact, wave variable is seen as a reformulation of scattering transformation.

   These techniques achieve elegantly a stable time-delayed bilateral teleoperation but the level of transparency is remarkably affected by the coding/decoding steps. Therefore, the transparency achieved using wave variable techniques has improved through its combination with predictors as in [Ching and Book, 2006] or with the transmission of interaction measurements as in [Tanner and Niemeyer, 2005]. Further application and discussion can be raced in [Baier and Schmidt, 2004] [Nuño et al., 2011] [Kawashima et al., 2009].

2. **Time domain passivity :** Firstly introduced to provide a stable haptic feedback of virtual environments in [Hannaford and Ryu, 2002], this approach addresses the virtual environment as a 1-port network and defines a passivity observer to monitor the stability of input-output relationship. If the passivity condition is violated, a passivity controller is applied to maintain the stability. This controller consists of an adaptive dissipative element coupled in series or in parallel with the designed 1-port network. [Ryu et al., 2004] adapted this technique to fit the time-delayed communication line design problem. Designed as 2-port network, a passivity observer and controller are

placed on each port. The series of networks are seen as one-port network at the concerned port and the energy flow is monitored to be tuned when it violates the passivity conditions. This approach improves the time-delayed MSN's transparency because it limits the stability-transparency trade-offs to the unstable cases.

This algorithm has been further improved by letting the local controllers of master and slave robots exchange with the remote site the locally estimated time delay as in [Artigas et al., 2007] or locally estimatied energy as in [Ryu et al., 2010]. The drawbacks of this improvements [Tzafestas et al., 2008] were overcome in [Kawashima et al., 2008] by defining the local passivity controller as an adaptive model based on the remote robot model.

3. **Bounded-Energy approach:** Similarly to time domain passivity algorithm, Bounded-Energy algorithm is also inspired from haptics literature to resolve time-delay problem in bilateral teleoperation context [Kim and Ryu, 2009]. It consists of placing an energy monitoring algorithm at each port of the communication layer. If the energy surpassed a parametrically calculated bounds, then the energy excess is dissipated [Seo et al., 2008]. This method suffers from a limited transparency.
4. **Geometrically extended passivity** A standard tool to design a stable bilateral teleoperation system has been summarised in absolute stability (Llewellyn) criteria [Lawrence, 1993]. The stability criteria can be mapped using a special operator derived from scattering mapping [Haddadi and Hashtrudi-Zaad, 2010] [Haddadi and Hashtrudi-Zaad, 2013] or via Mobius transformation [Jazayeri and Tavakoli, 2015].

In conclusion, this section introduces the design of communication layer in teleoperation literature. the necessary procedures to transmit haptic data between master and slave sites could impose a time-delay on the transmitted data. The induced time delay in the communication layer affects teleoperation stability and transparency. The main approaches to overcome time-delay effects on teleoperation stability are introduced and the attempts to improve the resultant transparency are discussed. The following section introduces the 4^{th} topic of research in teleoperation literature which is slave system design.

2.4.4 Slave System

Slave system replaces human operator in performing the required task(s) at a remote (inaccessible) environment by reserving, in teleoperative context, human reasoning and judgement capacity. Slave system consists of an adequate vision system, action system (robotic arms) and optionally an auditory system. The design of each of these components is task dependant. In other words, the core technology used to design these sub-systems adapts to fit the task requirements and the host environment constraints. Haptic teleoperation takes place through the action layer and therefore this discussion will be restricted to the robotic arm system. Moreover, this thesis focus scope is medical telerobotic, accordingly the other applications in telerobotic context are intentionally ignored. Nevertheless,

the tools used to realise the slave robot can be found in robotic state of art in terms of kinematic structures, control and technological choice of materials [Khalil and Dombre, 2004] [Spong et al., 2006] [Siciliano et al., 2009] [Corke, 2011].

Medical teleoperation literature addresses slave system usually as surgical robots. A dedicated survey on robotic presence in medical service can be traced in [Dario et al., 1996] [Taylor et al., 2008] [Bozovic, 2008] [Rosen et al., 2011] and [Troccaz, 2013]. ***Dombre et al.*** in ([Troccaz, 2013], Chapter 5) and [Taylor et al., 1995] provide guidelines to design a medical robot. For the seek of clarity and abbreviation, this guidelines will be introduced for surgical (interventional) robot in MIS context. The author thinks that this guidelines can be applied for any other given context (tasks and environment).

This section investigates the role of slave system design in the achieved transparency. Therefore, we first explore the sequence of steps followed to design a slave platform (surgical robot). These steps can be summarised under the following three main points: Task analysis, Electromechanical structure design and Control and safety. Understanding the design constraint imposed on the surgical robot exposes the major factors that influence teleoperation transparency. These factors are discussed within a brief conclusion.

a. Task analysis:

The efficient design of a slave has to start with environment and tasks analysis to quantify the tasks requirements and the environment constraint. These requirements and constraints have a direct influence on the system transparency because it determines the methods of action generation and reaction acquisition. Task analysis in the Operating Room (OR) (Fig. 2.13) consists of the analysis of three main relationships which are: robot-surgeon [Rosen et al., 2006], robot-staff [Higuchi and Gettman, 2011] and robot-patient [Dombre et al., 2004] relationships. The output of this analysis is organised under a set of requirements (*in terms of forces & motion workspace, kinematic constraints, etc.*) and constraints to design suitable HMI interfaces and control functions that satisfy the need of OR staff and safety standards. Example on task analyse for surgical robots can be sought in BlueDragon robot [Richards et al., 2000] and ROBEA MARGE project [Dombre et al., 2004].

In MIRS context, the robotic arm is inserted inside patient body through small holes after placing a troccar. An example of optimal ports placing for beating heart endoscopic surgery can be found in [Rodriguez and Chitwood, 2009] [Srivastava et al., 2010]. These ports impose on the surgical instrument kinematic constraints as their position has to stay constant all the time to prevent the damage to patient body. This constant point is addressed technically as the Remote Centre of Motion (RCM) and binds 2 DoFs of robot motion [Zemiti et al., 2007]. An example of in-vivo data base of surgical task analysis in MIS context is shown in (Table. 2.1). Further details can be traced in [Lum et al., 2009], [Çavusoglu et al., 2003] and ([Rosen et al., 2011], Chapter 8). Surgeon motion lays inside a conical rang with vertex angle of 60° (the dexterous workspace). To reach every part in the abdomen cavity, surgeon's hand motion lays inside workspace of an elliptical cone shape

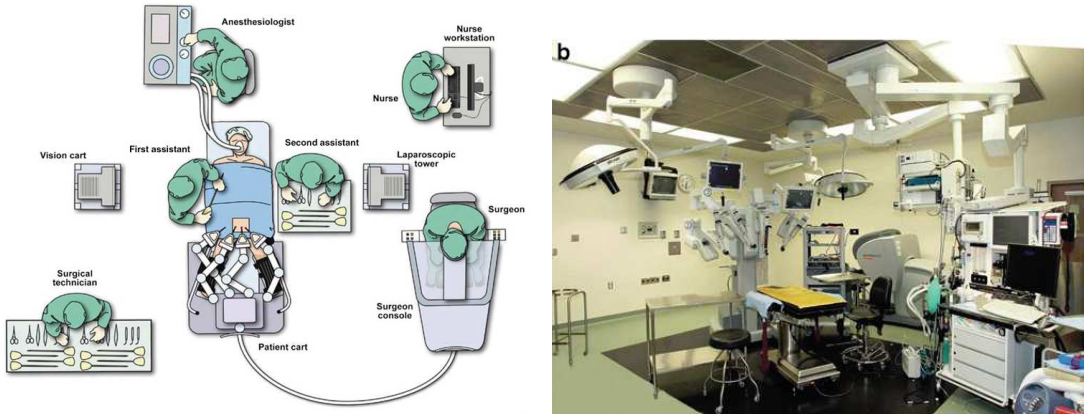

Figure 2.13: Operating room set-up [Higuchi and Gettman, 2011]

with vertex angle of $60° - 90°$ (the extended dexterous workspace) (Fig. 2.14.a). This is a small example of the set of requirements and constraints that have to considered in the design of surgical robot electromechanical structure.

In conclusion, two main pints withdrew the attention: first, the interaction forces peak noted in (Table. 2.1) could be violated in the absence of haptic sense and second, the RCM constraints (Fig. 2.14.a) confines the interaction measurement modality. This last point will be discussed with some details in (Section.2.4.5 and Section.2.4.5).

b. Electromechanical structure design:

The technological choices made to realise the slave robot affects the teleoperation transparency mainly by defining the robot-environment (tool-tissue) interaction. This section revises briefly the surgical robot design as a part of teleoperation design. The requirements and constraints defined in task analysis step are considered as an input to this phase.

The most important constraint present in OR and that affects teleoperation transparency is the RCM [Aghakhani et al., 2013]. In laparascopic surgery, the fulcrum con-

Table 2.1: Task requirements of abdomen surgery in terms of workspace and interaction wrench [Rosen et al., 2011]

Quantity	Requirement			Unite
Orientation	$\triangle\theta_x = 53.80°$	$\triangle\theta_y = 36.38°$	$\triangle\theta_z = 148.09°$	[Deg]
Position	$\triangle X = 0.1026$	$\triangle Y = 0.0815$	$\triangle Z = 0.0877$	[m]
Velocity	$\omega_x = 0.432$	$\omega_y = 0.486$	$\omega_z = 1.053$	[rad/s]
Peak force	$F_x = 14.73$	$F_y = 13.2$	$F_z = 67.4$	[N]
Torque	$T_x = 2.4$	$T_y = 1.6$	$t_z = 0.05$	[N.m]

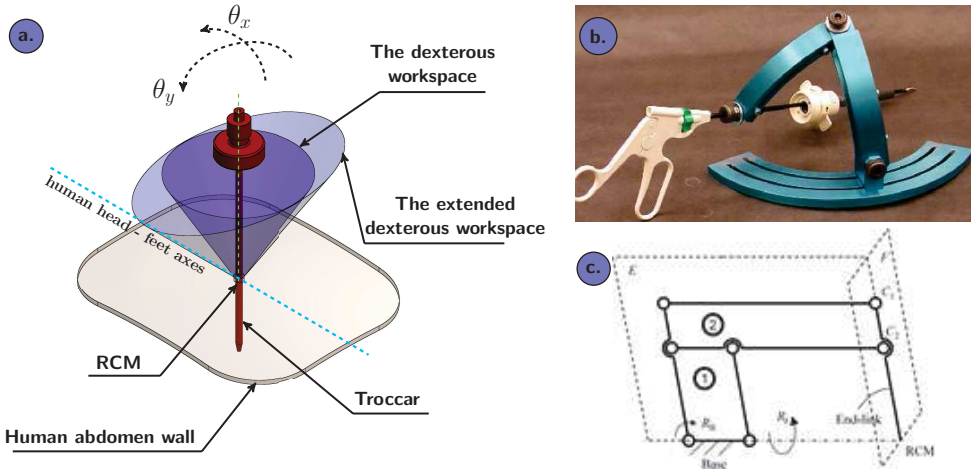

Figure 2.14: a. Remote centre of motion (RCM) constraints and surgeon workspace, b. spherical and c. the parallelogram mechanisms to satisfy RCM constraints [Rosen et al., 2011]

straint (RCM) is satisfied either mechanically or by control [Krupa et al., 2004]. Several structures are available in mechanisms theory to impose mechanically the RCM [Faraz and Payandeh, 1998] [Beira, 2013]. They can be organised in two main categories: the parallelogram (Fig. 2.14.c ex. Da Vinci Robot) [Madhani, 1997] [Çavuşoğlu et al., 1999] [Herman et al., 2009], and the spherical mechanism which is used in several forms as in Otelo robot [Al Bassit, 2005] [Delgorge et al., 2005], ViKY-LER robot [Berkelman et al., 2003a] [Berkelman, 2009] and MC^{2}E robot [Zemiti et al., 2007] where the driving motors are mounted directly on the concerned joints. Another approach of spherical mechanism is to place the motors away from the mechanical chain and driving the joint through capstan motion transmission as in Raven robot [Li and Payandeh, 2002] [Lum et al., 2009] with an optimised workspace[Lum et al., 2006].

Further discussion on the technological choices in terms of mechanical structure, actuation, and sensory redundancy can be sought in *Dombre et al.* ([Troccaz, 2013] Chapter 5) [Duchemin et al., 2004] and [Rosen et al., 2011].

c. Control and safety :

Control aspect in surgical robotics can be presented in three main folds: First, the basic requirements of robot control and HMI. Second, additional specific features like disturbance compensation and robustness. Finally, the teleoperation context. Even though our concern focuses the last point, the first two aspects are necessary in each robotic device and therefore are introduced [Rosen et al., 2011] [Troccaz, 2013].

The necessary functions requested from a robotic device to perform concisely its activity (sensing, calculating, acting, etc.) are driven by a computation kernel under real time constraints with fixed computation (sampling) rate. In case of necessity of interaction control between the robot and its environment, a proper interaction control algorithm has to be implemented (compliance, impedance or force control). In most cases, the robot is sufficiently driven under motion control low with a proper HMI to satisfy the operating room staff [Pierrot et al., 1999] [Duchemin et al., 2004]. Fore example, some vital organs in human body contains an inherent disturbance that overburden the surgeon task and the robotised arm helps to compensate automatically this disturbance (Section. 2.4.5). Finally, safety issue should be given a special attention because the robot perform its tasks in a human-occupied environment and this is basically imposed through control intelligence [Rovetta, 2000].

In Conclusion, the main effect of the adopted slave design on teleoperation transparency can be summarized in one question: How precise is possible to acquire the haptic data of a required interaction? For example, RCM constraint confines the location of force sensing modality required to measure the tool-tissue interaction force. Consequently, the measured force contains in uncouples state the interaction data mixed with tool-trocar friction, tool-other tissues contact, etc. This section treats the effect of slave design on teleoperation transparency through three points: task analysis, electromechanical structure design and control and safety issues. The next section introduces the role of environment in teleoperation transparency.

2.4.5 Environment and interaction modelling

Environment is the last station in teleoperation sequence and is generally inaccessible (in terms of scale, distance and/or hostility) to human operator. The term ***environment*** is used broadly in teleoperation literature to address the host of targeted remote (set of) task(s). In medical applications (ex. telesurgery) context, the environment is the operated human vital organs and soft tissues. To insure the teleoperation task success, the most effecting constraints, that are present in the task environment, has to be considered and this what is meant here by the environment modelling in its general sense.

From haptic teleoperation stand point, environment modelling can be reduced to the analysis of tool-tissue interaction. This analysis is necessary not only for the success of the teleoperation task but also to maximize the MSN transparency by identifying and considering (through its design) the maximum of constraints which are present in the operated environment and can limits the MSN performance. The main factors that affect teleoperation transparency and can be classified under environment modelling are organised under the following main points:

* *Tool-tissue interaction modelling.*
* *The presence of motion disturbance.*
* *The accuracy of haptic data acquisition.*

Before detailing each of these points, it is worth to note the following: (1) The environment is modelled in teleoperation literature as 1-port network system which has generally robot position rate as input and its reaction force as an output. (2) The interaction velocity (v) and force (F) are referred in the literature as haptic data and defines the tool-tissue exchanged power. (3) Teleoperation literature uses the term ***interaction port*** to designate the physical area of interaction where tool-tissue energy exchange happens.

a. Tissue modelling (Interaction modelling):

Interaction modelling of soft tissue helps to estimate the reaction force of this living tissue by knowing the amount of shape deformation imposed by this tissue on the robotic tool. Providing accurate models of such interaction helps the surgical robot to predict and control the interaction forces imposed on the operated living tissues, helps to predict the task scenario and therefore improves the teleoperation performance and is useful in substituting the lake of some important information. The most clearer effect of tissue modelling accuracy on teleoperation transparency can be seen in force control based haptic teleoperation as in the case of [Park and Khatib, 2006] [Cortesão et al., 2006]. Tissue interaction modelling is introduced through the following two parallel axis of developments: first, interaction modelling by direct measurement of the haptic data and second, force estimation by an adequate mathematical modelling of tool-tissue interaction.

Direct acquisition of interaction forces in robotic surgery is still a developing area. The accuracy of force substitution of a required interaction in telesurgery represents one of the major constraints that prevents introducing haptic technology to the OR. This point will be introduced later with some details in haptic data acquisition accuracy point. An overview of force sensing methods can be sought in [Fahlbusch and Fatikow, 1998] and for commercialised force/ tactile sensors comparison in [Fässler, 2010]. Moreover, for an adequate review on tactile and force acquisition modalities in minimally invasive surgery context, see [Puangmali et al., 2008] [Konstantinova et al., 2014] and [Lu et al., 2006] for micromanipulation scale. Finally, interaction force measurement and estimation based on vision sensors is also possible [Greminger and Nelson, 2004] [Chawda and Malley, 2011]. If the interaction force is available through direct measurement, it is fed back directly after filtering to feedback to human operator through master device.

In the absence of direct force measurement utility, a successful estimation of the interaction force becomes mandatory to perform bilateral teleoperation. This problem is called also interaction modelling and its main objective is to provide useful estimation algorithms to guess slave-environment interaction forces based on the available and pre-known information of master and environment. Several approaches have bee proposed to provide a useful construction of interaction force with soft tissue in haptic telesurgery context and yet it seems to be far from being matured.

Slave-environment interaction forces can be estimated based on the driving torques of the robot in and without contact beside the knowledge of joint position information

through the usage of function parameter matrix and recursive least-squares method [Son et al., 2010] or by using Kalman filter [Mitsantisuk et al., 2012]. Moreover, interaction forces can be estimated based on visual acquisition of shape deformation [Aviles et al., 2014] but this method requires often an established model of the deformed tissue [Kim et al., 2010]. Traced-back in interaction and impedance control [Love and Book, 1995], numerous contribution enriched deformation modelling of soft tissues [Fung, 1993] [Erickson et al., 2003] [Diolaiti et al., 2005] [Misra and Okamura, 2006] [Bensamoun et al., 2008] [Yamamoto et al., 2008] [Yamamoto et al., 2009] [Fong, 2009] [Bickel et al., 2009] [Gao et al., 2010] [Boonvisut and Cavusoglu, 2013] [Moreira et al., 2014] and yet it seems to be a fertile area of scientific production. The utility of a meaningful soft tissue deformation model passes beyond force sensor substitution to encompasses several applications, Virtual reality, augmented reality, sensory redundancy to improve intervention safety, etc.

b. Physiological activities estimation and modelling

This discussion is reduced to focus on haptic telesurgery directly related issue i.e. the physiological motion disturbance. Involuntary motion is an inherent property of many vital organs in human body. Breathing motion directed by the involuntary activity of diaphragm. Heart beats motion directed by the involuntary electrical activity of heart muscle. The effect of these activities pass beyond the boundary of thoracic area to its neighbourhood in abdomen cavity and neck due to its close place and/or the blood transferred through vessels. The presence of such disturbance strains the natural direct or robotic surgical intervention. The most obvious example is cardiac surgery. Heart performs a complex 3D motion that consists of a quasi-periodic contraction and simultaneous twist with high frequency (2 Hz) which surpasses the human capacity of manual compensation [Jacobs et al., 2003]. Moreover, even if the breathing motion frequency is small, the precise micro scale low frequency nature of surgeon gestures on vital organs highlight the importance of providing an automatic compensation of such disturbance [Riviere et al., 2006].

First concern was to provide an accurate estimation of this physiological motion [Wang et al., 1995] [Hunter et al., 2003] [Ortmaier et al., 2005] [Shechter et al., 2006] [Bachta et al., 2009]. Followed by a serious effort to provide an automatic cancellation of respiratory/-heartbeat motion disturbance [Ginhoux et al., 2005] [Riviere et al., 2006] [Bebek and Çavusoglu, 2007] [Groeger et al., 2008] [Bachta et al., 2010] [Richa et al., 2010] [Bachta et al., 2011]. And yet, the integration in operating room is not achieved [Azizian et al., 2014]. Researchers nowadays are thinking about a faithful method to construct the interaction force with the moving organ with compensating its motion.

Haptic data acquisition accuracy

Haptic data as aforementioned is force and velocity information of the interaction region. The accurate acquisition of this data affect remarkably the system transparency and it is therefore the subject of this section.

Because the robotic tool is far stiffer in comparison to the operated soft tissue, interaction velocity can be considered equal to this of the robotic tool. Every robotic structure is provided with an adequate position measurement modality and an accurate models to perform task/ joint space transformation. In conclusion, the position rate information of any required interaction can be obtained accurately.

On the other hand, obtaining the interaction forces (through measurement or tissue modelling) is subject to several technical constraints. First, The force measurement facility that fits operating room constraints (ex. sterilization) adds a considerable cost to the surgical intervention. Furthermore, the up to date proposed location of the force sensing modality (ex. respecting the trocar constraints) does not provide a faithful acquisition of the reaction forces of the targeted interaction (i.e. in most cases the acquired forces lump several uncoupled measures like tool-trocar friction, tool interaction with tissues other than the required interaction, etc.). Consequently , the haptic and interaction control in medical context is still confined to laboratories prototypes. [Berkelman et al., 2003b] [Takahashi et al., 2006] [Puangmali et al., 2012].

In conclusion, this research topic addressed the role of environment modelling in providing a transparent teleoperation through three main points: the accuracy of toot-tissue interaction modelling, the effect of motion disturbance presence and the accuracy of haptic data acquisition. The following topic focusses on assessing the overall teleoperation.

2.4.6 Teleoperation design and assessment

Teleoperator is the inter-medium between human operator as a task executer and remote environment as a task host. The objective of the (1 to 5) precedent research thematics is to provide a close overview of the MSN components and to define the major factors that affect a MSN transparency. This topic of research addresses the MSN design and evaluation issue through three main points: (1) Modelling (2) Design (Stability) (3) Evaluation (Transparency).

a. Modelling

In its early days and up to the end of 80s, precisely 1989, MSNs had been designed and evaluated experimentally [Sheridan, 1992] [Hirzinger et al., 1998]. The analytic tools to design and evaluate MSNs have been inspired from network theory and interaction theory, thanks to the simultaneous effort of ***Tomas Sheridan***, ***Antal Bejczy***, ***Neville Hogan*** and their teams. Nowadays, it is widely accepted in teleoperation community that the MSN (i.e.

Master-Slave Network) and its components (i.e. Master, communication and slave sytems) can be modelled as two port networks that transmits the injected energy by the human operator to the remote environment and conveys back this latter reactions to the operator. Moreover, Human operator and environment are modelled as a one port network with an active source or energy [Hannaford and Fiorini, 1988] [Raju et al., 1989] [Hogan, 1989] [Kazerooni et al., 1990]. In most cases the MSN is designed to interact with pre-known well-structured passive environment. Through each interaction port an energy flows and can be identified through the local flow and effort values [Anderson and Spong, 1988] [Anderson and Spong, 1989] (Fig. 2.15). Further steps have been achieved in [Lawrence, 1993] and [Hashtrudi-Zaad and Salcudean, 2001] by providing a comprehensive structure of teleoperation system, called 4-channel architecture, to serve in the technical design of MSNs. A sufficient technical details on MSN's modelling will be introduced in the following chapter.

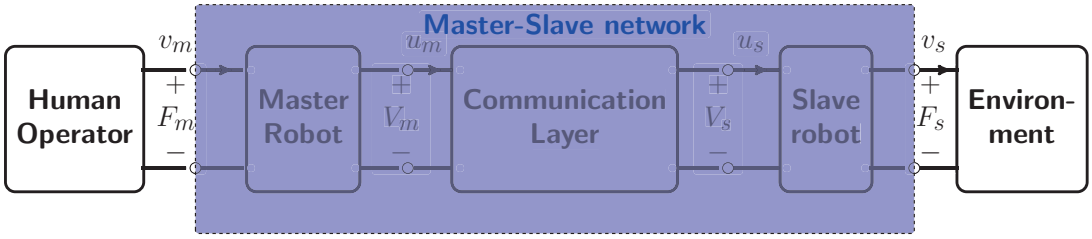

Figure 2.15: Bilateral Teleoperation Modelling

b. Stability

Several techniques have been adopted to insure the stability of teleoperation through MSN. To the best of author knowledge, these techniques can be organised under three main categories: (1) Teleoperation design using Linear system stability tools. (2) Teleoperation design using nonlinear systems design tools. (3) Passivity based absolute stability.

It is possible for simple teleoperation control structures as 2-channel architectures, under some assumptions, to rearrange the teleoperation control structure into unity-feedback structure. By introducing a loop shaping compensator, it is possible to use the conventional linear system design tools to provide a stable teleoperation [Hannaford, 1989b] [Fite et al., 2001] [Fite et al., 2004].

Moreover, Teleoperation is, from control design stand-point, a multi-variable system with several sources of non-linearities like time delay, friction, models uncertainties, measurements' noise, etc[Hirche et al., 2007]. Therefore, it is possible to use nonlinear system design tools to provide a stable teleoperation by combining H_∞ optimization with μ synthesis [Leung et al., 1995], through optimal design tools as in [Yan and Salcudean, 1996] or by using frequency domain damping design [Suzuki and Ohnishi, 2013].

Modelling the MSN as a 2-port network enabled its design under network theory design context. Indeed, considering the MSN as a transmission line that conducts energy, the design of stable teleoperation can be reduced to the design of stable MSN if the latter ends with passive terminations (ports) [Hannaford, 1989a] [Anderson and Spong, 1989]. [Colgate, 1988] [Lawrence, 1993] and [Hashtrudi-Zaad and Salcudean, 2001] formulated the design tools derived from passivity theorem to fit teleoperation literature. Absolute stability design tools can be summarised by ***Llewellyn's criteria*** that ensure the passivity of the MSN and its components [Hashtrudi-Zaad and Salcudean, 2001]. These design tools can be extended to include the stability of multi-master/multi-slave teleoepration systems [Khademian and Hashtrudi-Zaad, 2013], the stability of sampled-data bilateral teloperation systems [Jazayeri and Tavakoli, 2013] or even relaxing the conditions to involve some non-passive driving point termination [Jazayeri and Tavakoli, 2015].

c. Transparency

The ultimate objective of teleoperation is to provide a complete/controllable kinaesthetic coupling between Human operator and remote environment [Raju et al., 1989] [Hannaford, 1989a] [Lawrence, 1993], in other words, to design a transparent MSN that enables the operator to feel as if he/she is touching directly the remote environment [Hannaford and Okamura, 2008] [Niemeyer et al., 2008] [Okamura et al., 2011b]. Stability and transparency are contrasting measures and a trade-off is mandatory [Daniel and McAree, 1998] [Hashtrudi-Zaad and Salcudean, 2001]. Several approaches have been adopted to evaluate the transparency of a designed MSN. Further technical details on these evaluation criteria can be traced in (Section. 3.3) and can be summarized as follows:

First approach evaluates a MSN performance by comparing the corresponding values at human-master and slave-environment interaction ports [Yokokohji and Yoshikawa, 1994] [Moreau et al., 2012], where three ideal responses are defined to evaluate a MSN by comparing position and force information at human-master and slave-environment interactions. These ideal responses are that master and slave robot have identical position rate, identical interaction forces or both simultaneously.

The second approach evaluates teleoperation by comparing the environment impedance to the impedance sensed by human operator [Lawrence, 1993] [Hashtrudi-Zaad and Salcudean, 2002] [Kim et al., 2013] [Tavakoli et al., 2007] where these impedances are the transfer functions that describe force and position rate relationship at slave-environment and human-master interaction ports respectively.

The last approach to evaluate transparency is acquired from haptic literature and divides the sensed impedance by human operator into two main measures, the minimum impedance that can be sensed by human operator which is the impedance of the MSN itself when the slave performs a free space motion and the second is the range of impedances that can be reflected through the designed MSN [Colgate and Brown, 1994] [Hashtrudi-Zaad and Salcudean, 2001] [Cavusoglu et al., 2001] [Son et al., 2011].

2.5 Conclusion

The design of bilateral teleoperation can be summarised in stability-transparency trade-offs. These trade-offs depend extremely on MSN components. Transparency is an important measure in operating room and it is proved to improve the intervention quality. The design of a transparent bilateral MSN for medical applications requires a serious awareness from designer to each component effect on the system transparency.

This chapter provides a short overview on the research effort performed in the context of bilateral teleoperation for MIS applications. Starting with a brief introduction to teleoperation history and its added value to operating room, we proposed a new elaborated point-of view to explore the vast literature of haptic teleoperation by dividing it into six sub-topics of research. The contribution of each sub-topic in providing a transparent haptic teleoperation is analysed and the main factors affecting transparency are extracted. This chapter explored haptic teleoperation literature treatment of human as a subject to decide his/her need of haptic sense, the method(s) of its stimulation and the human performance in teleoperation closed loop. Furthermore, we explored the role(s) of each of master, communication layer, slave robot design and environment modelling in providing a transparent teleoperation. Finally, the design and assessment of the overall teleoperation is discussed.

Based on these detailed investigation, some but not limited to the major effective factors on a teleoperation performance (transparency) are identified as follows:

- Master design: defines action generation and haptic sense stimulation methods.
- Slave design: defines haptic variables acquisition accuracy of a required interaction.
- The implemented control architecture to achieve master-slave bilateral coupling.
- Action-perception latency (Time delay).
- Disturbance and uncertainties presence in the operated environment.
- Tissue model accuracy affects the force control based haptic teleoperation.

In the following chapters, and considering the MSN is known, the last four factors are brought to the focus point of interest. The next chapter explore the necessary definitions and tools that will be used to design a stable teleoperation and evaluate its performance.

CHAPTER

3 Teleoperation Design and Evaluation

Preamble

This chapter addresses the technical tools that will be used through this thesis to design a haptic bilateral teleoperator and assess its performance.

The ultimate objective of teleoperation systems is to provide a stable bilateral haptic telepresence of human operator with enough (controllable) amount of transparency. In this chapter, we present the essential tools that enable the design and evaluation of bilateral teleoperators. We start with modelling to present the analytic tools of representing teleoperation systems that are necessary for the design and assessment procedures. Teleoperator design addresses the stability of MSN and the affecting variables on this stability. Finally, the performance of the designed teleoperator has to be assessed through transparency criteria. Transparency investigates the matching between the manipulated environment and the operator sense based on set of criteria and measures.

3.1 Modelling

Teleoperator is seen, as introduced in the previous chapter, as a power transmission line that conveys the injected energy by operator to a remote environment and reflects back concurrently environment reactions to operator [Anderson and Spong, 1989]. This analysis is based on robot-environment interaction theory [Hogan, 1985a] which concludes that during interactions, robot and its environment exchange energy through interconnection bonds (ports). This concept is borrowed from system theory and depends on energy conservation concepts which considers *power*, the rate of energy transport be-

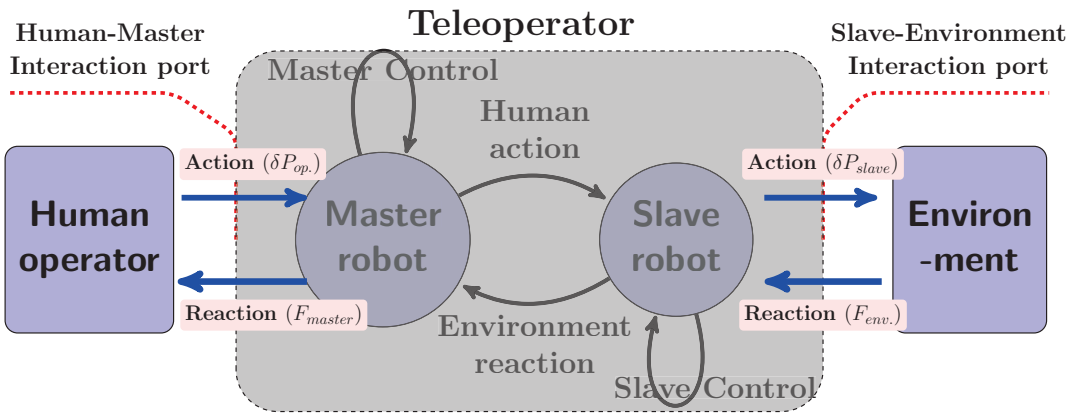

Figure 3.1: Teleoperation Modelling

tween components, as the universal currency of physical systems [Gawthrop and Bevan, 2007].

Intuitively, the exchanged energy between human-teleoperator and teleoperator-environment is a mechanical energy (kinetic and potential). Furthermore, teleoperation is a hybrid system where energy changes from one form to another. This energetic interpretation led to a comprehensive modelling of complex systems such as teleoperation systems [Hannaford, 1989a] based on physical systems analogy principles [Gawthrop and Bevan, 2007].

The following section aims to introduce briefly the fundamental concepts used in teleoperation modelling. First, we start with the basic notions of systems analogy, causality and interaction ports. Second, human, robot, communication line and environment models are addressed, to finish with a detailed introduction of teleoperation modelling.

3.1.1 Basic Notions

Systems Analogies :

It has been early remarked an analogy in behaviour and modelling of physical systems of different nature (mechanical, electrical, fluid, chemical, magnetic, thermal etc.). This analogy can be showed in three levels, *signals analogy* (Table 3.1), *components analogy* (Table 3.2) and *connections analogy* [Rosenberg and Karnopp, 1983]. These analogies have eased the reformulation of bilateral teleoperator model under 2-port network frame [Hannaford, 1989a] [Anderson and Spong, 1989].

1. ***Signals analogy :*** describes power variables similarity of mechanical and electrical systems [Gawthrop and Bevan, 2007] (Table 3.1).

Table 3.1: Signals analogy of mechanical-electrical systems

Generalized signals	**Mechanical systems** Translation		Rotation		**Electrical systems**	
Effort, e	Force F	(N)	Torque τ	$(N.m)$	Voltage v	$(volt)$
Flow, f	Linear velocity v	$(\frac{m}{s})$	Angular velocity ω	$(\frac{rad}{s})$	Current i	(Amp)
Integrated effort : $p = \int e\, dt$	Momentum	$\frac{kg\ m}{s}$	Angular momentum,	$\frac{kg\ m^2}{s}$	Flux λ	$Volt.s$
Integrated flow : $q = \int f\, dt$	Position, x	m	Angle, θ	rad	Charge q	C
***Power* = *effort* × *flow (Watt)*,**			***Energy* = ∫ *Power* . *dt (Joule)***			

2. ***Components analogy :*** highlights the behaviour similarities of frequenlty used physical systems components [Gawthrop and Bevan, 2007] (Table 3.2).

Table 3.2: Components analogy of mechanical-electrical systems

Generalized components	**Mechanical components** Translation		Rotation		**Electrical systems**	
Effort source S_e	Applied force	N	Applied torque	Nm	Applied voltage	volt
flow source S_f	Applied velocity	$\frac{m}{s}$	Applied angular velocity	$\frac{rad}{s}$	Applied current	Amp
M	Mass, m	kg	Inertia, J	$kg.m^2$	Inductor, L	H
D	Damper, d	$\frac{N.s}{m}$	Rot. Damper, d	$\frac{N.m.s}{rad}$	Resistor, R	Ω
S	Spring, K	$\frac{N}{m}$	Tor. Spring, K	$\frac{N.m}{rad}$	Capacitor, C	F

3. ***Connections analogy :*** In its serial and/or parallel combinations of components, systems exhibit always a certain level of performance analogy. Serial connections divide ***effort*** while ***flow*** stays the same in all serially connected components similarly to Kirchhoff's current law. On the other hand, parallel connections obey Kirchhof's voltage law and partition the ***flow*** while the same ***effort*** is applied on termination of parallel connected components.

Applying the aforementioned analogy on teleoperation hybrid systems enabled its reformulation under networks frame where MSN is decomposed into a cascade serial connection of 2-port networks while human operator and environments are modelled as 1-port network (Fig. 2.15) [Nahvi and Edminister, 2003].

Interaction port :

Places at which the subsystems (of different natures) can be interconnected are places at which power can flow between the subsystems. Such places are called *interaction ports* [Karnopp et al., 2012]. Teleoperator has two interaction ports, one with human operator and the second with the treated environment (Fig. 3.1). The region at which human operator grasps the master robot represents the first interaction port while the interaction region between slave and manipulated environment is the second port. At these ports the power flows between the human, teleoperator and environment where the teleoperator works as a transmission network. Power flow is quantified by knowing *flow* and *effort* quantities at the concerned interaction port.

Causality :

Causality relationship addresses system dynamics modelling and its input-output relationship. Considering effort and flow relationship in physics, systems can be modelled as impedance, admittance or immittance. *Impedance* (Z) is the mapping relationship between *flow* (***f***) as an input and *effort* (***e***) as an output i.e. $e(s) = Z(s)f(s)$ where $Z(s)$ is a transfer function for each DoF and s denotes Laplace variable. Likewise, *Admittance* (Y) is the mapping relationship between *effort* (***e***) as an input and *flow* (***f***) as an output $f(s) = Y(s)e(s)$. The *immittance* mapping (P) combines both impedance (Z) and admittance (Y) mapping and is used generally to describe system's dynamics when its input and output are vectors of mixed flow and effort values. In other words, a system has an immittance causality means that this system has either impedance or admittance model. (Fig. 3.2) provides an illustration of causality mapping for Mass Damper Spring (MDS) system.

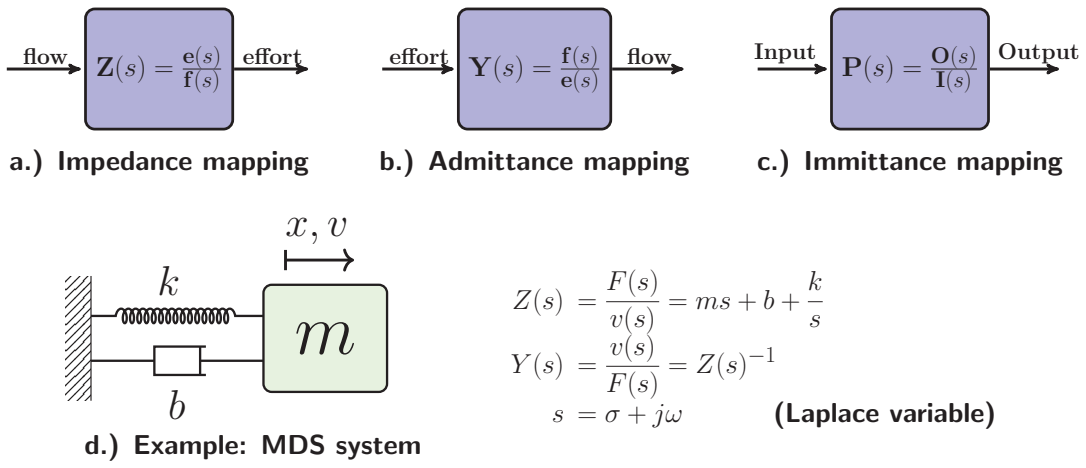

Figure 3.2: Teleoperation Modelling

Immittance causality mapping is a transfer function (or a matrix of transfer functions) that represents the system dynamics and enables its stability evaluation as will be introduced in passivity section. Impedance and admittance mapping of the same dynamic system are equivalent (see Property3.1.1) and therefore the evaluation of any dynamic system can be reduced to the evaluation of its impedance mapping causality.

Property 3.1.1. *Let H, a dynamic system that possesses an admittance causality mapping $\mathbf{f}(s) = \mathbf{Y}(s)\mathbf{e}(s)$, $\mathbf{Y}(s) \in \mathbb{R}^{n\times n}$ where $\mathbf{f}(s)$, $\mathbf{e}(s) \in \mathbb{R}^n$, denote the system output (flow) and input (effort) receptively, and $[\mathbf{I_n} + \mathbf{Y}(s)]^{-1}$ exists, i.e. the model is invertible where $\mathbf{I_n} \in \mathbb{R}^{n\times n}$ is the identity matrix and $\mathbf{Z}(s) = \mathbf{Y}(s)^{-1}$ is the impedance causality mapping of the system H, then:* ***If*** *$\mathbf{Y}(s)$* ***is positive real,*** *$\mathbf{Z}(s)$* ***is positive real*** ■

3.1.2 Human and Environment modelling

Human represents the decision making part of teleoperation closed loop control. The analysis of human-in-loop role in teleoperation context has been previously addressed in human-master interconnection (section 2.4.1) and master system design (section 2.4.2). Human performance in teleoperation context when one of his limbs is driving a master robot consists of two main components: first an active component that represents the operator's voluntary decision and second a passive component that indicates the reflexive part of human actions (generally depends on an external effect (input) like master robot motion). Briefly, the reflexive component is modelled as a passive impedance $\mathbf{Z_h}$ that takes the connected device's position rate as an input to generate a reflexive force. The reflexive force is summed with the active component of human action F_h^* to generate the human-master interaction force F_h [Hogan, 1989] [Burdet et al., 2001] (Fig3.3) and (Eq. 3.1).

Likewise, a passive environment can be modelled under impedance causality form as $\mathbf{Z_e}$. If the environment contains any source of activity, an external source of effort (F_e^*) or flow x_e^* (depends on the modelled case) can be added in serial with the reflexive component. In teleoperation context, environment is generally supposed to be passive i.e. $F_e^* = 0$.

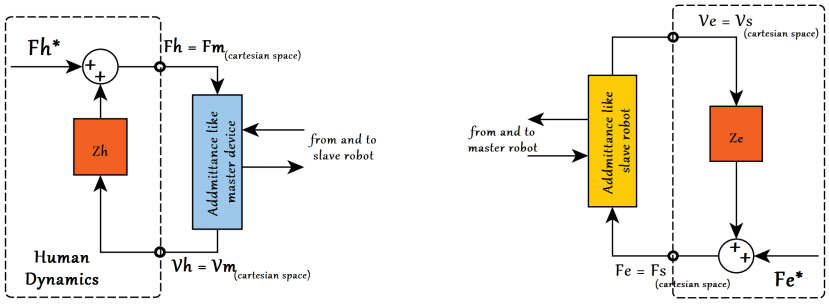

Figure 3.3: Human and environment dynamics modelling

Consequently, environment's reaction forces due to a robot input is defined only by the mechanical properties of the environment impedance. Dedicated survey can be sought in environment and interaction modelling section (section 2.4.5)(Eq. 3.2).

$$\mathbf{F_h} = \mathbf{Z_h v_h} + \mathbf{F_h}^*, \tag{3.1}$$

$$\mathbf{F_e} = \mathbf{Z_e v_e} + \mathbf{F_e}^*. \tag{3.2}$$

3.1.3 Teleoperator's model

Treating teleoperator as a transport line of energy between the operator and the environment enables its' modelling under 2-port network theory (Fig. 3.4). The transported energy is quantified through haptic (power) variables i.e. (*flow and effort*) at each interaction port. By selecting two variables as an input vector and the other two as an output, teleoperator can be modelled using impedance model (Eq. 3.3), admittance model (Eq. 3.4), hybrid model (Eq. 3.5) or inverse hybrid model (Eq. 3.6) [Christiansson and van der Helm, 2007] [Hashtrudi-Zaad and Salcudean, 2001]. Each member of $\mathbb{Z}$, $\mathbb{Y}$, $\mathbb{H}$, $\mathbb{G}$ matrices is a transfer function that represents the dynamics of the physical components (master, slave and communication facilities) used to realise the designed teleoperator.

$$\mathbf{y_z} = \mathbb{Z}\mathbf{u_z} \quad , \quad \begin{pmatrix} F_m \\ F_s \end{pmatrix} = \begin{pmatrix} z_{11} & z_{12} \\ z_{21} & z_{22} \end{pmatrix} \begin{pmatrix} v_m \\ -v_s \end{pmatrix}, \tag{3.3}$$

$$\mathbf{y_y} = \mathbb{Y}\mathbf{u_y} = \mathbb{Z}^{-1}\mathbf{u_y} \quad , \quad \begin{pmatrix} v_m \\ -v_s \end{pmatrix} = \begin{pmatrix} y_{11} & y_{12} \\ y_{21} & y_{22} \end{pmatrix} \begin{pmatrix} F_m \\ F_s \end{pmatrix}, \tag{3.4}$$

$$\mathbf{y_h} = \mathbb{H}\mathbf{u_h} \quad , \quad \begin{pmatrix} F_m \\ -v_s \end{pmatrix} = \begin{pmatrix} h_{11} & h_{12} \\ h_{21} & h_{22} \end{pmatrix} \begin{pmatrix} v_m \\ F_s \end{pmatrix}, \tag{3.5}$$

$$\mathbf{y_g} = \mathbb{G}\mathbf{u_g} = \mathbb{H}^{-1}\mathbf{u_g} \quad , \quad \begin{pmatrix} v_m \\ F_s \end{pmatrix} = \begin{pmatrix} g_{11} & g_{12} \\ g_{21} & g_{22} \end{pmatrix} \begin{pmatrix} F_m \\ -v_s \end{pmatrix}. \tag{3.6}$$

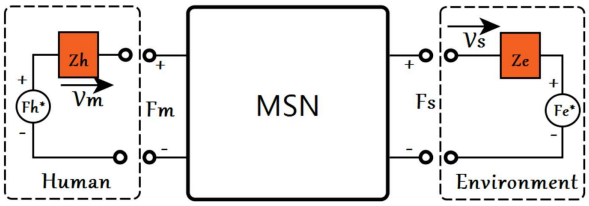

Figure 3.4: Bilateral Teleoperation Modelling

An ideal teleoperator imitates a light stiff stick that transports human-master Cartesian motion (v_m) to a remote environment and reflects faithfully its reaction (F_s). These two

variables are inputs in (Eq. 3.5). The hybrid model is therefore most present in teleoperation analysis literature and is interpreted as follows (eq. 3.5):

$$\begin{pmatrix} F_m \\ -v_s \end{pmatrix} = \begin{pmatrix} h_{11} & h_{12} \\ h_{21} & h_{22} \end{pmatrix} \begin{pmatrix} v_m \\ F_s \end{pmatrix} = \begin{pmatrix} Z_m & \gamma_f \\ \frac{-1}{\gamma_p} & Z_s \end{pmatrix} \begin{pmatrix} v_m \\ F_s \end{pmatrix}, \tag{3.7}$$

where Z_m, Z_s represent master and slave dynamics while γ_p and γ_f stand for position and force scale respectively. Any pair of the aforementioned representations (Eqs. 3.3 to 3.6) are equivalent and can be summarized under immittance mapping category $Y = \mathbb{P}u$ where the immittance matrix $\mathbb{P}$ can be $\mathbb{Z}$, $\mathbb{Y}$, $\mathbb{H}$ or $\mathbb{G}$. Consequently, the analysis of LTI teleoperator is independent of the used model to perform this analysis because the following property is always satisfied:

$$\mathbf{y}^T.\mathbf{u} = \mathbf{y}_z^T.\mathbf{u}_z = \mathbf{y}_y^T.\mathbf{u}_y = \mathbf{y}_h^T.\mathbf{u}_h = \mathbf{y}_g^T.\mathbf{u}_g = F_m v_m - F_s v_s. \tag{3.8}$$

Robot model:

The kinematic model of a robot that consists of n joints ($\mathbf{q} \in \mathbb{R}^n$) end effector that moves in $SE(3) := \{ \mathbb{R}^3 \times SO(3) \}$ can be described as follows:

$$\mathbf{v}(t) = \mathbf{J}(\mathbf{q}(t)) \dot{\mathbf{q}}(t), \tag{3.9}$$

$$\tau(t) = \mathbf{J}^T(\mathbf{q}(t)) \mathbf{F}(t). \tag{3.10}$$

Where $\mathbf{v}, \mathbf{F} \in \mathbb{R}^6$ are the Cartesian (linear and angular) velocities vector and the corresponding Cartesian forces and moments vector that are applied by the robot on its environment. $\mathbf{J}(\mathbf{q}) \in \mathbb{R}^{6\times n}$ is the robot Jacobian matrix, $\dot{\mathbf{q}}, \tau \in \mathbb{R}^n$ are the joint velocities and torques vectors respectively. On the other hand the robot dynamic performance is described using the following equations where the time variable is dropped for simplicity and clarity:

$$\mathbf{A}(\mathbf{q})\ddot{\mathbf{q}} + \mathbf{C}(\mathbf{q},\dot{\mathbf{q}})\dot{\mathbf{q}} + \mathbf{G}(\mathbf{q}) + \tau_{\mathbf{f}} = \tau_{\mathbf{m}} - \tau_{\mathbf{ext}} \tag{3.11}$$

Where $\mathbf{q}$, $\dot{\mathbf{q}}$, $\ddot{\mathbf{q}}$, $\tau_{\mathbf{m}}$, $\tau_{\mathbf{f}}$, $\tau_{\mathbf{ext}}$ and$\mathbf{G}(\mathbf{q}) \in \mathbb{R}^n$ are vectors of joint position, velocity, acceleration, controlled torques, friction torques, external interaction torques and gravity torques respectively, while $\mathbf{A}(\mathbf{q}), \mathbf{C}(\mathbf{q},\dot{\mathbf{q}})\,\dot{\mathbf{q}}$ are the symmetric positive definite inertial matrix and the Coriolis centrifugal torque vector respectively. To partially linearise the dynamic model in (Eq. 3.11), the control torque is calculated as follows:

$$-\mathbf{D}\,\dot{\mathbf{q}} + \hat{\mathbf{C}}(\mathbf{q},\dot{\mathbf{q}})\dot{\mathbf{q}} + \hat{\mathbf{G}}(\mathbf{q}) + \tau_{\mathbf{c}} = \tau_{\mathbf{m}} \tag{3.12}$$

$$\mathbf{A}(\mathbf{q})\ddot{\mathbf{q}} + \mathbf{D}\,\dot{\mathbf{q}} = \tau_{\mathbf{c}} - \tau_{\mathbf{ext}}, \tag{3.13}$$

- $\mathbf{D}$ is a diagonal positive definite gain matrix that represents the damping term required to pre-stabilise the linearised robot inner loop. $\mathbf{D}\,\dot{\mathbf{q}}$ is equivalent to friction term and therefore it is considered to include $\tau_{\mathbf{f}}$.

- $\hat{\mathbf{C}}(\mathbf{q},\dot{\mathbf{q}})\dot{\mathbf{q}}$: Coriolis centrifugal compensation vector.
- $\hat{\mathbf{G}}(\mathbf{q})$: Gravity compensation term.
- $\tau_{\mathbf{c}}$ the new joint control torque vector.

Considering that the robot workspace is evolving around a working posture ($\mathbf{q_0}$). Therefore, the dynamic model in (Eq. 3.13) can be locally linearised by considering a constant inertial matrix, i.e. $\mathbf{A}(\mathbf{q_0}) = \mathbf{A}$, and the dynamic model becomes:

$$\mathbf{A}\,\ddot{\mathbf{q}}(t) + \mathbf{D}\,\dot{\mathbf{q}}(t) \;= \tau_{\mathbf{c}}(t) - \tau_{\mathbf{ext}}(t), \tag{3.14}$$

Robot interacts with its environment (human or task) in Cartesian space, the fact that solicits the Cartesian space dynamic model construction. The transformation between joint and Cartesian space can be performed based on the kinematic model in (Eqs. 3.9 and 3.10). Consequently, the robot dynamic model becomes:

$$\mathbf{M}\,\dot{\mathbf{v}}(t) + \mathbf{B}\,\mathbf{v}(t) \;= \mathbf{F_c}(t) - \mathbf{F_{ext}}(t), \tag{3.15}$$

and in Laplace space:

$$(\,\mathbf{M}\,s + \mathbf{B}\,)\,\mathbf{v}(s) \;= \mathbf{Z}(s)\,\mathbf{v} \;= \mathbf{F_c}(s) - \mathbf{F_{ext}}(s), \tag{3.16}$$

The dynamic model presented in (Eq. 3.16) is used to represent master and slave mechanisms in teleoperation literature. The main difference is the external force (F_{ext}) sign. In master robot, the external force is human-master interaction force (F_h) and this force is a collaborating force that helps the control force at master cite (Fcm) to overcome the master mechanism dynamics (Z_m) and therefore it takes a positive signal (Eq. 3.17). On the other hand, the control forces imposed by the slave robot motors (F_{cs}) has to overcome slave mechanism dynamics (Z_s) plus slave-environment interaction forces (F_e) (Eq. 3.18):

$$\mathbf{Z_m v_m} = \mathbf{F_h} + \mathbf{F_{cm}}, \tag{3.17}$$

$$\mathbf{Z_s v_s} = -\mathbf{F_e} + \mathbf{F_{cs}}. \tag{3.18}$$

The objective of MSN (Fig. 3.4) is to provide a complete kineasthetic coupling between human operator and remote environment by conrolling master and slave device such that the exchanged energy at human-master interaction port equals to this at slave-environment interaction port. Therefore, the deriving forces at master (F_{cm}) and slave (F_{cs}) mechanisms has to be claculated based on the haptic variables (position rate and force) at teleoperator interaction ports i.e. $F_m,\ v_m,\ F_s,\ v_s$.

Communication layer model:

As previously introduced in communication layer design, in bilateral teleoperation context, the haptic information at master site has to be subject to a suitable parametric reduction and transformation before being sent through the communication facility. Once

it arrives to slave site, the transformation has to be inverted and the data has to replicated to reconstruct the original data. The haptic data sent from slave to master robot has to be subject to an equivalent procedure [Nuño et al., 2011].

The main influence of communication procedure is the imposed time latency between human action and environment sensed response. Hence, each information of F_m, v_m, F_s and v_s is changed through one communication channel that is characterised by its constant or variable time delay. If $*_{ms}$ denotes the information received at slave site coming from master site (i.e. master to slaver), $*_{sm}$ denotes the information received at master site coming from slave site (i.e. slave to master) and (T) the communication time delay, then:

$$F_{ms}(t) = F_m(t-T), \quad v_{ms}(t) = v_m(t-T), \tag{3.19}$$
$$F_{sm}(t) = F_s(t-T), \quad v_{sm}(t) = v_s(t-T). \tag{3.20}$$

And in Laplace domain (Eq. 3.19 and 3.20) take the following form:

$$F_{ms}(s) = F_m(s)\, e^{-sT}, \quad v_{ms}(s) = v_m(s)\, e^{-sT}, \tag{3.21}$$
$$F_{sm}(s) = F_s(s)\, e^{-sT}, \quad v_{sm}(s) = v_s(s)\, e^{-sT}. \tag{3.22}$$

Teleoperation model:

[Lawrence, 1993] rearranged the teleoperation control scheme based on the aforementioned basis in a comprehensible structure and called it 4-channel teleoperation control architecture. Because each distant site sends and receives two signals, this structure is refereed by the number of communication channels. Later, [Hashtrudi-Zaad and Salcudean, 2001] expanded Lawrence structure by adding a force control loop around master and slave mechanisms to enhance teleoperation stability-transparency trade-off(Fig. 3.5). [Hashtrudi-Zaad and Salcudean, 2001] had also explored all the possible compination of master impedance or admittance like mechanism with slave impedance or admittance like mechanism for 4-channel structure and 2-channel structures.

Briefly, the master and slave are modelled as in the precedent section as LTI systems:

$$Z_m v_m = F_h + F_{cm} \tag{3.23}$$
$$Z_s v_s = -F_e + F_{cs}, \tag{3.24}$$

with $Z_m = M_m\, s$, $Z_s = M_s\, s$ as master and slave mechanism dynamic impedance. $v_h = v_m$, $F_h = F_m$, haptic variables (velocity and force) at master-human interaction port. $v_e = v_s$, $F_e = F_s$ haptic variables (velocity and force) at slave-environment interaction port. F_{cm} and F_{cs} are master and slave driving control inputs and can be calculated based on the following form [Lawrence, 1993] and [Yokokohji and Yoshikawa, 1994]:

$$F_{cm} = -C_m v_m - C_4 e^{-sT_d} v_s + C_6 F_m - C_2 e^{-sT_d} F_s, \tag{3.25}$$
$$F_{cs} = -C_s v_s + C_1 e^{-sT_d} v_m - C_5 F_s + C_3 e^{-sT_d} F_m, \tag{3.26}$$

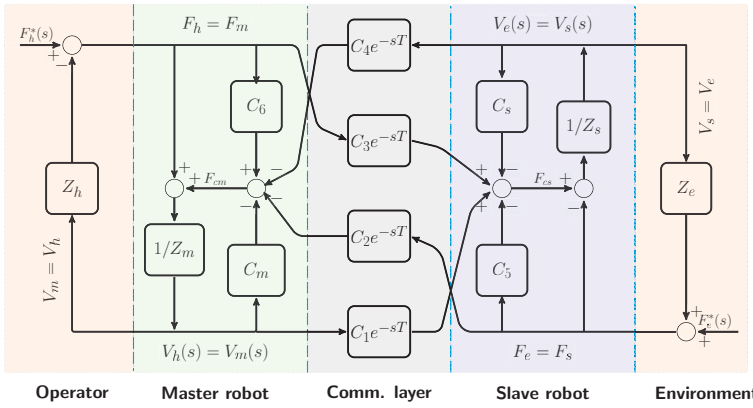

Figure 3.5: Extended Lawrence 4-Channel Teleoperation Control Architecture

with T_d stands for the communication layer induced time delay. $C_m = B_m + K_m/s$ and $C_s = B_s + K_s/s$ are position controllers around master and slave mechanisms and based on local position measurements. It can be noted the negligence of acceleration based terms (the controllers is limited to damper and spring components and the inertia component is neglected) due to its very noisy nature. C_1, C_2, C_3 and C_4 categorize the communication layers' transfer functions applied the exchanged position and force measurements (Fig. 3.5). By restitution of (Eqs. 3.25 and 3.26) in (Eqs. 3.23 and 3.24), bilateral teleoperation control lows can be rearranged to take the following form:

$$Z_{cm}v_m + C_4e^{-sT_d}v_s = (1+C_6)F_m - C_2e^{-sT_d}F_s, \tag{3.27}$$

$$Z_{cs}v_s - C_1e^{-sT_d}v_m = -(1+C_5)F_s + C_3e^{-sT_d}F_m, \tag{3.28}$$

$$Z_{cm} := (Z_m + C_m) \quad , \quad Z_{cs} := (Z_s + C_s). \tag{3.29}$$

Eq. 3.27 and Eq. 3.28 describe teleoperator dynamics and can be rearranged under input-output form as in (Eqs. 3.3-3.6). Because the models in (Eqs. 3.3-3.6) are equivalent from stability analysis stand-point, the preferred model is the one that makes teleoperator stability analysis simpler. Hereafter the 4-Channel *hybrid model* (Eq. 3.5) is presented:

$$h_{11} = \frac{Z_{cm}Z_{cs} + C_1C_4e^{-2sT_d}}{(1+C_6)Z_{cs} - C_3C_4e^{-2sT_d}}, \tag{3.30}$$

$$h_{12} = \frac{C_2Z_{cs}e^{-sT_d} - C_4(1+C_5)e^{-sT_d}}{(1+C_6)Z_{cs} - C_3C_4e^{-2sT_d}}, \tag{3.31}$$

$$h_{21} = -\frac{C_3Z_{cm}e^{-sT_d} + C_1(1+C_6)e^{-sT_d}}{(1+C_6)Z_{cs} - C_3C_4e^{-2sT_d}}, \tag{3.32}$$

$$h_{22} = \frac{(1+C_5)(1+C_6) - C_2C_3e^{-2sT_d}}{(1+C_6)Z_{cs} - C_3C_4e^{-2sT_d}}. \tag{3.33}$$

Teleoperator detailed model is constructed and ready to be analysed and evaluated.

3.2 Design

First objective in teleoperation is to design a stable teleoperator that is capable of interacting with wide variety of human operators and environments. The energy based interpretation of teleoperator interaction with human and environment led to an energy based design [Colgate and Hogan, 1988]. The energy based design can be summarized in **Passivity-Based Control (PBC)** which focuses basically on reshaping the interaction energy between the dynamically interacting systems [Ortega et al., 2001] without paying attention to the inner states of the interacting systems. Considering a dynamic system (H) with an input $u \in \mathbb{R}^m$ and output $y \in \mathbb{R}^m$ and state vector $x \in \mathbb{R}^n$ where u and y are power variables:

$$H : \begin{cases} \dot{x} = f(x,u) \\ y = g(x,u). \end{cases} \tag{3.34}$$

The system dynamics is assumed to satisfy the following energy-balance equation as a universal property of physical systems:

$$\underbrace{E[x(t)] - E[x(0)]}_{\text{Stored energy}} = \underbrace{\int_0^t u^T(\tau) y(\tau) d\tau}_{\text{Supplied energy}} - \underbrace{D(t)}_{\text{dissipated}}, \tag{3.35}$$

where $E[x]$ is the total energy function, $D(t)$ is a non-negative function that represents the dissipated energy and the function $h(u,y) := u^T(t)y(t) : \mathbb{R}^m \times \mathbb{R}^m \longrightarrow \mathbb{R}$, represents energy supply rate function. Such a system is passive (stable) if it is dissipative and does not participate in energy producing. Dissipativity property of the system given by (Eq. 3.34) appears when the system stored energy is less than the supplied energy i.e. $D(t) \geq 0$ and:

$$E[x(t)] - E[x(0)] \leq \int_0^t u^T(\tau) y(\tau) d\tau. \tag{3.36}$$

This property facilitates the design of interconnecting dynamic systems. Passivity theorem provides the necessary tools to monitor and shape the interconnection energy to produce a passive coupling between dynamic systems and ensuring the system stability through monitoring its input-output relationship. Teleoperation as introduced in (Fig. 3.4) is a serial sequence of interconnecting one and 2-port networks. Therefore we limit our concern to the design of 1-port and 2-port networks and its application in teleoperator design [Desoer and Vidyasagar, 1975] [Colgate, 1988] [Sepulchre et al., 1997] [Khalil, 2002].

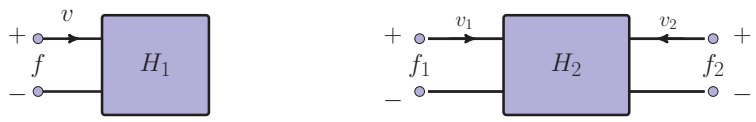

a.) One port network **b.) Two port network**

Figure 3.6: One and two-port networks as a basic components in teleoperation system

Definition 3.2.1. ***1-port network passivity [Colgate, 1988]:***
A one-port network, H_1 (Fig. 3.6.a), is said to be passive if and only if the energy flow through its identified port satisfies:

$$E(t) = \int_0^t f(\tau)\, v(\tau)\, d\tau \geq -c^2, \qquad \forall\, c \in \mathbb{Q}, \qquad v, f, E \in \mathbb{R} \tag{3.37}$$

where $-c^2 = E(0)$, a fixed number often associated with the initial stored energy($E(0)$). If the system H_1 has an impedance causality model $Z(s) = f(s)/v(s) \in \mathbb{R}$, then the system H_1 is passive if $Z(s)$ is positive real (PR) i.e. if and only if:

1. *$Z(s)$ has no poles in the right half plane.*
2. *Any imagunary poles of $Z(s)$ are simple and have positive real residues.* (3.38)
3. $\Re(Z(j\omega)) \geq 0, \qquad \forall \omega \geq 0.$

(Eq. 3.37) suggests that the supplied energy into the one-port network, quantified by the integral, is greater than its initial stored energy. In other-words, this energy is consumed (dissipated) by H_1 and the system does not inject any energy through its concerned interaction port. Systems that possess an admittance type causality can be also analysed through (Eqs. 3.38) as a consequence of (property 3.1.1).

Definition 3.2.2. ***2-port network passivity [Colgate, 1988]:***
Two-port network passivity is treated as a special case of N-port network passivity as follows:

A two-port network, H_2 (Fig. 3.6.b), is said to be passive if and only if the energy flow through its identified ports satisfies:

$$E(t) = \int_0^t \big(f_1(\tau)\, v_1(\tau) + f_2(\tau)\, v_2(\tau)\big)\, d\tau \geq -c^2 \tag{3.39}$$

for all admissible forces (efforts) (f_1, f_2) and velocities (flows) (v_1, v_2) with $-c^2 = E(0)$, the system's initial stored energy. If the system H_2 has an impedance causality model $f(s) = Z(s)v(s)$, $Z(s) \in \mathbb{R}^{2\times 2}$, $f = \big[f_1, f_2\big]^T$, $v = [v_1, v_2]^T$, then the system H_2 is passive if the matrix

($Z(s)+Z^{\dagger}(s)$) is non-negative definite Hermitian where $Z^{\dagger}(s)$ is the conjugate transpose of $Z(s)$, i.e. if and only if [Colgate, 1988]:

$$\begin{array}{ll} 1. & Z(s)+Z^{\dagger}(s) \text{ has no poles in the right half plane.} \\ 2. & \text{Any imaginary poles are simple and have positive real residues.} \\ 3. & Z(j\omega)+Z^{T}(-j\omega)\geq 0, \qquad \forall \omega \geq 0. \end{array} \tag{3.40}$$

Comparing the 2-port network in (Fig. 3.6.b) with the teleoperator model in (Fig. 3.4), one cannote that in the former case the energy flow is supposed to be in the H_2 network through both ports while in the latter the energy flows in teleoperator network through human-teleoperator interaction port and out the teleoperator network through teleoperator-environment interaction port. Hence the passivity condition in (Eq. 3.39) can be easily adapted by substituting (v_2) by $(-v_s)$. Furthermore, considering the immittance mapping $Y=\mathbb{P}u$ that encompasses (Eq. 3.3-3.8), Teleoperator stability study becomes:

Definition 3.2.3. ***Teleoperator stability [Hashtrudi-Zaad and Salcudean, 2001]:***
A LTI 2-port network teleoperator as in (Fig 3.4) is passive if and only if:

$$E(t) = \int_0^t Y^T(\tau)u(\tau)d\tau = \int_0^t \left(f_m(\tau)\ v_m(\tau) - f_s(\tau)\ v_s(\tau)\right)d\tau \ \geq\ 0, \qquad \forall t \geq 0 \tag{3.41}$$

for all admissible forces (f_*) and velocities (v_*) where ($*=m,s$) stands for master and slave. Considering the immittance mapping (i.e. $Y=\mathbb{P}u$) and p_{ij}, $(i,j=1,2)$ are the elements of the immittance matrix $\mathbb{P}$, the condition (Eq 3.41) is valid if and only if:

$$\begin{array}{ll} 1. & p_{11} \text{ and } p_{22} \text{ have no poles in the open right half plane.} \\ 2. & \text{Any imaginary poles of } p_{11} \text{ and } p_{22} \text{ are simple and have positive} \\ & \text{real residues, and for all } \omega \geq 0 : \\ 3. & \Re\{p_{11}(j\omega)\}\geq 0, \\ & \eta_p(\omega) := -\dfrac{\Re\{p_{12}\ p_{21}\}}{|p_{12}\ p_{21}|}+2\dfrac{\Re\{p_{11}\}\,\Re\{p_{22}\}}{|p_{12}\ p_{21}|} \\ & \qquad := -cos(\angle p_{12}\ p_{21})+2\dfrac{\Re\{p_{11}\}\,\Re\{p_{22}\}}{|p_{12}\ p_{21}|}\geq 1. \end{array} \tag{3.42}$$

Where $cos(\angle z) := \dfrac{\Re\{z\}}{|z|}$ for any complex $(z=\sigma+j\omega)$. The presented condition in (Eq. 3.42) are addressed in the literature as Llewellyen's criteria [Adams and Hannaford, 1999] [Hashtrudi-Zaad and Salcudean, 2002] and used to investigate and design a stable teleoperator. Based on (Eq. 3.8), teleoperator's stability using Llewellyen's criteria can use any type of representation in (Eqs. 3.3-3.6), i.e. $\eta_p(\omega)=\eta_Z(\omega)=\eta_Y(\omega)=\eta_H(\omega)=\eta_G(\omega)$. As a conclusion, the simplest representation of the teleoperator can be used to design the stability and state a clear conclusion on the effect of the controller parameters used in master and slave on the overall teleoperator's stability. That is because the absolute stability

in Llewellyen's criteria depends only on the master slave network parameters and is not subject to environment and/or human dynamic behaviour. Finally, stability margins of a passivity-based teleoperator can be assigned through the shortage and excess of passivity [Sepulchre et al., 1997] [Jazayeri and Tavakoli, 2015]. This margins can be used to improve the system transparency (see following section) through stability-transparency trade-off process.

3.3 Evaluation

Once the teleoperator is designed and the stability margins are assigned, the system performance has to be evaluated and the possible opportunities to improve its transparency has to be investigated. Teleoperator performance can be evaluated through at least one of the following measure:

Definition 3.3.1. ***Teleoperator ideal response:*** *[Yokokohji and Yoshikawa, 1994]*
Teleoperator has one of the following ideal responses:
Ideal Response I: $x_m \equiv x_s$ *whatever the environment dynamics.*
Ideal Response II: $f_m \equiv f_s$ *whatever the environment dynamics.*
Ideal Response III: $x_m \equiv x_s$ *and* $f_m \equiv f_s$ *whatever the environment dynamics.*

Definition 3.3.2. ***Impedance matching:*** *[Lawrence, 1993]*
A teleoperator (MSN) (Fig. 3.4) is transparent under the kinematic correspondence condition $v_m = v_s$ *if and only if:*

$$Z_{to} \equiv Z_e \tag{3.43}$$

where $Z_{to} = f_m / v_m$ *is the impedance felt by operator at human-master interaction port and* $Z_e = f_s / v_s$ *is the environment impedance at sensed at slave-environment interaction port.*

Definition 3.3.3. ***The Dynamic range of achievable impedance "*** Z_{width} ***":*** *[Colgate and Brown, 1994] [Hashtrudi-Zaad and Salcudean, 2001]*
The performance of a teleoperator (MSN) (Fig. 3.4) can be evaluated through the dynamic range of impedances that can be reflected as follows:

$$Z_{tomin} := Z_{to}|_{Z_e=0}, \tag{3.44}$$

$$Z_{towidth} := Z_{to}|_{Z_e \longrightarrow \infty} - Z_{tomin}, \tag{3.45}$$

where Z_{to} *and* Z_e *have the same definition as in (Eq. 3.43),* Z_{tomin} *is the impedance felt by human when the remote slave is in free-space (unconstrained) motion and* $Z_{towidth}$ *represents the range of possible impedances that can be reflected through the teleoperator in question.*

Transparent teleoperator is stiff and massless and can be achieved when $\|Z_{tomin}\| \longrightarrow 0$ *and* $\|Z_{towidth}\| \longrightarrow \infty$.

Stability-transparency trade-off:

Considering the hybrid representation of MSN (eq. 3.7), the impedance matching as introduced in (definition 3.3.2) can be reformulated under the following form [1]:

$$Z_{to} = \frac{h_{11} + \triangle h.Z_e}{1 + h_{22}Z_e} \tag{3.46}$$

$$\triangle h := h_{11}h_{22} - h_{12}h_{21}. \tag{3.47}$$

To achieve a transparent performance as in (eq. 3.43) and by considering the ideal kinaesthetic master-slave coupling as in (definition 3.3.1-*ideal performance III*), the hybrid matrix has to have the following form:

$$\begin{bmatrix} F_m \\ -\dot{x}_s \end{bmatrix} = \begin{bmatrix} h_{11} & h_{12} \\ h_{21} & h_{22} \end{bmatrix} \begin{bmatrix} \dot{x}_m \\ F_s \end{bmatrix} = \begin{bmatrix} 0 & 1 \\ -1 & 0 \end{bmatrix} \begin{bmatrix} \dot{x}_m \\ F_s \end{bmatrix}. \tag{3.48}$$

Examining the stability of this ideal system (eq. 3.48) though Llewellyen's criteria gives:

1. $\Re\{(h_{11})\} = 0, \Re\{(h_{22})\} = 0,$
2. h_{11} and h_{22} have no imaginary poles,
3. $\eta_h(\omega) = -\frac{\Re\{h_{12}h_{21}\}}{|h_{12}h_{21}|} + 2\frac{\Re\{h_{11}\}\Re\{h_{22}\}}{|h_{12}h_{21}|} = 1,$

suggesting that master and slave mechanisms have no dynamics as in (conditions 1 & 2) and the MSN is marginally stable. These conditions are unachievable. Therefore, perfect transparency and stability are conflicting parameters and a trade-off is necessary in any design process. To provide an insight of these trade-offs process, the ideal response of a haptic display is borrowed into teleoperation as in (definition 3.3.3). Consequently, the performance measures in (definition 3.3.3) become:

$$Z_{tomin} = Z_{to}|_{Z_e \longrightarrow 0} = \frac{\triangle h}{h_{22}} - \frac{h_{12}\,h_{21}}{h_{11}} = h_{11} \tag{3.49}$$

$$Z_{towidth} = Z_{to}|_{Z_e \longrightarrow \infty} - Z_{to}|_{Z_e \longrightarrow 0} = -\frac{h_{12}\,h_{21}}{h_{11}}. \tag{3.50}$$

A simple substitution of (eqs. 3.30-3.33) in (eqs. 3.49 and 3.50) gives:

$$Z_{tomin} = \frac{Z_{cm}Z_{cs} + C_1C_4e^{-2sT_d}}{(1 + C_6)Z_{cs} - C_3C_4e^{-2sT_d}} \tag{3.51}$$

$$Z_{towidth} = -\frac{\left(C_2Z_{cs}e^{-sT} - C_4(1 + C_5)e^{-sT}\right)\left(C_3Z_{cm}e^{-sT} + C_1(1 + C_6)e^{-sT}\right)}{\left(Z_{cm}Z_{cs} + C_1C_4e^{-2sT_d}\right)\left((1 + C_6)Z_{cs} - C_3C_4e^{-2sT_d}\right)}. \tag{3.52}$$

1. The required prove is presented in Appendix B

Considering that the time delay is negligible ($T_d = 0$) for simplicity, to achieve an optimized transparent teleoperator (Eq. 3.48) and (definition 3.3.3), the bilateral controller parameters have to satisfy the following conditions:

$$C_1 = Z_{cs} \tag{3.53}$$
$$C_2 = 1 + C_6 \tag{3.54}$$
$$C_3 = 1 + C_5 \tag{3.55}$$
$$C_4 = -Z_{cm}, \tag{3.56}$$

such that master and slave dynamics are cancelled out using the inverse dynamics, and the local interaction force is assured to track this on the remote site.

3.4 Conclusion

Through this chapter we explored the necessary tools to design and evaluate a bilateral teleoperator. The energy interpretation of human-master, slave-environment interaction and haptic signals transmission enabled the teleoperator reformulation (modelling) under network theory context based on physical systems duality. Furthermore, the passivity based stability design of networks is adapted to fit bilateral teleoperator under the form of Llwellyens criteria (eq. 3.42). Finally, the designed teleoperator performance is evaluated using transparency design measure (definitions 3.3.1-3.3.3). The capture is closed with a numerical example to demonstrate the usability of the introduced tools.

CHAPTER

4 On the Selection of Teleoperation Control Architecture

Preamble

Telesurgery has been more and more popular in robot-assisted medical intervention. Most existing teleoperation architectures for medical applications adopt 2-channel architectures. The 2-channel architectures have been evaluated in literature and it is shown that some architectures, e.g. position-force (P-F), are able to provide the surgeon a reliable haptic sense of the treated environment (transparency). However, stability of these P-F architecture is still a considerable concern especially when physiological disturbances exist in the remote environment. Furthermore, This architecture and the other 2-Channel architectures offer a limited choice of tunable parameters which constrains the possibility to obtain a satisfactory stability-transparency tradeoff.

On the other hand, P-PF architecture is proved to provide a convenient alternative. With one more channel, 3-channel teleoperation architectures present promising options due to their augmented design flexibility. This chapter [Albakri et al., 2013] evaluates stability and transparency of general 3-channel bilateral teleoperation control architectures and provides a design framework guidelines to improve the architectures' stability robustness and optimize the transparency. Simulation evaluations are provided to illustrate how the optimal 3-channel teleoperation architecture is chosen for medical applications given their dedicated requirements.

4.1 Introduction

Telesurgery integrates MSN in operating room and represents a sensitive application due to the treated environment nature. Providing the surgeon with faithful kinaesthetic representation of the manipulated tissue biomechanical properties is proved to improve the surgical intervention quality. As previously introduced through the precedent chapters, this kinaesthetic coupling between surgeon and treated tissues using MSN is evaluated by means of transparency and can be achieved by bilaterally controlling master and slave modalities. It is also shown that an optimally stable teleoperator is marginally stable. Therefore a stability-transparency trade-off is necessary.

The main idea of bilateral teleoperation is to control robot-environment interaction (power) variables at each site such that they are forced to track the remote interaction variables. The power variables in mechanical interactions are force (F) as *effort* and velocity ($v = \dot{x}$) as *flow*. In other words, position (P) and force (F) information of each interaction are necessary to be exchanged with the remote site. Each signal is transmitted through one communication channel. Having 2-port teleoperator (i.e. Human-master and slave-environment interconnection) means there is four signals to be exchanged (P_*, F_* with $* = m,\ s$ for master and slave) and therefore four channels. As a conclusion, it is thought that a complete transparency can be achieved by applying a 4-channel control architecture [Lawrence, 1993] which has been extended in [Hastrudi-Zaad and Salcudean, 1999] [Hashtrudi-Zaad and Salcudean, 2002] by adding a local force controller at master and slave sites to improve stability-transparency trade-off possibilities.

Due to its technical and technological implementation challenges, 4-channel architecture is used in limited number of applications. 2-channel control architectures [Hashtrudi-Zaad and Salcudean, 2002] are preferred due to their simplicity (less number of channels reduces the cost, analysis burden, implementation time ...) where each site sends and receives one signal (P or F). It has been recently proved that not all the four channels are necessary to achieve an optimal transparency [Naerum and Hannaford, 2009] [Naerum et al., 2012]. Unfortunately, 2-channel architectures are limited with the following facts:

1. Not all the available 2-channel architectures are transparent. Transparent architecture appears when the two remote sites exchange different signals.
2. Transparent architectures suffer from a limited available margins to perform stability-transparency trade-offs.

In telesurgical context, some 2-channel control architectures (CA) are compared with one of the 3-channel CAs in [Çavuşoğlu et al., 2002a]. With one additional exchanged information, the concerned 3-channel CA showed a superior performance in comparison with the studied 2-channel CAs [Flemmer and Wikander, 2003] [Kubo et al., 2007] [Susa et al., 2008] [Zandsteeg et al., 2010] [Sherman et al., 2000]. Unfortunately, to the author best knowledge, there is no complete discussion of all the 3-Channel CAs.

This chapter uses the modelling, analysis and evaluation tools presented in the precedent chapter to perform a comparative study of all 3-channel CAs and to provide simultaneously the teleoperator designer with initial guidelines to perform a convenient stability-transparency trade-off optimization. The study is limited to impedance-impedance type MSN (i.e. impedance like master and impedance like slave [1]). Furthermore, the surgical applications require a low inertia master and slave mechanisms, low frequencies of applications, low impedances, negligible time delay and highly sensitive teleoperator which has an impedance discrimination step less than human threshold sensitivity (JND). Finally, simulation studies are carried out to evaluate different architectures and illustrate how an optimal 3-channel architecture is chosen for a soft tissue telesurgery application scenario.

Notation

In this and the following chapters, teleoperation CA will be addressed by the names of communication channels that combine the two remote sites. As the human operator is the source of injected energy, we propose to call the control architecture by a series of letters. Each letter stands for one communication channel. Starting with the signals sent from master site to slave followed by dash and then by the signals sent from slave to master, the notation is as follows (Fig. 4.1):

1. ***4-channel control architecture:*** referred as $(PF-PF)$.
2. ***2-channel CAs:*** which are $(P-P)$, $(P-F)$, $(F-P)$ and $(F-F)$
3. ***3-channel CAs:*** which are $(P-PF)$, $(F-PF)$, $(PF-P)$ and $(PF-F)$

Each architecture of 2-channel and 3-channel groups can be directly deduced from 4-channel CA by setting the corresponding removed communication channel transfer function to zero. Fig. 4.1 provides a graphical representation of these CAs. The architectures in green are considered as transparent architectures while those in blue are considered non-transparent architectures because exchanging two different signals between the two remote sites is a necessary condition [Naerum and Hannaford, 2009]. Furthermore, it is worth to note that these notations are the inverse to the conventions used in [Hashtrudi-Zaad and Salcudean, 2001] [Hashtrudi-Zaad and Salcudean, 2002] where the used notation starts with the signals feed-forwarded from slave to master. The used notation in this document follows the natural sequence of teleoperation system where the master send a command to the slave robot and receives a feedback.

Modelling, analysis and evaluation tools

To perform the intended comparative study we start from the LTI model of master and slave control loop in bilateral teleoperation context presented in (Eqs. 3.27-3.29). The con-

1. By definition, an impedance device applies force to its environment in response to its measured position [Adams and Hannaford, 1999]

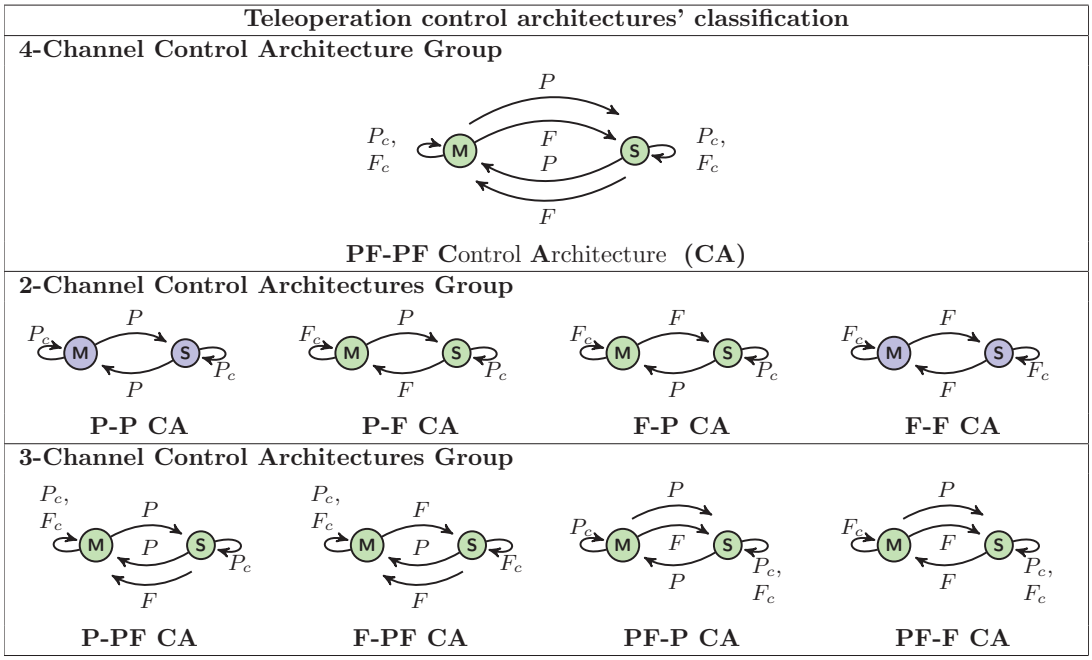

Figure 4.1: Bilateral Control Architectures, M: master, S: slave, P, Pc position signal and position based control, F and F_c force and force based control.

trol low for each 3-channel CA is deduced directly from this model by substituting the removed channel gain to zero. To analyse the stability of the CA in question, the simplest model of (Eqs. 3.3 - 3.6) will be considered as the condition (Eq. 3.8) is always valid. Stability is examined using Llewellyen's criteria (definition 3.2.3 - Eq. 3.42). On the other hand, transparency of the examined CA is evaluated through the dynamic range of achievable impedances introduced in definition (3.3.3 Eqs. 3.44-3.47, 3.49-3.52) which is essentially based on hybrid model representation of (Eqs. 3.5, 3.30-3.33).

Finally, it is worth to repeat that to carry out our intended comparative study and derive a useful generic conclusion, we kept the conventions imposed in [Lawrence, 1993] and [Hastrudi-Zaad and Salcudean, 1999], meaning that the force signals are normally passed through scalar positive gains C_2, C_3 C_5 and C_6. In practice, force signals are noisy and a filtering step has to be performed with condition that the used filter is passive (i.e. it has positive real part). In the following (table 4.1), we give a small reminder of the 4-Channel Extended Lawrence Architecture (ELA) block diagram components and their meaning with unified values to serve for numerical analysis of each one of the 3-Channel CAs and for comparative studies.

After addressing the analysis of each architecture, its stability and performance will

Table 4.1: Teleoperator Parameters

Block	Type	Model	Simulation Parameters	
			Simulation #1	Simulation #2
Z_m	Mass (Inertia)	$M_m s$	$00.7s$	$00.7s$
Z_s	Mass (Inertia)	$M_s s$	$50.0s$	$50.0s$
C_m	Damper spring (PI)	$B_m + \frac{K_m}{s}$	$50 + \frac{630}{s}$	$100 + \frac{1500}{s}$
C_s	Damper spring (PI)	$B_s + \frac{K_s}{s}$	$800 + \frac{40000}{s}$	$1100 + \frac{50000}{s}$
C_5	Scalar gain	–	0.1	0.7
C_6	Scalar gain	–	0.1	0.7
$M_m, M_s > 0$ & $B_m, B_s, K_m, K_s, C_5, C_6 \geq 0$				
M, B, and K are respectively a mass, damping and stiffness coefficients				
C_1	Impedance filter	–	$800 + \frac{40000}{s}$	$5500 + \frac{50000}{s}$
C_2	Scalar gain	–	1.1	1
C_3	Scalar gain	–	1.1	1
C_4	Impedance filter	–	$-(50 + \frac{630}{s})$	$-(30 + \frac{850}{s})$
T_d	Time delay		0 (ms)	0.02 (20 ms)
Z_e	Environment Impedance (Soft tissue model)	$B_e + \frac{K_e}{s}$	$120 + \frac{650}{s}$	(Kelvin-Voigt model)

be analysed experimentally by performing a comparison between a set of four different experiments that are the following:

* 1^{st} Sim. : the 3-channel CA in question using the parameters of sim. #1 in table 4.1.
* 2^{nd} Sim. : the 3-channel CA in question using the parameters of sim. #2 in table 4.1.
* 3^{rd} Sim. : improving the CA stability bandwidth by changing the controller parameters of sim. #1 in table 4.1 according to the excluded design guideline [2]. This simulation is intended to visualise the idea of stability-transparency trade-off.
* 4^{th} Sim.: the 4-channel CA using the parameters of sim. #1 in table 4.1. Sim. #1 employs the optimized configuration and can, in 4-channel CA case, provide a complete (optimized) transparency. This simulation is considered as a reference with which the performance of the studied 3-channel CA will be compared.
* MSN's parameters are considered as in [Hashtrudi-Zaad and Salcudean, 2001] in order to enable the performance comparison between 2 and 3-channel CAs if needed.
* A MSD model is used to represent the operated environment. Often, the environment in surgical context is organs' soft tissue. The mass coefficient of the identified

2. The design guidelines of each CA is deduced based on stability evaluation of the considered MSN using Llewellyn criteria. It gives an indication on how to modify the bilateral controller parameters such that to increase (or decrease) the stability bandwidth. See for example (Eq.4.12) as a design guideline for P-PF CA.

MSD model for soft tissues are generally very small and negligible which gives rise to Kelvin-Voigt model. Because the accuracy of tissue model is not the focus of this study, the Kelvin-Voigt is considered for its simplicity. The used model in (table 4.1) is identified through ex-vivo experiment on Lamb's heart tissue (Appendix A).

Performing a comparative analysis of these four simulations on the same scale highlights geometrically the characteristics of the analysed CA and the adequate methodology of employing the proposed guidelines. That is because the 1^{st} simulation of table 4.1 adopts the optimal transparency conditions presented in (Eqs. 3.53-3.56) with a neglected presence of time delay while the 2^{st} simulation of table 4.1 is a non optimized CA with time delay. The performance of each architecture will be evaluated by comparing Z_{to} defined in (Eq. 3.46) with Z_e presented in the (table 4.1). The values of Z_e are experimentally estimated values of Kelvin-Voigt modelled lamb's heart tissue.

4.2 Contributions

First step in realizing a transparent haptic teleoperator is the careful and prudent selection of the applied CA. It is proved that not all the 4 channels are necessary to provide transparency [Naerum and Hannaford, 2009]. It is also demonstrated that to establish a transparent teleoperator, the two remote sites have to exchange different signals [Naerum and Hannaford, 2009]. This fact enabled to distinguish between transparent CAs (in green) and non-transparent CAs (in blue) (Fig. 4.1).

4-channel and 2-channel CAs are well analysed in the literature [Lawrence, 1993] [Hashtrudi-Zaad and Salcudean, 2001]. For medical application, the architectures $(P-P)$, $(P-F)$ and $(P-PF)$ are analysed and their performances are compared [Cavusoglu et al., 2001] [Çavuşoğlu et al., 2002a]. As a conclusion to their analysis the 3-channel CA showed a higher performance in comparison with the 2-channel CAs. This fact rises the following question: what about the three other 3-channel CAs? It can be easily found through surveying the literature the lack of such necessary comparative study [Sherman et al., 2000] [Hashtrudi-Zaad and Salcudean, 2002] [Flemmer and Wikander, 2003] [Okamura, 2004] [Abbott and Okamura, 2006] [Christiansson and van der Helm, 2007] [Kubo et al., 2007] [Susa et al., 2008] [Zandsteeg et al., 2010] [Son et al., 2011] [Sanchez et al., 2013].

This first contribution aims at providing a comparative study of all the possible teleoperation CAs that rise from 3 communication channel combinations in MSN for surgical application. The CAs under examination are $(P-PF)$, $(F-PF)$, $(PF-P)$ and $(PF-F)$ CAs (Fig. 4.2). Furthermore, a design guideline to perform an efficient stability-transparency trade-off is provided for each architecture. Finally, given a specific application, a methodology to select a suitable CA is illustrated through simulation studies.

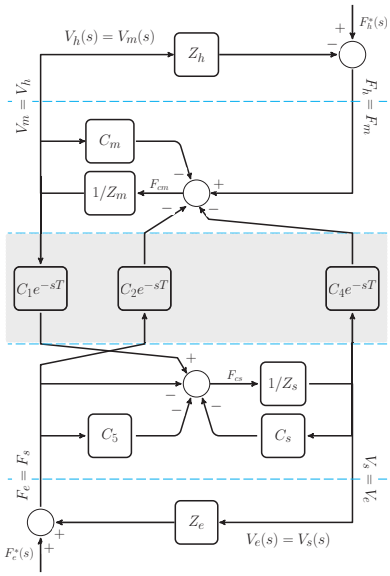

a.) P-PF Structure

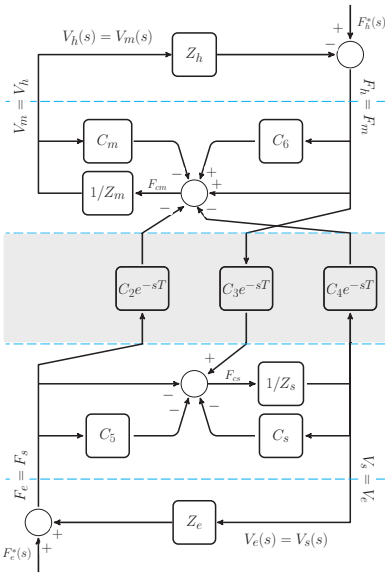

a.) F-PF Structure

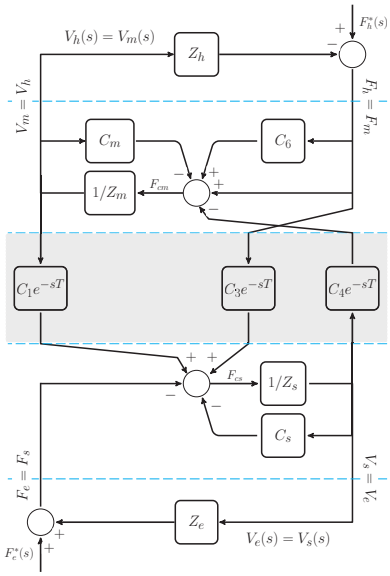

a.) PF-P Structure

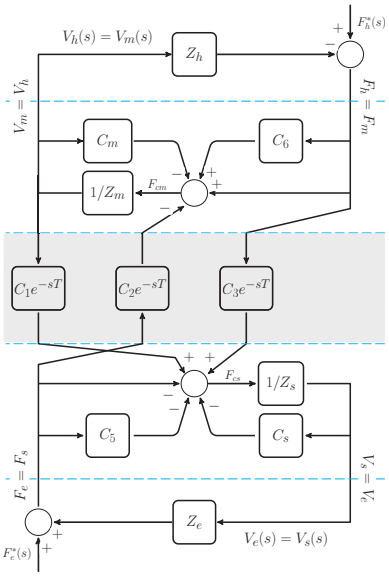

a.) PF-F Structure

Figure 4.2: Three-Channel teleoperation control architectures

4.3 Stability and Performance Analysis of 3-Channel Architectures

The target application of this study is haptic teleoperation on soft tissues which are subject to motion disturbance (e.g. abdomen and thoracic robotic assisted surgeries). The architecture's stability has to be guaranteed for a relatively wide range of frequencies. To maximize transparency of teleoperation on soft tissues, good performance values Z_{tomin} and $Z_{towidth}$ are expected. Nevertheless enough range of impedances $Z_{towidth}$ that can be reflected to the human operator is necessary, minimizing $|Z_{tomin}|$ (i.e. $|Z_{tomin}| \rightarrow 0$) is still a priority in medical telesurgery context since most operations are in contact with soft tissue or in free space. In fact, the condition $|Z_{tomin}| \rightarrow 0$ implies that the sensed impedance of the teleoperator is small enough to distinguish between free-space and in-contact state of slave with a small impedance soft tissues. ¿In the following, each one of 3-channel CAs is brought to the focus of interest to be analysed in terms of stability and transparency, to summarize the factors that affect each of this measures and to provide guidelines to perform effective stability-transparency required trade-offs.

4.3.1 Position-Position Force Control Architecture ($P-PF$, $Fig.4.2.a$)

This architecture can also be called as (Flow forward, Flow backward, Effort backward) and has already been used in medical context [Abbott and Okamura, 2006]. It can be deduced from ELA by setting direct effort forward gain to zero, i.e. $C_3 = 0$. Sherman et al. [Sherman et al., 2000] showed through experiments that this architecture has better fidelity[3]. over P-P and P-F architectures. Nevertheless, no explicit evaluation of its stability and performance has been provided in literature.

Absolute Stability

Since $\eta_h = \eta_z = \eta_g = \eta_y$, to make the stability analysis easier and to extract a useful clear guidelines and conclusions, the matrix that provides the simplest representation, here the impedance matrix $\mathbb{Z}$, will be used to evaluate the absolute stability of P-PF architecture. The impedance matrix in the model given by Eq. 3.3 has the following elements:

$$z_{11} = \frac{(1+C_5)Z_{cm} + C_1C_2e^{-2sT_d}}{(1+C_5)(1+C_6)} \tag{4.1}$$

$$z_{12} = \frac{C_2Z_{cs} - C_4(1+C_5)}{(1+C_5)(1+C_6)}e^{-sT_d} \tag{4.2}$$

3. The fidelity of haptic feedback is defined as the ratio between transmitted impedance (Z_{to}) discrimination to the environment impedance (Z_e) discrimination i.e. (fidelity = $\left|\frac{dZ_{to}}{dZ_e}\right|$)

$$z_{21} = \frac{C_1}{(1+C_5)} e^{-sT_d} \tag{4.3}$$

$$z_{22} = \frac{Z_{cs}}{(1+C_5)}. \tag{4.4}$$

Considering Llewellyn's criteria (definition 3.2.3 - Eq. 3.42), the positive realness of $\Re\{z_{11}\}$ and $\Re\{z_{22}\}$ implies the passivity of the master and slave robots when they are not coupled, that is when $C_i = 0$ $(i = 1,...,4)$. The passivity of the decoupled master (z_{11}) and slave (z_{22}) is guaranteed since Z_{cm} and Z_{cs} are passive:

$$\Re\{z_{11}\}|_{C_{i=1,...,4}=0} = \Re\{\frac{(1+C_5)Z_{cm}}{(1+C_5)(1+C_6)}\} = \frac{\Re\{Z_{cm}\}}{(1+C_6)} = \frac{B_m}{(1+C_6)} \geq 0 \tag{4.5}$$

$$\Re\{z_{22}\}|_{C_{i=1,...,4}=0} = \frac{\Re\{Z_{cs}\}}{(1+C_5)} = \frac{B_s}{(1+C_5)} \geq 0, \tag{4.6}$$

where:

$$\Re\{Z_{cm}(j\omega) = \Re\{M_m s + B_m + \frac{K_m}{s}\}|_{s=j\omega} = B_m, \tag{4.7}$$

$$\Re\{Z_{cs}(j\omega) = \Re\{M_s s + B_s + \frac{K_s}{s}\}|_{s=j\omega} = B_s. \tag{4.8}$$

Noting that because C_5 and C_6 are positive scalars, the division (multiplication) of the numerator and the denominator of any fraction by $(1+C_5)$ and/or $(1+C_6)$ does not affect the conclusion. Moreover, stability of coupled master-slave via $(P-PF)$ teleoperation CA can be evaluated through the third condition of (Eq. 3.42) as follows:

$$\eta_{p-pf}(\omega) = \eta_{1p-pf}(\omega) + \eta_{2p-pf}(\omega) = -cos(\angle z_{12}z_{21}) + 2\frac{\Re\{z_{11}\}\Re\{z_{22}\}}{|z_{12}z_{21}|} \tag{4.9}$$

$$\begin{aligned} &= -cos(\angle \frac{C_1}{(1+C_5)} \frac{C_2 Z_{cs} - C_4(1+C_5)}{(1+C_5)(1+C_6)} e^{-2j\omega T_d}) \\ &+ 2\frac{\Re\{\frac{(1+C_5)Z_{cm}+C_1C_2e^{-2j\omega T_d}}{(1+C_5)(1+C_6)}\}\Re\{\frac{Z_{cs}}{(1+C_5)}\}}{|\frac{C_1}{(1+C_5)}\frac{C_2Z_{cs}-C_4(1+C_5)}{(1+C_5)(1+C_6)}e^{-2j\omega T_d}|} \end{aligned} \tag{4.10}$$

$$\begin{aligned} &= sgn(1+C_6)[-cos(\angle C_1(C_2Z_{cs} - C_4(1+C_5))\ e^{-2j\omega T_d}) \\ &+ 2\frac{\Re\{(1+C_5)Z_{cm} + C_1C_2e^{-2j\omega T_d}\}\Re\{Z_{cs}\}}{|C_1(C_2Z_{cs} - C_4(1+C_5))|}] \geq 1. \end{aligned} \tag{4.11}$$

To avoid the effect of time delay on $\eta_{1p-pf}(\omega)$, the architecture's absolute stability is guaranteed if $\eta_{2p-pf}(\omega) \geq 2$, that is because $\eta_{1p.pf(\omega)} = -cos(\angle\chi) \in [-1,+1]$ for any complex χ. Moreover, $|e^{-2j\omega T_d}| = 1$ limits time delay effect only to the numerator of η_{2p-pf}. Therefore, stability of time delayed P-PF is guaranteed when the following condition holds:

$$\Re\{Z_{cm}\} \geq \frac{-C_2}{(1+C_5)}\Re\{C_1e^{-2j\omega T_d}\} + \frac{sgn(1+C_6)|C_1|}{(1+C_5)\Re\{Z_{cs}\}}|C_2Z_{cs} - C_4(1+C_5)|. \tag{4.12}$$

This equation shows clearly that the master damping ($\Re\{Z_{cm}\} = B_m$) has a significant effect on the system's stability and has to be greater than a minimum amount regulated by (4.12). Time delay effect can be studied through numerical analysis. For example, if C_1 is designed to take the form $C_1 = a + \frac{b}{s}$, then:

$$\Re\{C_1 e^{-2j\omega T_d}\} = \sqrt{a^2 + \frac{b^2}{\omega^2}}\ \ cos(\varphi - 2\omega\ T_d), \qquad \varphi = \arctan(-\frac{b}{a\omega}) \tag{4.13}$$

and therefore $\Re\{C_1 e^{-2j\omega T_d}\} \in [-a,\ a]$ for high frequencies i.e. when $\omega \gg 10(rad/s)$, that is because $(\frac{b^2}{\omega^2})$ becomes too small and negligible. Otherwise, $|C_1|$ has a dominant effect. In the OR, time delay induced in the telesurgical system is very small and hence negligible. Therefore, the absolute stability condition can be simplified to:

$$\eta_{p.pf}(\omega) = sgn(1+C_6)[-cos(\angle C_1(C_2 Z_{cs} - C_4(1+C_5))) + 2\frac{\Re\{(1+C_5)Z_{cm} + C_1 C_2\}\Re\{Z_{cs}\}}{|C_1(C_2 Z_{cs} - C_4(1+C_5))|}] \geq 1. \tag{4.14}$$

In this case, it should be noticed that $\eta_{1p.pf}(\omega) = -cos(\angle T(j\omega))$, where $T(j\omega)$ is a transfer function that can be assigned by the designer and written under the form $T(s) = a_t s + b_t + \frac{c_t}{s}$. This characteristic enables the designer to improve the stability margin of the architecture using $\eta_{1p.pf}(\omega)$ by assigning suitable parameters to $T(s)$. The architecture's stability investigation is performed using the condition $\eta_{2p.pf}(\omega) \geq 2$ and:

$$\Re\{Z_{cm}\} \ \geq\ -\frac{C_2\Re\{C_1\}}{(1+C_5)}\ \frac{sgn(1+C_6)|C_1|}{(1+C_5)\Re\{Z_{cs}\}}|C_2 Z_{cs} - C_4(1+C_5)|. \tag{4.15}$$

Increasing the damping on the master/slave robots i.e $\Re\{Z_{cs}\}$, $\Re\{Z_{cm}\}$ and/or decreasing $|C_1|$ especially $\Re\{C_1\}$ improves the architecture's stability. Moreover, because:

$$\frac{|C_1|}{\Re\{Z_{cs}\}}|C_2 Z_{cs} - C_4(1+C_5)| \ \geq\ 0 \qquad \forall\ \omega\ \in [0,\ \infty], \tag{4.16}$$

designing $-C_2\Re\{C_1\}$ and $sgn(1+C_6)$ in a way to have counteractive signs will improve the stability. Because C_2 is frequency independent, the stability robustness can be enhanced by scaling down the slave-environment interaction force before feedback it to the master with $0 \leq C_2 \leq 1$. Nevertheless, this tuning has a counteractive effect on architecture's transparency where it reduces the range of impedances that can be reflected to the teleoperator.

To visualize the aforementioned analytical main points, a simulation study is carried out using the parameters addressed in (Table 4.1) for *simulation #1* and *simulation #2*. A third simulation (*simulation #3*) is added considering the aforementioned analysis recommendations to improve the systems stability margins. (Fig. 4.3 & 4.4) highlight the following main points:

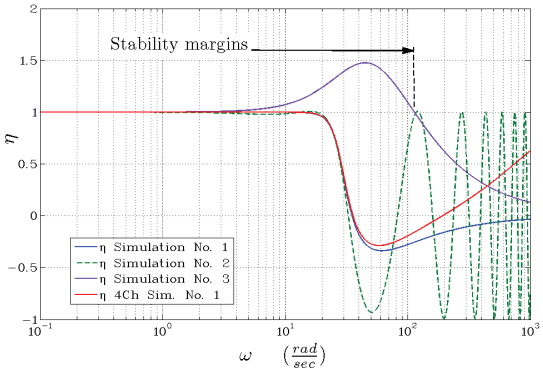

Figure 4.3: Stability condition $\eta \geq 1$

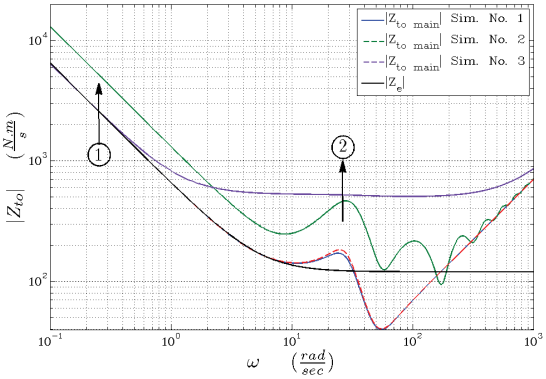

Figure 4.4: Transparency: $Z_{to} \equiv Z_e$

- $(P-PF)$ CA provides performance and stability margins (in blue) that are remarkably close to these of 4-channel CA (in red) and which are convenient for surgical activities ($\omega \in [0,\ 20]\ \frac{rad}{s}$).
- Time delay reduces stability margin and its effect appears clearly for activities with high frequencies (simulation 2 in green includes only 20 ms of time delay).
- Considering (Eq. 4.15), stability margins can be improved by increasing B_m, B_s and $|Z_{cs}|$. Therefore, by applying the following changes ($B_m = 500\frac{N.m}{s}$, $B_s = 4000\frac{N.m}{s}$ and $K_s = 1.e^5\frac{N}{m}$) to simulation #1, simulation #3 shows a clear improvement in stability margins as in (Fig. 4.3) but as the same time reduces remarkably the system transparency (Fig. 4.4). The transparency degradation can be clearly seen by comparing $|Z_{to}|_{simulation\ No.\ 3}$ to $|Z_e|$ at region 2.
- In MDS LTI model, the stiffness affects static and quasi-static condition (i.e. low frequencies), the damper affects the mid-range frequencies i.e. $\omega \in [1,\ 100]\ \frac{rad}{s}$ while the effect of the mass appears for high frequencies ($\omega \geq 100\ \frac{rad}{s}$). This fact can be used as a design guideline where increasing the controller stiffness at master and/or slave site will appear at region (1) in (Fig. 4.4) while increasing the controller damping effect will appear in the region (2).

Transparency

The performance is analysed using (Eqs. 3.44-3.47, 3.49-3.52) as follows:

$$Z_{tomin} = h_{11} = \frac{Z_{cm}}{(1+C_6)} + \frac{C_1\ C_4 e^{-2sT_d}}{(1+C_6)Z_{cs}} \tag{4.17}$$

$$Z_{towidth} = -\frac{h_{12}\ h_{21}}{h_{22}} = \frac{C_1 e^{-2sT_d}}{(1+C_5)(1+C_6)Z_{cs}}[Z_{cs}C_2 - C_4(1+C_5)]. \tag{4.18}$$

Because Transparency evaluation is characterized by the study of $|Z_{tomin}|$ and $|Z_{towidth}|$ and considering $|e^{-2j\omega T_d}| = 1$, the role of time delay is reduced to only affecting $|Z_{tomin}|$. As it is already mentioned, good performance can be achieved if $|Z_{tomin}| \to 0$ and $|Z_{towidth}| \to \infty$. $|Z_{tomin}| = 0$ is achieved for non-delayed system when $C_1 = Z_{cs}$ and $C_4 = -Z_{cm}$. However, since mass in Z_{cm}, and Z_{cs} cannot be zero, perfect transparency cannot be achieved and has to be subject to a trade-off with the absolute stability margin. This can be easily seen by substituting these two conditions in the original stability condition of non-delayed system. Indeed, using a, b in C_1, C_4 as $C_1 = a.Z_{cs}$ and $C_4 = -b.Z_{cm}$ may help to obtain better trade-off between stability and transparency. $|Z_{tomin}|$ can also be improved by decreasing $|C_1|$ which will reduce the range of impedances that can be reflected to the teleoperator $|Z_{towidth}|$. Increasing the damping in slave controller ($\Re\{Z_{cs}\} = B_s$) improves simultaneously the architecture's performance and absolute stability. Increasing $(1+C_6)$ has no effect on the stability parameter, but it reduces $|Z_{tomin}|$ and at the same time the range of the reflected impedances $|Z_{towidth}|$. Here it should be noted that generally $|Z_{towidth}|$ of the designed teleoperator is wide enough for surgical applications that does not involve contacts with bones and therefore the most tricky design requirement is minimizing $|Z_{tomin}|$ and (C_6) plays a useful role in this case. Finally C_2 can be used to achieve the trade-off between $|Z_{towidth}|$ and $\eta_{p.pf}$ depending on specific system setup, increasing $|C_2|$ increases $|Z_{towidth}|$, without affecting $|Z_{tomin}|$ but reduces stability margins.

It can be seen that stability and performance analysis of 3-channel architecture is much more complicated than 2-channel architectures. Except few parameters whose roles are easy to identify, other parameters need to be tuned carefully to achieve good trade-off of absolute stability and performance depending on specific application requirements and system set-up. Finally, performing simulation #1 & #2 presented in (Table 4.1) and simulation #3 presented in the aforementioned stability discussion gives the results introduced in (Figs. 4.5 & 4.6) and the following points can be highlighted:

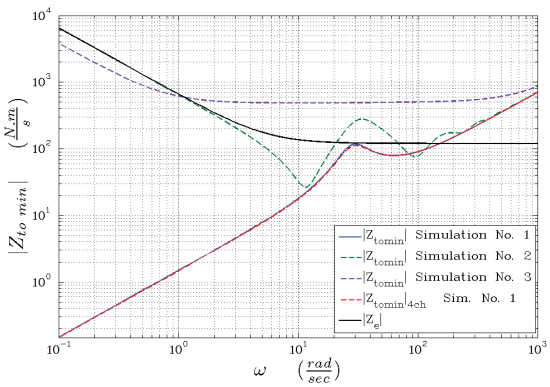

Figure 4.5: $|Z_{tomin}| < |Z_e|$

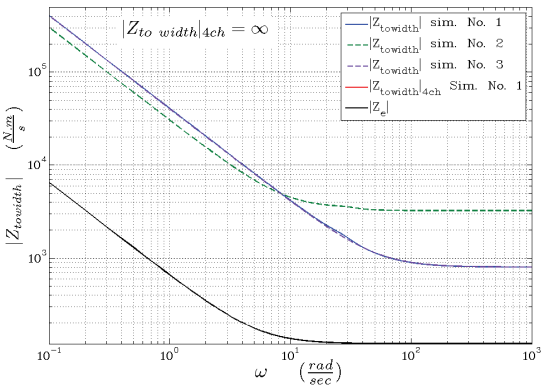

Figure 4.6: Transparency: $|Z_{towidth}| > |Z_e|$

- A transparent feedback of a given manipulated impedance $|Z_e|$ is achievable if and only if $|Z_{tomin}| < |Z_e|$ and $(|Z_{tomin}| + |Z_{towidth}|) > |Z_e|$.
- If the former condition is not achieved then the operator would feel one of the limits i.e. he will feel $|Z_{tomin}|$ if $|Z_{tomin}| > |Z_e|$ or $(|Z_{tomin}| + |Z_{towidth}|)$ if $(|Z_{tomin}| + |Z_{towidth}|) < |Z_e|$.
- Nevertheless $|Z_{towidth}|_{(P-PF)} \lll |Z_{towidth}|_{(4ch)}$, $|Z_{tomin}|_{(P-PF)} \approxeq |Z_{tomin}|_{(4ch)}$ and $(P-PF)$ CA is still capable of achieving complete transparency.
- The time delay induced in the 2^{nd} simulation controller degrades remarkably the transparency by increasing $|Z_{tomin}|_{sim.\ No.\ 2}$.
- Increasing stability margins reduces the transparency where $|Z_{tomin}|$ is mainly affected and one can clearly note $|Z_{tomin}|_{sim.\ No.\ 3} > |Z_e| \forall \omega \geq 2(\frac{rad}{s})$.

4.3.2 Force-Position Force Control Architecture ($F-PF$, $Fig.4.2.b$)

This work is the first time for the architecture F-PF (Effort forward, Flow backward, Effort backward) to be analysed in terms of absolute stability and transparency. This architecture can be deduced from ELA by setting master coordinating force feedforward controller to zero, that is $C_1 = 0$.

Absolute Stability

Stability is investigated based on alternative hybrid matrix $\mathbb{G}$ (Eq. 3.6) which provides comparatively to other models a simple representation and has the following members:

$$g_{11} = \frac{(1+C_5)(1+C_6) - C_2C_3e^{-2sT_d}}{(1+C_5)Z_{cm}} \tag{4.19}$$

$$g_{12} = -\frac{C_2Z_{cs} - C_4(1+C_5)}{(1+C_5)Z_{cm}}e^{-sT_d} \tag{4.20}$$

$$g_{21} = \frac{C_3}{(1+C_5)}e^{-sT_d} \tag{4.21}$$

$$g_{22} = \frac{Z_{cs}}{(1+C_5)}. \tag{4.22}$$

First two conditions in Llewellyn's criteria are guaranteed due to the passivity of non-connected master and slave, i.e.:

$$\Re\{g_{11}\}|_{C_{i=1,\dots,4}=0} = \Re\{\frac{(1+C_5)(1+C_6)}{(1+C_5)Z_{cm}}\} = \frac{(1+C_6)}{\Re\{Z_{cm}\}} = \frac{(1+C_6)}{B_m} \geq 0 \tag{4.23}$$

$$\Re\{g_{22}\}|_{C_{i=1,\dots,4}=0} = \frac{\Re\{Z_{cs}\}}{(1+C_5)} = \frac{B_s}{(1+C_5)} \geq 0. \tag{4.24}$$

The third condition evaluates the stability of F-PF CA:

$$\eta_{f-pf}(\omega) = \eta_{1f-pf}(\omega) + \eta_{2f-pf}(\omega) \tag{4.25}$$

$$= -cos(\angle g_{12}g_{21}) + 2\frac{\Re\{g_{11}\}\Re\{g_{22}\}}{|g_{12}g_{21}|} \tag{4.26}$$

$$= -cos(\angle - \frac{C_3}{Z_{cm}}(C_2Z_{cs} - C_4(1+C_5))e^{-2\omega T_d j}) + 2\frac{\Re\{(1+C_5)(1+C_6) - C_2C_3e^{-2\omega T_d j}\}\Re\{Z_{cs}\}}{\frac{\Re\{Z_{cm}\}}{|Z_{cm}|}|C_3||C_2Z_{cs} - C_4(1+C_5)|}] \geq 1. \tag{4.27}$$

Because $\eta_{1f.pf} \in [-1,+1]$ and includes $e^{-2\omega T_d j}$, the absolute stability of the system can be guaranteed only when $\eta_{2f.pf} \geq 2$, and therefore to guarantee the structure absolute stability, the following condition must hold:

$$\Re\{Z_{cs}\} \geq \frac{cos(\angle Z_{cm})|C_3|.|C_2Z_{cs} - C_4(1+C_5)|}{\Re\{(1+C_5)(1+C_6) - C_2C_3e^{-2\omega T_d j}\}}. \tag{4.28}$$

Since C_2, C_3, C_5 and C_6 are considered as scalar gains, the role of time delay becomes clearer by inspecting the most critical case of $\Re\{e^{-2\omega T_d j}\} = cos(2\omega T_d) \in [-1,\ 1]$, and when: $\Re\{(1+C_5)(1+C_6) - C_2C_3e^{-2\omega T_d j}\} = (1+C_5)(1+C_6) - C_2C_3\Re\{e^{-2\omega T_d j}\} = 0$. This means that time delay may cause the system to lose absolute stability for certain frequencies. When time delay is negligible ($T_d = 0$), absolute stability parameter takes the form:

$$\eta_{f-pf}(\omega) = -cos(\angle - \frac{C_3}{Z_{cm}}(C_2Z_{cs} - C_4(1+C_5))) + 2\frac{((1+C_5)(1+C_6) - C_2C_3)\Re\{Z_{cs}\}}{\frac{\Re\{Z_{cm}\}}{|Z_{cm}|}|C_3||C_2Z_{cs} - C_4(1+C_5)|}] \ \geq\ 1\,. \tag{4.29}$$

Again, noting that $\eta_{1f-pf}(\omega) = -cos(\angle T(j\omega)) \in [-1,1]$ for any transfer function $T(j\omega)$, the system absolute stability of can be guaranteed only when $\eta_{2f-pf}(\omega) \geq 2$. Therefore, in the absence of time delay the criterion in (Eq. 4.28) becomes:

$$\frac{\Re\{Z_{cs}\}}{cos(\angle Z_{cm})} = \frac{B_s}{B_m}|Z_cm| \geq \frac{|C_3||C_2Z_{cs} - C_4(1+C_5)|}{(1+C_5)(1+C_6) - C_2C_3}\,. \tag{4.30}$$

Because $\Re\{Z_{cm}\} = B_m \geq 0$, $-\frac{\pi}{2} \leq \angle Z_{cm} \leq \frac{\pi}{2}$ holds and hence $cos(\angle Z_{cm}) = \frac{\Re\{Z_{cm}\}}{|Z_{cm}|} \in [0,1]$. Accordingly, Increasing M_m (for high frequencies) and K_m (for low frequencies) in the imaginary part of Z_{cm} and decreasing master damping B_m, so that $cos(\angle Z_{cm}) \rightarrow 0$, and improves architecture's stability. The formula (4.30) shows that force controller gains C_2, C_3, C_5 and C_6 have a dominant role on the stability of the architecture. This conclusion can be justified easily because the two remote sites are exchanging basically force signals

in addition to the position information received from slave side. However, optimized transparency architecture cannot be realized because applying $(1+C_5)(1+C_6)-C_2C_3 \rightarrow 0$ implies extremely high damping on slave robot. This may justify the benefit of adding local force controller C_5 and C_6 on the master and slave. It is also worth to note that increasing the damping $\Re\{Z_{cs}\}$ on slave part and decreasing $|Z_{cs}|$ by reducing its imaginary part improves the architecture's stability. Consequently, the position controller on slave side has more significant effect on the absolute stability than this on master side.

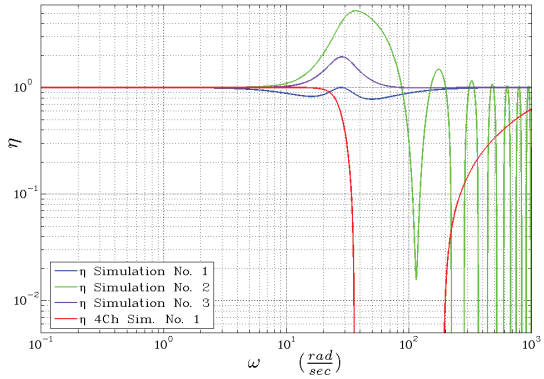

Figure 4.7: Stability condition $\eta \geq 1$

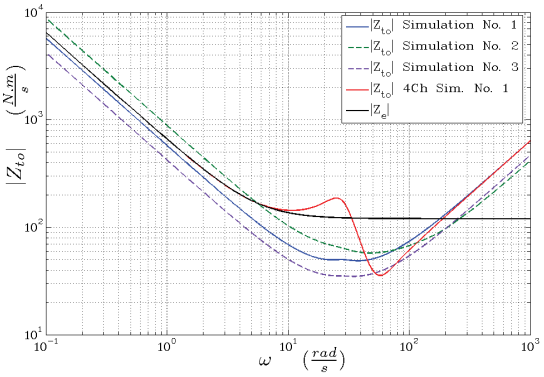

Figure 4.8: Transparency: $Z_{to} \equiv Z_e$

A simulation studies (*simulation #1, #2* and *#3*) are carried out to visualize the characteristics of $(F-PF)$ CA and presented in (Fig. 4.7 & 4.8):

- The optimised transparency combination of $(F-PF)$ CA has a low stability margin as formerly justified during the analytical study.
- The stability can be easily improved by increasing the force controller C_5 and/or C_6 gains. Indeed, simulation #3 has the same controller as simulation #1 with a single change in the value of $C_6 = 0.5$.
- The presence of time delay and improving the stability margins reduce the system transparency.
- $(F-PF)$ optimised transparency CA is not a completely transparent architecture. This conclusion can be clearly red by comparing read, blue and black lines in (Fig4.8)
- Time delay effect appears clearly for activities with high frequencies.

Transparency

Performance investigation is carried out by applying the equations (3.44-3.47 and 3.49-3.52) on F-PF hybrid matrix to get:

$$Z_{tomin} = \frac{Z_{cm}Z_{cs}}{(1+C_6)Z_{cs} - C_3C_4e^{-2sT_d}} \tag{4.31}$$

$$Z_{towidth} = \frac{(C_2Z_{cs} - C_4(1+C_5))C_3Z_{cm}e^{-2sT_d}}{((1+C_6)Z_{cs} - C_3C_4e^{-2sT_d})((1+C_5)(1+C_6) - C_2C_3e^{-2sT_d})}. \tag{4.32}$$

The role of time delay is very complicated and needs numerical analysis to evaluate its effect on a specific teleoperator. On the other hand, it can be remarked that $|Z_{towidth}| = T(j\omega)|Z_{tomin}|$, with $T(j\omega) = \frac{(C_2 - \frac{C_4}{Z_{cs}}(1+C_5))C_3e^{-2sT_d}}{(1+C_5)(1+C_6) - C_2C_3e^{-2sT_d}}$. This means that minimizing $|Z_{tomin}|$ will lead to reduced range of impedances that can be reflected and the parameters need to be compromised. This analytic conclusion can be easily read in (Figs. 4.9 & 4.10) where $|Z_{towidth}|$ of the controllers in simulation #2 & #3 are quite small to be able to feedback enough variety of low impedance soft tissues.

Comparing (Eq. 4.30) with (Eq. 4.31- 4.32) shows clearly the necessity of the trade-of step between the stability margin and the architecture's performance. $|Z_{tomin}|$ can be minimized by minimizing $|Z_{cm}Z_{cs}|$ and/or increasing $|(1+C_6)Z_{cs} - C_3C_4e^{-2sT_d}|$. The latter can be done by increasing C_6. Increasing the range of impedance that can be reflected through the teleoperator demands to decrease force controller gains C_5 and C_6. $|Z_{cm}|$ plays an important role to improve and compromise $|Z_{towidth}|$.

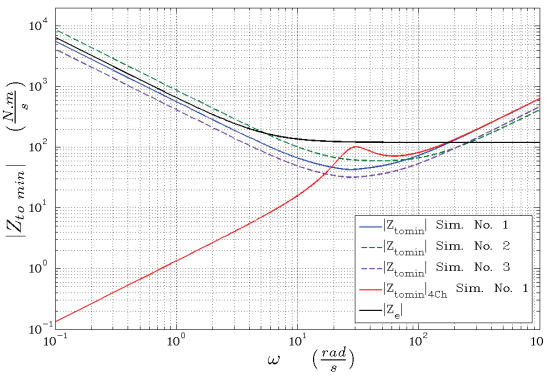

Figure 4.9: $|Z_{tomin}| < |Z_e|$

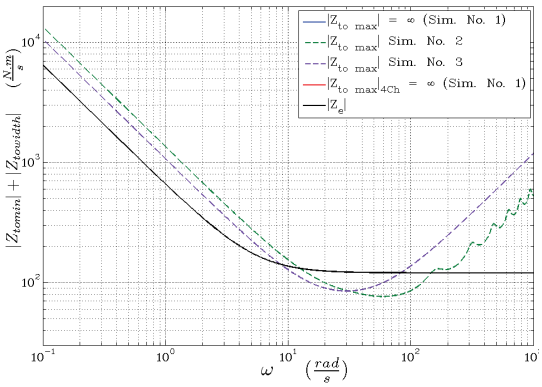

Figure 4.10: Transparency: $|Z_{tomax}| > |Z_e|$

- The simulation studies presented in (Figs. 4.9 & 4.10) shows a bad transparency of $(F-PF)$ CA even for the optimized transparency configuration. Furthermore to feedback a sufficient range of low impedance as in soft tissue a low stiffness controller has to be used affecting by consequent the stability.

- A limited range of impedances can be reflected through such controller because $|Z_{towidth}|$ is very limited.

4.3.3 Position Force-Position Control Architecture ($PF-P$, $Fig.4.2.c$)

Addressed as *Flow forward, Effort forward, Flow backward* CA, Hashtrudi-Zaad et al. discussed in [Hashtrudi-Zaad and Salcudean, 2002] this architecture's transparency as a special case realized from optimized ELA by applying $C_6 = -1$, requiring C_2 to be zero. However, stability analysis of this architecture has not been reported yet.

Absolute Stability

Stability evaluation is performed based on ELA using alternative hybrid matrix ($\mathbb{G}$) in (Eq. 3.6) by removing the direct force feed-forward from slave to master i.e. $C_2 = 0$:

$$g_{11} = \frac{(1+C_6)}{Z_{cm}} \tag{4.33}$$

$$g_{12} = \frac{C_4 e^{-sT_d}}{Z_{cm}} \tag{4.34}$$

$$g_{21} = \frac{C_3 Z_{cm} + C_1(1+C_6)}{(1+C_5)Z_{cm}} e^{-sT_d} \tag{4.35}$$

$$g_{22} = \frac{Z_{cm}Z_{cs} + C_1 C_4 e^{-2sT_d}}{(1+C_5)Z_{cm}} \tag{4.36}$$

First two conditions in Llewellyn's stability criteria hold because non-coupled master and slave are passive.:

$$\Re\{g_{11}\}|_{C_{i=1,\dots,4}=0} = \Re\{\frac{(1+C_6)}{Z_{cm}}\} = \frac{(1+C_6)}{B_m} \geq 0 \tag{4.37}$$

$$\Re\{g_{22}\}|_{C_{i=1,\dots,4}=0} = \frac{\Re\{Z_{cm}Z_{cs}\}}{(1+C_5)\Re\{Z_{cm}\}} \geq 0. \tag{4.38}$$

Teleoperator stability is evaluated using 3^{rd} condition of Llewellyn's stability criteria:

$$\eta_{pf-p}(\omega) = \eta_{1pf-p}(\omega) + \eta_{2pf-p}(\omega) \tag{4.39}$$

$$= -cos(\angle g_{12}g_{21}) + 2\frac{\Re\{g_{11}\}\Re\{g_{22}\}}{|g_{12}g_{21}|} \tag{4.40}$$

$$= sgn(1+C_5)[-cos(\angle C_4 \frac{C_3 Z_{cm} + C_1(1+C_6)}{Z_{cm}^2\, e^{2j\omega T_d}})$$

$$+ 2\frac{(1+C_6)}{cos^2(\angle Z_{cm})} \frac{\Re\{Z_{cm}Z_{cs} + C_1C_4e^{-2j\omega T_d}\}}{|C_4||C_3Z_{cm} + C_1(1+C_6)|} \geq 1 \tag{4.41}$$

Because $\eta_{1p-.p}(\omega) \in [-1,\ 1]\ \forall\ \omega \geq 0$, the system absolute stability is guaranteed when $\eta_{2pf-p} \geq 2$ which can be reformulated under the following condition:

$$\Re\{Z_{cm}Z_{cs}\} \geq -\Re\{C_1C_4e^{-2j\omega T_d}\} + \frac{sgn(1+C_5)}{(1+C_6)}cos^2(\angle Z_{cm})|C_4||C_3Z_{cm}+C_1(1+C_6)| \quad (4.42)$$

Time delay effect on stability evaluation is reduced to $\Re\{C_1C_4e^{-2j\omega T_d}\}$. Significant effect of time delay can be handled by decreasing $|C_1C_4|$ and especially $|C_4|$. Condition (4.42) shows that minimum amount of $\Re\{Z_{cm}Z_{cs}\}$ is necessary to guaranty the stability. Moreover, it is noted that $\angle Z_{cm}$ has a significant effect on system's stability. If a certain design of a teleoperator is imposed, stability margin can be improved when $\angle Z_{cm} \rightarrow \pm\frac{\pi}{2}$. Because two remote sites are exchanging basically position information supported by force information sent from master site toward slave one, position feedforward gains C_1, C_4 and position controllers on each site C_m, C_s have major effect to achieve a stable architecture and to compromise stability robustness with architecture transparency. However, decreasing C_3 or increasing $|1+C_6|$ may also improve the stability.

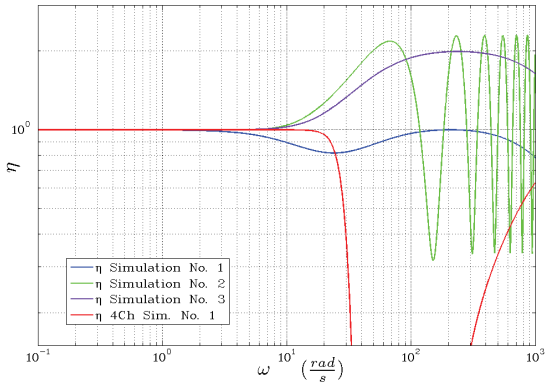

Figure 4.11: Stability condition $\eta \geq 1$

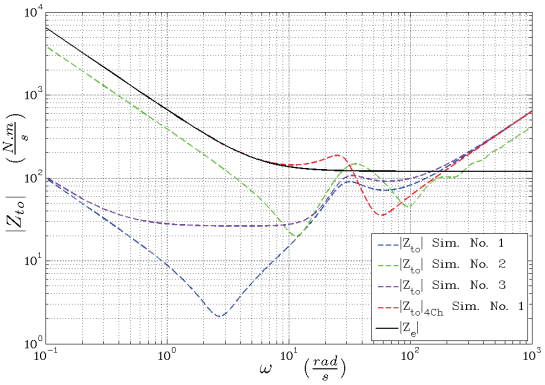

Figure 4.12: Transparency: $Z_{to} \equiv Z_e$

The numerical analysis through simulation shows that $(PF-P)$ structure has low stability and performance measure (Fig. 4.11 & 4.12). The low stability bandwidth of *simulation #1* structure can be increased by simply increasing the damping applied in master controller as in *simulation #3* where the solely change in comparison with *simulation #1* is $B_m = 75\frac{N.m}{s}$ (Fig. 4.7).

Transparency

Performance evaluation is carried out by applying the equations (3.44-3.47 and 3.49-3.52) on PF-P hybrid representation to get:

$$Z_{tomin} = h_{11} = \frac{Z_{cm}Z_{cs} + C_1C_4e^{-2sT_d}}{(1+C_6)Z_{cs} - C_3C_4e^{-2sT_d}} \tag{4.43}$$

$$Z_{towidth} = -\frac{h_{12}h_{21}}{h_{22}} = -\frac{C_4}{(1+C_6)} \frac{C_3Z_{cm} + C_1(1+C_6)}{(1+C_6)Z_{cs} - C_3C_4e^{-2sT_d}} e^{-2sT_d}. \tag{4.44}$$

Time delay affects clearly the performance of this architecture, especially the minimum impedance reflected to the operator. Nevertheless, this effect can be reduced by decreasing $|C_4|$ mainly and/or decreasing $|C_1|$, $|C_3|$. Examining performance parameters shows an opposition between them and their assignment is subject to specific application requirements.

In telesurgery on soft tissues, low $|Z_{tomin}|$ and high sensitivity are most demanded in a teleoperator. Therefore, after designing a stable teleoperator, minimum reflected impedance characteristic is first of all to be achieved. Then additional margin can be used to improve impedance bandwidth. $|Z_{tomin}|$ can be decreased by increasing $|Z_{cs}|$ and $|C_3|$ or decreasing $|Z_{cm}|$, $|C_1|$ and $|C_6|$. On the other hand, bigger $|Z_{towith}|$ needs increasing $|Z_{cm}|$, $|C_1|$ and $|C_3|$ and/or decreasing $|Z_{cs}|$ and $|C_6|$. As consequence, bigger $|C_3|$ and smaller $|C_6|$ are preferred to achieve better performance.

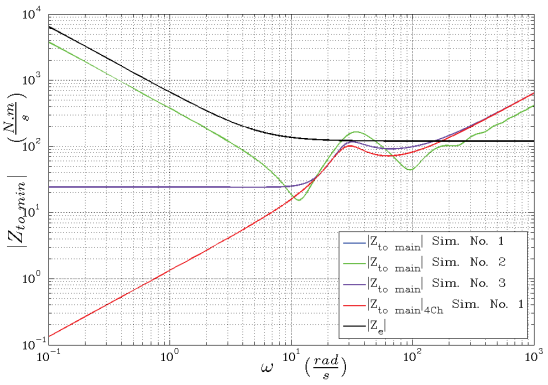

Figure 4.13: $|Z_{tomin}| < |Z_e|$

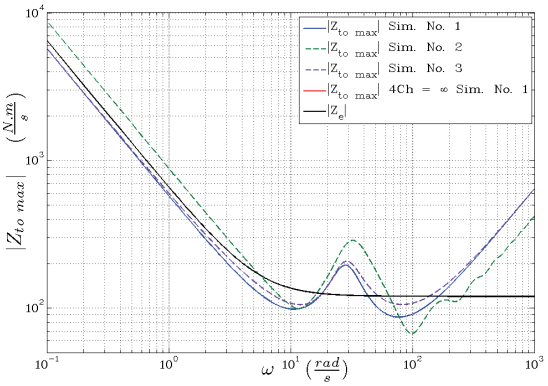

Figure 4.14: Transparency: $|Z_{tomax}| > |Z_e|$

Fig. 4.13 shows the minimum impedances that can be reflected through $(PF-P)$ CA for simulation 1, 2 and 3. $|Z_{tomin}|_{PF-P}$ has a considerably low values which enables the rendering of soft tissue with low impedance. Unfortunately, this architecture suffers from a low $|Z_{towidth}|$ where $|Z_{tomax}|$[4] $\lesssim Z_e$ in some cases as in Fig. 4.14.

4. $|Z_{tomax}| = |Z_{tomin}| + |Z_{towidth}|$

4.3.4 Position Force-Force Control Architecture ($PF-F$, $Fig.4.2.d$)

To the authors' knowledge, the analysis of PF-F *(Flow forward, Effort forward, Effort backward)* in terms of stability and transparency has not been yet addressed in the literature. To derive this architecture from Extended Lawrence Architecture (ELA), coordinating force feedforward from slave to mater needs to be removed by setting C_4 to zero.

Absolute Stability

Stability evaluation is performed by applying Llewellyn's criterions on hybrid matrix ($\mathbb{H}$) in (Eq. 3.6) which has the following members:

$$h_{11} = \frac{Z_{cm}}{(1+C_6)} \tag{4.45}$$

$$h_{12} = \frac{C_2}{(1+C_6)} e^{-sT_d} \tag{4.46}$$

$$h_{21} = -\frac{C_3 Z_{cm} + C_1(1+C_6)}{(1+C_6) Z_{cs}\, e^{sT_d}} \tag{4.47}$$

$$h_{22} = \frac{(1+C_5)(1+C_6) - C_2 C_3 e^{-2sT_d}}{(1+C_6) Z_{cs}} \tag{4.48}$$

decoupled master-slave passivity is guaranteed because Z_{cm} and Z_{cs} are passive:

$$\Re\{h_{11}\}|_{C_{i=1,\dots,4}=0} = \Re\{\frac{Z_{cm}}{(1+C_6)}\} = \frac{B_m}{(1+C_6)} \geq 0 \tag{4.49}$$

$$\Re\{h_{22}\}|_{C_{i=1,\dots,4}=0} = \frac{(1+C_5)}{\Re\{Z_{cs}\}} = \frac{(1+C_5)}{B_s} \geq 0. \tag{4.50}$$

(PF-F) teleoperator's stability is evaluated depending on the 3^{rd} condition of Llewellyn's criterions as follows:

$$\eta_{pf-f}(\omega) = \eta_{1pf-f}(\omega) + \eta_{2pf-f}(\omega) \tag{4.51}$$

$$= -cos(\angle h_{12} h_{21}) + 2\frac{\Re\{h_{11}\}\Re\{h_{22}\}}{|h_{12} h_{21}|} \tag{4.52}$$

$$= -cos(\angle - \frac{C_2}{Z_{cs}}(C_3 Z_{cm} + C_1(1+C_6)) e^{-2j\omega T_d}) + 2\frac{\Re\{Z_{cm}\}\Re\{(1+C_5)(1+C_6) - C_2 C_3 e^{-2j\omega T_d}\}}{cos(\angle Z_{cs})|C_2||C_3 Z_{cm} + C_1(1+C_6)|} \geq 1. \tag{4.53}$$

To circumvent time delay effect inside η_{1pf-f}, absolute stability of the system can be guaranteed only when $\eta_{2pf.f}(\omega) \geq 2$. To realize a stable PF-F architecture for certain range of frequencies, the following condition must hold:

$$\Re\{Z_{cm}\} \geq \frac{cos(\angle Z_{cs})|C_2||C_3 Z_{cm} + C_1(1+C_6)|}{(1+C_5)(1+C_6) - C_2 C_3 cos(-2\omega T_d)} \tag{4.54}$$

To satisfy (4.54), small $|C_2|$ and $cos(\angle Z_{cs})$ are preferred. Minimizing $|C_2|$ leads to reducing time delay effect and improve simultaneously architecture's stability. However, condition (4.54) shows clearly the necessity of minimum amount of damping on master to guarantee system's stability. Increasing local force controllers on each sites (C_5 & C_6) and/or adjusting $\angle Z_{cs}$ in such way that $\angle Z_{cs} \rightarrow \pm\frac{\pi}{2}$ will also improve architecture's stability. When time delay is negligible, $\eta_{1pf.f}(\omega)$ can be used to improve stability margin for certain range of frequencies by adjusting the transfer function appeared inside the cosine function.

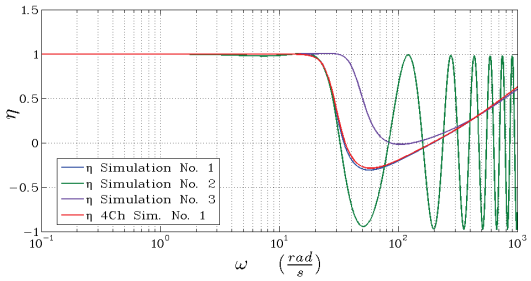

Figure 4.15: Stability condition $\eta \geq 1$

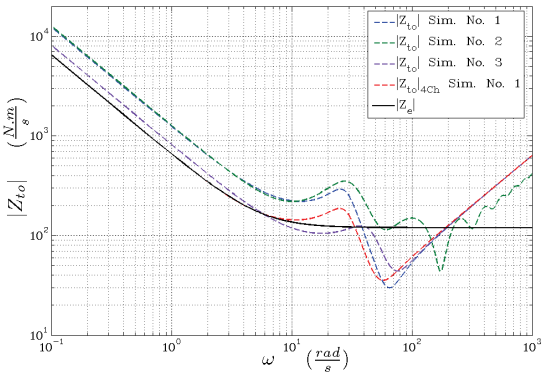

Figure 4.16: Transparency: $Z_{to} \equiv Z_e$

$(PF-F)$ seems to provide good performance in terms of stability and transparency as illustrated by (Figs. 4.15 & 4.16). Although the stability performance of $(PF-F)$ CA is very close to this of 4-Ch, the effect of loosing one information channel can be clearly seen on transparency measure where the operator feels a higher impedance than the real impedance of manipulated tissue ($|Z_{to}|_{simulation\ No.\ 1} > |Z_e|$). Furthermore, the main effect of time delay appears for high frequency activities but it can also destroy the stability for low frequency application (simulation #2 in green). Following the suggestion of (Eq. 4.54) which indicates that $\angle Z_{cs}$ plays an important role in improving the architecture stability. Therefore changing the slave controller stiffness and damping in (simulation #1) to have the values of $B_s = 1500\frac{N.m}{s}$ and $K_s = 1.e^5\frac{N}{m}$ and performing simulation # 3, this suggested improvement has increased simultaneously the system transparency (Figs. 4.11 & 4.12).

Transparency

Applying (3.44-3.47 and 3.49-3.52) on PF-F hybrid representation gives:

$$Z_{tomin} = h_{11} = \frac{Z_{cm}}{(1+C_6)} \tag{4.55}$$

$$Z_{towidth} = -\frac{h_{12}h_{21}}{h_{22}} = \frac{C_2}{(1+C_6)}\frac{C_3Z_{cm}+C_1(1+C_6)}{(1+C_5)(1+C_6)-C_2C_3e^{-2sT_d}}e^{-2sT_d}. \tag{4.56}$$

$|Z_{tomin}|$ can be minimized by decreasing $\Im m\{Z_{cm}\}$ and thus $|Z_{cm}|$ without affecting (4.54) or by increasing $|C_6|$. Note that reducing $\angle Z_{cm}$ won't affect system's stability. Moreover, time delay doesn't affect $|Z_{tomin}|$. On the other hand, increasing $|Z_{towidth}|$ requires decreasing C_3, C_5, C_6 and/or increasing $|C_1|$, C_2 and $|Z_{cm}|$. Again, as trade-off, smaller $|Z_{cm}|$, $|C_5|$ and bigger $|C_1|$ and C_2 are preferred for better transparency.

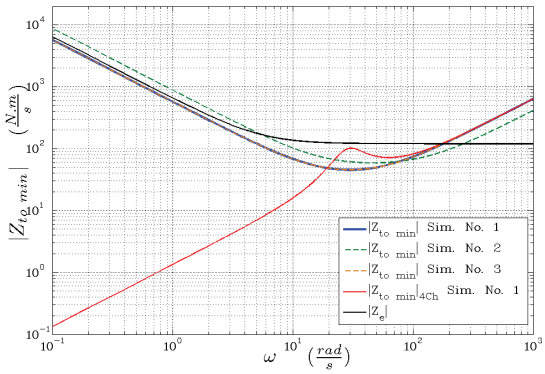

Figure 4.17: $|Z_{tomin}| < |Z_e|$

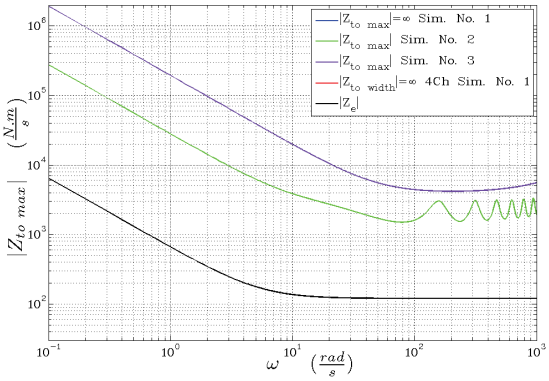

Figure 4.18: Transparency: $|Z_{towidth}| > |Z_e|$

A specific teleoperator with a specific stable CA is capable of reflecting a required interaction to the operator if and only if the environment impedance lies inside its dynamic range of rendered impedances i.e. $|Z_{tomin}| < |Z_e| < |Z_{tomax}|$. $(PF-F)$ architecture has a relatively bad measure of $|Z_{tomin}|$ even for the optimised architecture and consequently the interaction with some soft tissues that have low impedance is difficult to feedback (Fig. 4.17). Furthermore, the impression gained from (Figs. 4.15 & 4.16) that, in some cases, increasing the stability margins could improve the system transparency is not completely correct. As seen in (Fig. 4.18), the suggested improvement has reduced severely $|Z_{towidth}|$ measure. By consequent, the architecture selection is highly dependant on the application in terms of the required impedances to feedback and at which frequency.

4.4 Teleoperation control architecture for medical application

Each CA has its own specific characteristics that impose on the designer a limitation on system stability and achievable transparency. Consequently, the designer should be aware of the characteristic of each architecture to be able to select a suitable one for given requirements. In this section, the two simulation studies in (table 4.1) are carried out to analyse the performance and the absolute stability of different 3-channel architectures and illustrate how an optimal 3-channel architecture is selected according to the analysis and given application specifications to achieve a good trade-off between stability and transparency.

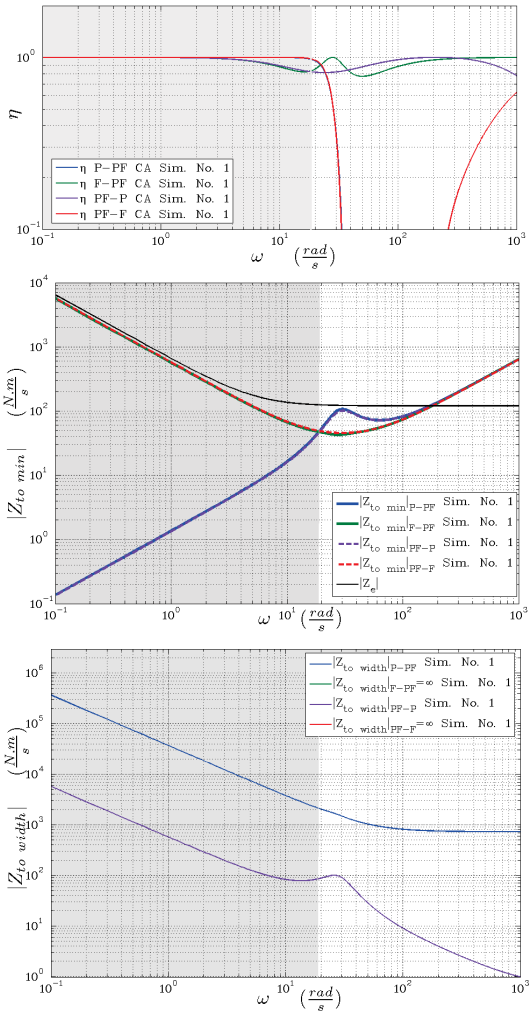

Figure 4.19: 1^{st} Example: Absolute stability parameter (upper), Performance parameters $|Z_{tomin}|$ (middle) and $|Z_{towidth}|$ (lower).

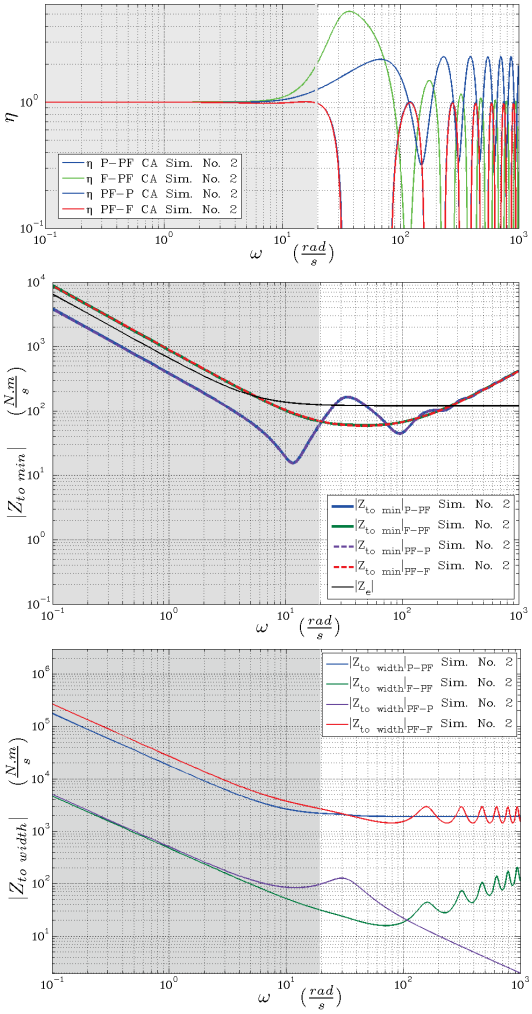

Figure 4.20: 2^{st} Example: Absolute stability parameter (upper), Performance parameters $|Z_{tomin}|$ (middle) and $|Z_{towidth}|$ (lower).

One of the most challenging application of telesurgery is beating heart minimally invasive surgery. Beating heart is a very challenging environment and its main motion frequency is up to 2 Hz. Thus, the motion disturbance frequencies in thoracic telesurgery lie in the range $0 \sim 2$ Hz ($0 \sim 12.6$ rad/s) [Bachta et al., 2009]. In these simulations, the target range of frequencies for stable teleoperation is set to 20 rad/sec. Because soft tissues has usually low impedances, $|Z_{tomin}| \rightarrow 0$ is a more important characteristic to consider for

transparency. However, enough range of $Z_{towidth}$ still has to be guaranteed. Teleoperator fidelity as another measurement for soft tissue MIS is beyond the scope of this chapter and hence is not discussed.

After evaluating the stability and performance of each architecture solely and in the objective of selecting a suitable architecture for medical applications, a comparative study of all the 3-channel CAs has to be performed. This comparative study is performed analytically through simulations using the system parameters introduced in (Table 4.1 simulation # 1 and #2). Simulation results are shown in Fig.4.19 and Fig.4.20. The upper part of each figure introduces the absolute stability parameter η. An architecture is said to be absolutely stable when $\eta \geq 1$ as in (3.42). In fact, each architecture can be tuned to be absolutely stable for certain range of frequencies but then the architecture's performance will degrade. The middle part of each figure shows the minimum impedance that can be felt through the teleoperator i.e. when $Z_e = 0$. $|Z_{tomin}|$ as a performance measurement has to be very small and its preferred lower limit depends on target application (for example for medical application it is expected to have very small values because the soft tissue has ordinary very low biomechanical impedance). The lower part provides the range of impedance that can be reflected through the teleoperator. This range is expected be as wide as possible to enable the teleoperator to reflect a big variety of environments.

The first simulation is performed based on optimized transparency architectures without time delay mimicking the case as in OR. The teleoperator's controllers can be tuned to guaranty the architectures' stability in the target range of frequencies (frequency width for beating heart telesurgery is up to $2\ Hz = 4\,\pi \frac{rad}{sec} < 20 \frac{rad}{sec}$). Therefore the design frequency width is take up to $20 \frac{rad}{sec}$ as indicated by the dark region. The middle part of Fig.4.19 shows that low $|Z_{tomin}|$ can be achieved by P-PF and PF-P architectures while F-PF and PF-F give poor performance. In the lower figure PF-P and F-PF are not shown since they possess high enough $|Z_{towidth}|$ over large range of frequencies. P-PF architecture is shown to have enough reflected impedance range. Comparatively, PF-P architecture offers very low $|Z_{towidth}|$. This simulation study shows that P-PF architecture presents the optimal choice for our targeted application. In fact, this conclusion won't be changed using different control parameters. Fig.4.20 shows a non-optimized transparency case with time delay. The above discussions and conclusions are shown to still stand valid. Hence, P-PF presents the most suitable architecture for our application (soft tissues MIS).

Nevertheless, it can be noticed that if $|Z_{tomin}| \rightarrow a$ instead of $|Z_{tomin}| \rightarrow 0$ is expected (e.g. applications that use hydraulic teleoperator) where a is a small enough impedance, then PF-F architecture (black line) may be the suitable option. In fact PF-F architecture is more suitable for heavy environment and big impedances. Actually, P-PF and PF-F architecture are based on P-F architecture (which mimics the ideal teleoperator) supported by position information from slave side in P-PF and by force information from master side in PF-F. The additional information channel provides more freedom to achieve stability/-transparency trade-off, which again justify the use of 3-channel architectures.

4.5 Conclusions

In this chapter, a general evaluation procedure for 3-channel architecture is established based on Llewellyn's absolute stability criteria and Z_{width} notion for transparency. All possible 3-channel architectures have been evaluated using these tools in an uniformed manner and design guidelines are provided after each evaluation considering the specific concerns of medical applications. Simulation studies have been carried out to evaluate the stability and performance of each 3-channel architecture. The P-PF architecture is recommended based on analysis of simulation evaluation results.

CHAPTER

5 Environment Modeling with Physiological Motion Disturbance for Surgical Teleoperation

Preamble

One of major issues that affects teleoperation transparency, in addition to the applied control architecture identified in the precedent chapter, is the significant presence of disturbances in the operated tissues. These disturbances take several forms because of the non-linear nature of robot-tissue interaction, friction presence in trocar, vital motion disturbance present in some organs, etc. This chapter [Albakri et al., 2014] tries to analyse the effects of motion disturbance on the rendered impedance. In the following, we propose a modelling method for the interaction impedance of a remote soft tissue that contains quasi-periodic physiological motion disturbance. The interaction impedance, in such case, depends not only on the soft tissue impedance but also on the relationship between the robotic tool motion and the soft tissue motion disturbance. Through this study, it is shown that the interaction with such environment is not passive and its influence should be considered in the teleoperator design. An illustrative case study is presented to demonstrate how to analyse the environment interaction impedance in real application.

5.1 Introduction

As previously explored in the second chapter, MIRS is introduced to Operating Room (OR) to optimize the outcome of laparascopic surgery for both patient and surgeon [Troccaz, 2013] [Rosen et al., 2011]. Furthermore, Minimally Invasive Beating Heart Surgery(MIBHS) provides an advantageous alternative approach to traditional open chest heart surgery (e.g. minimizing the postoperative risks) [Murkin et al., 1999] [Gersak and Sutlic, 2002]. Due to its complex shape and high Dynamics, the region under operation in

MIBHS has to be stabilized using mechanical stabilizer while the significant residual motion is compensated automatically by synchronizing the tools and endoscope movements with the residual motion. This approach allows the surgeon to operate on the beating heart and avoiding the cardiopulmonary bypass pump [Bozovic, 2008] [Riviere et al., 2006].

On the other hand, providing the surgeon with haptic sensation of the manipulated tissues has been proved to improve the surgical intervention's quality [Bethea et al., 2004]. This improvement is, as formerly discussed, due to the teleoperator's increased transparency. Several methods have been explored to provide the human operator with an adequate haptic representation of the remote environment [Okamura, 2004]. Nevertheless, haptic teleoperation has its inherent limitations (e.g. stability, bandwidth) [Daniel and McAree, 1998]. To this limit, all the considered operated tissues in telesurgical context are assumed to be either static or quasi-static passive tissues.

As previously explored in the precedent chapters, the concern of designing a stable transparent bilateral teleoperator that interacts with a wide spectrum of possible environment impedances (Z_e) and human impedances (Z_h), is treated through passivity of 2-port network that represents the designed teleoperator. Briefly, the teleoperation is stable if the interaction energy out of the teleoperator at slave-environment interaction port is equal or less than the energy injected by human operator at human-master interaction port (Fig. 5.1). In other words, the human operator has to be the only source of energy in the teleoperation closed loop. As such, the majority of the teleoperators are loosely designed using the assumption that the remote environment does not involve any external forces i.e. $F_e^* = 0$ [Lawrence, 1993] [Hashtrudi-Zaad and Salcudean, 2001].

The beating heart is quite different in comparison to the other static (or quasi-static) living tissues which could be considered passive. The main challenge of any kind of surgical intervention in the thoracic area is the significant amplitude (up to 10 mm) and relatively high rate inherent motion disturbance (up to 2 Hz). This disturbance results from both breathing and heart beat vital functions and its effects pass beyond the thoracic area to many other vital organs (liver, kidney, etc.). Intuitively, the presence of breathing and heart beat motion suggests that the robot-tissue interaction in likewise affected organs is not a passive interaction. In other words, the energy flow at slave-environment interaction port is not only from teleoperator to environment, indicating human action application on the remote environment, but also the environment itself that injects some (bounded)

Figure 5.1: Teleoperation Modelling

energy in the teleoperator network. Nevertheless, the passivity of robot-beating heart interaction port has not so far been rigorously investigated and represents an open issue.

This chapter aims to investigate the effect of soft tissue physiological motion on the impedance perceived at slave-tissue interaction region. Hereafter we consider the interaction with a beating heart tissue as an exemplary case study because its motion is influenced by the heart beat and breath function simultaneously, and its study can lead to a general conclusion. Firstly, by analysing the physiology of beating heart and robot-tissue interaction, the teleoperation scheme can be reformulated to enable the port's power quantification. Then, a new mathematical formula is proposed to describe the impedance sensed by the slave robot, which we propose to call as "interaction impedance". The interaction impedance depends not only on the soft tissue impedance but also on the relativity (ratio) between the environment motion and the robotic tool motion. Finally, the proposed model of the interaction impedance can be used to analyse the passivity of the interaction port with these category of environments by examining the real part of its transfer function [1]. Through numerical analysis, it is shown that interaction port with quasi-periodically moving tissues could be non-passive.

5.2 Teleoperation Scheme Reformulation

As previously introduced in the Section 3.1.2, the dynamic performance of any environment that interacts with a robotic device takes, in the constrained state, the form of passive impedance joint in serial with external active source of energy (effort source F_e^*) to represent the external activity induced in the treated environment (Fig. 5.2). In most cases handled in teleoperation context, the treated environments are supposed to be well structured static or quasi-static, the fact that enables the assumption ($F_e^* = 0$). However, in many cases, as in beating heart and/or breathing physiological activities, this assumption is not always valid and there is no clear way to quantify, measure or model accurately this effort source. In this section we revise the heart tissue and activity modelling to derive a suitable representation of its impedance and source of energy while interacting with a surgical instrument to facilitate its study under the standard/classical teleoperation framework. We approach this problem through two aspects: First, by identifying the source of energy and its physical measures that may help to quantify the external source of energy (F_e^*) and revisiting the existing model(s) of heart tissue mechanical properties; Second, by reformulating teleoperation standard scheme (Fig. 5.2) to fit tool-tissue interaction in MISBH context. Finally the result of this analysis will be used to propose a new interaction model that takes the environment motion disturbance in consideration.

1. A 1-port network is passive when the transfer function representing its dynamics is positive real.

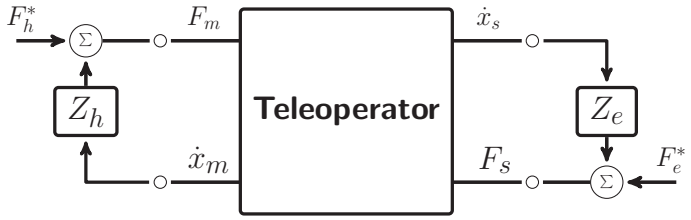

Figure 5.2: Conventional teleoperation modelling

5.2.1 Heart electromechanical properties

Heart performs its role as a bump that pushes blood into lungs and other parts of the body through contraction of cardiac muscles (atrial, ventricular, and specialized excitatory and conductive muscles). These contractions are due to the physical presence of heart rhythmic electrical excitation of S-A and A-V nodes (Fig. 5.3) accompanied with changes in heart walls' thickness and chambers volumes leading to an adequate change in blood pressure inside the chambers (Fig. 5.4). This volume-pressure change quantifies the work executed by the active driving force generated by the heart muscle [Guyton and Hall, 2010].

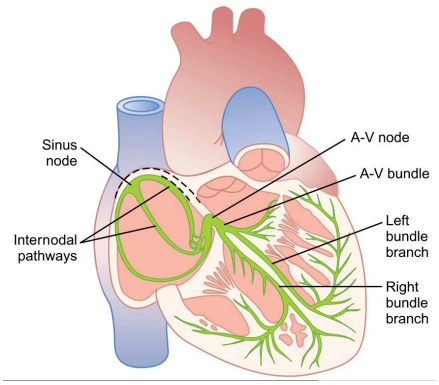

Figure 5.3: Heart conducting system [Guyton and Hall, 2010]

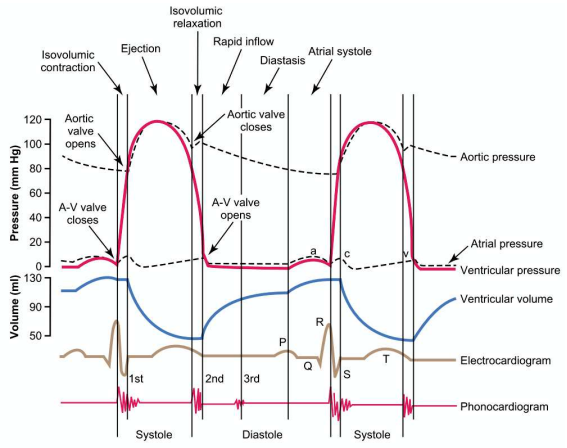

Figure 5.4: The cardiac cycle for left ventricular function [Guyton and Hall, 2010]

On the other hand, the myocardium bundles have a spiral form. Therefore, the motion of a point of interest (POI) on heart wall is subject to a composition of three-dimensional displacements and contractions. In other words, the region of interest (ROI) does not change only its position in time but also it is subject to shape changes under the form of stretch and shrinkage [Richa et al., 2010]. Furthermore, passive soft tissues consist of multi inhomogeneous layers and have consequently non-linear properties. In myocardium, the

spiral form of muscle fibres implies that the impedance of the passive myocardium tissue changes with the considered point position i.e. $Z_e = f(X),\ X = [x\ y\ z]^T \in \mathbb{R}^3$. Moreover, the muscle contraction-relaxation phases are due to periodic electrochemical changes that take place inside the heart wall accompanied with an instantaneous change in the wall thickness. Therefore, the"passive" impedance of the heart wall is time variant and $Z_e = f(X,\ t)$. Thus, heart wall tissue modelling represents a complex problem and some assumption and simplifications are necessary [Pinto and Fung, 1973] [Fung, 1984] [Winters and Woo, 1990] [Huyghe et al., 1991] [Jeremic and Nehorai, 2000] [Roger, 2004] [Sermesant et al., 2006] [Guyton and Hall, 2010] [Fung, 1993].

Two main assumptions considered in this analysis are summarized as follows:

* The blood medium inside the heart being incompressible, when the heart muscle comes to interact with an external effect (e.g. surgical tool), the main changes of volume happen inside the myocardium walls or vessels tissues.
* Despite the numerous source of non-linearities in the muscle tissues, a minimum amount of linearisation is imposed to reduce the problem complexity.
* Muscle fibre model is composed of a contractile element (CE) that represents the active part joint with a combination of passive elements in serial (serial element(s) (SE)) and/or in parallel (parallel element (PE)) (Fig. 5.6) [Blaustein et al., 2011].
* Any soft tissue that is subject to a considerable physiological motion can be approximated to the case of blood vessel wall (Fig. 5.5). In other words, to consider the heart wall completely passive and the energy is supplied by the inner medium (blood) as a pressure on the inner face of heart wall.
* The virtual source of pressure produces the same effects as the heart beat.

5.2.2 Problem reformulation

In telesurgery context, the surgeon performs a slow careful precise action. Consequently, the motion disturbance produced by heart beat and breath physiology is relatively

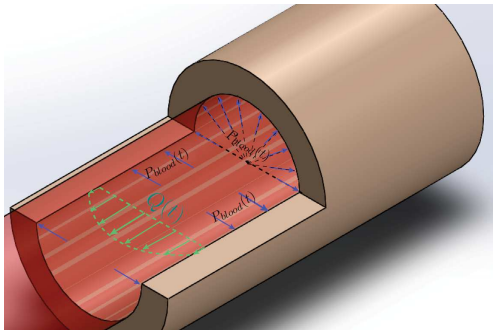

Figure 5.5: Section in a blood vessel

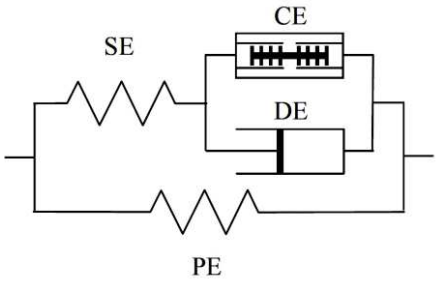

Figure 5.6: Muscle fibre general model

great enough and cannot be treated as noise. Considering the aforementioned assumptions, tool-heart interaction problem can be described as follows (Fig. 5.8):

* The incompressible blood medium affects the inner face of the heart wall with pressure that varies in time and space i.e. $p = f(X,t)$, X and t denoting the POI position on heart wall inner face and time respectively. This pressure is rhythmic and quasi-periodic with an approximated period (T) i.e. $p(X,t) = p(X,t+T)$.
* Considering heart muscle (wall) to be completely passive, blood represents the active medium. This medium is capable of reproducing an effect equivalent to this of myocardium contraction (i.e. position variation of a POI $X_e^*(t) = X_e^*(t+T)$).
* The position of a POI on the surface of an unconstrained heart, its velocity and acceleration X_e^*, $\dot{X}_e^*$, $\ddot{X}_e^*$ are continuous, periodic and can be estimated.
* In free state, a point on the outer face of the heart wall reproduces the motion of a point on the inner face of the heart wall with position shift $\delta X = [\delta x\ \delta y\ \delta z]^T$.
* When a surgical tool approaches the heart with a continuous motion $X_s(t)$, $\dot{X}_s(t)$, $\ddot{X}_s(t)$, it imposes its position on heart wall because the tool is infinity stiff in comparison with the heart tissue impedance $X_{POI}(t) = X_s(t)$, $\dot{X}_{POI}(t) = \dot{X}_s(t)$, $\ddot{X}_{POI}(t) = \ddot{X}_s(t)$.
* Heart tissue impedance is variant in time and space. This impedance is bounded $Z_e(X,t) \in [Z_e^{max}(X,t),\ Z_e^{min}(X,t)]$ and has a quasi-periodic variance $Z_e(X,t) = Z_e(X,t+T)$. In conclusion, it is possible to construct an approximate function that describes heart tissue impedance variance of a POI knowing its maximal (Z_e^{max}) and minimal (Z_e^{min}) limits and its frequency spectrum of changes.
* Z_e and p have the same frequency spectrum as heart motion X_e^*.

In conclusion, heart tissue can be considered as a passive member that is compressed from its two extremities with position X_e^* at the first extremity and X_s at the second one (Fig. 5.8). For further illustration, let us suppose that the tissue involved in the analysis has

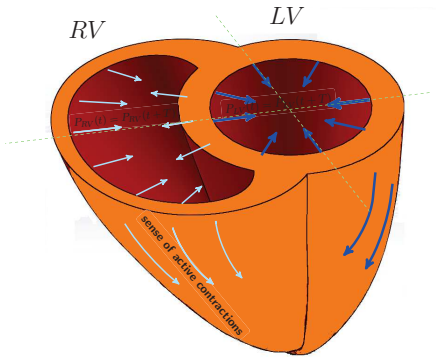

Figure 5.7: Myocardium model (reconstructed [Marieb and Hoehn, 2007])

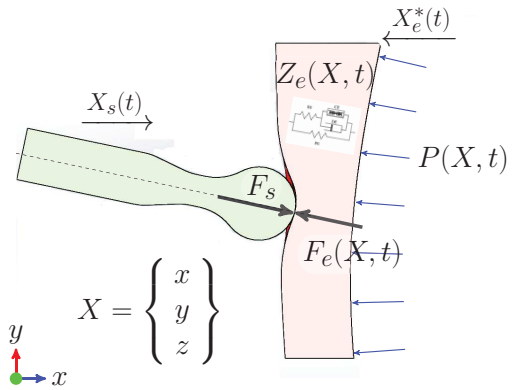

Figure 5.8: Tool-tissue interaction

a MSD model with negligible mass term as for the majority of soft tissues. The resulting model is composed of a spring (k_e) in parallel with a damper (b_e). Tool-tissue interaction force in this simplified case can be calculated as follows:

$$F_s(X,t) = F_e(X,t) \tag{5.1}$$
$$= k_e(X,t)(x_e^*(X,t) + x_s(X,t)) + b_e(X,t)(\dot{x}_e^*(X,t) + \dot{x}_s(X,t)), \tag{5.2}$$

where F_e denotes the tissue reaction force while F_s is the force at slave tip sensed by a suitable force measurement modality. Considering a specific POI, the variable X in each function can be dropped down to concentrate on the time variance of the physical quantities. Furthermore, supposing that the involved tissue has a constant model coefficients (i.e. time independent k_e and b_e), (Eq. 5.2) can be simplified to:

$$F_s(t) = F_e(t) = k_e\ (x_e^*(t)) + x_s(t)) + b_e\ (\dot{x}_e^*(t) + \dot{x}_s(t)) \tag{5.3}$$

Applying Laplace transform on the previous equation (Eq. 5.3) gives:

$$F_s(s) = k_e\ (X_e^*(s)) + X_s(s)) + b_e\ (sX_e^*(s) + sX_s(s)) \tag{5.4}$$
$$= (\frac{k_e}{s} + b_e)(s\ X_e^*(s)) + s\ X_s(s)) \tag{5.5}$$
$$= Z_e(s)\ (s\ X_e^*(s) + s\ X_s(s)) \tag{5.6}$$
$$= F_e^*(s) + Z_e(s)(s\ X_s(s)), \tag{5.7}$$

with $F_e^*(s) = Z_e(s)(sX_e^*(s))$ denoting the active force generated by the heart muscle in Laplace domain. In fact (Eq. 5.6) represents a generic model of tool-tissue interaction when the tissue is subject to a motion disturbance (X_e^*) in condition that the tissue is represented by a time invariant model where Z_e could involve a different forms of tissue modelling. Accordingly, teleoperation scheme in (Fig. 5.2) can be reproduced to have the form in (Fig. 5.9). The main advantage of the new scheme is that the teleoperation scheme has X_e^* as input which is known for a POI or can be estimated [Bozovic, 2008]. This reformulation enables the analysis of the interaction with wide varieties of soft tissues that are subject to a non-negligible motion disturbance.

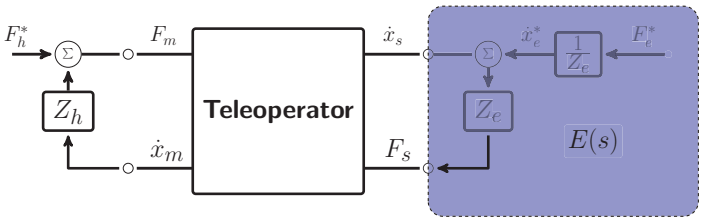

Figure 5.9: Teleoperation scheme reformulation

5.2.3 Environment Impedance

In the following, the tissue impedance sensed at the robot tool end-effector from robot stand point will be addressed as interaction impedance. The interaction impedance of passive environment ($F_e^* = 0$) is the transfer function between its reaction force and the external robotic position rate i.e. $Z_e(s) = F_s(s)/(s\ X_s(s))$ with $F_s(s)$, $X_s(s)$, $Z_e(s)$ denoting tissue-robot interaction force, slave robot end-effector position and environment (tissue) impedance in Laplace domain respectively. On the other hand, when the manipulated environment contains an inherent motion disturbance X_e^*, the interaction impedance E_e can be calculated in terms of the soft tissue impedance Z_e based on the aforementioned approximation as follows (Fig.5.9):

$$E_e(s) = \frac{F_s(s)}{sX_s(s)} = \frac{Z_e(s)\left(sX_e^*(s) + sX_s(s)\right)}{sX_s(s)} \tag{5.8}$$

$$= Z_e(s)\left(1 + \frac{X_e^*(s)}{X_s(s)}\right). \tag{5.9}$$

As demonstrated by Eq.(5.9), the interaction impedance depends not only on the environment passive impedance Z_e but also on the relative relationship between the robot end-effector motion and the disturbance motion. When the disturbance amplitude is small enough to be neglected ($|X_e|^* \leq \varepsilon$ with ε a small positive constant), the interaction impedance becomes equivalent to the tissue impedance at the concerned point $E_e(s)|_{|X_e^*|\to 0} = Z_e(s)$. On the other hand, when environment disturbance magnitude is remarkable, it cannot be neglected and has to be considered in the analysis. As in telesurgery, especially MIBHS context, surgeon performs acute actions with relatively low frequency motion in comparison with heartbeat/breath motion disturbance (ex. suturing). In the following we propose a methodology to calculate this impedance in real time during the surgical intervention. Such model is useful for surgical training through developing a virtual reality environment and in surgical assistance through augmented reality applications as virtual fixture for example.

5.3 Interaction Impedance with a Moving Environment

In this section each term in (Eq.5.9) is discussed to construct a suitable algorithm to calculate the interaction impedance model of a soft tissue that is subject to an external source of disturbance. First soft tissue impedance modelling is discussed then motion modelling of the surgical tool and physiological disturbance, to finish with establishing the interaction impedance transfer function. This model is useful for surgical training and assistance.

5.3.1 Soft Tissue Modeling $Z_e(s)$

To describe accurately the viscoelastic behaviour of tool-tissue contact, a non-linear model might be necessary. However, several linear models proposed in literature have prove efficiency in describing force-deformation relationship for inhomogeneous tissues. Further discussion of tissue modelling can be found in [Fung, 1993] and is not the concern of this chapter. To carry out our analysis, a LTI Mass Spring Damper (MSD) model is used to describe the dynamic behaviour of an interaction with a soft tissue, this model is addressed in literature as Kelvin-Voigt model[Erickson et al., 2003] [Misra and Okamura, 2006]. Although mass term for soft tissues is usually very small and can be neglected, it is considered in this analysis to insure the generality of the conclusion. It is worth to note that the used model to represent Z_e in following is only used as an exemplary case study in the purpose of demonstrating the proposed model usability (i.e. Z_e could take the form of any model to describe better the analysed environment dynamics). The dynamic behavior of tool-tissue interconnection can be described using LTI MSD model as follows:

$$Z_e(s) = \frac{F(s)}{sX(s)} = M_e s + B_e + \frac{K_e}{s}, \tag{5.10}$$

with $M_e, B_e, K_e \in \mathbb{R}^+$ are respectively the mass, damping and stiffness coefficients of MSD model. In the frequency domain (Eq. 5.10) takes the following form:

$$\begin{aligned} Z_e(j\omega) &= B_e + (M_e\omega - \frac{K_e}{\omega})\,j & (5.11)\\ &= \Re(Z_e(\omega)) + \Im(Z_e(\omega))\,j, & (5.12) \end{aligned}$$

This impedance is passive since:

$$\Re\{Z_e(j\omega)\} = \Re\{M_e\omega\, j + B_e + \frac{K_e}{\omega\, j}\} = B_e \geq 0. \tag{5.13}$$

One of the main limitation of LTI model as the aforementioned example is that this model neglects the viscoelasticity of living soft tissues. Furthermore, in the case of beating heart soft tissue model, heart wall is subject to changes of thickness, chemical and electrical structure during the beat cycle. Therefore the impedance of any POI must have a time variant coefficients rather than constants, i.e. $M_e = f(t)$, $B_e = g(t)$, $K_e = h(t)$.

5.3.2 Motion Modelling

Two types of motion sources can be distinguished in telesurgery, *surgeon motion* and *physiological tissue motion*. Although the surgeon performs several simultaneous tasks that may affect his/her hand motion during the surgery (eg. stereo instrument motion, pedal activity, etc.), his/her hand motion can be divided, based on the protocol used to

carry out the intervention, to several continuous trajectories [Ahmidi et al., 2013]. Moreover, the physiological motion of organs inside human body can be attributed mainly to two main sources of motion: breathing and heart beating. The main characteristic of this motion is its continuous quasi-periodical property. Any continuous differentiable motion trajectory can be approximated as a sum of finite series of functions as follows:

$$x(t) = \sum_{i=1}^{n} \Big(\lambda_i \, f_i(t) \Big) \qquad \forall \; t \geq 0, \tag{5.14}$$

where $f_i(t)$ is a time dependant function. Actually, $f_i(t)$ can be sinusoidal function for periodical and quasi-periodical motion and it may be a sort of power series of time for small scale motion, or sum of both sinusoidal and exponential.

Physiological motion modeling

Many vital organs in human body are subject to a periodic or quasi-periodic non-negligible motion disturbance. This motion is due to the physiological activities induced in the thoracic area and can be described using Fourier transform under a series of triangular functions as follows:

$$x_e^*(t) = x_e^*(0) + \sum_{i=1}^{n} \Big(a_i \; sin(b_i \; t) \Big). \tag{5.15}$$

Where $x_e^*(t)$ and $x_e^*(0)$ denote the environment position at time t and its initial position when $t = 0$ while a_i and b_i are Fourier transform coefficients and the corresponding frequency respectively. Applying Laplace transform on (Eq. 5.15) gives the following equation:

$$X_e^*(s) = \frac{x_e^*(0)}{s} + \sum_{i=1}^{n} \Big(\frac{a_i \; b_i}{s^2 + b_i^2} \Big) \tag{5.16}$$

$$= \frac{x_e^*(0)}{s} + \sum_{i=1}^{n} \frac{\Big(s \; a_i \; b_i \prod\limits_{ii=1}^{i-1} (s^2 + b_{ii}^2) \prod\limits_{ii=i+1}^{n} (s^2 + b_{ii}^2) \Big)}{s \prod\limits_{ii=1}^{n} (s^2 + b_{ii}^2)} \tag{5.17}$$

$$= \frac{\alpha(s)}{s \prod\limits_{ii=1}^{n} (s^2 + b_{ii}^2)}, \tag{5.18}$$

where:

$$\alpha(s) = x_e^*(0) \prod_{ii=1}^{n} (s^2 + b_{ii}^2) + \sum_{i=1}^{n} \Big(s \; a_i \; b_i \prod_{ii=1}^{i-1} (s^2 + b_{ii}^2) \prod_{ii=i+1}^{n} (s^2 + b_{ii}^2) \Big). \tag{5.19}$$

In frequency domain, the function in (Eq. 5.19) can be simplified as follows:

$$\alpha(j\omega) = \Re(\alpha(j\omega)) + \Im(\alpha(j\omega))\, j, \tag{5.20}$$

where:

$$\begin{cases} \Re(\alpha(j\omega)) = x_e^*(0) \prod_{ii=1}^{n} (b_{ii}^2 - \omega^2) \\ \Im(\alpha(j\omega)) = \sum_{i=1}^{n} \Big(\frac{\omega a_i b_i}{b_i^2 - \omega^2} \prod_{ii=1}^{n} (b_{ii}^2 - \omega^2) \Big). \end{cases}$$

Robotic tool end-effector motion modelling

Surgical robot end-effector displacement is controlled by surgeon's hand motion. This motion varies widely depending on the surgeon's experience. However, the motion of an expert surgeon hand is not random and follows the certified protocol used to perform the intervention with the purpose of minimizing the tool path and avoiding the collision with vital structures. Using Frenet Frames (FF), the surgeon hand trajectory can be decomposed into a sum of continuous time differentiable segments [Ahmidi et al., 2012] [Ahmidi et al., 2013]. At each segment, the trajectory can be interpolated using Eq. (5.14) and the time dependent function that describes the tool displacement during the performance of a specific segment of the intervention can be constructed.

Observing the surgeon hand motion when intervening on vital organs that contains motion disturbance shows that this motion is a slow small range motion. We assume that the surgeon hand motion during one segment performance before changing the motion direction can be interpolated through the following power series of time where c_k is constant [Flash and Hogan, 1985]:

$$\dot{x}_s(t) = \sum_{k=0}^{m} c_k \, t^k, \tag{5.21}$$

which takes in Laplace domain the following form:

$$s \, X_s(s) = \sum_{k=0}^{m} \frac{c_k \, k!}{s^{k+1}} = \frac{c_m m! + \sum_{k=0}^{m-1} c_k k! s^{(m-k)}}{s^{m+1}} \tag{5.22}$$

$$= \frac{\beta(s)}{s^{m+1}}, \tag{5.23}$$

Without loss of generality, suppose the series length m to be odd ($c_{m+1} = 0$ for even) and by considering $m = 2\tau - 1$ and $m - k = r$, the function $\beta(s)$ becomes:

$$\begin{aligned} \beta(s) &= c_m m! + \sum_{k=0}^{m-1} c_k k! s^{m-k} \\ &= c_m m! + \sum_{r=1}^{\tau} c_{m-2r} \, (m-2r)! \, s^{2r} + \sum_{r=1}^{\tau} c_{m-2r+1} \, (m-2r+1)! \, s^{2r-1}. \end{aligned} \tag{5.24}$$

Generally m does not exceed 5 for most cases of motion in small segments as performed in MIS [Flash and Hogan, 1985]. With $v = m - 2r$:

$$\beta(\omega\ j) = \Re(\beta(j\omega)) + \Im(\beta(j\omega))\,j \tag{5.25}$$

$$= \left(c_m m! + \sum_{r=1}^{\tau} c_{m-2r}\ (m-2r)!\ (-1)^r \omega^{2r}\right) + \left(\sum_{r=1}^{\tau} c_{m-2r+1}(m-2r+1)!(-1)^{r-1}\omega^{2r-1}\right) j, \tag{5.26}$$

$$\begin{cases} \Re(\beta(j\omega)) = c_m m! + \sum_{r=1}^{\tau} c_v\ v!\ (-1)^r \omega^{2r} \\ \Im(\beta(j\omega)) = \sum_{r=1}^{\tau} c_{v+1}(v+1)!(-1)^{r-1}\omega^{2r-1}. \end{cases} \tag{5.27}$$

5.3.3 Interaction modeling

When the remote manipulated environment contains a non-negligible disturbance motion i.e. $|\dot{x}_e^*(t)| \neq 0$, the local interaction impedance $E_e(s)$ at the slave-environment interaction port depends not only on the environment impedance $Z_e(s)$ but also on the environment and robotic tool motions as seen in Eq.(5.9). Actually, $\left(1 + \frac{X_e^*(s)}{X_s(s)}\right)$ is unitless and represents the relativity between the robot's end-effector motion and the environment's induced motion. The effect of this locally induced motion "$\dot{x}_e^*$" can be considered when $\frac{X_e^*(s)}{X_s(s)} \geq \varepsilon$ where ε is a small enough decimal (e.g. $\varepsilon = \pm 0.1$). By substituting (Eqs. 5.18, 5.23) in (Eq. 5.9) we can conclude the following:

$$E(s) = Z_e(s)\left(1 + \frac{s^{m+1}\ \alpha(s)}{\beta(s)\ \prod_{ii=1}^{n}(s^2 + b_{ii}^2)}\right) \tag{5.28}$$

$$= Z_e(s)\left(\frac{\beta(s)\ \prod_{ii=1}^{n}(s^2 + b_{ii}^2) + s^{m+1}\ \alpha(s)}{\beta(s)\ \prod_{ii=1}^{n}(s^2 + b_{ii}^2)}\right) \tag{5.29}$$

$$= \frac{Z_e(s)A(s)}{\beta(s)\ \prod_{ii=1}^{n}(s^2 + b_{ii}^2)} = \frac{N(s)}{D(s)}. \tag{5.30}$$

where

$$A(s) = \beta(s)\ \prod_{ii=1}^{n}(s^2 + b_{ii}^2) + s^{m+1}\ \alpha(s). \tag{5.31}$$

To define the real part of the interaction impedance and considering this last equation, the length of the slave robot's motion interpolation series m plays a decisive role. m is

imposed to be odd and the member $(j\omega)^{m+1}$ is a real part:

$$A(j\omega) \quad = \quad \Re(A(j\omega)) + \Im(A(j\omega))\, j, \tag{5.32}$$

where $\Re(A(j\omega))$ and $\Im(A(j\omega))$ are defined as follows:

$$\begin{cases} \Re(A(j\omega)) = \Re(\beta(j\omega)) \prod\limits_{ii=1}^{n} (b_{ii}^2 - \omega^2) + (j\omega)^{m+1} \Re(\alpha(j\omega)) \\ \Im(A(j\omega)) = \Im(\beta(j\omega)) \prod\limits_{ii=1}^{n} (b_{ii}^2 - \omega^2) + (j\omega)^{m+1} \Im(\alpha(j\omega)) \end{cases} \tag{5.33}$$

$$\begin{cases} \Re(A(j\omega)) & = \Big(c_m m! + \sum\limits_{r=1}^{\tau} (c_v\ v!\ (-1)^r \omega^{2r}) \\ & \quad + (-1)^{\tau} (\omega)^{2\tau} x_e^*(0) \Big) \prod\limits_{ii=1}^{n} (b_{ii}^2 - \omega^2) \\ Im(A(j\omega)) & = \Big(\sum\limits_{r=1}^{\tau} c_{v+1} (v+1)! (-1)^{r-1} \omega^{2r-1} \\ & \quad + (-1)^{\tau} (\omega)^{2\tau+1} \sum\limits_{i=1}^{n} \frac{a_i b_i}{b_i^2 - \omega^2} \Big) \prod\limits_{ii=1}^{n} (b_{ii}^2 - \omega^2) \end{cases} \tag{5.34}$$

The environment interaction impedance is frequency dependent in this case and can be written as follows:

$$E_e(j\omega) = \frac{N(j\omega)}{D(j\omega)} = \frac{\Re(N(j\omega)) + \Im(N(j\omega))\, j}{\Re(D(j\omega)) + \Im(D(j\omega))\, j} \tag{5.35}$$

$$= \Re(E_e(j\omega)) + \Im(E_e(j\omega))\, j. \tag{5.36}$$

Supposing that $R_n = \Re(N(j\omega))$, $I_n = \Im(N(j\omega))$, $R_d = \Re(N(j\omega))$ and $I_d = \Im(N(j\omega))$, the real and imaginary parts of the interaction impedance E_e can be calculated as follows:

$$\Re(E_e(j\omega)) = \frac{R_n R_d + I_n I_d}{R_d^2 + I_d^2} \tag{5.37}$$

$$\Im(E_e(j\omega)) = \frac{R_d I_n - R_n I_d}{R_d^2 + I_d^2}. \tag{5.38}$$

As it is noted in Eq. (5.30): $N(s) = Z(s)A(s)$ and $D(s) = \beta(s) \prod\limits_{ii=1}^{n} (s^2 + b_{ii}^2)$, then:

$$\begin{cases} R_n = \Re(Z_e(j\omega))\Re(A(j\omega)) - \Im(Z_e(j\omega))\Im(A(j\omega)) \\ I_n = \Re(Z_e(j\omega))\Im(A(j\omega)) + \Im(Z_e(j\omega))\Re(A(j\omega)) \\ \\ R_d = \Re\{\beta(\omega\ j)\} \prod\limits_{ii=1}^{n} (b_{ii}^2 - \omega^2) \\ I_d = \Im\{\beta(\omega\ j)\} \prod\limits_{ii=1}^{n} (b_{ii}^2 - \omega^2) \end{cases}$$

$$\begin{cases} R_n = B_e Re(A(j\omega)) - (M_e\omega - \dfrac{K_e}{\omega}) Im(A(j\omega)) \\ I_n = B_e Im(A(j\omega)) + (M_e\omega - \dfrac{K_e}{\omega}) Re(A(j\omega)). \end{cases} \tag{5.39}$$

$$\begin{cases} R_d = \left(c_m m! + \sum_{r=1}^{\tau} c_v v!(-1)^r \omega^{2r}\right) \prod_{ii=1}^{n} (b_{ii}^2 - \omega^2) \\ I_d = \left(\sum_{r=1}^{\tau} c_{v+1}(v+1)!(-1)^{r-1}\omega^{2r-1}\right) \prod_{ii=1}^{n} (b_{ii}^2 - \omega^2). \end{cases} \tag{5.40}$$

The recursive calculation of Eqs. (5.12), (5.3.2), (5.27), (5.33), (5.39), (5.40) and (5.38) enables the calculation of the interaction impedance demonstrated by Eqs. (5.9) and (5.36). Hereafter, one of the employments of such model will be explored. The constructed model of the interaction impedance will be used to evaluate the passivity of the interaction port between the beating heart and the robotic tool. To evaluate the passivity of the interaction impedance, it is sufficient to examine its positivity realness i.e. $Re(E_e(j\omega)) \geq 0$. The real part of the interaction impedance can be written under the form:$Re(E_e(j\omega) = B_e\gamma(j\omega) + (M_e\omega - \frac{K_e}{\omega})\lambda(j\omega)$.

It is noted that this impedance is frequency dependant and is not possible to be positive real for all the frequencies, then the interaction port between the slave robot and the quasi-periodically moving tissue is not passive. This conclusion implies that the used methods to evaluate the teleoperator, used to interact with such environment, has to be revised or to include the environment model in the stability design process of the teleoperation.

5.4 Case Study

Assume a complete interaction between the robotic tool and the beating heart tissue during the whole evaluation time. First the interpolation function of the motion of the beating heart environment is established. Second, respecting the previously mention assumption, a model of the robotic tool end-effector is proposed. Then the interaction impedance model is obtained and analysed.

5.4.1 Beating heart motion modeling

The used data of heart motion to perform the numerical analysis is recorded during *in-vivo* experiments on a pig's heart [Sauvée et al., 2007]. We have selected one axis data for analysis (z_{axis}) [Liu et al., 2011]. The dominant frequencies and their corresponding amplitudes can be obtained through Discrete Fourier Transform (DFT) (Table 5.1). Fig. 5.10 shows the beating heart motion along z_{axis} with its interpolation function which constants (amplitudes and frequencies) are calculated from off-line fast Fourier transform.

Table 5.1: Interpolation using DFT

i	0	1	2	3	4	5
$a_i(mm)$	-1.0	-2.6000	-1.13300	-0.3867	-0.750	-0.807
$f_i\ (Hz)$	0.0	0.3356	0.6714	0.9765	1.251	2.380
$b_i = 2\pi f_i$	0.0	2.11	4.22	6.14	7.86	14.95

$$x_e(t) = a_0 + \sum_{i=1}^{n} a_i\ sin(2\pi f_i\ t + \alpha),\quad x_e^*(0) = a_0,\quad \alpha = \pi/5$$

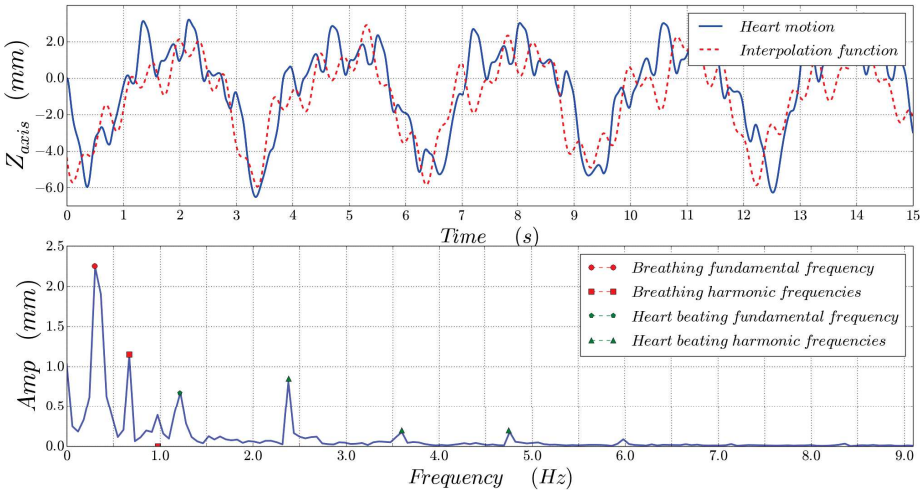

Figure 5.10: Heart motion data

The environment motion disturbance is approximated by the following equation:

$$\begin{aligned} x_e(t) &= -1 - 2.6sin(0.67\pi t + \frac{\pi}{5}) - 1.13sin(1.34\pi t + \frac{\pi}{5}) \\ &- 0.39\ sin(1.95\pi t + \frac{\pi}{5}) - 0.75\ sin(2.5\pi t + \frac{\pi}{5}) - 0.81\ sin(4.76\pi t + \frac{\pi}{5}). \end{aligned} \quad (5.41)$$

5.4.2 Slave Robot Motion Modelling

As previously mentioned, the slave robot's end-effector motion is controlled by surgeon's hand motion. This motion can be separated, when the expert surgeon performs a certified protocol, to several segments. Considering the small available workspace, and to avoid damaging the vital structure with unnecessary movement, the surgeon performs careful and small range movement. This movement can be modelled using the time series in Eq. (5.21) as follows:

$$x_s(t) = c_0 + c_1\ t + c_2\ t^2 + c_3\ t^3. \quad (5.42)$$

Considering the motion expressed by Eq. (5.41) and Fig. 5.10, to achieve a complete interaction between the robotic tool and the moving tissue, this imposes some constraint on the modelled motion of the robotized end-effector like: $x_{robot} \leq 0$.

The robot starts from a suposed initial position of its end-effector along z_{axis} and moves slowly in the negative direction. With respect to the values in table 5.1 and Fig. 5.10, this implies that: $c_0 \geq 4mm$ while c_1 and c_2 can be selected arbitrarily with considering a slow motion. We assume that $c_0 = 5mm$, $c_1 = -10mm/s$, $c_2 = 0mm/s^2$ and $c_3 = 0mm/s^3$.

5.4.3 Interaction Impedance

Because the beating heart soft tissue is subject to non-negligible motion disturbance, the stiffness and inertia parameters in the environment model represented by Eq. (5.10) have to be considered. Considering the parameters of the MSD model of the soft tissue as: $M_e = 0.0005\frac{N.s^2}{mm}$, $K_e = 0.4\frac{N}{mm}$ and $B_e = 0.25\frac{N.s}{mm}$, and using it in the equations (5.33), (5.36), (5.38), (5.39), (5.40), (5.41) and Table (5.1), let us define the following terms as:

$$\Phi = \prod_{ii=1}^{5} (b_{ii}^2 - \omega^2) = (4.45 - \omega^2)(17.8 - \omega^2)(37.64 - \omega^2)(61.78 - \omega^2)(223.62 - \omega^2), \tag{5.43}$$

$$\Omega = \sum_{i=1}^{5} \frac{a_i b_i}{b_i^2 - \omega^2} = \frac{5.486}{4.45 - \omega^2} + \frac{4.781}{17.8 - \omega^2} + \frac{2.374}{37.64 - \omega^2} + \frac{5.895}{61.78 - \omega^2} + \frac{12.065}{223.62 - \omega^2} \tag{5.44}$$

and

$$\Re(\alpha(j\omega)) = x_e^*(0)\ \Phi, \qquad \Im(\alpha(j\omega)) = \omega\ \Omega\ \Phi. \tag{5.45}$$

$$\Re(\beta(j\omega)) = -c_1\omega^2, \qquad \Im(\beta(j\omega)) = -c_0\omega^3. \tag{5.46}$$

$$R_d = -c_1\omega^2 \prod_{ii=1}^{5} (b_{ii}^2 - \omega^2) = 10\ \omega^2\ \Phi \tag{5.47}$$

$$I_d = -c_0\omega^3 \prod_{ii=1}^{5} (b_{ii}^2 - \omega^2) = -5\ \omega^3\ \Phi \tag{5.48}$$

$$R_d^2 + I_d^2 = (100 + 25\omega^2)\ \omega^4\ \Phi. \tag{5.49}$$

$$R_n = \Big(B_e\Big(-c_1 + \omega^2 x_e^*(0)\Big) - (M_e\omega^2 - K_e)\Big(-c_0 + \omega^3\Omega\Big)\Big)\omega^2\Phi \tag{5.50}$$

$$I_n = \Big(B_e\Big(-c_0 + \omega^2\Omega\Big)\omega^3 + (M_e\omega^2 - K_e)\Big(-c_1\omega + \omega^3 x_e^*(0)\Big)\Big)\Phi \tag{5.51}$$

$$R_n = \Big(0.5 - 0.2475\omega^2 - (5.10^{-4}\omega^2 - 0.4)\omega^3\Omega\Big)\omega^2\Phi \tag{5.52}$$

$$I_n = \Big(-4\omega - 0.845\omega^3 - 0.0005\omega^5 + \omega^5\Omega\Big)\Phi \tag{5.53}$$

$$R_nR_d + I_nI_d = \Big(B_e\Big(c_1^2 + c_0^2\omega^2 - c_1\omega^2 x_e^*(0) - c_0\omega^4\Omega\Big) + (M_e\omega^2 - K_e)\Big(-c_0 x_e^*(0) + c_1\omega\Omega\Big)\omega^2\Big)\omega^4\Phi \tag{5.54}$$

$$= \Big(25 + 1.75\omega^2 + 25.10^{-4}\omega^4 + (4 - 1.255\omega^2)\omega^2\Omega\Big)\omega^4\Phi. \tag{5.55}$$

Then, for the interaction impedance:

$$\Re(E(\omega)) = \frac{R_nR_d + I_nI_d}{R_d^2 + I_d^2} \tag{5.56}$$

$$= \Big(\frac{25 + 1.75\omega^2 + 25.10^{-4}\omega^4}{100 + 25\omega^2}\Big) + \frac{4 - 1.255\omega^2}{100 + 25\omega^2}\,\omega^2 \sum_{i=1}^{5} \frac{a_i b_i}{b_i^2 - \omega^2}. \tag{5.57}$$

For this case study, the real part of the interaction impedance in the frequency domain is represented as:

$$\Re(E(\omega)) = \Big(\frac{25 + 1.75\omega^2 + 25.10^{-4}\omega^4}{100 + 25\omega^2}\Big) + \frac{4 - 1.255\omega^2}{100 + 25\omega^2}\,\omega^2\Big(\frac{5.486}{4.45 - \omega^2} + \frac{4.781}{17.8 - \omega^2} + \frac{2.374}{37.64 - \omega^2} + \frac{5.895}{61.78 - \omega^2} + \frac{12.065}{223.62 - \omega^2}\Big). \tag{5.58}$$

Its value with respect to different frequencies are shown geometrically in Fig. (5.11):

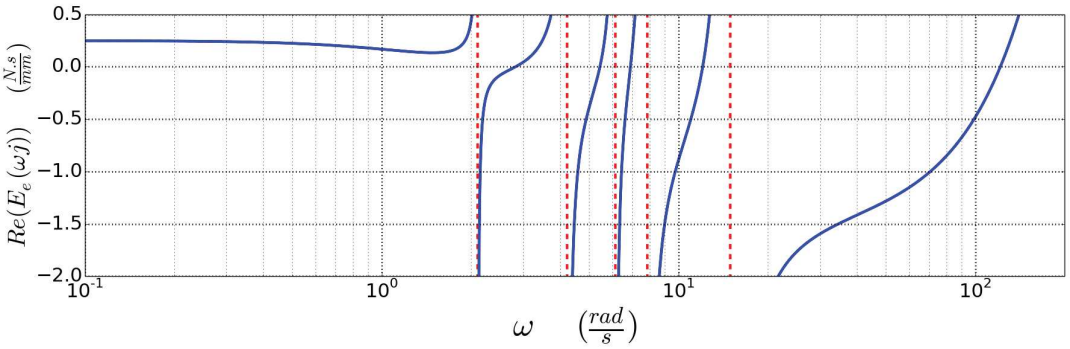

Figure 5.11: The real part of the interaction impedance

Equation (5.58) shows that: $\lim_{\omega\to 0} Re(E(\omega)) = Re(Z_e) = B_e$. This conclusion is also demonstrated through the plot of $Re(E_e(j\omega))$ in Fig.5.11. This interaction impedance is not positive real and the interaction with such environment is hence not passive. This conclusion suggests that the evaluation concepts and criterions of the teleoperated interaction with active and bounded active environments should be reconsidered for moving environment involving different motion frequencies.

5.5 Conclusion

This chapter investigates the effect of physiological disturbance presence on the impedance sensed at slave tip. A reality based analysis lead to establishing the interaction impedance model. In the presence of motion disturbance, the sensed impedance at robot tip depends not only on the physical properties of the treated tissue (environment) but also on the ratio between robot end-effector motion and the disturbance motion. The proposed interaction model highlights the importance of motion synchronisation between tool tip and organ motion. Furthermore, this work proposes an analytical method to evaluate and calculate the interaction impedance in the frequency space, which could be useful in evaluating a teleoperator transparency in the presence of physiological motion disturbance. Finally a case study of interaction between slave robot and beating heart surface is introduced to illustrate the algorithm application.

CHAPTER

6 Slave-Environment Interaction Control Based Haptic Teleoperation

Preamble

The previous chapter developed a general model of tool-tissue interaction by considering the presence of an inherent motion disturbance in the operated tissue. This interaction model depends on the soft tissue impedance, robot and tissue motion (i.e. $E_{int} = f(Z_e, \dot{x}_s, \dot{x}_e^*)$). In this chapter, we analyse the effects of the interaction model used to represent the interaction with a constant soft tissue (i.e. $Z_e = E_{int}\big|_{\dot{x}_e^* \longrightarrow 0}$) on the performance of interaction control based haptic teleoperation.

In telesurgery context and because the robot is executing his task in human occupied environment, an interaction based control of the surgical robot is a desired feature. This chapter introduces a new haptic teleoperation CA that applies an interaction control algorithm on slave site. This algorithm requires a model of the tool-tissue interaction. Hunt-Crossley model describes better the viscoelastic properties of soft tissues. Therefore, the performance of the interaction control based haptic teleoperation is improved for medical applications by integrating Hunt-Crossly to represent tool-soft tissue interaction. First, the nonlinear Hunt-Crossly model is linearised around a work point in order to implement model-based AOB algorithm [Cortesão et al., 2006] and to investigate finally the stability and transparency of the proposed architecture. The results are supported experimentally by in-vitro validation using Raven II- Sigma7 teleoperation test-bed.

6.1 Introduction

Medicine preformed wide steps during the precedent century. One of the main landmarks was the integration of surgical robot in OR to assist surgeons and enable more complex and sometimes unachievable therapeutic techniques [Troccaz, 2013] [Bozovic, 2008] [Rosen et al., 2011]. There are still many details to improve, one of them is represented by the haptic feedback integration in the telesurgical platform. Furthermore, because the surgical robot is acting in a human occupied environment, an interaction based control of the surgical robot is a desired feature. Haptic augmentation aims to enable surgeons to exert the forces required to execute successfully a targeted task and to perceptive the operated tissues mechanical properties. Consequently, the excess in tool-tissue interaction forces will be reduced [Kitagawa et al., 2002] [Wagner et al., 2002]. On the other hand, an interaction based control of the surgical robot would increase the intervention safety by increasing the surgical robot compliance and sensitivity toward any unexpected changes in the interaction with the environment.

The minimum requirements to establish a transparent (haptic) teleoperation is to realise ($P-F$ CA) [Albakri et al., 2013] [1]. In this CA, human actions are sent as a reference position to the slave robot while the master receives environment reaction forces as a reference to feedback to the human operator. The slave robot is driven consequently using a position based controller and therefore its sensitivity toward the interaction with the operated environment is poor [2] . [Park and Khatib, 2006] treated the aforementioned problem by proposing an interaction based control of the slave robot and by conserving simultaneously the haptic nature of the implemented teleoperation CA (figure 6.1). The interaction control algorithm requires a model of robot-environment interaction and [Park and Khatib, 2006] uses a virtual spring (elastic) model. [Cortesão et al., 2006] improved the system performance by imposing a real-time adaptive stiffness on the virtual spring. This method, proposed in the mobile robotics community, is adapted for surgical community by [Zarrad et al., 2007]. The elastic model is incapable of describing the viscoelastic properties of living tissues' interaction. Therefore, a well known state of art linear models (ex. Kelvin-Voigt, Kelvin-Boltzmann, etc. [Diolaiti et al., 2005][Fung, 1993]) are integrated in slave robot controller design to improve the performance on the interaction control based haptic teleoperation [Sánchez et al., 2012] [Moreira et al., 2014].

In this CA (figure 6.1), the directions, that subject to interaction (force) control, receive f_d as a reference. The reference force signal f_d is calculated based on master-slave position correspondence error using k_{vir} transfer function. k_{vir} represents a virtual spring and can adopt any adequate model to represent robot-environment interaction. Furthermore, the

1. In transparent teleoperation, the two remote sites have to exchange different types of signals [Naerum et al., 2012]. In medical context ($P-PF$ CA) represents the optimal candidate while ($P-F$ CA) represents the minimum requirement with confined choises to perform stability-transparency trade-off(chapter 4).

2. Robot end-effector is very stiff in comparison with the operated soft tissue. Position based control of the robot imposes its position on the environment leading to undesired performance (consequences).

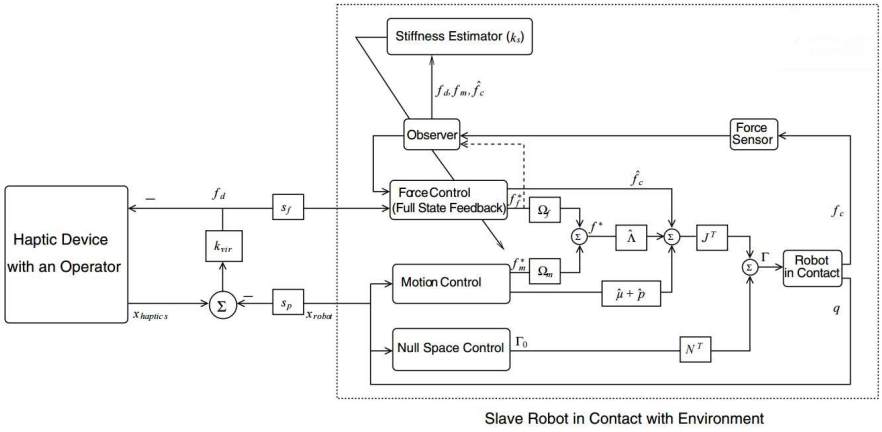

Figure 6.1: Interaction control based haptic teleoperation as proposed in [Park and Khatib, 2006]

desired force f_d is fed back to the master device to feedback to the operator. Unfortunately, this CA suffers from several limitations which are summarized as follows:

i. Due to its complex nature, to organize the CA under teleoperation standard framework (as a 2-port network) is an arduous task. Consequently, the designer choices are confined to the linear systems tools in place of teleoperation tools to perform the design and assessment step of the teleoperation system.

ii. The haptic feedback sense to human operator is governed by k_{vir}. In other words, the operator feels the virtual model dynamics rather than this of the real environment.

iii. To realize the interaction control algorithm, a force sensor on the slave site is required to measure robot-environment interaction forces. Nevertheless, The measured forces are not used to feedback through the haptic interface. Consequenlty, the operator feels a virtual forces while the real interaction forces are available.

iv. The interaction control algorithm uses a linear model to describe tool-tissue interaction. Linear models fails to describe the living tissues' viscoelastic (nonlinear) properties leading to a corresponding inaccuracy in the interaction control performance.

This chapter improves the aforementioned concept in two aspects: First, A new approach is proposed to replace the precedent CA (figure 6.1) by conserving its main features (i.e. transparent teleoperation CA and interaction based control of the slave robot). The proposed CA adopt the standard $P-F$ CA form and can be consequently designed using teleoperation tools. Second, tool-tissue interaction's viscoelastic properties are better described by integrating Hunt-Crossly model in the interaction control algorithm design.

6.2 Chapter Contributions and Organisation:

The contributions of this chapter can be organized in the following three main folds:

I. ***A new teleoperation CA:***
   1. Proposition of new transparent CA with interaction based control of slave robot.
   2. Design and assessment of the proposed CA.

II. ***An enhanced interaction controller***
   1. Based on relaxation test analysis, the importance of Hunt-Crossly model is highlighted in better describing soft tissues' viscoelastic properties.
   2. Hunt-Crossly model is linearised around a working point to design AOB controller.
   3. Design of Hunt-Crossly model based AOB interaction controller.

III. ***Experimental validation***
   1. The Hunt-Crossly model based AOB controller is tested on Raven II robot.
   2. The dynamics of the used haptic interface (Sigma 7) is identified.
   3. The designed bilateral teleoperation is realized on (Raven II-Sigma 7) test-bed for elastic and Hunt-Crossly models and the results are discussed.

To address these contributions, this chapter is organised in three main sections as follows: First, the teleoperation control architecture is proposed and the required modelling, design and assessment are addressed. The second section focuses on the design and implementation of the enhanced interaction controller by introducing Hunt-Crossly model to the design of AOB controller. Finally the experimental validation of the proposed teleoperation CA is introduced and the results are discussed.

6.3 Teleoperation Structure

Figure 6.2 presents our proposed CA. On the master site, the forces generated by the interface motors F_{cm}, in the purpose of reproducing the haptic sense, collaborate with these generated by the human operator F_h to derive the interface mechanism Z_m. The resultant human hand (master) motion V_m is captured and transferred to the slave site after being scaled with β_p. Based on the velocity (position) correspondence error between master and slave motion (i.e. $\beta_p V_m - V_s$), a desired value F_d of slave-environment interaction force is generated using G_v transfer function. An adequate interaction controller (in this chapter, we use AOB model based interaction controller [Cortesão et al., 2006] [3]) is realized on the slave such that slave-environment interaction forces F_e follows the desired forces F_d with

3. The advantages of this observer-based state space controller is its robustness toward uncertainties, thank you to the presence of Kalman recursive formula to calculate the observer gain and to the augmented state which predict stochastically the non-modelled errors and uncertainties.

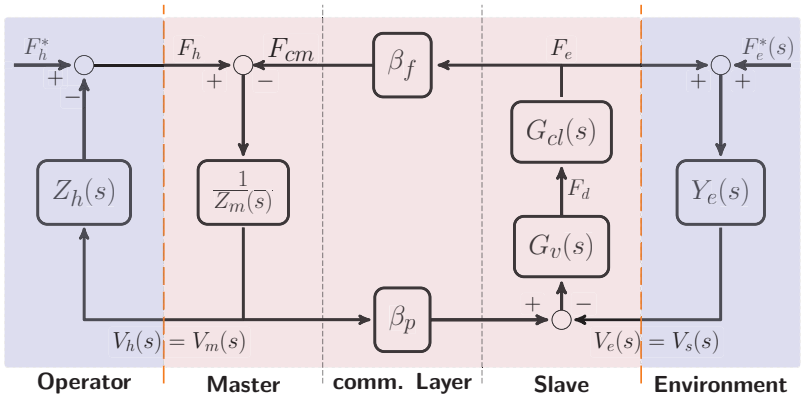

Figure 6.2: Bilateral teloperation scheme

a designed desired dynamics G_{cl}. The measured interaction forces F_e are scaled by β_f and fed back to the master robot to deliver a corresponding haptic sense to the operator.

This CA adopt $P-F$ CA form. and can consequently achieve a complete transparency. Moreover, this CA implements an interaction controller on the slave robot as a desired feature in the medical context. The transmission between the velocity error $\dot{e} = \beta_p V_m - V_s$ and the desired force F_d is achieved through G_v transfer function. The following section discusses the design of this CA and the constraints imposed on G_v transfer function to optimise the CA transparency while guaranteeing the system absolute stability.

6.3.1 Modelling

To analyse the CA introduced in (Figure 6.1), [Park and Khatib, 2006] proposed to establish the equivalent open loop structure between the human input F_h and the slave output X_s. This concept is adopted in [Cortesão et al., 2006] and [Zarrad et al., 2007] who decomposed the operator hand motion into voluntary motion and involuntary (reflexive) motion.

This section analyses the structure illustrated by figure 6.2 based on its hybrid model. Thanks to its $P-F$ CA form, the hybrid model of the proposed CA (figure 6.2) can be deduced as follows:

$$Z_m V_m = F_h - \beta_f F_e \tag{6.1}$$

$$G_{cl} G_v (\beta_p V_m - V s) = F_e, \tag{6.2}$$

which can be reformulated as:

$$F_h = Z_m V_m + \beta_f F_e \tag{6.3}$$

$$G_{cl} G_v (-V s) = -G_{cl} G_v \beta_p V_m + F_e. \tag{6.4}$$

Then the system hybrid model takes the following form:

$$\begin{bmatrix} F_h \\ -V_s \end{bmatrix} = \begin{bmatrix} Z_m(s) & \beta_f \\ -\beta_p & \frac{1}{G_{cl}(s)G_v(s)} \end{bmatrix} \begin{bmatrix} V_m \\ F_e \end{bmatrix} \tag{6.5}$$

Comparing the precedent form with the ideal performance form in (Eq. 3.48) gives the designer a quick indication to where he/she should pay more attention in the design process. This comparison suggests that, to have good performance, the master device inertial properties has to minimized (ideally $Z_m = 0$) and the G_v has to be designed to minimise also $\frac{1}{G_{cl}(s)G_v(s)}$. On the other hand, the condition $\beta_p = \beta_f = 1$ can be relaxed by considering $\beta_p\beta_f = 1$ where the essential objective from energetic point of view is that the energy at the two remote interaction ports (master and slave) are identical. The following section discusses the stability of the proposed CA based on Llewellyn criteria.

6.3.2 Stability

Based on Llewellyn criteria, this 2-port network (figure 6.2) is stable if:

$$\Re\{h_{11}\} = \Re\{Z_m(\omega j)\} \geq 0, \tag{6.6}$$

$$\Re\{h_{22}\} = \Re\{\frac{1}{G_{cl}(\omega j)G_v(\omega j)}\} \geq 0, \tag{6.7}$$

$$\begin{aligned} \eta_h(\omega) &= -\frac{\Re\{h_{12}h_{21}\}}{|h_{12}h_{21}|} + 2\frac{\Re\{h_{11}\}\Re\{h_{22}\}}{|h_{12}h_{21}|} \\ &= -\frac{\Re\{-\beta_p\beta_f\}}{|-\beta_p\beta_f|} + 2\frac{\Re\{Z_m(\omega j)\}\Re\{\frac{1}{G_{cl}(\omega j)G_v(\omega j)}\}}{|-\beta_p\beta_f|} \geq 1. \end{aligned} \tag{6.8}$$

Considering $\beta_p,\ \beta_f \in \mathbb{R}^+$ (positive scalars), $G_{cl}(s) = \dfrac{e^{-sT_d}}{(1+T_{cl}s)^2}$ [4] with $T_d = 0.0$ ms and the master dynamics can be described as $Z_m = M_m s + B_m + \dfrac{K_m}{s}$ with M_m, B_m and K_m the Cartesian inertia, damping and stiffness properties of the haptic interface on the analysed direction. Consequently, the stability conditions becomes:

$$\Re\{Z_m(j\omega)\} = B_m \geq 0, \tag{6.9}$$

$$\Re\{\frac{1}{G_{cl}(j\omega)G_v(j\omega)}\} \geq 0, \tag{6.10}$$

$$\frac{2B_m}{\beta_p\beta_f}\Re\{\frac{1}{G_{cl}(j\omega)G_v(j\omega)}\} \geq 0. \tag{6.11}$$

4. G_{cl} represents the controlled dynamics of slave-environment interaction which will be designed to have this desired form. More details can be traced in AOB controller design.

Because the master system is designed to be stable, the first condition is always achieved. Furthermore the second and third conditions can be summarized in the following condition which rules the stability transparency trade-offs through G_v adjustment:

$$\Re\{\frac{1}{G_{cl}(\omega j)G_v(\omega j)}\} \geq 0. \tag{6.12}$$

Considering that G_v can be written under the form $G_v(\omega j) = \Re(G_v(\omega j)) + \Im(G_v(\omega j))$ and $G_{cl}(\omega j) = \frac{1}{(1+T_{cl}\omega j)^2}$, then based on the this last condition, the teleoperation system is stable if the following condition stands for all targeted frequencies:

$$\frac{\Re(G_v(\omega j)}{\Im(G_v(\omega j)} \geq \frac{2T_{cl}\omega}{1-T_{cl}^2\omega^2} \quad \Leftrightarrow \quad \angle G_v(\omega j) \geq \angle G_{cl}(\omega j) \quad \forall \quad \omega \geq 0. \tag{6.13}$$

6.3.3 Transparency

Following the discussion of the 3^{rd} chapter, teleoperation performance (transparency) can be evaluated using two closely related criteria, the first analyses the dynamic range of reflected impedances and the second focuses on the matching between environment impedance and this sensed by the remote operator. Unfortunately, following the dynamic range of reflected impedances criteria does not give a satisfactory analysis because:

$$Z_{tomin} = h_{11} = Z_m \tag{6.14}$$

$$Z_{towidth} = -\frac{h_{12}h_{21}}{h_{11}} = \frac{\beta_p\beta_f}{Z_m}. \tag{6.15}$$

Minimizing Z_{tomin} would lead to maximize $Z_{towidth}$ which is a good property of this CA. But this specific criteria do not comment the contribution of the other decisive components (i.e. G_v and G_{cl}). Consequently we follows the second method to evaluate our proposed CA where the sensed impedance by human operator can be calculated using (Eq. 3.46) as follows:

$$\Delta h = \frac{Z_m}{G_{cl}C_v} + \beta_p\beta_f = \frac{Z_m + \beta_p\beta_f G_{cl}G_v}{G_{cl}C_v} \tag{6.16}$$

$$Z_{to}(s) = \frac{h_{11}(s) + \Delta h(s)Z_e(s)}{1 + h_{22}(s)Z_e(s)} = Z_m(s) + \frac{\beta_p\beta_f G_{cl}(s)G_v(s)Z_e(s)}{G_{cl}(s)G_v(s) + Z_e(s)} \tag{6.17}$$

$$Z_{to}(s) = Z_m(s) + \frac{\beta_p\beta_f G_{cl}(s)G_v(s)}{1 + G_{cl}(s)G_v(s)Z_e^{-1}(s)}. \tag{6.18}$$

The same form of Z_{to} in (Eq. 6.18) can be obtained following the steps of [Park and Khatib, 2006] [Zarrad et al., 2007] by reformulating the teleoperation scheme in (Fig. 6.2)

under the form of (Fig. 6.3) and considering that the real dynamics of the environment Z_e is well described by the model $G_e \approxeq Z_e$. The sensed impedance by the human operator is:

$$Z_{to}(s) = \frac{F_h(s)}{V_h(s)} = Z_m(s) + \frac{\beta_p \beta_f G_v(s) G_{cl}(s)}{1 + G_v(s) G_{cl}(s) G_e^{-1}(s)} \tag{6.19}$$

According to (Eq. 6.18 and Eq. 6.19), transparency is affected by the selection of $G_v(s)$ as illustrated in (fig. 6.3) and (eq. 6.19). Considering rate tracking error as input ($\beta_p V_m - V_s$), $G_v(s)$ is used to obtain the necessary desired force F_d to perform an adequate force control on the slave site and is used to optimize the system transparency. Distinguishing between $G_e(s)$ which represents the environment dynamic model and $Z_e(s)$ the real dynamic of the environment tissue, $G_v(s)$ can be calculated using two methods, approximative and precise.

Approximative calculation of $G_v(s)$:

Usually, the master robot is a haptic interface which is adequate targeted application. The haptic devices are designed to maximize the system transparency by involving low inertia and a good level of gravity and friction compensation. These facts makes the $Z_m(s)$ involved in the teleoperation very small and hence its possible to design the MSN such that the sensed impedance by the human operator has the form:

$$Z_{to} = Z_m + Z_e. \tag{6.20}$$

Consequently, comparing (eq. 6.20) to (eq. 6.18) gives rise to:

$$G_v(s) = \frac{Z_e(s)}{(\beta_p \beta_f - 1) G_{cl}(s)}. \tag{6.21}$$

Because robot-environment interaction measurements F_e and V_s are available, Z_e can be calculated directly by applying $Z_e(k) = F_e(k)/v_s(k)$. Otherwise, if the environment model

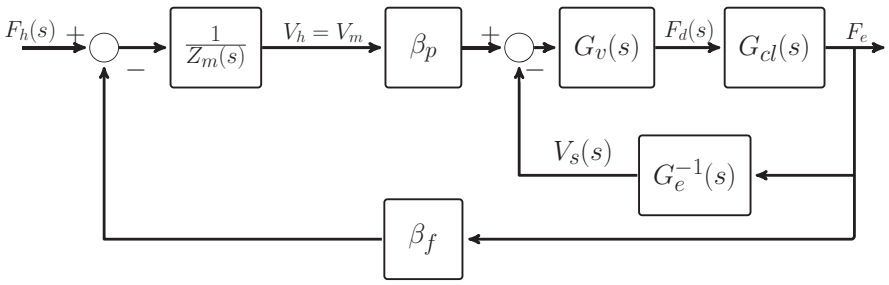

Figure 6.3: Teleoperation scheme reformulation

is accurate enough to consider $Z_e \cong G_e(s)$ then:

$$G_v(s) = \frac{G_e(s)}{(\beta_p \beta_f - 1) G_{cl}(s)}. \tag{6.22}$$

The drawback of this simplified method is that Eq. 6.22 shows clearly that the complete transparency cannot to realise because considering $\beta_p \beta_f = 1$ makes G_v indeterminable.

Precise calculation of $G_v(s)$:

Transparency is achieved when the impedance sensed by the operator equals the treated tissue impedance i.e.:

$$Z_{to} := Z_e. \tag{6.23}$$

Consequently, comparing (eq. 6.23) to (eq. 6.18) gives rise to:

$$G_v(s) = \frac{(Z_e - Z_m) Z_e(s)}{(\beta_p \beta_f Z_e(s) - Z_e + Z_m) G_{cl}(s)} \tag{6.24}$$

$Z_e(k) = F_e(k) / v_s(k)$ or $Z_e \cong G_e(s)$ for precise model, then:

$$G_v(s) = \frac{(G_e(s) - Z_m) G_e(s)}{((\beta_p \beta_f - 1) G_e(s) + Z_m) G_{cl}(s)} \tag{6.25}$$

In fact, including Z_m in $G_v(s)$ calculation improves the transparency where, at least mathematically, the optimised transparency when $\beta_p \beta_f = 1$ is admissible and accordingly:

$$G_v(s) = \frac{(G_e(s) - Z_m) G_e(s)}{Z_m G_{cl}(s)} \tag{6.26}$$

The following section discusses the need G_v transfer function, its role and the imposed constraints of G_v design to optimize the system performance.

6.3.4 The role of G_v transfer function (a discussion)

The simplest way to introduce G_v is to consider it equivalent to the environment model G_e. Consequently, the incremental motion imposed by human actions and represent by $\dot{e} = \beta_p v_m - v_s$ will be transformed through $G_v = G_e$ into a corresponding force F_d that predict the interaction output (force). This model-based calculated interaction force is used as desired reference to the interaction controller that roles the slave performance. Furthermore, in this concept, any changes in the environment motion v_e would be reflected in a corresponding changes in the desired and interaction forces F_d and F_e respectively. In other words, the robot itself will respond to the interaction changes before even the human himself sense it through the haptic interface.

The aforementioned case appears when the slave is isolated from teleoperation context. In teleoperation, further constraints has to be imposed on G_v to guarantee the stability and transparency of the considered system as discussed in the precedent sections. A general recursive formula to calculate G_v for tissue interaction models treated in this thesis can be deduced. Considering that master and slave dynamics has the following form:

$$Z_m(s) = m_m s + b_m \tag{6.27}$$

$$G_{cl}(s) = \frac{1}{(1+T_{cl}s)^2} = \frac{1}{(1+2T_{cl}s+T_{cl}^2s^2)}. \tag{6.28}$$

The considered models to represent tool-tissue interaction are: elastic model, KV, KB and linearised HC model. It can be noted that the previous models can be deduced from KB model by assigning the non-involved parameters to zero. Consequently, the recursive formula to establish G_v transfer function is deduced based on KB model where environment dynamics is represented as follows:

$$G_e(s) = \frac{F_e(s)}{V_e(s)} = \frac{k_e + b_e s}{s(1+\alpha_e s)}. \tag{6.29}$$

- For elastic model $b_e = 0$ and $\alpha_e = 0$.
- For KV and linearised HC model $\alpha_e = 0$.
- In KB model all the parameters are involved.

Approximative G_v

$$G_v(s) = \frac{G_e(s)}{(\beta_p\beta_f - 1)G_{cl}(s)}, \tag{6.30}$$

$$G_v(s) = \frac{F_d(s)}{se(s)} = \frac{k_e + (b_e + 2T_{cl}k_e)s + (T_{cl}^2k_e + 2T_{cl}b_e)s^2 + T_{cl}^2b_es^3}{(\beta_p\beta_f - 1)s(1+\alpha_e s)}. \tag{6.31}$$

Then:

$$G_v(s) = \frac{F_d(s)}{se(s)} = \frac{a_0 + a_1 s + a_2 s^2 + a_3 s^3}{s(1+\alpha_e s)} \tag{6.32}$$

with $a_0 = \dfrac{k_e}{\beta_p\beta_f - 1}$, $a_1 = \dfrac{b_e + 2T_{cl}k_e}{\beta_p\beta_f - 1}$, $a_2 = \dfrac{T_{cl}^2k_e + 2T_{cl}b_e}{\beta_p\beta_f - 1}$, $a_3 = \dfrac{T_{cl}^2b_e}{\beta_p\beta_f - 1}$ and $se(s) = \beta_p V_m(s) - V_s(s)$.

$$(1+\alpha_e s)F_d(s) = (a_0 + a_1 s + a_2 s^2 + a_3 s^3)e(s). \tag{6.33}$$

The stability condition of teleoperation system has to be verified before implementing G_v.

Precise calculation of $G_v(s)$

$$G_v(s) = \frac{(G_e(s) - Z_m)G_e(s)}{Z_m G_{cl}(s)} \tag{6.34}$$

$$G_e(s) - Z_m(s) = \frac{K_e + B_e s}{s(1+\alpha_e s)} - (m_m s + b_m) = \frac{b_0 + b_1 s + b_2 s^2 + b_3 s^3}{s(1+\alpha_e s)} \tag{6.35}$$

$$\begin{aligned} b_0 &= K_e \\ b_1 &= B_e - b_m \\ b_2 &= -(m_m + \alpha_e b_m) \\ b_3 &= -\alpha_e m_m \end{aligned}$$

$$(G_e(s) - Z_m(s))G_e(s) = \frac{b_0 + b_1 s + b_2 s^2 + b_3 s^3}{s(1+\alpha_e s)} \; \frac{K_e + B_e s}{s(1+\alpha_e s)} = \frac{c_0 + c_1 s + c_2 s^2 + c_3 s^3 + c_4 s^4}{s^2(1 + 2\alpha_e s + \alpha_e^2 s^2)} \tag{6.36}$$

$$\begin{aligned} c_0 &= b_0 K_e = K_e^2 \\ c_1 &= b_0 B_e + b_1 K_e = (2B_e - b_m)K_e \\ c_2 &= b_1 B_e + b_2 K_e = (B_e - b_m)B_e - (m_m + \alpha_e b_m)K_e \\ c_3 &= b_2 B_e + b_3 K_e = -(m_m + \alpha_e b_m)B_e - \alpha_e m_m K_e \\ c_4 &= b_3 B_e = -\alpha_e m_m B_e \end{aligned}$$

$$Z_m G_{cl}(s) = \frac{b_m + m_m s}{1 + 2T_{cl} s + T_{cl}^2 s^2} \tag{6.37}$$

$$\begin{aligned} G_v(s) = \frac{(G_e(s) - Z_m)G_e(s)}{Z_m G_{cl}(s)} &= \frac{(c_0 + c_1 s + c_2 s^2 + c_3 s^3 + c_4 s^4)(1 + 2T_{cl} s + T_{cl}^2 s^2)}{s^2 b_m (1 + 2\alpha_e s + \alpha_e^2 s^2)(1 + \frac{m_m}{b_m} s)} \\ &= \frac{a_0 + a_1 s + a_2 s^2 + a_3 s^3 + a_4 s^4 + a_5 s^5 + a_6 s^6}{s^2(1 + e_1 s + e_2 s^2 + e_3 s^3)} \end{aligned} \tag{6.38}$$

$$
\begin{aligned}
a_0 &= \frac{c_0}{b_m} = \frac{K_e^2}{b_m} \\
a_1 &= \frac{c_1 + 2T_{cl}c_0}{b_m} = (2B_e - b_m)K_e + 2T_{cl}K_e^2 = (2B_e - b_m + 2T_{cl}K_e)\frac{K_e}{b_m} \\
a_2 &= \frac{c_2 + 2T_{cl}c_1 + T_{cl}^2 c_0}{b_m} = \Big(B_e - b_m\Big)\frac{B_e}{b_m} + \Big(-m_m - \alpha_e b_m + 2T_{cl}(2B_e - b_m) + T_{cl}^2 K_e\Big)\frac{K_e}{b_m} \\
a_3 &= \frac{c_3 - 2T_{cl}c_2 + T_{cl}^2 c_1}{b_m} \\
&= \Big(-(m_m + \alpha_e b_m) + 2T_{cl}(B_e - b_m)\Big)\frac{B_e}{b_m} + \Big(-\alpha_e m_m - 2T_{cl}(m_m + \alpha_e b_m) + T_{cl}^2(2B_e - b_m)\Big)\frac{K_e}{b_m} \\
a_4 &= \frac{c_4 + 2T_{cl}c_3 + T_{cl}^2 c_2}{b_m} \\
&= \Big(-\alpha_e m_m - 2T_{cl}(m_m + \alpha_e b_m) + T_{cl}^2(B_e - b_m)\Big)\frac{B_e}{b_m} + \Big(-2T_{cl}\alpha_e m_m - T_{cl}^2(m_m + \alpha_e b_m)\Big)\frac{K_e}{b_m} \\
a_5 &= \frac{2T_{cl}c_4 + T_{cl}^2 c_3}{b_m} = \Big(-2T_{cl}\alpha_e m_m - T_{cl}^2(m_m + \alpha_e b_m)\Big)\frac{B_e}{b_m} + \Big(-T_{cl}^2\alpha_e m_m\Big)\frac{K_e}{b_m} \\
a_6 &= \frac{T_{cl}^2 c_4}{b_m} = -T_{cl}^2\alpha_e m_m \frac{B_e}{b_m}
\end{aligned}
\tag{6.39}
$$

It can be noted that the order of G_v numerator is higher than its denominator which make it difficult to analyse and implement in discrete time. To overcome this burden it is possible either to descretize its inverse i.e. $G_v^{-1}(z) = \frac{e_v(z)}{F_e(z)}$ or to multiply G_v by low-pass filter (i.e. $\frac{a}{s+a}$) where $a \geq 1000$ to make numerator and denominator orders equivalent.

6.4 An Enhanced Interaction Controller

Slave robot in OR is a surgical robot and performs his task on a living tissues environment. Therefore, interaction based control of this surgical robot is always considered as desired function to exert a sufficient forces to execute the required task. In other words, to reduce the exceed in forces exerted by the robot on the operated tissues. Our proposed haptic CA involves interaction control of slave robot. The applied control algorithm adopts AOB model based interaction control. The main advantage of this controller is its robustness toward uncertainties. Nevertheless, model accuracy of tool-tissue interaction plays a decisive role in the performance of this special interaction controller. Therefore we explore the performance of AOB based controller which uses Hunt-Crossly model to describe tool-tissue interaction.

This section introduces some of the famous model used to model tissue interaction dynamics and justify the use of Hunt-Crossly model. Furthermore, it introduces the corresponding AOB model based interaction controller.

6.4.1 Tissue interaction model

Tissue interaction model describes deformation-interaction force (stress-strain) relationship of tool-tissue dynamic interaction. This model characterizes the tissue interaction impedance. The real physical dynamics of the operated soft tissue is represented by the transfer function $Y_e(s)$:

$$Y_e(s) = \frac{1}{Z_e(s)} = \frac{V_e(s)}{F_e(s) + F_e^*(s)}. \tag{6.40}$$

Generally we do not have an accurate description of these dynamics rather than by knowing the input and the output at a given instant. Providing an accurate model to the force-deformation relationship of a living soft tissue is a quite challenging problem because of its viscoelasticity and non-linear properties (i.e. inhomogeneous multi-layers) of soft tissues. A wide variety of linear and non-linear models are available in the literature to describe soft tissue deformation dynamics. Table 6.1 summarises the most famous ones.

Model	**Constitutive law**	$G_e(s) = Z_e(s)$
Elastic	$F(t) = k_e x(t)$	$\frac{k_e}{s}$
Maxwell (MW)	$F(t) = b_e \dot{x}(t) - \alpha_e \dot{F}(t)$	$\frac{b_e}{s(1+\alpha_e s)}$
Kelvin-Voigt (KV)	$F(t) = k_e x(t) + b_e \dot{x}(t)$	$\frac{k_e + b_e s}{s}$
Kelvin-Boltzmann (KB)	$F(t) = k_e x(t) + b_e \dot{x}(t) - \alpha_e \dot{F}(t)$	$\frac{k_e + b_e s}{s(1+\alpha_e s)}$
Hunt-Crossly (HC)	$F(t) = k_e x^{\beta_e}(t) + \lambda_e x^{\beta}(t)\dot{x}(t)$	$G_{e_{HC}}$

Table 6.1: Candidate models

Model selection:

In the aim of selecting the model that describes better tool-tissue interaction dynamics, we carried out an *in vitro* experimental comparison between the performance of these models (Table 6.1) in AOB model based interaction control on Raven II robot using a piece of lamb's heart as a tissue. The model coefficients are identified and the AOB algorithm is implemented. In the purpose of clarity and to escape repetition trap, the identification

and comparison result are introduced in (Appendix A). These results show the superiority of Hunt-Crossly based interaction control and therefore it is used to realise the actual interaction control based haptic teleoperation.

Linearisation of Hunt-Crossly non-linear model:

Because Hunt-Crossly model provides a better representation of soft tissues, the environment model $G_e(s)$ necessary to establish the model based interaction control algorithm on the slave robot is using Hunt-Crossly model. This model is described as follows:

$$F(t) = k_e x^{\beta}(t) + \lambda_e x^{\beta_e}(t)\dot{x}(t) \tag{6.41}$$

To better present the viscoelastic properties of tool-tissue interaction, Hunt-Crossly model proposes time variant coefficient to spring-damper system (Kelvin-Voigt model). To establish the adequate model based force controller on the slave robot; the model in (eq.6.41) has to be linearised. The linearisation is performed around an equilibrium position (steady state) (x_s) that the model achieves under a constant input (F_d) starting from initial position (x_0) (Fig. 6.4).

A non-linear function $F_e(x,\dot{x})$ can be linearised using Taylor expansion. Considering the first order terms of this expansion $F_e(x,\dot{x})$ has the following expression:

$$F_e(x,\dot{x}) \approx F_e(x_s,\dot{x}_s) + \left.\frac{\partial F_e}{\partial x}\right|_{x_s,\dot{x}_s}(x-x_s) + \left.\frac{\partial F_e}{\partial \dot{x}}\right|_{x_s,\dot{x}_s}(\dot{x}-\dot{x}_s). \tag{6.42}$$

The equilibrium state conditions are $\dot{x}_s = 0$ and $F_d = F_e$ then:

$$F_d = F_e(x_s,\dot{x}_s)|_{\dot{x}_s=0} = kx_s^{\beta} + \lambda x_s^{\beta}\dot{x}_s = kx_s^{\beta}, \tag{6.43}$$

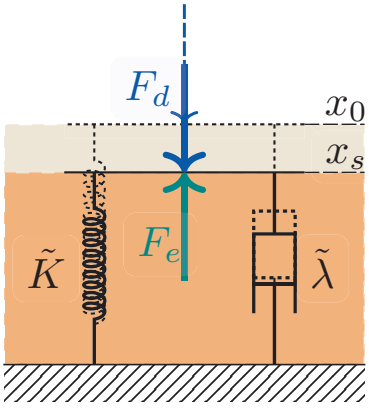

Figure 6.4: Hunt-Crossly model linearisation around an equilibrium configuration

and

$$x_s = \sqrt[\beta]{\frac{F_d}{k}}. \tag{6.44}$$

(Eq. 6.42) becomes:

$$F_e(x,\dot{x}) \approx F_d + \tilde{K}(x - x_s) + \tilde{\lambda}\dot{x}, \tag{6.45}$$

with

$$\tilde{K} = \left.\frac{\partial F_e}{\partial x}\right|_{x_s,\dot{x}_s=0} = k\beta x_s^{\beta-1} = k\beta\left(\frac{F_d}{k}\right)^{\frac{\beta-1}{\beta}}, \tag{6.46}$$

$$\tilde{\lambda} = \left.\frac{\partial F_e}{\partial \dot{x}}\right|_{x_s,\dot{x}_s=0} = \lambda x_s^{\beta} = \lambda\frac{F_d}{k}. \tag{6.47}$$

Consequently the linearised function of the Hunt-Crossley model for the given desired force F_d can be obtained as

$$F_e(x,\dot{x}) = \tilde{K}x + \tilde{\lambda}\dot{x} + (1-\beta)F_d. \tag{6.48}$$

and

$$G_e(s) = \frac{F_e(s)}{X(s)} = \tilde{K} + \tilde{\lambda}s \tag{6.49}$$

The neglected high order terms would be considered as modelling errors and handled by the control algorithm. The following section introduces the the use of Hunt-Crossly model in AOB model based controller.

6.4.2 Model based interaction controller

This controller is applied on the slave robot and therefore, it is introduced, for the purpose of clarity, in the following main steps: first, the robot model and its linearisation is presented. Second, the controlled plant is defined as the coupled robot-tissue. Finally, the observer based controller is addressed and its stability is discussed.

Robot Modelling and Linearisation

While the robot interaction task is executed using its end-effector in the Cartesian space, the robot control is performed in joint space. Robot dynamics in Cartesian and joint space is described as follows:

$$M(q)\ddot{q} + V(q,\dot{q}) + G(q) + \tau_f = \tau_c - J^T(q)F_e \tag{6.50}$$

$$M_x(q)\ddot{X} + V_x(q,\dot{q}) + G_x(q) + F_f = F_c - F_e, \tag{6.51}$$

$q \in \mathbb{R}^n$ and $X \in \mathbb{R}^m$, $m \leq 6 \in \mathbb{R}^+$ represent the generalised joints and Cartesian space vectors respectively. $M(q) \in \mathbb{R}^{n\times n}$, $V(q) \in \mathbb{R}^n$ and $G(q) \in \mathbb{R}^n$ are respectively the inertia matrix,

the Coriolis and centrifugal torques and the gravity compensation torques in joint space. $M_x(q) \in \mathbb{R}^{m\times m}$, $V_x(q) \in \mathbb{R}^m$ and $G_x(q) \in \mathbb{R}^m$ are the same as previous measures in Cartesian space. τ_f & $\tau_m \in \mathbb{R}^n$, F_f, F_m & $F_e \in \mathbb{R}^m$ are the generalized friction and motors torques in joint space, their equivalent (friction and control forces vector) in Cartesian space and the robot-environment interaction forces vector respectively. The transformation from Cartesian to joint space and vice-versa can be performed using the robot kinematic model as follows[Khatib, 1987] :

$$\dot{X} = J(q)\dot{q} \tag{6.52}$$

$$\tau_m = J^T(q)F_m \tag{6.53}$$

$$M_x(q) = J^{-T}(q)M(q)J^{-1}(q) \tag{6.54}$$

$$V_x(q,\dot{q}) = J^{-T}(q)V(q,\dot{q}) - M_x(q)\dot{J}(q)\dot{q} \tag{6.55}$$

$$G_x(q) = J^{-T}(q)G(q). \tag{6.56}$$

Where $J(q) \in \mathbb{R}^{m\times n}$ is the robot jacobian matrix that describes its kinematic model (Eq. 6.52). Robot dynamic model introduced in (Eqs. 6.50 and 6.51) is non-linear. Applying an accurate modelling and calibration process and by selecting a new control input as follows:

$$F_m = \hat{M}_x(q)u + \hat{V}_x(q,\dot{q}) + \hat{G}_x(q) + \hat{F}_f + \hat{F}_e, \tag{6.57}$$

where $(\hat{*})$ is the estimation measure of $(*)$. An accurate modelling and calibration process enables the assumption $(\hat{*} = *)$ and consequently the robot dynamics in (Eqs.6.51) is decoupled and linearised to act as a double integrator with acceleration equivalent input:

$$U = \ddot{X}. \tag{6.58}$$

This control low is disturbed by two main sources of error which can be distinguished by comparing (Eq. 6.57) to (Eq. 6.51) as modelling errors and measurement error. To improve the resultant system robustness with respect to these errors, the desired plant poles at the origin are shifted to the LHP by adding an inner loop of velocity damping with a coefficient diagonal matrix $K_v \in \mathbb{R}^+$. The new control input of the (i^{th}; $\forall i \in [0,n]$) DoF takes the following form:

$$U_i = \ddot{X}_i + K_v^i \dot{X}_i. \tag{6.59}$$

In conclusion one DoF of a linearised decoupled robot has a dynamics that can be represented by the following transfer function (Fig. 6.5):

$$G_r(s) = \frac{X_s}{U} = \frac{1}{s(s+K_v)}. \tag{6.60}$$

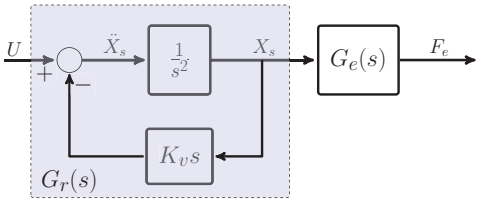

Figure 6.5: Linearised decoupled model of a robot control in Cartesian space

System plant

The system plant is the robot in coupled state with the environment (the tissue). System plant for the various considered model is organised in the following table (table 6.2). To control the concerned system dynamics, a proper state space control technique will be proposed. In most cases the system states are non-measurable therefore a proper observer is necessary to estimate the system state. We control robot-tissue interaction using AOB technique which concept is presented in (fig. 6.6) [Cortesão, 2007].

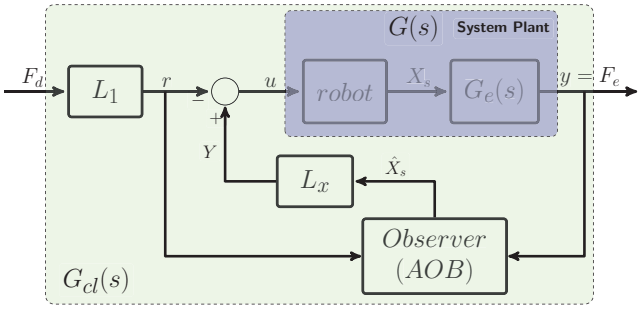

Figure 6.6: Observer based slave controller

State space representation

For the Hunt-Crossly model, using the Observable Canonical Form, one obtains:

$$\begin{bmatrix} \dot{x}_1 \\ \dot{x}_2 \end{bmatrix} = \begin{bmatrix} -K_v & 1 \\ 0 & 0 \end{bmatrix} \begin{bmatrix} x_1 \\ x_2 \end{bmatrix} + \begin{bmatrix} \tilde{\lambda} \\ \tilde{K} \end{bmatrix} u = Ax + Bu \tag{6.61}$$

$$y(t) = \begin{bmatrix} 1 & 0 \end{bmatrix} \begin{bmatrix} x_1 \\ x_2 \end{bmatrix} = Cx. \tag{6.62}$$

For the computer controlled systems the plant model of the system (6.61) has to be discretized with a sample time T_s. The discrete state space representation is given at the in-

Model	$G_e(s)$	$G(s) = G_r(s)G_e(s)$
Elastic	k_e	$\frac{k_e}{s(s+K_v)}$
MW	$\frac{b_e}{1+\alpha_e s}$	$\frac{b_e}{s(s+K_v)(1+\alpha_e s)}$
KV	$k_e + b_e s$	$\frac{k_e + b_e s}{s(s+K_v)}$
KB	$\frac{k_e + b_e s}{1+\alpha_e s}$	$\frac{k_e + b_e s}{s(s+K_v)(1+\alpha_e s)}$
HC	$\tilde{K} + \tilde{\lambda} s$	$\frac{\tilde{K} + \tilde{\lambda} s}{s(s+K_v)}$

Table 6.2: Robot-Environment system plant

stant k by:

$$\begin{aligned} x(k) &= \Phi x(k-1) + \Gamma u(k-1) + \xi(k) \\ y(k) &= Cx(k) + \eta(k), \end{aligned} \tag{6.63}$$

where $\omega(k)$, $\eta(k)$ denote respectively model and measurement uncertainties while Φ, Γ are the discrete state matrix and the discrete input matrix respectively and can be obtained in the absence of time delay ($T_d = 0$) as follows:

$$\Phi = e^{AT_s} = I + AT_s + \frac{A^2T_s^2}{2!} + \frac{A^3T_s^3}{3!} + ... \tag{6.64}$$

$$\Gamma = \int_0^{T_s} e^{AT_s} B d\tau = BT_s + AB\frac{T_s^2}{2!} + A^2B\frac{T_s^3}{3!} + ... \tag{6.65}$$

where A, B are the matrix defined in (6.61) and I is the identity matrix.

State space control and closed loop dynamics

The control law of the obtained system (eq 6.63) can be designed following the state feedback regulation method as:

$$u(k) = r(k) - Lx(k) \tag{6.66}$$

where L is the state feedback gain that can be calculated according to poles' assignment method using Ackermann's formula:

$$L = \begin{bmatrix} 0 & \dots & 0 & 1 \end{bmatrix} W_c^{-1} P(\Phi), \tag{6.67}$$

$$W_c = \begin{bmatrix} \Gamma & \Phi\Gamma \end{bmatrix}, \tag{6.68}$$

$$P(\Phi) = (\Phi^2 + a_1\Phi + a_2), \tag{6.69}$$

where W_c and $P(\Phi)$ are respectively the controllability matrix of the system (eq 6.63) and the desired characteristic polynomial of the closed loop performance with coefficients $a_1 = -2e^{-\xi\omega_n T_s} cos(\sqrt{(1-\xi^2)}\omega_n T_s)$ and $a_2 = e^{-2\xi\omega_n T_s}$. The coefficient a_1 and a_2 are selected in the objective to have a critically damped transient response with time constant T_{cl} and a null static error i.e. :

$$\xi = 1, \quad and \quad \omega_n = \frac{1}{T_{cl}}. \tag{6.70}$$

The reference signal $r(k)$ is calculated based on the desired force input F_d as follows:

$$r(k) = L_1 F_d(k). \tag{6.71}$$

To impose a unitary static gain, L_1 is selected to be equal to the first element of the state feedback gain $L = [L_1\ L_2\ ...\ L_n]$. Consequently, the closed loop dynamics of a state space controlled (coupled robot-environment) system can be described by the following transfer function G_{cl} which describes the robot-environment interaction force F_e regarding the desired interaction force F_d:

$$G_{cl} = \frac{F_e}{F_d} = \frac{1}{(1 + T_{cl}s)^2}. \tag{6.72}$$

The necessary system states to perform the control cannot be measured and need to be estimated. Therefore a state space observer based control is proposed to solve this problem. Moreover Kalman filter is adapted to calculate the state control gained of the proposed observer (referred as AOB). Finally, the estimation and measurement errors are predicted and lumped in an augmented state to correct the estimation output. In the following section we present AOB structure and design.

AOB Concept:

The proposed state space control low (eq. 6.66) requires a full definition of the state vector through direct measurement, which is generally difficult and most likely infeasible because some states themselves do not have a physical meaning, or an indirect estimation method through an adequate observer. The discrete state space representation of the system dynamics can be written as:

$$x(k) = \Phi_r x(k-1) + \Gamma_r u(k-1) + \xi_{x_r}(k) \tag{6.73}$$

$$y(k) = C_r x(k) + \eta(k) \tag{6.74}$$

As can be seen in (eqs. 6.73 and 6.74), the system dynamics is disturbed by two types of uncertainties; modelling uncertainties coupled in ξ_{x_r} and output measurement uncertainties lumped in η. State observer dynamics can be summarised as follows:

$$\hat{x}(k) = \Phi_r \hat{x}(k-1) + \Gamma_r u(k-1) + E_k(y(k-1) - \hat{y}(k-1)) \tag{6.75}$$
$$\hat{y}(k) = C_r(\Phi_r \hat{x}(k-1) + \Gamma_r u(k-1)) \tag{6.76}$$

The system output $y(k)$ is supposed to be measurable while the output estimation $\hat{y}$ is calculated based on the previous input and estimated state as in (eq. 6.76). $E_k \in \mathbb{R}^{2\times 1}$ is the output estimation error gain and is calculated based on a Kalman procedure such that the estimation error converges to zero i.e.:

$$\lim_{k\to\infty} e(k) = \lim_{k\to\infty} (x(k) - \hat{x}(k)) = 0. \tag{6.77}$$

Notice that observer based state space control low form of (eq. 6.66) becomes:

$$u(k) = r(k) - L\hat{x}(k) \tag{6.78}$$
$$= r(k) - L(x(k) - e(k)) \tag{6.79}$$
$$= r(k) - L\,x(k) + L\,e(k). \tag{6.80}$$

Substituting (eq. 6.80) back in (eq. 6.73) gives:

$$x(k) = (\Phi_r - \Gamma_r L)x(k-1) + \Gamma_r r(k-1) + \Gamma_r L\,e(k-1) + \xi(k) \tag{6.81}$$
$$y(k) = C_r x(k) + \eta(k) \tag{6.82}$$

This system ca be reformulated under the following form:

$$\begin{bmatrix} x(k) \\ Le(k) \end{bmatrix} = \begin{bmatrix} \Phi_r - \Gamma_r L & 0 \\ 0 & 1 \end{bmatrix} \begin{bmatrix} x(k-1) \\ Le(k-1) \end{bmatrix} + \begin{bmatrix} \Gamma_r \\ 0 \end{bmatrix} r(k-1) + \begin{bmatrix} \xi_x(k) \\ \xi_e(k) \end{bmatrix} \tag{6.83}$$
$$y(k) = [C_r\ 0] \begin{bmatrix} x(k) \\ Le(k) \end{bmatrix} + \eta(k) \tag{6.84}$$

This reformulation uses the known reference signal $r(k) = L_1 F_d(k)$ as an input and augments the state space with one new state, so called active state p. Active state is a stochastic definition of modelling errors due to higher order dynamics, parameters mismatch and/or unknown disturbance The N th-order evolution of the active state is described as follows:

$$p(k) = Le(k) \tag{6.85}$$
$$p(k) = \sum_{j=1}^{N} (-1)^{j+1} \frac{N!}{j!(N-j)!} p(k-j) + {}^{N-1}\xi_p(k) \tag{6.86}$$

In the following analysis, a first-order evolution (i.e. $N = 1$) is considered to describe the active state dynamics with $\xi_p(k)$ a zero mean Gaussian variable. Consequently:

$$p(k) = p(k-1) + \xi_p(k) \tag{6.87}$$

$$E[\xi_p \xi_p^T] = Q_{p_k}\, I \tag{6.88}$$

with I is the identity matrix, $E[.]$ to represent the expected value and Q_{p_k} is the positive definite covariance matrix. The higher this value is, the more effective the error compensation will be. The resulting system is:

$$\begin{bmatrix} x(k) \\ p(k) \end{bmatrix} = \begin{bmatrix} \Phi_r - \Gamma_r L & 0 \\ 0 & 1 \end{bmatrix} \begin{bmatrix} x(k-1) \\ p(k-1) \end{bmatrix} + \begin{bmatrix} \Gamma_r \\ 0 \end{bmatrix} r(k-1) + \begin{bmatrix} \xi_x(k) \\ \xi_p(k) \end{bmatrix} \tag{6.89}$$

$$y(k) = [C_r\ 0] \begin{bmatrix} x(k) \\ p(k) \end{bmatrix} + \eta(k) \tag{6.90}$$

ξ_x and η are also Gaussian white noise with zero mean and covariance matrices:

$$E[\xi_x \xi_x^T] = Q_{x_k}\, I \qquad E[\eta\eta^T] = R_k\, I \tag{6.91}$$

Supposing $\xi = [\xi_x^T\ \xi_p]^T$ is the disturbance noise that affects the new state vector $[x^T(k)\ \ p(k)]^T$ with covariance matrix Q_k defined as follows:

$$E[\xi\xi^T] = Q_k\, I \qquad Q_k = \begin{bmatrix} Q_{x_k} & 0 \\ 0 & Q_{p_k} \end{bmatrix} \tag{6.92}$$

The resulting new control input is defined as:

$$u(k) = r(k) - \begin{bmatrix} L & 1 \end{bmatrix} \begin{bmatrix} \hat{x}(k) \\ \hat{p}(k) \end{bmatrix} \tag{6.93}$$

with state observer defined as:

$$\begin{bmatrix} \hat{x}(k) \\ \hat{p}(k) \end{bmatrix} = \begin{bmatrix} \Phi_r - \Gamma_r L & 0 \\ 0 & 1 \end{bmatrix} \begin{bmatrix} \hat{x}(k-1) \\ \hat{p}(k-1) \end{bmatrix} + \begin{bmatrix} \Gamma_r \\ 0 \end{bmatrix} r(k-1) + K(k)\Big(y(k) - \hat{y}(k)\Big) \tag{6.94}$$

$$\hat{y}(k) = C_a\left(\begin{bmatrix} \Phi - \Gamma L & 0 \\ 0 & 1 \end{bmatrix} \begin{bmatrix} \hat{x}(k-1) \\ \hat{p}(k-1) \end{bmatrix} + \begin{bmatrix} \Gamma \\ 0 \end{bmatrix} r(k-1)\right) \tag{6.95}$$

$$C_a = [C_r\ 0] \tag{6.96}$$

$K(k)$ is the Kalman estimation gain and is calculated as follows:

$$K(k) = P_1(k) C_a^T [C_a P_1(k) C_a^T + R(k)]^{-1} \tag{6.97}$$

$$P_1(k) = \Phi_a P(k-1) \Phi_a^T + Q(k) \tag{6.98}$$

$$P(k) = P_1(k) - K(k) C_a P_1(k) \tag{6.99}$$

with

$$\Phi_a = \begin{bmatrix} \Phi_r & \Gamma_r \\ 0 & 1 \end{bmatrix},\ Q(k) = \begin{bmatrix} Q_{x(k)} & 0 \\ 0 & Q_{p(k)} \end{bmatrix}$$

System Stability

To evaluate the system stability, the most common criteria used are the phase and gain margins that can indicate both absolute and relative stability of the system. For the system considered here, one can compute the Loop Transfer Function (LTF) as the relationship between input $u(k)$ and the output Y, as shown in (Fig. 6.6). The corresponding state space representation is given by [Cortesão, 2007]

$$\begin{bmatrix} \hat{x}(k) \\ e(k) \end{bmatrix} = \begin{bmatrix} \Phi - \Upsilon\Gamma L & K(k)C\Phi \\ \Upsilon\Gamma L & \Phi - K(k)C\Phi \end{bmatrix} \begin{bmatrix} \hat{x}(k-1) \\ e(k-1) \end{bmatrix} \tag{6.100}$$

$$+ \begin{bmatrix} K(k)C\Gamma \\ (I - K(k)C)\Gamma \end{bmatrix} u(k-1) \tag{6.101}$$

$$Y = \begin{bmatrix} L & 0 \end{bmatrix} \begin{bmatrix} \hat{x}(k) \\ e(k) \end{bmatrix} \tag{6.102}$$

where $\Upsilon = I - K(k)C$. The transfer function of (6.100) can be obtained as:

$$H_{LTF} = [L\,0][I - \phi z^{-1}]^{-1}\gamma z^{-1} \tag{6.103}$$

where ϕ, γ are the state transition and command matrices of (6.100). Given H_{LTF}, one can plot the Bode diagram and compute the gain and phase margin of the system in (6.100), as illustrated in next section. It's worthwhile to notice that this stability analysis applies when the system works close to the equilibrium since a linearised approximation of the Hunt-Crossley model around the equilibrium is used in the control design.

6.5 Experimental validation:

The aforementioned CA with the model based interaction control of slave robot is tested on Raven II-Sigma 7 test-bed. To introduce the components of the experiment set-up, we follow teleoperation literature concept which divides teleoperation system in five main layers, i.e. operator, master robot, communication layer, slave robot and environment. This components are introduce in following experiment set-up section and is followed by the experiment results and discussion.

6.5.1 Experiments set-up

Master device

As discussed in the haptic interface design section (section 2.4.2) in the second chapter, the robot control torques are proportional to the feedback forces F_{cm} and collaborate or contrast the human imposed forces F_h to give him an engineered sense of touch, therefore it can be modelled as a passive mechanism deriven by the sum of motors' forces and

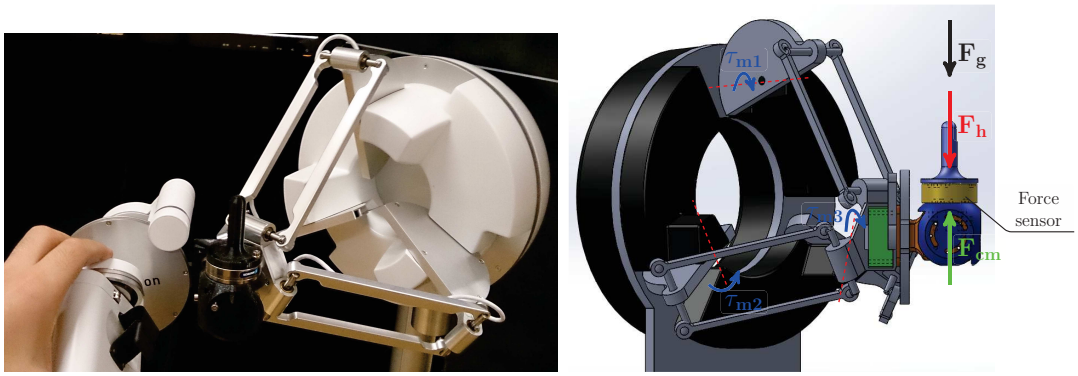

Figure 6.7: Master Sigma 7 robot

human-device interaction forces (Fig. 6.2):

$$Z_m(s) = \frac{F_h(s) + F_{cm}(s)}{V_m(s)}. \tag{6.104}$$

The experiment uses a Sigma 7 haptic interface running under Windows environment to guide the slave robot. Human-master interaction forces are measured using an ATI F/T sensing modality where the transducer is attached to the robot translational base with a proper home-made adapter (Fig. 6.7). These interaction forces are necessary to evaluate the system performance as introduced in the following experiment analysis section.

To quantify the exchanged energy between human operator and the haptic interface, a force sensor is necessary to measure human-robot interaction forces. Augmenting sigma7's translational base end-effector (Fig. 6.7) with force sensor and its adapter changes the dynamic characteristics of the haptic interface. The new dynamics has to be identified if the precise implementation of G_v transfer function is intended to be realized. In the following we identify the dynamic properties (mass and damping) of the used haptic interface (sigma7) augmented with a force sensor on the analysed axis (z direction). To achieve this objective, an identification process is defined as follows:

- Using **ForceDimention API** function (**dhdSetForce**(F_x, F_y, F_z, InterfaceID)), the interface is ordered to impose constant force $F_{cm} = [Fx\ Fy\ Fz]^T$ on its environment.
- Because the three Cartesian coordinates can be decoupled, teleoperation analysis is confined to the study of Z_{axis} without lose of generality. Consequently, $F_{cm} = [0\ 0\ Fz]^T$ is considered in the identification process. Haptic interface dynamic parameters are identified based on a three set of tests with different values of F_z: $F_z = 0$, 5 and 10 (N).
- Each set of tests encompasses 4 cases (3 tests per case). The considered cases are:
  * Static interaction to identify the gravity properties.
  * Slow motion

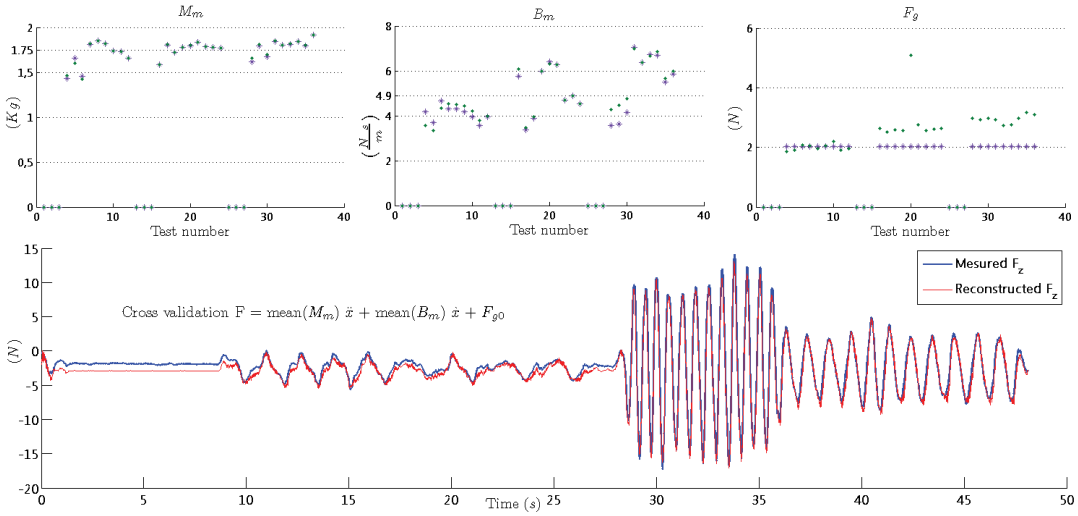

Figure 6.8

  - ∗ High motion
  - ∗ Mixed motion (static, slow and high)
- – The human imposes his motion on the interface. The position and velocity information of the resulting motion are detected based on the interface API while the corresponding forces are measured using the force sensor.
- – The sensed force is $F_{sensor} = F_h - F_{cm} = \hat{m}_m\ddot{x} + \hat{b}_m\dot{x} - F_{gravity}$ (Fig. 6.7).
- – Considering gravity compensation, two cases can be identified:
  - ∗ Gravity forces F_g can be identified based on static tests as follows: $F_{sensor} = F_{cm} - Fg$. Consequently, robot parameters can be identified (in dynamic case) based on the following equation: $F_{sensor} + F_{gravity} = F_h - F_{interface} = \hat{m}_m\ddot{x} + \hat{b}_m\dot{x}$
  - ∗ Gravity forces can be identified directly using least square method by applying the following equation $F_{sensor} = F_h - F_{interface} = \hat{m}_m\ddot{x} + \hat{b}_m\dot{x} - \hat{F}_g$ where the parameters with hats are the identified parameters.
- – The identified parameters are evaluated and the eccentric tests are neglected.
- – the considered values of the estimated parameters are the mean of estimations of all valid tests tests.

$$Z_m = m_m\ddot{x} + b_m\dot{x} = 1.75\ddot{x} + 4.9\dot{x} \tag{6.105}$$

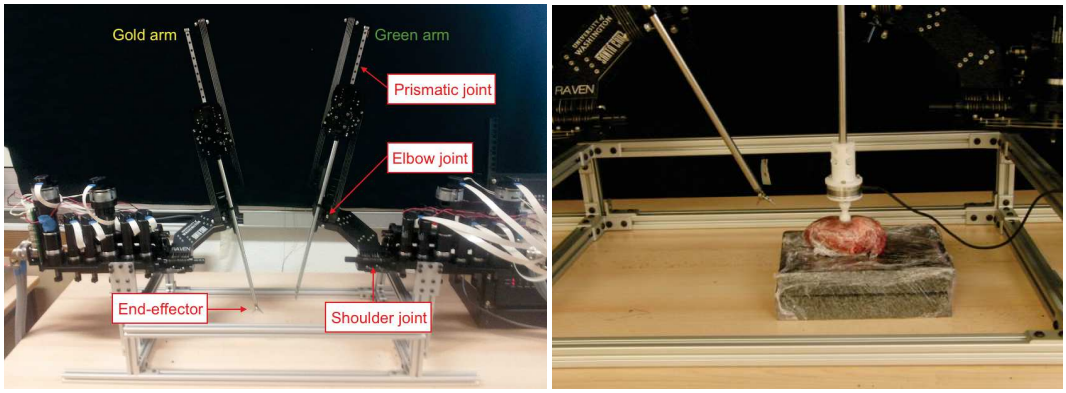

Figure 6.9: Raven II robot slave site

Communication layer

The communication layer is represented in (Fig. 6.2) by the scaling gains β_p and β_f of the exchanged position and force data respectively. These gains can be in the general case a transfer function that performs a certain type of filtering besides the signal scaling.

In the experimental set-up; the two distant running controllers exchanges their data through an Ethernet communication modality with UDP communication protocol. The exchanged data from master to slave and vice versa contains the Cartesian generalized position rate ($[]\Delta P \Delta\phi^T]^T$), the interaction forces (F), a variable that defines if the two remote robot are coupled in teleoperation or not ($teleop\_variable$) and security variable ($check\_sum$) to ensure data integrity. This data is organised under the following form:

$$[\ \Delta P \quad \Delta\phi \quad F \quad teleop\_variable \quad check\_sum\ ]^T \tag{6.106}$$

Slave robot

As previously introduced, we used Raven II as a slave robot. Raven II is a 7 DoF open architecture (software & hardware) robot dedicated for medical surgery research. The RCM is mechanically imposed through a spherical mechanism; the joints are cable driven by distant motors (the driving motors are placed far at the base of the robot) to ensure a light weight mechanism. To measure the environment-slave interaction forces; a suitable adapter is designed and made by 3D printing technique to attach the force sensor to the robot end-effector (fig. 6.9).

On the other hand; Raven robot is controlled under soft Linux_rt operating system using ROS environment with sampling time $T_s = 1\ ms$. The basic data exchanged with master robot are the position and orientation of the tool tip and the interaction forces in addition to a variable to distinguish the running state (if the two remote sites are coupled or not).

Environment:

These preliminary experiments are carried out using a synthetic phantom tissue with medium density PVC (70% soft + 30% hard PVC) to represent the operated environment (tissue), where the performed task is a palpation. The interaction model of this phantom can be identified using relaxation test and is introduced in the following (figure 6.10) for elastic model and in (figure 6.11) for the same trials but using Hunt-Crossly model. It can be noted from the hysteresis behaviour that the Hunt-Crossly model describes better the phantom interaction but the same time the used phantom has dominant elastic properties.

6.5.2 Haptic data measurements

As previously introduced in the second and third chapters, haptic data refers to the position and force information of a specified robot-environment (man or task) interaction. Raven II and Sigma 7 robots are equipped with suitable position measurement facilities at joint space (encoders) and have sophisticated kinematic models that enable good estimations of the robot end-effectors position. Because the robot end-effector is far more stiff than its environment, we propose that the position of the robot end-effector represents the position information of the analysed interaction.

On the other hand, these robots are not supplied with any type of interaction force measurement modality. Therefore, the end-effector of each robot is augmented with an adequate ATI/FT force measurement facility as introduced in (Fig. 6.12.b and 6.12.c). Fig. 6.12.a presents the components of ATI/FT force measurement system. This system is quite

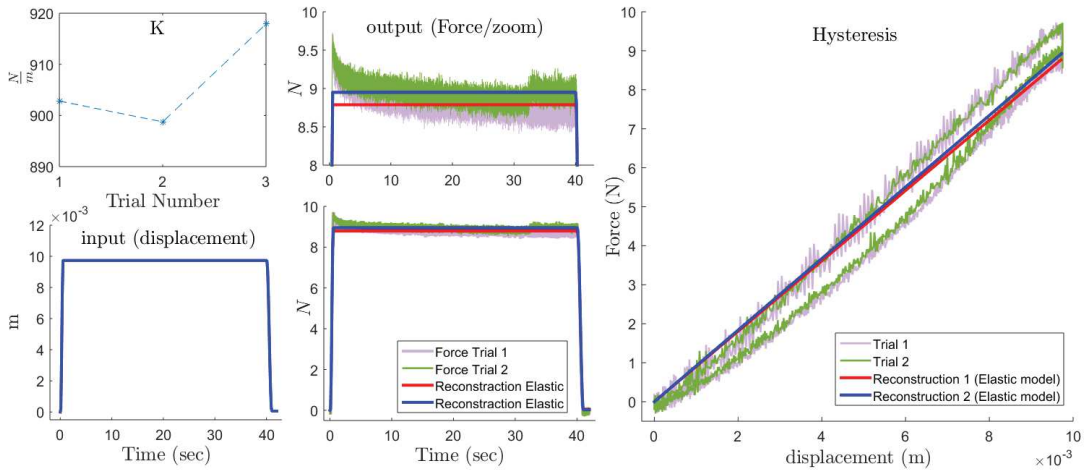

Figure 6.10: Relaxation test and model reconstruction behaviour

accurate as the measurement white noise does not surpass 0.5 N. More details on the interaction force acquisition hardware, software and phylosophy can be sought in [ATI Industrial automation].

6.5.3 Experiments results

The used parameters to realize these experiments are introduced in (Table 6.3) and the results of position and force correspondence are shown in (Fig. 6.13). The experiment is a preliminary one and hence a simplified G_v is used. The system transparency analysis through impedance matching test is visualised in (Fig. 6.14).

Table 6.3: Experimental Parameters

Transparency Controller TF	$G_v(s) = B_v + (M_v s + \frac{K_v}{s})$		
	$K_v = 1000\frac{N}{m}$	$B_v = 500\frac{Ns}{m}$	$M_v = 500\frac{Ns^2}{m}$
AOB Covariance Matrices	$R = 5e^{-5}$	$Q_x = 1e{-}3\ I_{2\times2}$	$Q_p = 1e{-}5$
Environment Model	$F_e(t) = \tilde{K}x_e(t) + \tilde{\lambda}\dot{x}_e(t)$		
	$\tilde{K} = k_e\beta_e\left(\frac{F_{d_{lin.}}}{k_e}\right)^{\frac{\beta_e-1}{\beta_e}}$	$\tilde{\lambda} = \lambda_e\frac{F_{d_{lin.}}}{k_e}$	$F_{d_{lin.}} = 5\ N$
	$k_e = 2000.0$	$\lambda_e = 40000.0$	$\beta_e = 1.21$
Scaling	position: $\beta_p = 0.5$	force: $\beta_f = 2$	$\beta_p\beta_f = 1$

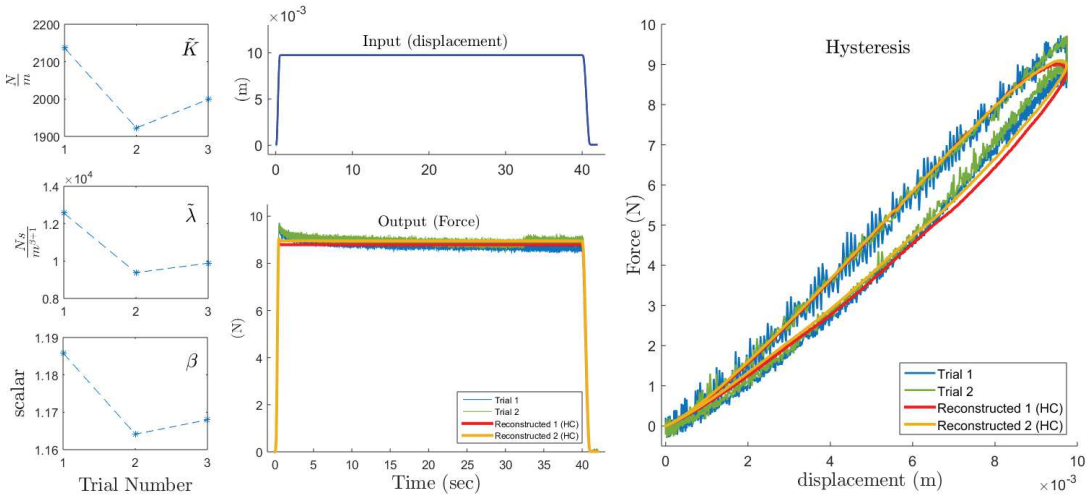

Figure 6.11: Relaxation test and model reconstruction behaviour

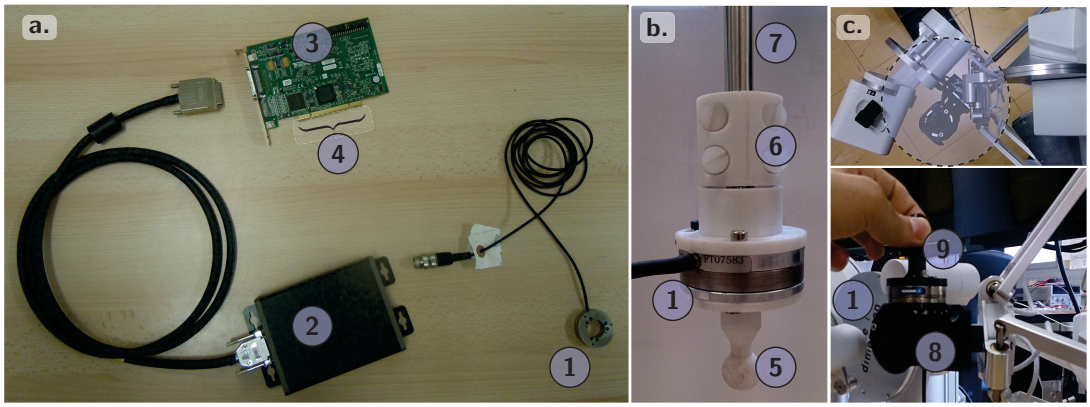

1.) Force sensor transducer
2.) Amplifier
3.) NI Acquisition card
4.) PCI port
5.) Sensor-environment mediator
6.) Addapter
7.) Slave robot end-effector
8.) Addapter
9.) Operator-environment mediator

Figure 6.12: Interaction force measurement facility: a.) ATI/FT force sensing system b.) force sensor transducer attached to slave end-effector c.) force sensor attached to sigma-7.

Force and Position Tracking:

To assess the performance (transparency) of the proposed Hunt-Crossly based haptic teleoperation, position and force information measured at operator-master and slave-environment interaction are compared as introduced in (Fig. 6.13). To show the control algorithm properties, this experiment contains three main phases:

- ***Phase 1:*** Slave robot in free space motion (represented by the region $t \leq 15\ sec$ on (Fig. 6.13) where $F_s \cong 0$). On this region, we can notice that the slave robot repeats the master motion (position and velocity) quite accurately while the sensed force at master site ($F_m > 0$) shows that human operator feels the teleoperator dynamics because $\beta_f F_m > Fs$. Because Sigma-7 has high resolution and its controller compensates accurately friction and gravity forces, the sense dynamics of teleoperator is small and negligible.
- ***Phase 2:*** Interaction phase represented by the region ($16 \leq t \leq 26\ sec$ on Fig. 6.13). We can se that the velocity is almost zero while the position and force measures matching are quite good. The small noticed position and force errors can be interpreted as a result of the unmodelled non-linearities (especially joints backlash).
- ***Phase 3:*** constrained motion phase represented by the region ($36 \leq t \leq 45\ sec$) on (Fig. 6.13). In this phase we try to move the master while slave robot is in interaction with the environment. We can note that the velocity measures oscillate around zero and consequently some mismatch can be noticed especially on interaction forces level. We think that the reason is because the operator changes his motion direction, consequently with the backlash presence, a remarkable force mismatching appears.

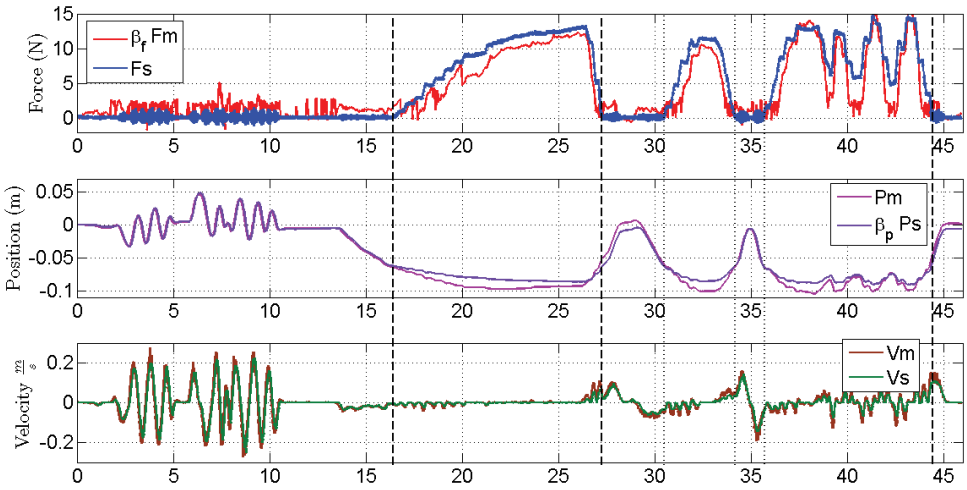

Figure 6.13: Force, Position and Velocity tracking measures on $Z_{direction}$; m: master and s: slave

Impedance matching:

The second method to evaluate the system performance is by comparing the impedance sensed by human operator $Z_{to} = F_m/v_m$ to the environment impedance $Z_e = F_s/v_s$ as in (Fig. 6.14). Equivalently to what we have experienced in the aforementioned analysis of P, F tracking measures, we note three main phases: ***Phase 1:*** ($t \leq 15\ s$) and $Z_{to} > Z_e \approxeq 0$ that is the human operator feels the system (teleoperator) dynamics (inertia). ***Phase 2:*** ($16 \leq t \leq 27\ s$), Z_{to} has the shape of Z_e with some mismatch. we think that the main reason for this mismatch is the present backlash on joint space in slave robot. That is because these joints are cable driven by motors located at the robot base. ***Phase 3:*** ($36 \leq t \leq 45\ s$), the slave robot is ordered to perform a constrained motion. The two impedances have the same shape with a remarkable mismatching and the reason as already explained in the above discussions may be the backlash presence.

6.6 Conclusion

In this chapter, we improve a force control based haptic teleoperation for surgical applications by integrating a better modelling to represent the tissue interaction dynamics and viscoelasticity. Hunt crossly model is capable of better representing the tissue viscoelastic properties by applying an interaction based damping and elastic coefficients. The nonlinear model is linearised to be joint to the robot linearised model to describe robot-environment dynamically interaction. The resulting system is written under state space

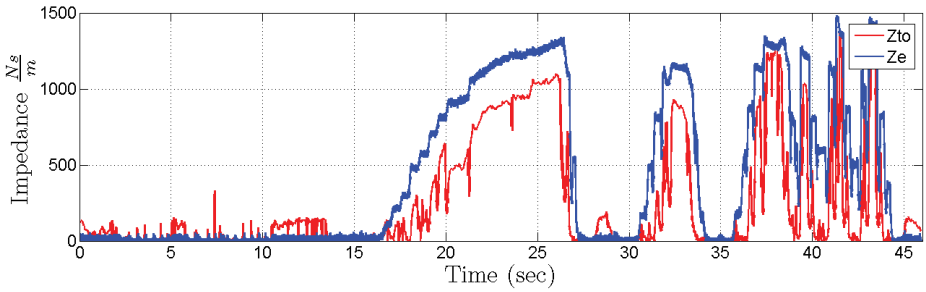

Figure 6.14: Impedance matching

representation to establish a proper state space controller. An Active OBserver (AOB) is used to estimate the system state while minimizing the estimation errors by integrating a stochastically driven augment state. The resulting system is integrated on Raven II robot and the gained results are shown and discussed.

CHAPTER

7 Conclusions and Discussion

7.1 Conclusions

We have conducted in the second chapter a wide elaborated state of art on haptic teleoperation subject. First the history of haptic teleoperation is browsed and its apported usfullness to medical community it highlighted. Then the conducted research that can be classified under haptic teleoperation framework has been organized under six sub-field of research based on the focus point of the proposed work. This sub-fields are the following:

1. Human-Master interconnection.
   * To define haptic sense receptors' locations, stimuli methods and thresholds.
   * To define the test scenarios required to assess human needs of a haptic feedback.
   * To provide a meaningful model of human-in-loop performance which could serve to predict and/or simulate his/her performance.
2. Master system design.
   * To quantify human requirement of haptic feedback as design measures.
   * To design a suitable electro-mechanical structure that meets the aforementioned requirements.
   * Haptic feedback of virtual environment.
   * Haptics to serve human health (applications).
3. Communication layer design.
   * To identify the set of processes required to be applied on haptic data passing through master-slave communication facility (i.e. coding, decoding, reduction, replication ...) and the resulting effects (ex. time delay).
   * Time delay in bilateral teleoperation affects the system stability and on the process transparency.
   * The used techniques to insure the stability and its reflection on the transparency.

4. Slave system design.
   * The slave robot (surgical robot) design is subject to the (set of) task(s) requirement.
   * The interaction shape and constraints besides the sensors location define the accuracy of the acquired haptic data of a specific interaction.
5. Slave-Environment interaction
   * Environment (task) modelling is necessary to design a transparent teleoperator.
   * The system transparency is remarkably affected by the presence of motion disturbances and the accuracy of the proposed model to robot-tissue interaction.
6. Teleoperator design and assessment.
   * This area pay attention to provide a suitable tools to assess the stability and performance of the coupled MSN.

This detailed sophisticated survey enabled the identification of major factors that affect haptic teleoperation transparency which can be listed as follows:

1. Master design: defines action generation and haptic sense stimulation methods.
2. Slave design: defines haptic variables acquisition accuracy of a required interaction.
3. The implemented control architecture to achieve master-slave bilateral coupling.
4. Action-perception latency (Time delay).
5. Disturbance and uncertainties presence in the treated environment.
6. Tissue model accuracy affects the force control based haptic teleoperation.

Our focus of interest during the available time is concentrated on the 3^{rd}, 5^{th}, 6^{th} factors which were investigated in details in the 4^{th}, 5^{th}, 6^{th} chapters respectively. While the third chapter introduces the basic technical tools required to develop the main contributions.

The applied control architecture plays a decisive role in achieving a desirable performance and providing a controllable level of transparency. In chapter 4, the possible control architectures to perform a bilateral teleoperation are explored and classified in haptic and non-haptic control architectures. The lake of 3-channel control architectures' analysis is fulfilled and their performance is compared in simulations for surgical applications.

In Chapter 5, we discussed the effect of the possible presence of motion disturbance in the treated soft tissue as a second factor that affects teleoperation transparency. Beating heart surgery represents an example of the interventions where the motion disturbance prevents the natural intervention due to the human limited capacity of manually compensating the disturbance. This chapter proposes an adequate analysis of robot-beating heart interaction and the affect of disturbance presence on the system transparency. Moreover, it presents a new model to tool-tissue interaction that can be useful in understanding the energy flow between the robot and the environment and can also be used in designing a model based interaction control with dynamic environments.

Finally, the accuracy of soft tissue model affects the transparency of interaction control based haptic teleoperation. Chapter 6 investigates this factor by introducing Hunt-Crossly model to AOB based haptic teleoperation. Hunt-Crossly based AOB interaction control showed a better performance in comparison with linear models for tool-soft tissue interaction. The resultant interaction control algorithm is employed to realise $P-F$ haptic teleoperation. The stability and transparency of these CA are analysed in theory and through experiments by its application on Raven II-Sigma 7 medical teleoperation test bed the exists in LIRMM and the result are discussed.

7.2 Future Directions

This thesis investigated a limited number of the main factors that affect a teleoperation transparency. Our first direct recommendation is to complete the analysis of the remaining factors through two main folds; first the effect of time latency between master and slave actions on the achieved transparency. Second fold is to investigate the role of master and slave design (i.e. the nature of operator-master and slave-environment interactions) on the system transparency. Furthermore, It is expected, after finishing the analysis of the role of each factor solely, to perform an overall evaluation by assessing the importance of each factor in affecting a teleoperation transparency.

On the other hand, we would like to draw the attention to the main points required, in our opinion, to complete the proposed contributions through this thesis as follows: *First*, to investigate the work proposed in the third chapter experimentally. Indeed; realizing an experimentally comparison of 3-channel CAs would highlight the CA sensitivity toward the measurement noise, the system inertia and the unmodelled nonlinearities besides the main gaol which is providing a suitable control architecture that provides an optimal stability-transparency trade-off. *Second*, improving the robustness of AOB and its prediction capabilities in force control based haptic teleoperation by integrating the developed model in the 4^{th} chapter in AOB based haptic teleoperation design.

Finally, on the long term objectives, we think that the work introduced in the 4^{th} chapter represents a step towards understanding the interaction with mobile environments and therefore designing a teleoperators that can deals with dynamic tasks (changing and/or not well-constructed environments). Such teleoperator has many promising applications.

APPENDIX

A Appendix A: Model based interaction control, a comparative study

This appendix introduces a comparative study on the performance of model-based interaction control using different models (Table 6.1). This study is carried out in simulation and in *in-vitro* experiments to define the model that describes better tissue interaction.

A.1 Model Identification

In order to analyse the relationship between tissue deformation and reacting force, it is common to perform relaxation tests on *in vitro* specimens. The relaxation test consists of generating a deformation along the direction normal to the tissue surface and measuring the corresponding force exerted by the tissue. Force and deformation depth data are saved to off-line estimate the parameters of candidate models and thus to reconstruct the exerted forces. For comparison of the experimental results for each model, both transient performance and overall force reconstruction errors are considered as selection criteria and evaluated through graphical inspection and numerical analysis, i.e. Mean Force Error (MFE) and corresponding Standard Deviation (STD).

A.1.1 Experiment Setup

The Raven-II surgical robot from Applied Dexterity (Seattle, WA, USA) was used for the relaxation tests as shown in (Fig. A.1). In the relaxation tests, the joint involved is the prismatic one of the right arm. As shown in (Fig. A.1), this arm was set in vertical configuration (along z axis) and a PID position control was used to generate the vertical motion to deform the tissue sample (a lamb's heart). The exerted force data were collected by an ATI MINI45 force sensor mounted on the wrist joint of the robot.

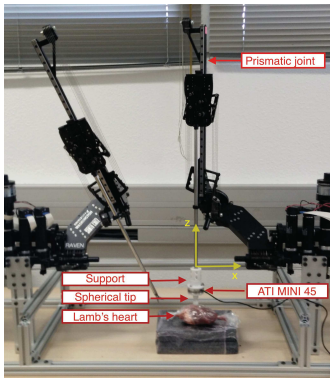

Figure A.1: Relaxation test using Raven II robot

Four relaxation tests were performed, giving a displacement depth of 15 mm from the undeformed surface with the ramp up time of 0.5 s and loading time of 20 s. In order to observe the hysteresis behavior, the unloading was also done with a ramp down time of 1 s. The data were recorded with a sampling time T_s of 1 ms (1 kHz). Fig. A.2 (a) shows the recorded displacement-force history of one test (Trial 3).

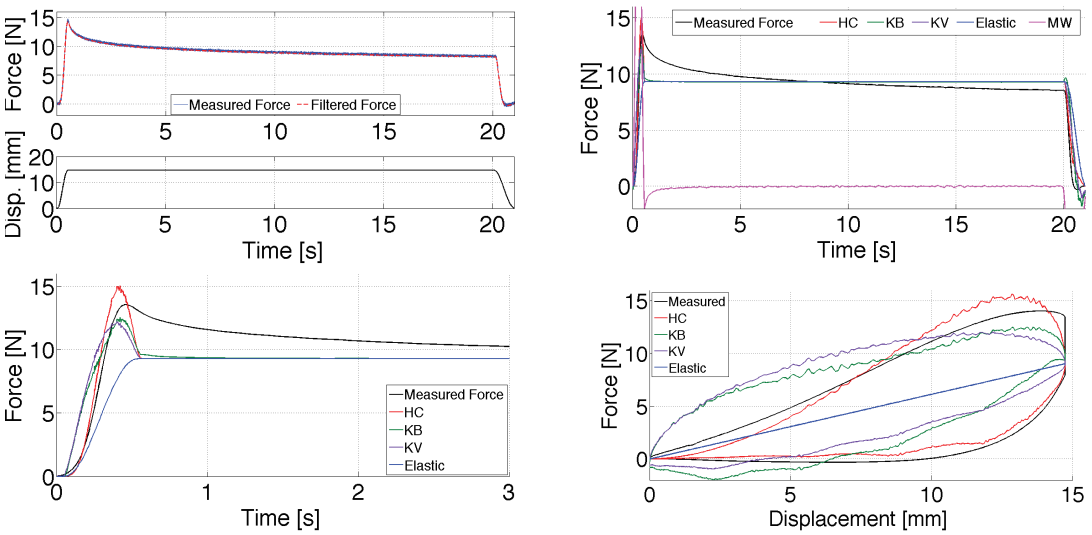

Figure A.2: Reconstructed forces for the Trial 3: (a) ramp deformation and force measurement, (b) reconstructed forces, (c) zoomed in reconstructed transient responses, (d) reconstructed hysteresis behaviors

A.1.2 Parameter Estimation

Based on the saved position information $x(t)$ and force measurement $F(t)$, off-line least squares method is used to estimate the parameters K, b, η, α, γ of the linear contact models (elastic, MW, KV, KB). $\dot{x}(t)$ and $\dot{F}(t)$ are calculated based on filtered position and force data using moving average technique. For the nonlinear HC model, the estimated parameters K, λ, β are calculated through nonlinear least squares method using the Levenberg-Marquardt algorithm [Levenberg, 1944][Marquardt, 1963]. The estimated parameters for the candidate models in the four tests are summarized in (Table A.1).

Model	Parameter	Mean	STD	STD/Mean [%]
Elastic	K	628.92	14.11	2.24
MW	b	349.58	13.39	3.83
	α	0.27	0.01	3.70
KV	K	629.11	14.11	2.24
	b	112.72	9.10	8.07
KB	K	636.05	16.21	2.55
	η	156.92	4.10	2.61
	γ	0.052	0.0046	8.85
HC	K	1732.23	275.82	15.92
	λ	41891.57	1314.90	3.14
	β	1.23	0.03	2.44

Table A.1: Values of the estimated parameters

A.1.3 Reconstructed Force Analysis

With the estimated parameters, the contact force can be reconstructed based on the recorded position information. Since all four tests generated similar results, only the reconstructed forces corresponding to Trial 3 are shown in (Fig. A.2).

Graphical inspection of the reconstructed forces as in (Fig. A.2.b) shows that all models give rise to the same descriptions for steady state contact forces except the Maxwell model, which presents a totally unrealistic reconstructed force (zero static contact force) and therefore is not considered in the further comparison and analysis. The pure elastic model clearly demonstrates the worst reconstructed force, as shown in (Fig. A.2.c). The reconstructed transient responses for the linear viscoelastic models (KV, KB) are similar and show a lead in phase compared to the real measured force at the beginning of contact. The

Hunt-Crossley model shows a quite accurate reconstructed transient response as the real force. The numerical analysis by means of the MFE and STD of reconstructed forces according to different contact models are summarized in (Table A.2). As it can be seen from this table, the Hunt-Crossley model exhibits the smallest reconstruction error.

Model	MFE	STD
Elastic	0.80	0.98
MW	9.27	8.88
KV	0.72	0.73
KB	0.71	0.71
HC	0.65	0.58

Table A.2: Average values of MFE [N] and STD [N] for the four relaxation tests

Moreover, the reconstructed loading and unloading behaviors of the candidate models are also shown in Fig. A.2 (d). The linear viscoelastic models (KV, KB) predict negative contact forces in the unloading phase and the Hunt-Crossley model shows a realistic hysteresis behaviour. Therefore, through the *in vitro* relaxation tests, Hunt-Crossley model has been identified as the most accurate one among all candidate models to describe the interaction between the robot's end-effector and the soft tissue.

A.2 Comparative Studies

In this section, the performance of the force controllers designed on the basis of different contact models are compared in simulation and in experiments. The application of Hunt-Corssly model in the interaction force controller is illustrated in (Chapter. 6). A similar steps are considered to implement the other models and the theory of implementation can be traced in [Cortesão, 2007][Sánchez et al., 2012][Moreira et al., 2014].

A.2.1 Numerical Studies

The performance of the force controllers developed using AOB based on elastic, Kelvin-Boltzmann and Hunt-Crossley contact models are considered to carry out these studies. Considering the estimated average values in (Table A.1), the corresponding contact model equations are:

$$\begin{aligned} F_{elastic}(t) &= 628.92\ x(t) \\ F_{KB}(t) &= 636.05\ x(t) + 156.92\ \dot{x}(t) - 0.052\ \dot{F}(t), \\ F_{HC}(t) &= 2\cdot 10^3\ x^{1.23}(t) + 4\cdot 10^4\ x^{1.23}(t)\dot{x}(t). \end{aligned} \tag{A.1}$$

In Fig. A.3, the performance of all three force control systems, based on different contact models with different closed-loop poles, are illustrated for direct graphical comparison. The simulation results of the force control methods under study are summarized in (Table A.3).

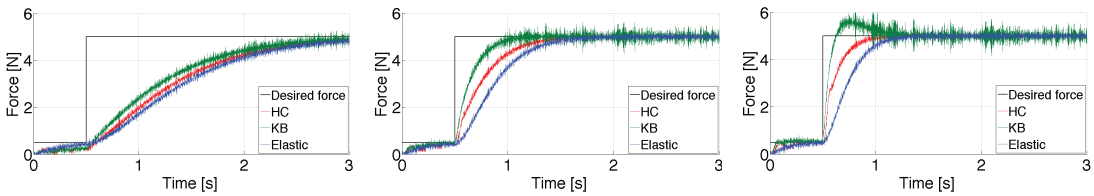

Figure A.3: System performances for different pole p assignments with $p = -2rad/s$ (left), $p = -5rad/s$ (middle) and $p = -8rad/s$ (right)

	Rise time		
Pole [rad/s]	**HC**	**KB**	**Elastic**
-2	1.21	1.11	1.28
-5	0.47	0.28	0.58
-8	0.23	0.08	0.36

Table A.3: Transient responses of the three control force

Among the three developed force control methods, the one based on KB model shows the fastest rise time in all cases, but the downside is that when a fast pole is assigned overshoot appears in the exerted force as seen in (Fig. A.3(right)), which should be minimized for surgical applications. In comparison, the HC model based control system shows slightly lower rise time and the elastic one presents the slowest response in all cases.
Remark: The elastic model represents the most often used contact model for force control in literature. The Kelvin-Boltzmann model is shown to be superior to elastic and other linear viscoelastic contact models in force control for soft tissues [Moreira et al., 2012]. Therefore, for the simulation studies of this section and the experimental studies in next section, only the elastic and Kelvin-Boltzmann model based controllers are considered for performance comparison with the Hunt-Crossley model based control method.

A.2.2 Experimental Studies

In this section, the experimental results for the force control methods based on the linearized Hunt-Crossley, the elastic and the linear viscoelastic Kelvin-Boltzmann models are reported and compared.

A step input of 5 N is set as the reference force command that should exert on a lamb's heart surface, in line with the simulation studies of last section. A small initial contact force around 0.5 N is exerted on tissue surface to ensure a real contact between robot and tissue at the beginning of experiment. Only motion along the normal direction (z axis) is allowed for the robot. The extra damping term K_v in the controller was set to $K_v = 0.05$, and based on the simulation studies the covariance matrices in AOB have been selected as follows

$$Q_{x(k)} = 10^{-6},\ Q_{p(k)} = 10^{-3},\ R(k) = 0.005$$

Fig. A.4-A.6 show the performance of the control methods based on Elastic, KB, HC models and for different closed-loop poles ($p = -2, -5, -8\ rad/s$) through *in vitro* experimental tests. To evaluate the control performance quantitatively, the contact force overshoot, rise time (RT) and the MFE/STD values of force tracking error (0-6 seconds) for each experiment are calculated and summarized in Table A.4.

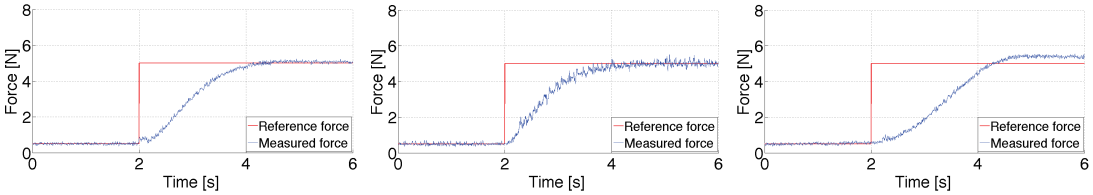

(*a.*) $Hunt-Crossley$ (*b.*) $Kelvin-Boltzmann$ (*c.*) $Elastic$

Figure A.4: Experiment results with pole at $p = -2\ rad/s$

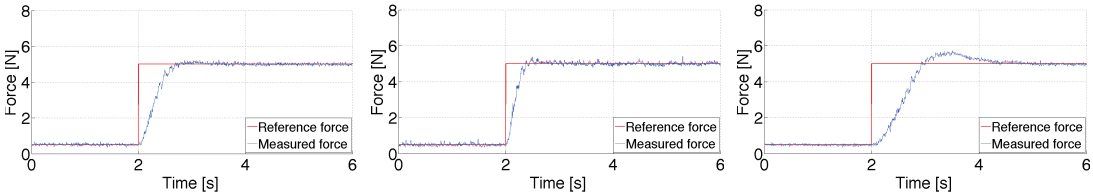

(*a.*) $Hunt-Crossley$ (*b.*) $Kelvin-Boltzmann$ (*c.*) $Elastic$

Figure A.5: Experiment results with pole at $p = -5\ rad/s$

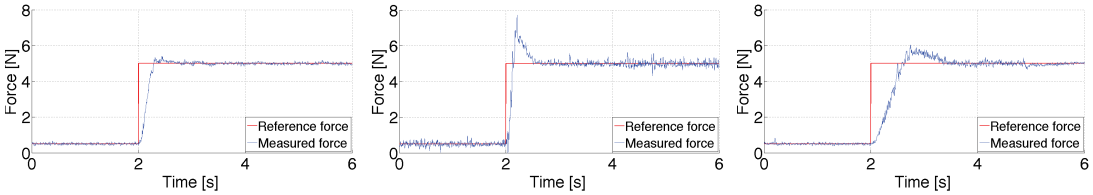

(*a.*) $Hunt-Crossley$ (*b.*) $Kelvin-Boltzmann$ (*c.*) $Elastic$

Figure A.6: Experiment results with pole at $p = -8\ rad/s$

From the experimental results it can be observed that the elastic model based control always presents the slowest responses and Kelvin-Boltzmann model based control shows the smallest rising time. The Hunt-Crossley model based control shows slightly slower but comparable responses. Both Kelvin-Boltzmann and Hunt-Crossley model based control show similar force tracking performance in terms of MFE and STD, while the Elastic model based control presents a bigger force tracking error.

Concerning overshoot, which is a criterion of particular importance for surgical applications, it can be noticed that Elastic model based control shows overshoot even for the slow system pole $p = -2\ rad/s$. The Kelvin-Boltzmann model based control remained stable for the fast pole $p = -8\ rad/s$ but the overshoot is over 50% (2.72 N) of the desired force (5 N). Comparatively, the Hunt-Crossley model based control showed very small overshoot for all three situations.

Model	**Pole**	**RT [s]**	**Overshoot [N]**	**MFE [N]**	**STD [N]**
Elastic		1.71	0.81	0.86	1.59
KB	-2	1.02	0.67	0.57	1.14
HC		1.34	0.23	0.68	1.30
Elastic		0.62	0.72	0.33	1.14
KB	-5	0.22	0.40	0.11	0.62
HC		0.40	0.23	0.21	0.81
Elastic		0.35	1.02	0.19	0.91
KB	-8	0.09	2.72	0.002	0.58
HC		0.16	0.40	0.10	0.60

Table A.4: Experimental results

A.2.3 Discussion

A.3 Conclusion

This appendix is addressed in the purpose of justifying our choice of Hunt-Crossly model in performing force control haptic teleoperation. This analysis considered three models: elastic, Kelvin-Boltzmann and Hunt-Crossly models. In the aim of contact models parameters identification, a relaxation test is performed experimentally *in vitro* on Raven II robot and using Lamb's heart tissue. The identified models are used to carry out a numerical and experimental studies. The results are presented and discussed.

APPENDIX

B

Appendix B: Prove of Equation 3.7

Hybrid representation of MSN as described in (eq. 3.7):

$$F_m = h_{11}\dot{x}_m + h_{12}F_s \tag{B.1}$$

$$-\dot{x}_s = h_{21}\dot{x}_m + h_{22}F_s \tag{B.2}$$

Then the impedance sensed by human operator can be described as follows:

$$Z_{to} = \frac{F_m}{\dot{x}_m} \tag{B.3}$$

$$= h_{11} + h_{12}\left(\frac{F_s}{\dot{x}_m}\right) \tag{B.4}$$

$$= h_{11} + h_{12}\left(\frac{F_s}{-\frac{1}{h_{21}}\dot{x}_s - \frac{h_{22}}{h_{21}}F_s}\right) \tag{B.5}$$

$$= h_{11} + h_{12}\left(\frac{h_{21}F_s}{-\dot{x}_s - h_{22}F_s}\right) \tag{B.6}$$

$$= h_{11} + h_{12}\,h_{21}\left(\frac{1}{-\frac{\dot{x}_s}{F_s} - h_{22}}\right) \tag{B.7}$$

$$= h_{11} - h_{12}\,h_{21}\left(\frac{1}{\frac{1}{Z_e} + h_{22}}\right) \tag{B.8}$$

$$= h_{11} - \frac{h_{12}\,h_{21}\,Z_e}{1 + h_{22}Z_e} \tag{B.9}$$

$$= \frac{h_{11} + (h_{11}h_{22} - h_{12}\,h_{21})\,Z_e}{1 + h_{22}Z_e} \tag{B.10}$$

$$= \frac{h_{11} + \triangle h\,Z_e}{1 + h_{22}Z_e} \tag{B.11}$$

APPENDIX

C Publications

1. A. Pappalardo, **A. Albakri**, C. Liu, L. Bascetta, E. De Momi and P. Poignet, "Hunt-Crossley Model Based Force Control For Minimally Invasive Robotic Surgery", 2015. Submitted to "Biomedical Signal Processing & Control".
2. É. Dorileo, **A. Albakri**, N. Zemiti and P. Poignet, "Simplified Adaptive Path Planning for Percutaneous Needle Insertions", *Robotic and Automation (ICRA), 2015 IEEE International Conference on*, 2015.
3. **A. Albakri,** C. Liu and P. Poignet, "Environment modeling with physiological motion disturbance for surgical teleoperation," *in Control Automation Robotics & Vision (ICARCV), 2014 13th International Conference on*, pp.1298-1303, Dec. 2014
4. **A. Albakri,** C. Liu and P. Poignet, "Stability and performance analysis of three-channel teleoperation control architectures for medical applications," *In Intelligent Robots and Systems (IROS), 2013 IEEE/RSJ International Conference on,* pp. 456-462, Nov. 2013.

Bibliography

J. Abbott and A. Okamura. Effects of position quantization and sampling rate on virtual-wall passivity. *Robotics, IEEE Transactions on*, 21(5):952–964, 2005. Cited page 25.

J. J Abbott and A. Okamura. Stable forbidden-region virtual fixtures for bilateral telemanipulation. *Journal of dynamic systems, measurement, and control*, 128(1):53–64, 2006. Cited pages 60 and 62.

R.J. Adams and B. Hannaford. Stable haptic interaction with virtual environments. *Robotics and Automation, IEEE Transactions on*, 15(3):465–474, 1999. Cited pages 51 and 57.

R.J. Adams and B. Hannaford. Control law design for haptic interfaces to virtual reality. *Control Systems Technology, IEEE Transactions on*, 10(1):3–13, Jan 2002. Cited page 25.

D. Adelstein and J. Rosen. Design and implementation of a force reflecting manipulandum for manual control research. *ASME DYN SYST CONTROL DIV PUBL DSC., ASME, NEW YORK, NY(USA), 1992,*, 42:1–12, 1992. Cited page 23.

N. Aghakhani, M. Geravand, N. Shahriari, M. Vendittelli, and G. Oriolo. Task control with remote center of motion constraint for minimally invasive robotic surgery. In *Robotics and Automation (ICRA), 2013 IEEE International Conference on*, pages 5807–5812, 2013. Cited page 30.

N. Ahmidi, G. Hager, L. Ishii, G. Gallia, and M. Ishii. Robotic path planning for surgeon skill evaluation in minimally-invasive sinus surgery. In *Medical Image Computing and Computer-Assisted Intervention (MICCAI) 2012*, volume 7510, pages 471–478. Springer Berlin Heidelberg, 2012. Cited pages 21 and 91.

N. Ahmidi, Y. Gao, B. Béjar, S. Vedula, S. Khudanpur, R. Vidal, and G. Hager. String motif-based description of tool motion for detecting skill and gestures in robotic surgery. In *Medical Image Computing and Computer-Assisted Intervention (MICCAI) 2013*, volume 8149, pages 26–33. Springer Berlin Heidelberg, 2013. Cited pages 21, 90, and 91.

L. Al Bassit. *Structure mécaniques à modules sphériques optimisées pour un robot médical de télé-échographie mobile*. PhD thesis, L'Univertié d'Orleans, 2005. Cited page 31.

A. Albakri, C. Liu, and P. Poignet. Stability and performance analysis of three-channel teleoperation control architectures for medical applications. In *Intelligent Robots and Systems (IROS), 2013 IEEE/RSJ International Conference on*, pages 456–462, 2013. Cited pages 55 and 100.

A. Albakri, C. Liu, and P. Poignet. Environment modeling with physiological motion disturbance for surgical teleoperation. In *Control Automation Robotics Vision (ICARCV), 2014 13th International Conference on*, pages 1298–1303, Dec 2014. Cited page 81.

S. Allin, Y. Matsuoka, and R. Klatzky. Measuring just noticeable differences for haptic force feedback: implications for rehabilitation. In *Haptic Interfaces for Virtual Environment and Teleoperator Systems, 2002. HAPTICS 2002. Proceedings. 10th Symposium on*, pages 299–302, 2002. Cited page 16.

J. An and D.S. Kwon. Stability and performance of haptic interfaces with active/passive actuators—theory and experiments. *The International Journal of Robotics Research*, 25 (11):1121–1136, 2006. Cited page 25.

R. Anderson and M.W. Spong. Hybrid impedance control of robotic manipulators. *Robotics and Automation, IEEE Journal of*, 4(5):549–556, Oct 1988. Cited page 36.

R. Anderson and M.W. Spong. Bilateral control of teleoperators with time delay. *Automatic Control, IEEE Transactions on*, 34(5):494–501, May 1989. Cited pages 36, 37, 39, and 40.

R.J. Anderson and M.W. Spong. Asymptotic stability for force reflecting teleoperators with time delay. *The International Journal of Robotics Research*, 11(2):135–149, 1992. Cited page 27.

J. Artigas, C. Preusche, and G. Hirzinger. Time domain passivity for delayed haptic telepresence with energy reference. In *IEEE International Conference on Intelligent Robots and Systems*, pages 1612–1617, 2007. Cited page 28.

ATI Industrial automation. URL http://www.ati-ia.com/. Cited page 125.

A. Aviles, P. Sobrevilla, and A. Casals. Unconstrained l_1—regularized minimization with interpolated transformations for heart motion compensation. In *Engineering in Medicine*

and Biology Society (EMBC), 2014 36th Annual International Conference of the IEEE, pages 5109–5112, 2014. Cited page 34.

M. Azizian, M. Khoshnam, N. Najmaei, and R. Patel. Visual servoing in medical robotics: a survey. part i: endoscopic and direct vision imaging–techniques and applications. *The International Journal of Medical Robotics and Computer Assisted Surgery*, 10(3):263–274, 2014. Cited page 34.

W. Bachta, P. Renaud, L. Cuvillon, E. Laroche, A. Forgione, and J. Gangloff. Motion prediction for computer-assisted beating heart surgery. *Biomedical Engineering, IEEE Transactions on*, 56(11):2551–2563, 2009. Cited pages 34 and 77.

W. Bachta, P. Renaud, E. Malis, K. Hashimoto, and J. Gangloff. Visual servoing for beating heart surgery. In *Visual Servoing via Advanced Numerical Methods*, pages 91–114. Springer, 2010. Cited page 34.

W. Bachta, P. Renaud, E. Laroche, A. Forgione, and J. Gangloff. Active stabilization for robotized beating heart surgery. *Robotics, IEEE Transactions on*, 27(4):757–768, 2011. Cited page 34.

S. R. Badaan and D. Stoianovici. Robotic systems: Past, present, and future. In A.K. Hemal and M. Menon, editors, *Robotics in Genitourinary Surgery*, chapter 59, pages 645–654. Springer-Verlag London Limited, 2011. Cited page 14.

H. Baier and G. Schmidt. Transparency and stability of bilateral kinesthetic teleoperation with time-delayed communication. *Journal of Intelligent and Robotic Systems*, 40(1):1–22, 2004. Cited page 27.

L. Basañez and R. Suárez. Teleoperation. In *Springer Handbook of Automation*, pages 449–468. Springer, 2009. Cited pages 8 and 15.

C. Basdogan and M. A. Srinivasan. Haptic rendering in virtual environments. *Handbook of virtual environments*, pages 117–134, 2002. Cited page 25.

R. L. Bashshur and G. W. Shannon. *History of telemedicine: Evolution, Context, and Transformation*. Mary Ann Liebert, Inc., 2009. Cited page 13.

R. Beasley. Medical robots: Current systems and research directions. *Journal of Robotics*, pages 1–14, 2012. Cited page 14.

O. Bebek and M. C. Çavusoglu. Intelligent control algorithms for robotic-assisted beating heart surgery. *Robotics, IEEE Transactions on*, 23(3):468–480, 2007. Cited page 34.

R. D. R. Beira. *Dexterous Mechanical Systems for Intuitive Telemanipulation in Minimally Invasive Surgery*. PhD thesis, 2013. Cited page 31.

O. Ben-Porat, M. Shoham, and J. Meyer. Control design and task performance in endoscopic teleoperation. *Presence: Teleoperators and Virtual Environments*, 9(3):256–267, 2000. Cited page 19.

S. Bensamoun, L. Wang, L. Robert, F. Charleux, J.P. Latrive, and M.C. Ho Ba Tho. Measurement of liver stiffness with two imaging techniques: magnetic resonance elastography and ultrasound elastometry. *Journal of Magnetic Resonance Imaging*, 28(5):1287–1292, 2008. Cited page 34.

J. Berkelman, P.and Ma. A compact modular teleoperated robot system for laparoscopic surgery. *The International journal of robotics research*, 2009. Cited page 31.

P. Berkelman, P. Cinquin, E. Boidard, J. Troccaz, C. Letoublon, and J.M. Ayoubi. Design, control and testing of a novel compact laparoscopic endoscope manipulator. *Proceedings of the Institution of Mechanical Engineers, Part I: Journal of Systems and Control Engineering*, 217(4):329–341, 2003a. Cited page 31.

P. Berkelman, L. Whitcomb, R. Taylor, and P. Jensen. A miniature microsurgical instrument tip force sensor for enhanced force feedback during robot-assisted manipulation. *IEEE Transactions on Robotics and Automation*, 19(5):917–922, 2003b. Cited page 35.

B. Bethea, A. Okamura, M. Kitagawa, T. Fitton, S. Cattaneo, V. Gott, W. Baumgartner, and D. Yuh. Application of haptic feedback to robotic surgery. *Journal of laparoendoscopic & advanced surgical techniques. Part A*, 14(3):191–195, 2004. Cited pages 19 and 82.

B. Bickel, M. Bächer, M. A. Otaduy, W. Matusik, H. Pfister, and M. Gross. Capture and modeling of non-linear heterogeneous soft tissue. *ACM Transactions on Graphics (TOG)*, 28 (3):89, 2009. Cited page 34.

L. Birglen, C. Gosselin, N. Pouliot, B. Monsarrat, and T. Laliberté. Shade, a new 3-dof haptic device. *Robotics and Automation, IEEE Transactions on*, 18(2):166–175, 2002. Cited page 24.

M. Blaustein, J. Kao, and D. Matteson. *Cellular Physiology and Neurophysiology*. Elsevier Health Sciences, 2011. Cited page 85.

P. Boonvisut and M. C. Cavusoglu. Estimation of soft tissue mechanical parameters from robotic manipulation data. *Mechatronics, IEEE/ASME Transactions on*, 18(5):1602–1611, 2013. Cited page 34.

V. Bozovic. *Medical robotics*. Sciyo. com, 2008. Cited pages 29, 82, 87, and 100.

Frederick P. Brooks, J., M. Ouh-Young, J. Batter, and P. J. Kilpatrick. Project gropehaptic displays for scientific visualization. In *ACM SIGGraph computer graphics*, volume 24, pages 177–185. ACM, 1990. Cited page 23.

T.L. Brooks. Telerobotic response requirements. In *Systems, Man and Cybernetics, 1990. Conference Proceedings., IEEE International Conference on*, pages 113–120, Nov 1990. Cited pages ix and 18.

E. Burdet, R. Osu, D. Franklin, T. Milner, and M. Kawato. The central nervous system stabilizes unstable dynamics by learning optimal impedance. *Nature*, 414(6862):446–449, 2001. Cited page 43.

P. Buttolo and B. Hannaford. Advantages of Actuation Redundancy for the Design of Haptic Displays. In *Proceedings ASME, Fourth Annual Symposium on Haptic Interfaces for Virtual Environment and Teleoperator Systems*, pages 623–630, 1995. Cited page 23.

G. Campion, Qi Wang, and V. Hayward. The pantograph mk-ii: a haptic instrument. In *Intelligent Robots and Systems, 2005. (IROS 2005). 2005 IEEE/RSJ International Conference on*, pages 193–198, Aug 2005. Cited page 24.

S. C. Cannon and G. I. Zahalak. The mechanical behavior of active human skeletal muscle in small oscillations. *Journal of Biomechanics*, 15(2):111–121, 1982. Cited page 20.

C. M. Çavusoglu, W. Williams, F. Tendick, and S. Shankar Sastry. Robotics for telesurgery: second generation berkeley/ucsf laparoscopic telesurgical workstation and looking towards the future applications. *Industrial Robot: An International Journal*, 30(1):22–29, 2003. Cited page 29.

M. C. Çavuşoğlu, F. Tendick, M. Cohn, and S. S. Sastry. A laparoscopic telesurgical workstation. *Robotics and Automation, IEEE Transactions on*, 15(4):728–739, 1999. Cited page 31.

M. C. Çavuşoğlu, A. Sherman, and F. Tendick. Design of bilateral teleoperation controllers for haptic exploration and telemanipulation of soft environments. *Robotics and Automation, IEEE Transactions on*, 18(4):641–647, 2002a. Cited pages 56 and 60.

M.C. Cavusoglu, A. Sherman, and F. Tendick. Bilateral controller design for telemanipulation in soft environments. In *Robotics and Automation, 2001. Proceedings 2001 ICRA. IEEE International Conference on*, volume 1, pages 1045–1052, 2001. Cited pages 22, 37, and 60.

M.C. Çavuşoğlu, D. Feygin, and F. Tendick. A critical study of the mechanical and electrical properties of the phantom haptic interface and improvements for highperformance control. *Presence: Teleoperators and Virtual Environments*, 11(6):555–568, 2002b. Cited page 23.

Jr. H. G. Chapman. Remote control manipulating apparatus, 4 nov. 1958. US Patent 2,858,947. Cited pages ix and 11.

V. Chawda and M. K. Malley. Vision-based force sensing for nanomanipulation. *Mechatronics, IEEE/ASME Transactions on*, 16(6):1177–1183, 2011. Cited page 33.

D. Checcacci, E. Sotgiu, A. Frisoli, C.A. Avizzano, and M. Bergamasco. Gravity compensation algorithms for parallel haptic interface. In *Robot and Human Interactive Communication, 2002. Proceedings. 11th IEEE International Workshop on*, pages 140–145, 2002. Cited page 23.

H. Ching and W. J. Book. Internet-Based Bilateral Teleoperation Based on Wave Variable With Adaptive Predictor and Direct Drift Control. *Journal of Dynamic Systems, Measurement, and Control*, 128(1):86–93, 2006. Cited page 27.

G. Christiansson and F. van der Helm. The low-stiffness teleoperator slave—a trade-off between stability and performance. *The International Journal of Robotics Research*, 26(3): 287–299, 2007. Cited pages 44 and 60.

D. A. Chu and G. Myer. *Plyometrics*. Human Kinetics, 2013. Cited pages ix and 17.

J. E. Colgate. *The control of dynamically interacting systems*. PhD thesis, Massachusetts Institute of Technology, 1988. Cited pages 37, 49, 50, and 51.

J. E. Colgate and N. Hogan. Robust control of dynamically interacting systems. *International Journal of Control*, 48(1):65–88, 1988. Cited pages 20, 22, 26, and 49.

J. E. Colgate and G. Schenkel. Passivity of a class of sampled-data systems: Application to haptic interfaces. *Journal of Robotic Systems*, 14(1):37–47, 1997. Cited page 25.

J.E. Colgate and J.M. Brown. Factors affecting the z-width of a haptic display. In *Robotics and Automation, 1994. Proceedings., 1994 IEEE International Conference on*, volume 4, pages 3205–3210, May 1994. Cited pages 22, 37, and 52.

F. Conti and O. Khatib. Spanning large workspaces using small haptic devices. In *Eurohaptics Conference, 2005 and Symposium on Haptic Interfaces for Virtual Environment and Teleoperator Systems, 2005. World Haptics 2005. First Joint*, pages 183–188, March 2005. Cited page 24.

F. Conti and O. Khatib. A new actuation approach for haptic interface design. *The International Journal of Robotics Research*, 28(6):834–848, 2009. Cited page 23.

P. Corke. *Robotics, vision and control: fundamental algorithms in MATLAB*, volume 73. Springer Science & Business Media, 2011. Cited page 29.

R. Cortesão. On kalman active observers. *Journal of Intelligent and Robotic Systems*, 48(2): 131–155, 2007. Cited pages 115, 120, and 136.

R. Cortesão, J. Park, and O. Khatib. Real-time adaptive control for haptic telemanipulation with kalman active observers. *Robotics, IEEE Transactions on*, 22(5):987–999, 2006. Cited pages 33, 99, 100, 102, and 103.

R. S. Dahiya, P. Mittendorfer, M. Valle, G. Cheng, and V. J. Lumelsky. Directions toward effective utilization of tactile skin: A review. *Sensors Journal, IEEE*, 13(11):4121–4138, 2013. Cited page 16.

R.W. Daniel and P.R. McAree. Fundamental limits of performance for force reflecting teleoperation. *The International Journal of Robotics Research*, 17(8):811–830, 1998. Cited pages 37 and 82.

P. Dario, E. Guglielmelli, B. Allotta, and M.C. Carrozza. Robotics for medical application. *Robotics & Automation Magazine, IEEE*, 3(3)(September):44–56, 1996. Cited pages 14 and 29.

E. De Vlugt, A. C. Schouten, and F. Van Der Helm. Adaptation of reflexive feedback during arm posture to different environments. *Biological cybernetics*, 87(1):10–26, 2002. Cited page 21.

E. De Vlugt, A. C Schouten, and F. Van Der Helm. Quantification of intrinsic and reflexive properties during multijoint arm posture. *Journal of neuroscience methods*, 155(2):328–349, 2006. Cited page 21.

C. Delgorge, F. Courrèges, L. A.l. Bassit, C. Novales, C. Rosenberger, N. Smith-Guerin, C. Brù, R. Gilabert, M. Vannoni, and G. Poisson. A tele-operated mobile ultrasound scanner using a light-weight robot. *Information Technology in Biomedicine, IEEE Transactions on*, 9(1):50–58, 2005. Cited page 31.

C. Desoer and M. Vidyasagar. *Feedback systems: input-output properties*, volume 55. SIAM, 1975. Cited page 49.

N. Diolaiti, C. Melchiorri, and S. Stramigioli. Contact impedance estimation for robotic systems. *Robotics, IEEE Transactions on*, 21(5):925–935, Oct 2005. Cited pages 34 and 100.

N. Diolaiti, G. Niemeyer, F. Barbag, and J. K. Salisbury. Stability of haptic rendering: Discretization, quantization, time delay, and coulomb effects. *Robotics, IEEE Transactions on*, 22(2):256–268, 2006. Cited page 25.

E. Dombre, M. Michelin, F. Pierrot, P. Poignet, P. Bidaud, G. Morel, T. Ortmaier, D. Sallé, N. Zemiti, and P. Gravez. Marge project: design, modeling and control of assistive devices for minimally invasive surgery. In *Medical Image Computing and Computer-Assisted Intervention–MICCAI 2004*, pages 1–8. Springer, 2004. Cited page 29.

G. Duchemin, P. Poignet, E. Dombre, and F. Pierrot. Medically safe and sound: The challenge of designing and manufacturing actuaed medical robot for saf human interaction. *IEEE Robotics and Automation Magazine*, 11(2):46–55, 2004. Cited pages 31 and 32.

R.E. Ellis, O.M. Ismaeil, and M.G. Lipsett. Design and evaluation of a high-performance haptic interface. *Robotica*, 14(03):321–327, 1996. Cited page 22.

R.E. Ellis, N. Sarkar, and M.A. Jenkins. Numerical methods for the force reflection of contact. *Journal of dynamic systems, measurement, and control*, 119(4):768–774, 1997. Cited page 25.

D. Erickson, M. Weber, and I. Sharf. Contact stiffness and damping estimation for robotic systems. *The International Journal of Robotics Research*, 22(1):41–57, 2003. Cited pages 34 and 89.

M. O. Ernst and M. S. Banks. Humans integrate visual and haptic information in a statistically optimal fashion. *Nature*, 415(6870):429–433, 2002. Cited page 19.

euroVR. Last visit june 2015. URL http://kb.eurovr-association.org/index.php/Haptic_Hardware. Cited pages ix, 23, and 24.

S. Fahlbusch and S. Fatikow. Force sensing in microrobotic systems-an overview. In *1998 IEEE International Conference on Electronics, Circuits and Systems. Surfing the Waves of Science and Technology*, volume 3, pages 259–262, 1998. Cited page 33.

A. Faraz and S. Payandeh. A robotic case study: optimal design for laparoscopic positioning stands. *The International Journal of Robotics Research*, 17(9):986–995, 1998. Cited page 31.

M. Fässler. Force Sensing Technologies, 2010. Cited page 33.

W. R. Ferell and T. Sheridan. Supervisory control of remote manipulation. *Spectrum, IEEE*, 4(10):81âĂŞ88, 1967. Cited page 26.

M. Ferre, M. Buss, R. Aracil, C. Melchiorri, and C. Balaguer, editors. *Advances in telerobotics*, volume 31. Springer, 2007. Cited page 8.

W. R. Ferrell. Remote manipulation with transmission delay. *Human Factors in Electronics, IEEE Transactions on*, (1):24–32, 1965. Cited page 26.

K. B. Fite, J. E. Speich, and M. Goldfarb. Transparency and stability robustness in two-channel bilateral telemanipulation. *Journal of Dynamic Systems, Measurement, and Control*, 123(3):400–407, 2001. Cited page 36.

K. B. Fite, L. Shao, and M. Goldfarb. Loop shaping for transparency and stability robustness in bilateral telemanipulation. *Robotics and Automation, IEEE Transactions on*, 20(3): 620–624, 2004. Cited page 36.

T. Flash and N. Hogan. The coordination of arm movements: An experimentally confirmed mathematical model. *The Journal of Neuroscience*, 5(7):1688–1703, 1985. Cited pages 21 and 91.

H Flemmer and J. Wikander. Transparency and stability analysis of a surgical teleoperator system. In *Haptic Interfaces for Virtual Environment and Teleoperator Systems, 2003. HAPTICS 2003. Proceedings. 11th Symposium on*, pages 382–389, 2003. Cited pages 56 and 60.

P. Fong. Sensing, acquisition, and interactive playback of data-based models for elastic deformable objects. *The International Journal of Robotics Research*, 28(5):630–655, 2009. Cited page 34.

T. Fong, J. Rochlis Zumbado, N. Currie, A. Mishkin, and D. L. Akin. Space telerobotics: Unique challenges to human—robot collaboration in space. *Reviews of Human Factors and Ergonomics*, 9(1):6–56, 2013. Cited page 11.

A. Frisoli and M. Bergamasco. Experimental identification and evaluation of performance of a 2 dof haptic display. In *Robotics and Automation, 2003. Proceedings. ICRA '03. IEEE International Conference on*, volume 3, pages 3260–3265, Sept 2003. Cited page 24.

Y.C. Fung. *Biodynamics: circulation*. Springer Science & Business Media, 1984. Cited page 85.

Y.C. Fung. *Biomechanics: mechanical properties of living tissues*. Springer Science & Business Media, 1993. Cited pages 34, 85, 89, and 100.

Z. Gao, K. Lister, and J. P. Desai. Constitutive modeling of liver tissue: experiment and theory. *Annals of biomedical engineering*, 38(2):505–516, 2010. Cited page 34.

E. Garcia, M. A. Jimenez, P. G. De Santos, and M. Armada. The evolution of robotics research. *Robotics & Automation Magazine, IEEE*, 14(1):90–103, 2007. Cited page 11.

P. J. Gawthrop and G. P. Bevan. Bond-graph modeling. *Control Systems, IEEE*, 27(2):24–45, 2007. Cited pages 40 and 41.

B. Gersak and Z. Sutlic. Aortic and mitral valve surgery on the beating heart is lowering cardiopulmonary bypass and aortic cross clamp time. In *Heart Surg Forum*, volume 5, pages 182–6, 2002. Cited page 81.

G.A. Gescheider, J.H. Wright, and R.T. Verrillo. *Information-processing channels in the tactile sensory system: A psychophysical and physiological analysis*. Psychology Press, 2010. Cited page 16.

J. J. Gil, A. Avello, A. Rubio, and J. Florez. Stability analysis of a 1 dof haptic interface using the routh-hurwitz criterion. *Control Systems Technology, IEEE Transactions on*, 12(4): 583–588, 2004. Cited page 25.

J. J. Gil, E. Sánchez, T. Hulin, C. Preusche, and G. Hirzinger. Stability boundary for haptic rendering: Influence of damping and delay. *Journal of Computing and Information Science in Engineering*, 9(1):011005, 2009. Cited page 25.

R. B. Gillespie and M. R. Cutkosky. Stable user-specific haptic rendering of the virtual wall. In *Proceedings of the ASME International Mechanical Engineering Congress and Exhibition*, volume 58, pages 397–406, 1996. Cited page 25.

R. Ginhoux, J. Gangloff, M. De Mathelin, L. Soler, M. M. A. Sanchez, and J. Marescaux. Active filtering of physiological motion in robotized surgery using predictive control. *Robotics, IEEE Transactions on*, 21(1):67–79, 2005. Cited page 34.

R. Goertz. 1954 electromechanical manipulator. URL http://cyberneticzoo.com/teleoperators/1954-electromechanical-manipulator-ray-goertz-american. Cited page 11.

R. Goertz. A force-reflecting positional servomechanism. *Nucleonics*, 10(11):43–45, 1952. Cited page 11.

R. Goertz. Mechanical master—slave manipulator. *Nucleonics*, 12(11):45–46, 1954. Cited page 25.

R. C. Goertz. Remote-control manipulator, 24 mars 1953. URL http://www.google.com/patents/US2632574. US Patent 2,632,574. Cited pages ix and 11.

E. Goldstein. *Sensation and perception*. Cengage Learning, 2013. Cited pages 16 and 17.

P. Gomes. Surgical robotics: Reviewing the past, analysing the present, imagining the future. *Robotics and Computer-Integrated Manufacturing*, 27(2):261–266, 2011. Cited page 14.

D. Grant. Two new commercial haptic rotary controllers. In *Proc. Eurohaptics*, page 451, 2004. Cited page 24.

M. Greminger and Br. J. Nelson. Vision-Based Force Measurement. *IEEE Transactions on Pattern Analysis and Machine Intelligence*, 26(3):290–298, 2004. Cited page 33.

M. Groeger, K. Arbter, and G. Hirzinger. Motion tracking for minimally invasive robotic surgery. In Vanja Bozovic, editor, *Medical Robotics*, pages 117–148. ITech, 2008. Cited page 34.

A. C. Guyton and J. E. Hall. *Textbook of Medical Physiology*. Elsevier Health Sciences, 12th edition edition, 2010. Cited pages x, 84, and 85.

A. Haddadi and K. Hashtrudi-Zaad. Bounded-impedance absolute stability of bilateral teleoperation control systems. *Haptics, IEEE Transactions on*, 3(1):15–27, Jan 2010. Cited page 28.

A. Haddadi and K. Hashtrudi-Zaad. Robust stability of teleoperation systems with time delay: A new approach. *Haptics, IEEE Transactions on*, 6(2):229–241, April 2013. Cited page 28.

A. Z. Hajian and R. D. Howe. Identification of the mechanical impedance at the human finger tip. *Journal of biomechanical engineering*, 119(1):109–114, 1997. Cited page 21.

M. Handlykken and T. Turner. Control system analysis and synthesis for a six degree-of-freedom universal force-reflecting hand controller. In *Decision and Control including the Symposium on Adaptive Processes, 1980 19th IEEE Conference on*, pages 1197–1205, 1980. Cited page 24.

B. Hannaford. A design framework for teleoperators with kinesthetic feedback. *Robotics and Automation, IEEE Transactions on*, 5(4):426–434, Aug. 1989a. Cited pages 8, 37, and 40.

B. Hannaford. Stability and performance tradeoffs in bi-lateral telemanipulation. In *Robotics and Automation, 1989. Proceedings., 1989 IEEE International Conference on*, volume 3, pages 1764–1767, May 1989b. Cited page 36.

B. Hannaford and P. Fiorini. A detailed model of bi-lateral teleoperation. In *Proceedings of the IEEE international conference on systems, man and cybernetics*, volume 1, pages 117–121, 1988. Cited page 36.

B. Hannaford and A. Okamura. Haptics. In B. Siciliano and O. Khatib, editors, *Springer Handbook of Robotics*, pages 719–739. Springer Berlin Heidelberg, 2008. Cited pages 8, 23, 24, and 37.

B. Hannaford and J.H. Ryu. Time-domain passivity control of haptic interfaces. *Robotics and Automation, IEEE Transactions on*, 18(1):1–10, Feb. 2002. Cited pages 25 and 27.

B. Hannaford, L. Wood, D.A. McAffee, and H. Zak. Performance evaluation of a six-axis generalized force-reflecting teleoperator. *Systems, Man and Cybernetics, IEEE Transactions on*, 21(3):620–633, May 1991. Cited page 19.

B. M. Harnett, C. R. Doarn, J. Rosen, B. Hannaford, and T. J. Broderick. Evaluation of unmanned airborne vehicles and mobile robotic telesurgery in an extreme environment. *Telemedicine and e-Health*, 14(6):539–544, 2008. Cited page 25.

K. Hashtrudi-Zaad and S. E. Salcudean. Analysis of control architectures for teleoperation systems with impedance/admittance master and slave manipulators. *The International Journal of Robotics Research*, 20(6):419–445, 2001. Cited pages 36, 37, 44, 47, 51, 52, 57, 59, 60, and 82.

K. Hashtrudi-Zaad and S.E. Salcudean. Transparency in time-delayed systems and the effect of local force feedback for transparent teleoperation. *Robotics and Automation, IEEE Transactions on*, 18(1):108–114, Feb 2002. Cited pages 37, 51, 56, 57, 60, and 71.

C. J Hasser and M. R. Cutkosky. System identification of the human hand grasping a haptic knob. In *Haptic Interfaces for Virtual Environment and Teleoperator Systems, International Symposium on*, pages 180–180. IEEE Computer Society, 2002. Cited page 21.

K. Hastrudi-Zaad and S.E. Salcudean. On the use of local force feedback for transparent teleoperation. In *Robotics and Automation, 1999. Proceedings. 1999 IEEE International Conference on*, volume 3, pages 1863–1869, 1999. Cited pages 56 and 58.

S. S. Haykin. *Active Network Theory*. Addison-Wesley, 1970. Cited pages 25 and 27.

V. Hayward. Toward a seven axis haptic device. In *Intelligent Robots and Systems 95. 'Human Robot Interaction and Cooperative Robots', Proceedings. 1995 IEEE/RSJ International Conference on*, volume 3, pages 133–139, Aug. 1995. Cited page 23.

V. Hayward and O. R. Astley. Performance measures for haptic interfaces. In *Robotics Research*, pages 195–206. Springer, 1996. Cited pages 22 and 23.

V. Hayward and K.E. MacLean. Do it yourself haptics: part i. *Robotics Automation Magazine, IEEE*, 14(4):88–104, Dec 2007. Cited pages 22, 23, and 24.

V. Hayward, O. R. Astley, M. Cruz-Hernandez, D. Grant, and G. Robles-De-La-Torre. Haptic interfaces and devices. *Sensor Review*, 24(1):16–29, 2004. Cited pages 21 and 23.

B. Herman, B. Dehez, K. T. Duy, B. Raucent, E. Dombre, and S. Krut. Design and preliminary in vivo validation of a robotic laparoscope holder for minimally invasive surgery. *The International Journal of Medical Robotics and Computer Assisted Surgery*, 5(3):319–326, 2009. Cited page 31.

T. Higuchi and M. T. Gettman. Robotic instrumentation, personnel and operating room setup. In *Atlas of Robotic Urologic Surgery*, chapter 2. Springer Science+Business Media, 2011. Cited pages ix, 29, and 30.

J. W. Hill and J. F. Jensen. Telepresence technology in medicine: Principles and applications. *Proceedings of the IEEE*, 86(3):569–580, 1998. Cited page 14.

P. Hinterseer, S. Hirche, S. Chaudhuri, E. Steinbach, and M. Buss. Perception-based data reduction and transmission of haptic data in telepresence and teleaction systems. *Signal Processing, IEEE Transactions on*, 56(2):588–597, 2008. Cited page 26.

S. Hirche and M. Buss. Human-oriented control for haptic teleoperation. *Proceedings of the IEEE*, 100(3):623–647, March 2012. Cited pages 4, 12, and 15.

S. Hirche, M. Ferre, J. Barrio, C. Melchiorri, and M. Buss. Bilateral control architectures for telerobotics. In *Advances in Telerobotics*, volume 31 of *Springer Tracts in Advanced Robotics*, pages 163–176. Springer Berlin Heidelberg, 2007. Cited page 36.

G. Hirzinger, B. Brunner, R. Koeppe, and J. Vogel. Advanced telerobotics. In *Autonomous Robotic Systems*, pages 97–124. Springer, 1998. Cited page 35.

N. Hogan. Impedance control: An approach to manipulation: Parts i-iii. *Journal of Dynamic Systems, Measurement, and Control*, 107(1):1–24, 1985a. Cited pages 20 and 39.

N. Hogan. The mechanics of multi-joint posture and movement control. *Biological Cybernetics*, 52(5):315–331, 1985b. ISSN 0340-1200. Cited page 21.

N. Hogan. Controlling impedance at the man/machine interface. In *Robotics and Automation, 1989. Proceedings., 1989 IEEE International Conference on*, volume 3, pages 1626–1631, 1989. Cited pages 20, 22, 36, and 43.

P. F. Hokayem and M. W. Spong. Bilateral teleoperation: An historical survey. *Automatica*, 42(12):2035–2057, 2006. Cited pages 4, 12, 15, and 26.

M. K. Holden. Virtual environments for motor rehabilitation: review. *Cyberpsychology & behavior*, 8(3):187–211, 2005. Cited page 22.

L. Huijun and S. Aiguo. Virtual-environment modeling and correction for force-reflecting teleoperation with time delay. *IEEE Transactions on Industrial Electronics*, 54(2):1227–1233, 2007. Cited page 26.

P. J. Hunter, A. J. Pullan, and B. H. Smaill. Modeling total heart function. *Annual review of biomedical engineering*, 5(1):147–177, 2003. Cited page 34.

J. M. Huyghe, D. H. van Campen, T. Arts, and R. M. Heethaar. The constitutive behaviour of passive heart muscle tissue: a quasi-linear viscoelastic formulation. *Journal of biomechanics*, 24(9):841–849, 1991. Cited page 85.

H. Igo Krebs, N. Hogan, M. L. Aisen, and B. T. Volpe. Robot-aided neurorehabilitation. *IEEE Transactions on Rehabilitation Engineering*, 6(1):75–87, 1998. Cited page 22.

H. Iwata. Artificial reality with force-feedback: development of desktop virtual space with compact master manipulator. In *Computer Graphics*, volume 24, pages 165–170, 1990. Cited page 23.

S. Jacobs, D. Holzhey, B. B. Kiaii, J. F. Onnasch, T. Walther, F. W. Mohr, and V. Falk. Limitations for manual and telemanipulator-assisted motion tracking—implications for endoscopic beating-heart surgery. *The Annals of thoracic surgery*, 76(6):2029–2035, 2003. Cited page 34.

A. Janot, C. Bidard, F. Gosselin, M. Gautier, D. Keller, and Y. Perrot. Modeling and identification of a 3 dof haptic interface. In *Robotics and Automation, 2007 IEEE International Conference on*, pages 4949–4955. IEEE, 2007. Cited page 24.

A. Jazayeri and M. Tavakoli. A passivity criterion for sampled-data bilateral teleoperation systems. *Haptics, IEEE Transactions on*, 6(3):363–369, 2013. Cited page 37.

A. Jazayeri and M. Tavakoli. Bilateral teleoperation system stability with non-passive and strictly passive operator or environment. *Control Engineering Practice*, 40:45–60, 2015. Cited pages 28, 37, and 52.

A. Jeremic and A. Nehorai. Estimating mechanical properties of the heart using dynamic modeling and magnetic resonance imaging. In *Acoustics, Speech, and Signal Processing, 2000. ICASSP '00. Proceedings. 2000 IEEE International Conference on*, volume 6, pages 3775–3778, 2000. Cited page 85.

L. Kaim and K. Drewing. Exploratory strategies in haptic softness discrimination are tuned to achieve high levels of task performance. *Haptics, IEEE Transactions on*, 4(4):242–252, July 2011. Cited page 19.

E. R. Kandel, T. M. Jessell, J. H. Schwartz, T. S. Siegelbaum, and A.J. Hudspeth. *Principles of neural science*, volume 4. McGraw-Hill New York, 2012. Cited page 16.

D. C. Karnopp, D. L. Margolis, and R. C. Rosenberg. *System Dynamic: Modeling, Simulation, and Control of Mechatronic Systems*. John Wiley & Sons, 2012. Cited page 42.

K. Kawashima, K. Tadano, G. Sankaranarayanan, and B. Hannaford. Model-based passivity control for bilateral teleoperation of a surgical robot with time delay. In *2008 IEEE/RSJ International Conference on Intelligent Robots and Systems, IROS*, number 2, pages 1427–1432, 2008. Cited page 28.

K. Kawashima, K. Tadano, and M.S. Fofana. Bilateral teleoperation with time delay using modified wave variable based controller. In *ASME 2009 International Mechanical Engineering Congress and Exposition*, pages 397–402. American Society of Mechanical Engineers, 2009. Cited page 27.

H. Kazerooni and M.G. Her. The dynamics and control of a haptic interface device. *Robotics and Automation, IEEE Transactions on*, 10(4):453–464, Aug 1994. Cited page 21.

H. Kazerooni and T.I. Tsay. On the stability of the constrained robotic maneuvers. In *American Control Conference, 1988*, pages 892–897, June 1988. Cited page 22.

H. Kazerooni, T.I. Tsay, and C.L. Moore. Telefunctioning: An approach to telerobotic manipulations. In *American Control Conference, 1990*, pages 2778–2783, May 1990. Cited pages 21 and 36.

A. Kazi. Operator performance in surgical telemanipulation. *Presence*, 10(5):495–510, 2001. Cited page 19.

B. Khademian and K. Hashtrudi-Zaad. A framework for unconditional stability analysis of multimaster/multislave teleoperation systems. *Robotics, IEEE Transactions on*, 29(3): 684–694, June 2013. Cited page 37.

H. K. Khalil. *Nonlinear systems*. Prentice hall New Jersey, 3rd edition, 2002. Cited pages 26, 27, and 49.

W. Khalil and E. Dombre. *Modeling, identification and control of robots*. Butterworth-Heinemann, 2004. Cited page 29.

O. Khatib. A unified approach for motion and force control of robot manipulators: The operational space formulation. *Robotics and Automation, IEEE Journal of*, 3(1):43–53, 1987. Cited page 114.

H. S. Kim. Mechanism design of haptic devices. In *Advances in Haptics*, pages 283–297. InTech, 2010. Cited page 23.

J. Kim, F. Janabi-Sharifi, and J. Kim. A haptic interaction method using visual information and physically based modeling. *Mechatronics, IEEE/ASME Transactions on*, 15(4):636–645, 2010. Cited page 34.

J. Kim, P. H. Chang, and H.S. Park. Two-channel transparency-optimized control architectures in bilateral teleoperation with time delay. *Control Systems Technology, IEEE Transactions on*, 21(1):40–51, 2013. Cited page 37.

J.P. Kim and J. Ryu. Robustly stable haptic interaction control using an energy-bounding algorithm. *The International Journal of Robotics Research*, 2009. Cited page 28.

W.S. Kim, B. Hannaford, and A.K. Fejczy. Force-reflection and shared compliant control in operating telemanipulators with time delay. *Robotics and Automation, IEEE Transactions on*, 8(2):176–185, Apr 1992. Cited page 26.

M. Kitagawa, A. Okamura, B. T. Bethea, V. L. Gott, and W. A. Baumgartner. Analysis of suture manipulation forces for teleoperation with force feedback. In *Medical Image Computing and Computer-Assisted InterventionâĂŤMICCAI 2002*, pages 155–162. Springer, 2002. Cited page 100.

R.L. Klatzky and B. Wu. Visual-haptic compliance perception. In M. Di Luca, editor, *Multisensory Softness*, Springer Series on Touch and Haptic Systems, pages 17–30. Springer London, 2014. Cited page 17.

G. Kokkonis, K. Psannis, M. Roumeliotis, and S. Kontogiannis. A survey of transport protocols for haptic applications. In *Proceedings of the 2012 16th Panhellenic Conference on Informatics, PCI 2012*, pages 192–197, 2012. Cited page 25.

J. Konstantinova, A. Jiang, K. Althoefer, P. Dasgupta, and T. Nanayakkara. Implementation of tactile sensing for palpation in robot-assisted minimally invasive surgery: A review. *IEEE Sensors Journal*, 14(8):2490–2501, 2014. Cited page 33.

A. Krupa, G. Morel, and M. De Mathelin. Achieving high-precision laparoscopic manipulation through adaptive force control. *Advanced Robotics*, 18(9):905–926, 2004. Cited page 31.

R. Kubo, N. Iiyama, K. Natori, K. Ohnishi, and H. Furukawa. Performance analysis of a three-channel control architecture for bilateral teleoperation with time delay. *IEEJ Transactions on Industry Applications*, 127(12):1224–1230, 2007. Cited pages 56 and 60.

M. Kuschel, M. Buss, F. Freyberger, B. Farber, and R.L. Klatzky. Visual-haptic perception of compliance: Fusion of visual and haptic information. In *Haptic interfaces for virtual environment and teleoperator systems, 2008. haptics 2008. symposium on*, pages 79–86, March 2008. Cited page 17.

M. Kuschel, P. Kremer, and M. Buss. Passive haptic data-compression methods with perceptual coding for bilateral presence systems. *Systems, Man and Cybernetics, Part A: Systems and Humans, IEEE Transactions on*, 39(6):1142–1151, 2009. Cited page 26.

Y.S. Kwoh, J. Hou, E.A. Jonckheere, and S. Hayati. A robot with improved absolute positioning accuracy for ct guided stereotactic brain surgery. *Biomedical Engineering, IEEE Transactions on*, 35(2):153–160, Feb 1988. Cited page 14.

D. Lawrence and J. D. Chapel. Performance trade-offs for hand controller design. In *Robotics and Automation, 1994. Proceedings., 1994 IEEE International Conference on*, pages 3211–3216, 1994. Cited page 22.

D. Lawrence, L. Y. Pao, A. M. Dougherty, M. Salada, and Y. Pavlou. Rate-hardness: A new performance metric for haptic interfaces. *Robotics and Automation, IEEE Transactions on*, 16(4):357–371, 2000. Cited page 22.

D. Lawrence, L. Y. Pao, A. C. White, and W. Xu. Low cost actuator and sensor for high-fidelity haptic interfaces. In *Haptic Interfaces for Virtual Environment and Teleoperator Systems, 2004. HAPTICS'04. Proceedings. 12th International Symposium on*, pages 74–81, 2004. Cited page 24.

D.A. Lawrence. Stability and transparency in bilateral teleoperation. *Robotics and Automation, IEEE Transactions on*, 9(5):624–637, Oct. 1993. Cited pages 28, 36, 37, 47, 52, 56, 58, 60, and 82.

S. J. Lederman and L. A. Jones. Tactile and haptic illusions. *Haptics, IEEE Transactions on*, 4(4):273–294, 2011. Cited page 16.

S. J. Lederman and R. L. Klatzky. Hand movements: A window into haptic object recognition. *Cognitive psychology*, 19(3):342–368, 1987. Cited pages ix and 17.

S. J. Lederman and R. L. Klatzky. Haptic aspects of motor control. *Handbook of neuropsychology*, 11:131–148, 1997. Cited pages ix and 17.

S. J. Lederman and R. L Klatzky. Haptic identification of common objects: Effects of constraining the manual exploration process. *Perception & psychophysics*, 66(4):618–628, 2004. Cited page 17.

S. J. Lederman and R. L. Klatzky. Haptic perception: A tutorial s. *Attention, perception & psychophysics*, 71(7):1439–1459, 2009. Cited page 16.

G. M.H. Leung, B. Francis, and J. Apkarian. Bilateral controller for teleoperators with time delay via μ-synthesis. *Robotics and Automation, IEEE Transactions on*, 11(1):105–116, 1995. Cited pages 27 and 36.

K. Levenberg. A method for the solution of certain non-linear problems in least squares. *Quarterly Journal of Applied Mathmatics*, II(2):164–168, 1944. Cited page 135.

T. Li and S. Payandeh. Design of spherical parallel mechanisms for application to laparoscopic surgery. *Robotica*, 20(02):133–138, 2002. Cited page 31.

C. Liu, P. Moreira, N. Zemiti, and P. Poignet. 3d force control for robotic-assisted beating heart surgery based on viscoelastic tissue model. In *Engineering in Medicine and Biology Society, EMBC, 2011 Annual International Conference of the IEEE*, pages 7054–7058, 2011. Cited page 94.

Longman Dictionary. URL http://www.ldoceonline.com/dictionary/. Cited page 7.

S. Louw, A. M.L. Kappers, and J. J. Koenderink. Haptic detection thresholds of gaussian profiles over the whole range of spatial scales. *Experimental brain research*, 132(3):369–374, 2000. Cited page 17.

L.J. Love and W.J. Book. Environment estimation for enhanced impedance control. In *Robotics and Automation, 1995. Proceedings., 1995 IEEE International Conference on*, volume 2, pages 1854–1859, May 1995. Cited page 34.

Z. L. Z. Lu, P. C. Y. Chen, and W. L. W. Lin. Force sensing and control in micromanipulation. *IEEE Transactions on Systems Man and Cybernetics Part C Applications and Reviews*, 36 (6):713–724, 2006. Cited page 33.

M. J.H. Lum, J. Rosen, M. N Sinanan, and B. Hannaford. Optimization of a spherical mechanism for a minimally invasive surgical robot: theoretical and experimental approaches. *Biomedical Engineering, IEEE Transactions on*, 53(7):1440–1445, 2006. Cited page 31.

M. J.H. Lum, D. C.W. Friedman, G. Sankaranarayanan, H. King, K. Fodero, R. Leuschke, B. Hannaford, J. Rosen, and M. N. Sinanan. The raven: Design and validation of a telesurgery system. *The International Journal of Robotics Research*, 28(9):1183–1197, 2009. Cited pages 29 and 31.

K. E. MacLean. Haptic interaction design for everyday interfaces. *Reviews of Human Factors and Ergonomics*, 4(1):149–194, 2008. Cited pages 8, 15, 17, 19, and 23.

K. E. MacLean and V. Hayward. Do it yourself haptics: Part ii [tutorial]. *Robotics Automation Magazine, IEEE*, 15(1):104–119, March 2008. Cited page 23.

A. J. Madhani. *Design of teleoperated surgical instruments for minimally invasive surgery*. PhD thesis, Massachusetts Institute of Technology, 1997. Cited page 31.

N. Mai, M. Avarello, and P. Bolsinger. Maintenance of low isometric forces during prehensile grasping. *Neuropsychologia*, 23(6):805–812, 1985. Cited page 17.

Elaine Nicpon Marieb and Katja Hoehn. *Human anatomy & physiology*. Pearson Education, 2007. Cited pages xi and 86.

D. W. Marquardt. An algorithm for least-squares estimation of nonlinear parameters. *Journal of the Society for Industrial & Applied Mathematics*, 11(2):431–441, 1963. Cited page 135.

T. H. Massie and J. K. Salisbury. The phantom haptic interface: A device for probing virtual objects. In *Proceedings of the ASME winter annual meeting, symposium on haptic interfaces for virtual environment and teleoperator systems*, volume 55, pages 295–300, 1994. Cited page 24.

M.J. Massimino and T. Sheridan. Variable force and visual feedback effects on teleoperator man/machine performance. *Proc. of NASA Conference on Space Robotic*, 1:89–98, 1989. Cited page 19.

D. McCloy and D.M.J. Harris. Chapter 10: Tele-operators. In *Robotics: An Introduction*, pages 238–263. Springer Science+Business Media Dordrecht, 1986. Cited page 12.

C. Melchiorri and G. Vassura. Development and application of wire-actuated haptic interfaces. *Journal of Robotic Systems*, 18(12):755–768, 2001. Cited page 23.

B.E. Miller, J.E. Colgate, and R.A. Freeman. On the role of dissipation in haptic systems. *Robotics, IEEE Transactions on*, 20(4):768–771, Aug 2004. Cited page 25.

P. Millman and J. E. Colgate. Design of a four degree-of-freedom force-reflecting manipulandum with a specified force/torque workspace. In *Robotics and Automation, 1991. Proceedings., 1991 IEEE International Conference on*, pages 1488–1493, 1991. Cited page 23.

M. Minsky, O.y. Ming, O. Steele, F. P. Brooks Jr, and M. Behensky. Feeling and seeing: issues in force display. *ACM SIGGRAPH Computer Graphics*, 24(2):235–241, 1990. Cited page 25.

S. Misra and A. Okamura. Environment parameter estimation during bilateral telemanipulation. In *Haptic Interfaces for Virtual Environment and Teleoperator Systems, 2006 14th Symposium on*, pages 301–307, March 2006. Cited pages 34 and 89.

P. Mitra and G. Niemeyer. Model-mediated telemanipulation. *The International Journal of Robotics Research*, 27(2):253–262, 2008. Cited page 26.

C. Mitsantisuk, K. Ohishi, and S. Katsura. Estimation of action/reaction forces for the bilateral control using kalman filter. *Industrial Electronics, IEEE Transactions on*, 59(11): 4383–4393, 2012. Cited page 34.

M. Mitsuishi, J. Arata, K. Tanaka, M. Miyamoto, T. Yoshidome, S. Iwata, M. Hashizume, and S. Warisawa. Development of a remote minimally-invasive surgical system with operational environment transmission capability. In *Robotics and Automation, 2003. Proceedings. ICRA'03. IEEE International Conference on*, volume 2, pages 2663–2670, 2003. Cited page 25.

R. Moreau, M. T. Pham, M. Tavakoli, M.Q. Le, and T. Redarce. Sliding-mode bilateral teleoperation control design for master–slave pneumatic servo systems. *Control Engineering Practice*, 20(6):584–597, 2012. Cited page 37.

P. Moreira, N. Zemiti, C. Liu, and P. Poignet. Viscoelastic model based force control for soft tissue interaction and its application in physiological motion compensation. *Computer methods and programs in biomedicine*, 116(2):52–67, 2014. Cited pages 34, 100, and 136.

Pedro Moreira, Chao Liu, Nabil Zemiti, and Philippe Poignet. Soft tissue force control using active observers and viscoelastic interaction model. In *Robotics and Automation (ICRA), 2012 IEEE International Conference on*, pages 4660–4666, 2012. Cited page 137.

M. Moreyra and B. Hannaford. A practical measure of dynamic response of haptic devices. In *Robotics and Automation, 1998. Proceedings. 1998 IEEE International Conference on*, volume 1, pages 369–374, 1998. Cited page 22.

G. P. Moustris, S. C. Hiridis, K. M. Deliparaschos, and K. M. Konstantinidis. Evolution of autonomous and semi-autonomous robotic surgical systems: a review of the literature. *The international journal of medical robotics and computer assisted surgery : MRCAS*, 7: 375–392, 2011. Cited page 14.

J. Murayama, L. Bougrila, Y. Luo, K. Akahane, S. Hasegawa, B. Hirsbrunner, and M. Sato. Spidar g&g: A two-handed haptic interface for bimanual vr interaction. In *Proceedings of EuroHaptics*, pages 138–146, 2004. Cited page 24.

J. M. Murkin, W. D. Boyd, S. Ganapathy, S. J. Adams, and R. C. Peterson. Beating heart surgery: why expect less central nervous system morbidity? *The Annals of thoracic surgery*, 68(4):1498–1501, 1999. Cited page 81.

F. A Mussa-Ivaldi, N. Hogan, and E. Bizzi. Neural, mechanical, and geometric factors subserving arm posture in humans. *The Journal of neuroscience*, 5(10):2732–2743, 1985. Cited page 21.

E. Naerum and B. Hannaford. Global transparency analysis of the lawrence teleoperator architecture. In *Robotics and Automation, 2009. ICRA'09. IEEE International Conference on*, pages 4344–4349, 2009. Cited pages 56, 57, and 60.

E. Naerum, O. J. Elle, and B. Hannaford. The effect of interaction force estimation on performance in bilateral teleoperation. *Haptics, IEEE Transactions on*, 5(2):160–171, 2012. Cited pages 56 and 100.

M. Nahvi and J. Edminister. *Schaum's outline of theory and problems of electric circuits*. McGraw-Hill New York, 2003. Cited page 41.

S. Najarian, M. Fallahnezhad, and E. Afshari. Advances in medical robotic systems with specific applications in surgery–a review. *Journal of medical engineering & technology*, 35(1):19–33, 2011. Cited page 14.

NASSSR14 presentations. 4th biennial north american summer school on surgical robotics/ slides, 2014. URL http://biorobotics.ri.cmu.edu/education/summerschool/slides.html. Cited page 14.

NASSSR14 videos. 4th biennial north american summer school on surgical robotics/ videos, 2014. URL http://www.ieee-ras.org/educational-resources-outreach/summer-schools/12-educational-resources-outreach/592-north-american-summer-school-on-surgical-robotics. Cited page 14.

G. Niemeyer. Telemanipulation with time delays. *The International Journal of Robotics Research*, 23(9):873–890, 2004. Cited page 27.

G. Niemeyer and J.-J.E. Slotine. Stable adaptive teleoperation. *Oceanic Engineering, IEEE Journal of*, 16(1):152–162, Jan 1991. Cited page 27.

G. Niemeyer, C. Preusche, and G. Hirzinger. Telerobotics. In B. Siciliano and O. Khatib, editors, *Springer Handbook of Robotics*, pages 741–757. Springer Berlin Heidelberg, 2008. Cited pages 8, 9, 11, 15, and 37.

M. Novak. Telemedicine predicted in 1925. URL http://www.smithsonianmag.com/history/telemedicine-predicted-in-1925-124140942/?no-ist. Cited pages ix, 11, and 12.

E. Nuño, L. Basañez, and R. Ortega. Passivity-based control for bilateral teleoperation: A tutorial. *Automatica*, 47(3):485–495, 2011. Cited pages 27 and 47.

A. Okamura. Methods for haptic feedback in teleoperated robot-assisted surgery. *Industrial Robot: An International Journal*, 31(6):499–508, 2004. Cited pages 60 and 82.

A. Okamura, M. J. Matarić, and H. I. Christensen. Medical and health-care robotics. *IEEE Robotics and Automation Magazine*, 17(3):26–37, 2010. Cited page 14.

A. Okamura, C. Basdogan, S. Baillie, and W. S. Harwin. Haptics in medicine and clinical skill acquisition, special section intro. *Haptics, IEEE Transactions on*, 4(3):153–154, 2011a. Cited page 19.

A. Okamura, L.N. Verner, T. Yamamoto, J. Gwilliam, and P.G. Griffiths. Force feedback and sensory substitution for robot-assisted surgery. In J. Rosen, B. Hannaford, and R. M. Satava, editors, *Surgical Robotics*, pages 419–448. Springer US, 2011b. Cited pages ix, 20, and 37.

R. Ortega, a. J. Van der Schaft, I. Mareels, and B. Maschke. Putting energy back in control. *IEEE Control Systems Magazine*, 21(2):18–33, 2001. Cited page 49.

T. Ortmaier, M. Groger, D.H. Boehm, V. Falk, and G. Hirzinger. Motion estimation in beating heart surgery. *Biomedical Engineering, IEEE Transactions on*, 52(10):1729–1740, Oct. 2005. Cited page 34.

T. Osa, K. Harada, N. Sugita, and M. Mitsuishi. Trajectory planning under different initial conditions for surgical task automation by learning from demonstration. In *Robotics and Automation (ICRA), 2014 IEEE International Conference on*, pages 6507–6513, 2014. Cited page 21.

M. A. Otaduy and M. C. Lin. Introduction to haptic rendering. In *ACM SIGGRAPH 2005 Courses*, page 3. ACM, 2005. Cited page 22.

Oxford Dictionary. URL http://www.oxforddictionaries.com/. Cited page 7.

A. E. Park and T. H. Lee. Evolution of minimally invasive surgery and its impact on surgical residency training. In R. Matteotti and S.W. Ashley, editors, *Minimally Invasive Surgical Oncology*, chapter 2, pages 11–22. Springer-Verlag Berlin Heidelberg, 2011. Cited page 14.

J. Park and O. Khatib. A haptic teleoperation approach based on contact force control. *The International Journal of Robotics Research*, 25(5-6):575–591, 2006. Cited pages xi, 33, 100, 101, 103, and 105.

C. Passenberg, A. Peer, and M. Buss. A survey of environment-, operator-, and task-adapted controllers for teleoperation systems. *Mechatronics*, 20(7):787 – 801, 2010. Special Issue on Design and Control Methodologies in Telerobotics. Cited pages 4, 12, and 15.

British Pathe. Mechanical hands 1948, 1948. URL http://www.britishpathe.com/video/mechanical-hands/query/atomic+manipulator. Cited pages ix and 11.

J. J. H. Payne. Remote-control manipulator, 12 july 1949. URL http://www.google.com/patents/US2476249. US Patent 2,476,249. Cited page 11.

A. Peer. *Design and Control of Admittance-Type Telemanipulation Systems*. PhD thesis, Technischen Universität München, 2008. Cited page 23.

A. Peer and M. Buss. A new admittance-type haptic interface for bimanual manipulations. *IEEE/ASME Transactions on Mechatronics*, 13(4):416–428, 2008. Cited page 23.

F. Pierrot, E. Dombre, E. Dégoulange, L. Urbain, P. Caron, S. Boudet, J. Gariépy, and J.L. Mégnien. Hippocrate: a safe robot arm for medical applications with force feedback. *Medical Image Analysis*, 3(3):285–300, 1999. Cited page 32.

J. G. Pinto and Y.C. Fung. Mechanical properties of the heart muscle in the passive state. *Journal of Biomechanics*, 6(6):597–616, 1973. Cited page 85.

R. P. Power. The dominance of touch by vision : sometimes incomplete. *Perception*, 9: 457–466, 1980. Cited page 19.

P. Puangmali, K. Althoefer, L. D. Seneviratne, D. Murphy, and P. Dasgupta. State-of-the-art in force and tactile sensing for minimally invasive surgery. *IEEE Sensors Journal*, 8(4): 371–380, 2008. Cited page 33.

P. Puangmali, H. Liu, L. D. Seneviratne, P. Dasgupta, and K. Althoefer. Miniature 3-axis distal force sensor for minimally invasive surgical palpation. *Mechatronics, IEEE/ASME Transactions on*, 17(4):646–656, 2012. Cited page 35.

G.J. Raju, G.C. Verghese, and T.B. Sheridan. Design issues in 2-port network models of bilateral remote manipulation. In *Robotics and Automation, 1989. Proceedings., 1989 IEEE International Conference on*, volume 3, pages 1316–1321, May 1989. Cited pages 22, 27, 36, and 37.

R. Richa, P. Poignet, and C. Liu. Three-dimensional motion tracking for beating heart surgery using a thin-plate spline deformable model. *The International Journal of Robotics Research*, 29(2-3):218–230, 2010. Cited pages 34 and 84.

C. Richards, J. Rosen, B. Hannaford, C. Pellegrini, and M. Sinanan. Skills evaluation in minimally invasive surgery using force/torque signatures. *Surgical endoscopy*, 14(9):791–798, 2000. Cited page 29.

M. A. Riley, J. B. Wagman, M.V. Santana, C. Carello, and M.T. Turvey. Perceptual behavior: Recurrence analysis of a haptic exploratory procedure. *PERCEPTION-LONDON-*, 31(4): 481–510, 2002. Cited page 18.

C. N Riviere, J. Gangloff, and M. De Mathelin. Robotic compensation of biological motion to enhance surgical accuracy. *PROCEEDINGS-IEEE*, 94(9):1705, 2006. Cited pages 34 and 82.

G. Robles-De-La-Torre. Principles of haptic perception in virtual environments. In *Human haptic perception: Basics and applications*, pages 363–379. Springer, 2008. Cited page 25.

E. Rodriguez and W.R. Chitwood. Robotics in cardiac surgery. *Scandinavian Journal of Surgery*, 98(2):120–124, 2009. Cited page 29.

M. Roger. *Cardiovascular Mechanics I, II, III.* Harvard-MIT, 2004. Cited page 85.

J. Rosen, J. D. Brown, L. Chang, M. N. Sinanan, and B. Hannaford. Generalized approach for modeling minimally invasive surgery as a stochastic process using a discrete markov model. *Biomedical Engineering, IEEE Transactions on*, 53(3):399–413, 2006. Cited page 29.

J. Rosen, B. Hannaford, and R. M. Satava. *Surgical Robotics: Systems Applications and Visions*. Springer Science & Business Media, 2011. Cited pages x, xiii, 29, 30, 31, 81, and 100.

L. B Rosenberg. How to assess the quality of force-feedback systems. *Medicine Meets Virtual Reality-Interactive Technology and the New Paradigm for Healthcare, IOS Press, Amsterdam*, 1995. Cited page 22.

R. C. Rosenberg and D. Karnopp. *Introduction to Physical System Dynamics*. McGraw-Hill, 1983. Cited page 40.

A. Rovetta. Telerobotic surgery control and safety. In *Robotics and Automation, 2000. Proceedings. ICRA'00. IEEE International Conference on*, volume 3, pages 2895–2900, 2000. Cited page 32.

J. H. Ryu, D. S. Kwon, and B. Hannaford. Stable teleoperation with time-domain passivity control. *IEEE Transactions on Robotics and Automation*, 20(2):365–373, 2004. Cited page 27.

J. H. Ryu, J. Artigas, and C. Preusche. A passive bilateral control scheme for a teleoperator with time-varying communication delay. *Mechatronics*, 20(7):812–823, oct. 2010. Cited page 28.

L. A. Sánchez, M.Q. Le, C. Liu, N. Zemiti, and P. Poignet. The impact of interaction model on stability and transparency in bilateral teleoperation for medical applications. In *Robotics and Automation (ICRA), 2012 IEEE International Conference on*, pages 1607–1613, 2012. Cited pages 100 and 136.

L. A. Sanchez, M.Q. Le, K. Rabenorosoa, C. Liu, N. Zemiti, P. Poignet, E. Dombre, A. Menciassi, and P. Dario. A case study of safety in the design of surgical robots: The araknes platform. In *Intelligent Autonomous Systems 12*, pages 121–130. Springer, 2013. Cited page 60.

G. Sankaranarayanan, H. I King, S.Y. Ko, M. Lum, D. Friedman, J. Rosen, and B. Hannaford. Portable surgery master station for mobile robotic telesurgery. In *Proceedings of the 1st international conference on Robot communication and coordination*, page 28. IEEE Press, 2007. Cited page 25.

M. Sauvée, A. Noce, P. Poignet, J. Triboulet, and E. Dombre. Three-dimensional heart motion estimation using endoscopic monocular vision system: From artificial landmarks to texture analysis. *Biomedical Signal Processing and Control*, 2(3):199–207, 2007. Cited page 94.

C. Seo, J. Kim, J.P. Kim, J. H. Yoon, and J. Ryu. Stable bilateral teleoperation using the energy-bounding algorithm: Basic idea and feasibility tests. In *Advanced Intelligent Mechatronics, 2008. AIM 2008. IEEE/ASME International Conference on*, pages 335–340, 2008. Cited page 28.

R. Sepulchre, M. Jankovic, and P. V. Kokotovic. *Constructive nonlinear control*. Springer Science & Business Media, 1997. Cited pages 49 and 52.

M. Sermesant, P. Moireau, O. Camara, J. Sainte-Marie, R. Andriantsimiavona, R. Cimrman, D. L.G. Hill, D. Chapelle, and R. Razavi. Cardiac function estimation from mri using a heart model and data assimilation: advances and difficulties. *Medical Image Analysis*, 10(4):642–656, 2006. Cited page 85.

C. Shahabi, M. R. Kolahdouzan, G. Barish, R. Zimmermann, K. Yao, D.and Fu, and L. Zhang. Alternative techniques for the efficient acquisition of haptic data. In *ACM SIGMETRICS Performance Evaluation Review*, volume 29, pages 334–335. ACM, 2001. Cited page 23.

G. Shechter, J. R. Resar, and E. R. McVeigh. Displacement and velocity of the coronary arteries: cardiac and respiratory motion. *Medical Imaging, IEEE Transactions on*, 25(3): 369–375, 2006. Cited page 34.

T. B. Sheridan. *Telerobotics, automation, and human supervisory control*. MIT press, 1992. Cited pages 4, 7, 9, 11, 12, 15, 26, and 35.

T.B. Sheridan. Telerobotics. *Automatica*, 25(4):487–507, jul. 1989. Cited pages 12 and 15.

T.B. Sheridan and W.R. Ferrell. Remote manipulative control with transmission delay. *Human Factors in Electronics, IEEE Transactions on*, HFE-4(1):25–29, Sept. 1963. Cited page 11.

A. Sherman, M. C. Çavusoglu, and F. Tendick. Comparison of teleoperator control architectures for palpation task. In *Proceedings of the ASME Dynamic Systems and Control Division, part of the ASME Internatioal Mechanical Engineering Congress and Exposition (IMECE 2000)*, pages 1261–1268, 2000. Cited pages 56, 60, and 62.

K. B. Shimoga. Finger force and touch feedback issues in dexterous telemanipulation. In *Intelligent Robotic Systems for Space Exploration, 1992. Proceedings. Fourth Annual Conference on*, pages 159–178, 1992. Cited page 18.

B. Siciliano, L. Sciavicco, L. Villani, and G. Oriolo. *Robotics: modelling, planning and control*. Springer Science & Business Media, 2009. Cited page 29.

I. Singh. Robotics in urological surgery: review of current status and maneuverability, and comparison of robot-assisted and traditional laparoscopy. *Computer aided surgery : official journal of the International Society for Computer Aided Surgery*, 16(1):38–45, 2011. Cited page 14.

M. R. Sirouspour, S. P. Dimaio, S.E. Salcudean, P. Abolmaesumi, and C. Jones. Haptic interface control-design issues and experiments with a planar device. In *Proceedings 2000*

ICRA. Millennium Conference. IEEE International Conference on Robotics and Automation. Symposia Proceedings, volume 1, pages 789–794, 2000. Cited page 25.

H. I. Son, T. Bhattacharjee, and D. Y. Lee. Estimation of environmental force for the haptic interface of robotic surgery. *The International Journal of Medical Robotics and Computer Assisted Surgery*, 6(2):221–230, 2010. Cited page 34.

H. I. Son, T. Bhattacharjee, and H. Hashimoto. Effect of scaling on the performance and stability of teleoperation systems interacting with soft environments. *Advanced Robotics*, 25(11-12):1577–1601, 2011. Cited pages 37 and 60.

M. W. Spong, S. Hutchinson, and M. Vidyasagar. *Robot modeling and control*, volume 3. Wiley New York, 2006. Cited page 29.

M. Srinivasan and C. Basdogan. Haptics in virtual environments: Taxonomy, research status, and challenges. *Computers & Graphics*, 21(4):393–404, 1997. Cited pages ix and 21.

M. A Srinivasan and J.S. Chen. Human performance in controlling normal forces of contact with rigid objects. In *Advances in Robotics, Mechatronics, and Haptic Interfaces, ASME*, volume 49, pages 119–125. ASME, 1993. Cited page 17.

S. Srivastava, S. Gadasalli, M. Agusala, R. Kolluru, R. Barrera, S. Quismundo, U. Kreaden, and V. Jeevanandam. Beating heart totally endoscopic coronary artery bypass. *The Annals of thoracic surgery*, 89(6):1873–1880, 2010. Cited page 29.

sssr13. European surgical robotic summer school, 2013. URL http://2013.sssr.fr/. Cited page 14.

E. Steinbach, S. Hirche, J. Kammerl, I. Vittorias, and R. Chaudhari. Haptic data compression and communication. *Signal Processing Magazine, IEEE*, 28(1):87–96, 2011. Cited page 26.

L. J. Stocco, S. E Salcudean, and F. Sassani. Optimal kinematic design of a haptic pen. *Mechatronics, IEEE/ASME Transactions on*, 6(3):210–220, 2001. Cited page 23.

C. Stüer, F. Ringel, M. Stoffel, A. Reinke, M. Behr, and B. Meyer. Robotic technology in spine surgery: Current applications and future developments. In M. N. Pamir, V. Seifert, and T. Kiris, editors, *Intraoperative Imaging*, volume 109, pages 241–245. Springer-Verlag/Wien, 2011. Cited page 14.

S. Susa, K. Natori, and K. Ohnishi. Three-channel micro-macro bilateral control system with scaling of control gains. In *Industrial Electronics, 2008. IECON 2008. 34th Annual Conference of IEEE*, pages 2598–2603. IEEE, 2008. Cited pages 56 and 60.

A. Suzuki and K. Ohnishi. Frequency-domain damping design for time-delayed bilateral teleoperation system based on modal space analysis. *Industrial Electronics, IEEE Transactions on*, 60(1):177–190, 2013. Cited pages 27 and 36.

H. Takahashi, S. Warisawa, M. Mitsuishi, J. Arata, and M. Hashizume. Development of high dexterity minimally invasive surgical system with augmented force feedback capability. In *Proceedings of the First IEEE/RAS-EMBS International Conference on Biomedical Robotics and Biomechatronics, 2006, BioRob 2006*, pages 284–289, 2006. Cited page 35.

A. Talasaz, A. L. Trejos, and R. V. Patel. Effect of force feedback on performance of robotics-assisted suturing. In *Biomedical Robotics and Biomechatronics (BioRob), 2012 4th IEEE RAS & EMBS International Conference on*, pages 823–828, 2012. Cited page 19.

H. Z. Tan, M. Srinivasan, B. Eberman, and B. Cheng. Human factors for the design of force-reflecting haptic interfaces. *Dynamic Systems and Control*, 55(1):353–359, 1994. Cited pages 17 and 22.

N. a. Tanner and G. Niemeyer. Improving perception in time-delayed telerobotics. *The International Journal of Robotics Research*, 24(8):631–644, 2005. Cited page 27.

M. Tavakoli, A. Aziminejad, and M. Patel, R. V.and Moallem. High-fidelity bilateral teleoperation systems and the effect of multimodal haptics. *Systems, Man, and Cybernetics, Part B: Cybernetics, IEEE Transactions on*, 37(6):1512–1528, 2007. Cited page 37.

R. Taylor, J. Funda, B. Eldridge, S. Gomory, K. Gruben, D. LaRose, M. Talamini, L. Kavoussi, and J. Anderson. A telerobotic assistant for laparoscopic surgery. *Engineering in Medicine and Biology Magazine, IEEE*, 14(3):279–288, May 1995. Cited page 29.

R. Taylor, A. Meciassi, G. Fichtinger, and P. Dario. Medical robotics and computer-integrated surgery. In B. Siciliano and O. Khatib, editors, *Springer Handbook of Robotics*, pages 1199–1222. Springer Berlin Heidelberg, 2008. Cited pages 14 and 29.

G. Tholey, J. P. Desai, and A. E. Castellanos. Force feedback plays a significant role in minimally invasive surgery: results and analysis. *Annals of surgery*, 241(1):102, 2005. Cited page 19.

A. Tobergte, P. Helmer, U. Hagn, P. Rouiller, S. Thielmann, S. Grange, A. Albu-Schaffer, F. Conti, and G. Hirzinger. The sigma.7 haptic interface for mirosurge: A new bi-manual surgical console. In *Intelligent Robots and Systems (IROS), 2011 IEEE/RSJ International Conference on*, pages 3023–3030, Sept 2011. Cited page 24.

J. Troccaz, editor. *Medical robotics*. John Wiley & Sons, 2013. Cited pages 29, 31, 81, and 100.

T. Tsuji, P. G. Morasso, K. Goto, and K. Ito. Human hand impedance characteristics during maintained posture. *Biological Cybernetics*, 72:475–485, 1995. Cited page 21.

C. Tzafestas, S. Velanas, and G. Fakiridis. Adaptive impedance control in haptic teleoperation to improve transparency under time-delay. In *Proceedings - IEEE International Conference on Robotics and Automation*, pages 212–219, 2008. Cited page 28.

M. Uchiyama, Y. Tsumaki, and W.K. Yoon. Design of a compact 6-dof haptic device to use parallel mechanisms. In *Robotics Research*, pages 145–162. Springer, 2007. Cited page 23.

F. C.T. Van der Helm, A. C. Schouten, E. de Vlugt, and G. G. Brouwn. Identification of intrinsic and reflexive components of human arm dynamics during postural control. *Journal of neuroscience methods*, 119(1):1–14, 2002. Cited page 21.

B. J. van der Horst and A. M.L. Kappers. Haptic curvature comparison of convex and concave shapes. *Perception*, 37(8):1137–1151, 2008. Cited page 18.

S.C. Venema and B. Hannaford. A probabilistic representation of human workspace for use in the design of human interface mechanisms. *Mechatronics, IEEE/ASME Transactions on*, 6(3):286–294, Sep 2001. Cited page 23.

J. Vertut and P. Coiffet. *Teleoperation and Robotics: Evolution and Development*, volume 3A of *NSRDS Bibliographic Series*. Springer, 1985. Cited page 11.

L. Villani and J. De Schutter. Force control. In B. Siciliano and O. Khatib, editors, *Springer Handbook of Robotics*, pages 161–185. Springer Berlin Heidelberg, 2008. Cited page 20.

H. S. Vitense, J. Jacko, and V. K. Emery. Multimodal feedback: an assessment of performance and mental workload. *Ergonomics*, 46(1-3):68–87, 2003. Cited page 19.

I. M.L.C. Vogels, A. M.L. Kappers, and J. J. Koenderink. Influence of shape on haptic curvature perception. *Acta psychologica*, 100(3):267–289, 1999. Cited page 18.

C. R. Wagner, R. D. Howe, and N. Stylopoulos. The role of force feedback in surgery: analysis of blunt dissection. In *haptics*, page 73, 2002. Cited page 100.

C. R. Wagner, N. Stylopoulos, P. G. Jackson, and R. D. Howe. The benefit of force feedback in surgery: Examination of blunt dissection. *Presence: teleoperators and virtual environments*, 16(3):252–262, 2007. Cited page 19.

Y. Wang, S. J. Riederer, and R. L. Ehman. Respiratory motion of the heart: kinematics and the implications for the spatial resolution in coronary imaging. *Magnetic Resonance in Medicine*, 33(5):713–719, 1995. Cited page 34.

D.W. Weir and J.E. Colgate. Stability of haptic displays. In *Haptic Rendering: Foundations, Algorithms, and Applications*, pages 151–189. 2008. Cited page 25.

D. E. Whitney. State space models of remote manipulation tasks. *Automatic Control, IEEE Transactions on*, 14(6):617–623, 1969. Cited page 26.

J.G.W. Wildenbeest, D.A. Abbink, C.J.M. Heemskerk, F.C.T. van der Helm, and H. Boessenkool. The impact of haptic feedback quality on the performance of teleoperated assembly tasks. *Haptics, IEEE Transactions on*, 6(2):242–252, April 2013. Cited page 19.

J. M. Winters and S. L.Y. Woo. *Multiple muscle systems: biomechanics and movement organization*. Springer New York, 1990. Cited page 85.

W.C. Wu, C. Basdogan, and M. Srinivasan. Visual, haptic, and bimodal perception of size and stiffness in virtual environments. 67:19–26, 1999. Cited page 17.

T. Yamamoto, M. Bernhardt, A. Peer, M. Buss, and A.M. Okamura. Techniques for environment parameter estimation during telemanipulation. In *Biomedical Robotics and Biomechatronics, 2008. BioRob 2008. 2nd IEEE RAS EMBS International Conference on*, pages 217–223, Oct 2008. Cited page 34.

T. Yamamoto, B. Vagvolgyi, K. Balaji, L. Whitcomb, and A. Okamura. Tissue property estimation and graphical display for teleoperated robot-assisted surgery. In *Robotics and Automation, 2009. ICRA'09. IEEE International Conference on*, pages 4239–4245, 2009. Cited page 34.

J. Yan and S. E. Salcudean. Teleoperation controller design using hâĹđ-optimization with application to motion-scaling. *Control Systems Technology, IEEE Transactions on*, 4(3): 244–258, 1996. Cited pages 27 and 36.

Y. Yokokohji and T. Yoshikawa. Bilateral control of master-slave manipulators for ideal kinesthetic coupling-formulation and experiment. *Robotics and Automation, IEEE Transactions on*, 10(5):605–620, Oct 1994. Cited pages 37, 47, and 52.

J. Yoon and J. Ryu. Design, fabrication, and evaluation of a new haptic device using a parallel mechanism. *Mechatronics, IEEE/ASME Transactions on*, 6(3):221–233, Sep. 2001. Cited page 23.

M. H. Zadeh, editor. *Advances in Haptics*. InTech, 2010. Cited page 22.

C.J. Zandsteeg, D.J.H. Bruijnen, and M.J.G. Van de Molengraft. Haptic tele-operation system control design for the ultrasound task: A loop-shaping approach. *Mechatronics*, 20 (7):767–777, 2010. Cited pages 56 and 60.

W. Zarrad, P. Poignet, R. Cortesão, and O. Company. Stability and transparency analysis of a haptic feedback controller for medical applications. In *Decision and Control, 2007 46th IEEE Conference on*, pages 5767–5772, 2007. Cited pages 100, 103, and 105.

N. Zemiti, G. Morel, T. Ortmaier, and N. Bonnet. Mechatronic design of a new robot for force control in minimally invasive surgery. *Mechatronics, IEEE/ASME Transactions on*, 12(2):143–153, 2007. Cited pages 29 and 31.

Index

causality, 42
Communication layer, 25, 46, 123

Evaluation, 52
    tools, 57

F-PF, 67

Haptic, 8, 16
    devices, 24
    exploration, 17
    freedback assessment, 18
    interface, 120
    interface control, 24
    perception, 17
    rendeing, 24
    teleoperation, 8, 9

Interaction port, 42

kinaesthetic, 8

Llewellyen's criteria, 51

Master
    desing, 23
    robot, 120
Master-Slave Network, 9

Model
    teleoperator's, 44
Modelling, 39
    environment, 81
    teleoperation,, 42, 44
    tools, 57

P-PF, 62
Passivity, 27, 36, 49, 51, 94
    1-port network, 50
    2-port network, 50
    based control (PBC), 49
Performance
    of 3-Ch, 62
PF-F, 74
PF-P, 71

Slave, 28
Stability, 36
    of 3-Ch, 62
    of AOB based teleoperator, 104
    teleoperator's, 51
Surgical
    assistance, 13
    robots, 13

Tactile, 8

Teleoperation, 7, 35, 83
AOB, 102
bilateral, 9, 10
control architecture for medical application, 76
for medical care, 13
haptic, 9
modelling, 36, 42, 44
multimodal, 10
scheme reformulation, 87
stability, 36
surgical, 81
three-channel control architectures, 61
transparency, 37
unilateral, 9, 10
Teleoperator, 8, 9, 35, 39
's model, 44
control architecture, 55
stability, 51
Telepresence, 8
Three-Channel
control architecture, 62
teleoperation, 61
Transparency, 37
of AOB based teleoperator, 105

Abstract

This thesis investigates the major factors affecting teleoperation transparency in medical robotics context. A wide state of art survey is carried out and a new point of view to examine haptic teleoperation literature is proposed in order to extract the decisive factors to achieve a transparent teleoperation. Furthermore, the roles of three aspects have been analysed.First, the role of the applied control architecture. To this aim, the performances of 3-channel teleoperation architectures are analysed and guidelines to select a suitable control architecture for medical applications are proposed. The validation of these guidelines are carried out through simulations. Second, the effects of motion disturbance in the manipulated environment on telepresence are analysed. Consequently, a new model of such moving environment is proposed and the applicability of the proposed model is shown through interaction port passivity investigation. The third analysed factor is the role of the interaction model accuracy on the transparency of interaction control based haptic teleoperation. This analysis is performed theoretically and experimentally based on the design and implementation of Hunt-Crossly model in AOB interaction control haptic teleoperation. The results are discussed and the future perspectives are proposed.

Keywords: *Haptics, Teleoperation, Bilateral teleoperation, Disturbance compensation, AOB*

Résumé

Dans ce travail de thèse, nous examinons les principaux facteurs affectant la transparence d'un schéma de téléopération dans le contexte de la robotique médicale. L'analyse approfondie de l'état de l'art a permis de proposer une nouvelle classification de schémas de téléopération avec retour haptique. Les principaux facteurs analysés sont liés à l'architecture de commande appliquée, aux perturbations provoquées par les mouvements physiologiques des tissus manipulés ainsi qu'à la précision du modèle d'interaction robot-tissue. Les performances du schéma de téléopération à architecture 3-canaux ont été mis en évidence en simulation. L'influence des mouvements physiologiques de l'environnement manipulé sur la transparence du système a également été évaluée et un nouveau modèle d'interaction avec des tissus mous a été proposé. Un schéma de commande de téléopération basé modèle d'interaction a été synthetisé en se basant sur une analyse de passivité du port d'interaction robot-environnement. Enfin, l'importance de la précision du modèle d'interaction (robot-tissue) sur la transparence du schéma de téléopération avec retour d'effort basé-modèle a été explorée. Cette analyse a été validée en théorie et expérimentalement en implémentant le modèle Hunt-Crossly dans une commande utilisant un AOB pour réaliser une téléopération avec retour haptique. En conclusion de ce travail, les résultats de cette thèse ont été discutés et les perspectives futures ont également été proposées.

Mots clefs : *Haptique, Téléopération, Compensation des Incertitudes, AOB*

LIRMM — 161, rue Ada — 34095 Montpellier cedex 5 — France